Scale-up of human pluripotent stem cell-based therapies for age-related macular degeneration

Iwan Thomas Roberts

UCL

EngD Bioprocess Leadership

I, Iwan Thomas Roberts confirm that the work presented in this thesis is my own. Where information has been derived from other sources, I confirm that this has been indicated in the thesis.

Abstract

This doctoral thesis was in collaboration with a research group from the Institute of Ophthalmology at Moorfields Eye Hospital and the London Project to Cure Blindness. The group was in late stage pre-clinical development creating a pluripotent stem cell (PSC) derived therapy to produce retinal pigment epithelium cells (RPE) for the treatment of Age Related Macular Degeneration (AMD). Creating effective treatments for AMD is vital given that it is the leading cause of blindness in the developed world with around 500,000 people in the UK afflicted with the disease, half of which are registered as visually impaired. In addition, for the dry form of the disease, which represents 85-90% of total cases, there is no effective treatment.

The current lab based manufacturing protocols intended for use during Phase 1 trials are not feasible for subsequent larger scale clinical trials or for the commercial manufacture of an affordable mass-produced therapy. The aim of this thesis was to explore the feasibility of applying methodologies and technologies from traditional biotechnology production to cell therapy manufacturing. Specifically use of bioreactors to scale up cell culture **(Chapter 2)**, the application of online monitoring and control to PSC culture **(Chapter 3)**, the use of a design of experiments (DoE) approach to PSC differentiation **(Chapter 4)** and cell-cell purification **(Chapter 5)**.

Taken as a whole it is clear that the application of traditional biomanufacturing technologies and approaches have much potential when applied to cell therapies, and specifically a PSC derived cell therapy to treat blindness. However much more work is needed to reduce variability in the process to better understand the impact of process parameters on critical quality attributes and how best to approach these in an environment where there is little clinical experience to define the target product profile.

Acknowledgements

I would like to give my thanks to my supervisors Professor Chris Mason and Professor Pete Coffey for their support, advice, and ultimately the confidence they had in me. Without their help I would not have enjoyed working on this thesis nearly as much as I did. I would also like to recognise my fellow researchers and the other academics at UCL who were kind enough to let me benefit from their expertise, time and experience; Amelia Lane, Shazeen Hasan, Sakina Gooljar, Ludmila Ruban, Diana Hernandez, Sofia Simaria and Suzanne Farid. I would also like to express my gratitude to the sponsors of this work for giving me this opportunity; the Engineering and Physical Science Research Council (EPSRC), the Industrial Doctoral Training Centre in Bioprocess Engineering Leadership (EP/G034656/1), and the UK Stem Cell Foundation. Lastly, the support from the entire Biochemical Engineering Department at UCL has been fantastic over the last 8 or so years and I am leaving with very fond memories of my time there.

Outside "the lab" I would like to thank my mum Margaret my dad Brian and my sister Rhiannon, particularly for their understanding that doctoral research is a "real job". Finally, I would like to thank Anna Lucock for her timeless patience for putting up with all the times I have been away working, especially the many late nights and weekends in the lab over the last 4 years.

Publications and presentations pertaining to this thesis

Publications

1) **Scale-up of Human Embryonic Stem Cell Culture Using a Hollow Fibre Bioreactor.**

   Roberts, I., Baila, S., Rice, R. B., Janssens, M. E., Nguyen, K., Moens, N., Ruban, L., Hernandez, D., Coffey, P. & Mason, C

   Biotechnology Letters, 34, 2307-15. 2012.

Poster Presentations

1) **Using a Design of Experiment (DoE) Approach to Optimise Pluripotent Stem Cell Differentiation for Subsequent Manufacturing***

   Roberts, I., Coffey, P. & Mason, C

   Scale-Up and Manufacturing of Cell-Based Therapies III (2014, San Diego, USA)

   **Winner of student abstract competition*

2) **Key Considerations when Scaling-Up Cell Culture for Therapies***

   Roberts, I., Coffey, P. & Mason, C

   Scale-Up and Manufacturing of Cell-Based Therapies II (2013, San Diego, USA)

   **Winner of young investigator of the year award*

3) **The Importance of Using Small-Scale Bioreactor Mimics to Scale-up Human Embryonic Stem Cell Culture**

   Roberts, I., Moens, N., Moncaubeig, F., Egloff, M., Coffey, P. & Mason, C

   International Society for Stem Cell Research 10th Annual Meeting (2012, Yokohama, Japan)

4) **The Scale-Up of Human Embryonic Stem Cell Culture using a Hollow Fibre Perfusion Bioreactor – The Quantum Cell Expansion System**

   Roberts, I., Baila, S., Rice, R. B., Janssens, M. E., Nguyen, K., Moens, N., Ruban, L., Hernandez, D., Coffey, P. & Mason, C

   International Society for Stem Cell Research 9th Annual Meeting (2011, Toronto, Canada)

Oral Presentations

1) 5 min poster summary including question and answer session

Key Considerations when Scaling-Up Cell Culture for Therapies*

Roberts, I., Coffey, P. & Mason, C

Scale-Up and Manufacturing of Cell-Based Therapies II (2013, San Diego, USA)

**Winner of young investigator of the year award*

2) First Impressions of the Quantum System

Roberts, I., Coffey, P. & Mason, C

UK Stem Cell User Group Annual Meeting (2010, London, UK)

List of chapters

List of Figures

List of tables

Chapter 1. Introduction

Chapter 2. Bioreactor culture of pluripotent stem cells using the Quantum Cell Expansion System

Chapter 3. Control of the pluripotent stem cell environment using the Xpansion One system

1. Introduction

1.1 Age related macular degeneration (AMD)

Age related macular degeneration (AMD) afflicts 8.69% of 45-85 year olds globally, with estimates that 195m people will suffer from the disease by 2020 and with and aging global population this will rise to 288m in 2040 (Wong et al.). AMD represents the advanced form of the deteriorative process that happens in all eyes primarily as a result of the ageing process, although other risk factors such as genetic predisposition, hypertension and smoking affect the age at onset of the disease pathology (Evans, 2001). AMD results in a characteristic loss of visual acuity in the central field of vision **Figure 1.1 a)** and **b)**. The cause of this photoreceptor death is the atrophy of the layer of retinal pigment epithelial (RPE) cells that support them, and the degeneration of Bruch's membrane on which the RPE adhere to (see **Figure 1.2 a)** and **b)** reproduced from Ramsden et al. (2013).

1.1.1 The role of RPE in AMD

The progression of AMD can be seen in colour fundus photographs, with **Figure 1.3 a), b)** and **c)** showing a healthy eye, and eyes afflicted with late stage dry and late stage wet AMD respectively. These images have been reproduced from Ebrahimi and Handa (2011). AMD causes damage to the fovea which makes up only a small percentage of the surface area of the eye but is responsible for the central field of vision where the greatest visual acuity is needed to perform everyday tasks such as reading and driving.

The RPE monolayer is derived from the neuroepithelium of the anterior neural plate in the developing embryo. It performs many important turnover functions to support the photoreceptors and makes up part of the physical barrier between the photoreceptors and the underlying blood supply. There are a considerable number of specific functions required of the RPE to maintain vision as outlined in **Table 1.1** adapted from Strauss (2005).

Late stage dry AMD is characterised by the build up of drusen deposits over the macular region (which contains the fovea) as seen in **Figure 1.3 b)**. These drusen aggregates are

formed from incomplete digestion of photoreceptor outer segments that form phagosomes within the RPE cells and other molecular by-products. RPE cells excrete this toxic lipofuscin which is non-degradable and so it accumulates on Bruch's membrane (Young, 1987). Lipofuscin is the same yellow brown pigmentation that causes "age spots" in post-mitotic cells (non-dividing) tissues. This accumulates as a function of age, resulting from a failure of molecular turnover mechanisms (Brunk and Terman, 2002).

Drusen combined with other age related toxic factors such as advanced-glycation end products (AGES) and a reduction in protective species such as the antioxidant α-tocopherol increases the oxidative stresses in the region (Strauss, 2005). In addition detailed analysis of drusen constituents showed the presence of proteins associated with immune-mediated and inflammatory systems thereby suggesting a role of these age sensitive systems in drusen formation (Hageman et al., 2001). These factors combined are believed to cause a reduction in RPE cell density due to apoptosis, reduction in pigmentation, destabilisation of intracellular membranes e.g. the tight junctions between RPE cells, and damage to Bruch's membrane (Strauss, 2005) visualised in **Figure 1.2 b)**. This process increases the amount of molecular debris that in turn leads to further degradation of the RPE cells as part of a positive feedback mechanism. Ultimately resulting in additional loss of the photoreceptors which the RPE support and so loss of sight (Young, 1987).

In wet or neovascular/exudative AMD the barrier between the blood supply in the choroid and the photoreceptors is penetrated by unwanted neovascular membranes (choroidal neovascularisation), this breached layer is made up of Bruch's membrane and the RPE (Chopdar et al., 2003). These vessels are leaky and so cause fluid oedema (extravasation of blood and lipid materials) and eventual dense fibrovascular scarring disrupting the architecture of the macular region and so photoreceptor death **(Figure 1.3 c)**. Wet AMD can cause rapid sight loss especially if the vessels rupture and haemorrhage. Both wet and dry AMD can exist in the same patient and the same eye.

1.1.2 Existing therapies for AMD

Wet AMD is treated using anti vascular endothelial growth factor (VEGF) treatments such as ranibizumab (Lucentis) which is a monoclonal antibody fragment made by Genentech. Bevacizumab (Avastin) is also used off-label which is a full monoclonal antibody also made by Genentech and EYLEA (aflibercept) a fusion protein from Regeneron Pharmaceuticals. These treatments inhibit the growth of penetrating vessels and require repeated injections into the eye. However no medicinal intervention is available for the dry form of AMD.

Some complex surgical interventions have shown a degree of success in small-scale trials for the treatment of AMD. For example, Macular Translocation is an operation in which the retina is detached (retinopathy) and the macula rotated to an area of undamaged RPE. In essence this is an RPE allograft. A review by da Cruz et al. (2007) describes cases where both the dry and wet forms of AMD have been treated with transplantations of RPE cells from RPE biopsies. These cells are either "allogeneic", being sourced from a donor, or "autologous" where the cells are sourced from the patients themselves. The mechanisms by which RPE transplantation rescues photoreceptor is unknown, but da Cruz et al. (2007) reports that the evidence points towards two types of interaction; 1) Direct contact between RPE and photoreceptor and/or, 2) Indirect contact through diffusible factors released by transplanted RPE, e.g. PEDF (see **Table 1.1**).

In the case of RPE transplantation to specifically treat Dry AMD there is evidence in the literature that visual function has been maintained in patients from the results of such RPE grafting. For example Algvere et al. (1997) reported that RPE cells from foetuses from 13-20 gestational age inserted into the subretinal space resulted in the disappearance of drusen and maintenance of visual function. In addition Joussen et al. (2006) reported success using the autologous Peripheral RPE-choroid method.

1.1.3 Pluripotent stem cell (PSC) therapy to treat AMD

It is important to consider that even though the previously described treatment methods appear to show efficacy in the treatment of AMD, they are not practical for treating the hundreds of thousands of prospective patients. Firstly, in the case of the allograft method

the surgery is complex due to the need harvest cells from the periphery before the transplantation, and if the RPE cells are dystrophic, meaning they are all dysfunctional, the method would be ineffective. Second, the primary cell sources listed for the allogeneic therapy are limited as foetal and cadaveric cells are hard to source and they lose their phenotype during in vitro expansion. This argument has been made by Vugler et al. (2008) which cites the following papers describing a loss of the following phenotypes in extended primary cultures (Dutt et al., 1989), a loss of Fc receptors (Davis et al., 1995), loss of cytoskeletal polarisation, and a down regulation of the proteins RPE65 and Cellular Retinaldehyde-Binding Protein (CRALBP) which are both involved in retinoid recycling, after only as few as 2-3 passages in vitro (Alge et al., 2003). Therefore, it is likely that there will never be enough cells available to achieve the economies of scale needed to provide a strong argument for a cellular therapy to treat AMD using these sources.

A potential alternative cell source is to use human pluripotent embryonic stem cells (PSCs). They have the capability of near indefinite expansion in culture whilst maintaining the ability to then differentiate into a large number of different cell types (pluripotency), making them an attractive cell source for many prospective cell replacement therapies. Human embryonic stem cells were first isolated by Thomson et al. (1998), and cells with the same pluripotent phenotype were generated through the use of genetic reprogramming to generate induced pluripotent stem cells (iPS) by a group lead by Yamanaka Takahashi et al. (2007); collectively these cells are named pluripotent stem cells (PSCs).

Advanced Cell Technology (ACT) and their collaborators first described PSCs as a source of human RPE for potential transplantation (Klimanskaya et al., 2004). Later a similar ACT collaboration was the first to show how PSC derived RPE (PSC-RPE) could rescue visual function in the royal college of surgeons (RCS) rat (Lund et al., 2006). The RCS rat being an animal model of RPE dystrophy (Mullen and LaVail, 1976). These results have been replicated using iPS cells by Carr et al. (2009). PSCs therefore present a potentially unlimited source of RPE cells. However their pluripotency and sensitivity to in vitro processing provides many novel technological challenges if they are to be used in a bioprocess in a future RPE cell therapy to treat AMD. Despite this PSC derived RPE have

already been successfully used to treat patients in early stage clinical trials. A trial by ACT reported in late 2014 that transplanted PSC-RPE in an open label study show initial promise of both safety and efficacy in the treatment of both AMD and Stargardt's macular dystrophy (a juvenile RPE dysfunctional disease) (Schwartz et al., 2014). Furthermore, the Riken institute in Japan released a press release in 2014 describing a successful RPE transplantation using iPS derived RPE cells.

1.2 Translating a PSC lab process into a therapeutic bioprocess

1.2.1 Current status of cell therapies

Although there are no existing PSC derived therapy with market approval there are clear examples of these therapies starting to transfer into the clinic. Therefore, this thesis focuses on looking beyond these initial small scale trials to explore how the current lab protocol used by Moorfields Eye Hospital could be scaled up into a novel, mass produced, and validated commercial bioprocess. Despite there being no PSC cell therapies with market approval (FDA, EMA regions) living cell therapies as a whole have been on the market for many years. For example the Apligraf[1] and Dermagraf[2] allogeneic products combined have treated over 300, 000 patients, primarily for venous leg and diabetic foot ulcers. Current estimates are now that over 1million patients have been treated with cellular therapies, this excludes those treated for hematologic malignancies (Professor Chris Mason, UCL[3]). Like most other examples of cell-based therapies with regulatory approval the cells are derived from a somatic cell biopsy (foreskin) administered to the exterior of the body.

However, regarding the internal administration of cell therapies into the body the field is at a much earlier stage of commercial exploitation (if an exclusion is made regarding bone marrow transplants). The two prime examples of such biotherapeutics are Provenge

[1] Bilayered skin substitute: an epidermal layer formed by human keratinocytes dermal layer is composed of human fibroblasts in a bovine Type I collagen lattice, from Organogenesis (USA). Used for venous leg ulcers (FDA 1998) diabetic foot ulcers (FDA 2001) and chronic ulcers and soft-tissue defects (Switzerland 2008)

[2] Cryopreserved human fibroblast-derivedermal substitute composed of fibroblasts, an extracellular matrix and a bioabsorbable scaffold, from Advanced BioHealing (USA) (originally Advanced Tissue Sciences/ Smith & Nephew). For the treatment of diabetic foot ulcers (FDA2001)

[3] London Regenerative Medicine Network, April 2015

(Dendreon), and Prochymal (Mesoblast). Provenge is a treatment of autologous dendritic cells loaded with prostate antigen prostatic acid phosphatase fused to granulocyte-macrophage colony-stimulating factor and which is approved by the FDA in prostate cancer. Whereas Phochymal consists of cells isolated from bone marrow expressing the CD34-marker (besides others) and is approved for the treatment of graft versus host disease. By administrating the cells directly into the blood stream the determination of the pharmacokinetics and pharmacodynamics of the therapy is vastly more complex than applying to external wounds, which results in an associated rise of clinical risk.

In short, development of novel allogeneic stem cell therapies from PSCs can draw on past experience from the growing commercial successes of somatic cell therapies and these first internally administered cells. However, development needs to be mindful of the evolving regulatory environment as regulators adjust to these new types of therapies for example the good tissue practice (GTP) final rule (FDA) and the advanced therapy medicinal products (ATMPs) regulation (EMA).

All biological therapies are approved on two criteria, efficacy and safety. To meet these criteria a PSC process needs to be able to reproducibly manufacture a defined population of cells to meet the target product profile (TPP). Understanding how the heterogeneous and transient nature of PSC cultures impact the TPP is key to scaling the lab protocol. The following sections explore some of the key considerations impacting the on safety and efficacy of the potential therapy that relate to the manufacturing process.

1.2.2 Safety concerns of PSC derived therapies

The main safety concerns of PSCs are that they have a transient and often highly heterogonous phenotype during differentiation. The phenotype is both highly susceptible to external stimuli and also hard to track during culture with there being few rapid or non-destructive analytical assays available. This heterogeneity means the safety of a PSC therapy will be dependent on a process's proven ability to deliver only the intended cell type to patients, being free of potentially harmful contaminant cells. Cellular contaminants can be put into 3 broad categories; 1) non-tumorigenic cells, 2) undifferentiated PSC, and 3)

proliferative cells. The presence of these cells, or masses they can form, could cause harm from either their metabolic activity and/or physical presence, particularly in anatomically sensitive areas such as the brain. The issue of stem cells and tumour formation is discussed in detail in the review by Anisimov et al. (2010).

1.2.3 Non-tumorigenic cells (contamination from spontaneous differentiation)

During differentiation protocols the PSC population not only changes into the intended therapeutic cell but also differentiates into a multitude of other cell types. Differentiation yields can be very low, for example Klimanskaya et al. (2004) reported <1% spontaneous differentiation of RPE from embryoid bodies after 6 weeks. However with protocol optimisation using nicotinamide and Activin A the efficiency can be increased to 33% for PSC-RPE differentiation (Idelson et al., 2009). More recently this has been further increased up to 80% with the addition of a larger number of defined factors at specific timings (Buchholz et al., 2013). Yet, this still leaves a substantial amount of contaminant "non RPE" cells (20%). Such contaminants can cause issues with the regulators, for example the Geron Corporation had their subsequently abandoned PSC clinical trial put on temporary hold when it was discovered that a certain unwanted cellular contaminant led to the formation of non-proliferative cysts[1]. This potential risk is termed it "graft overgrowth" were limited benign in vivo proliferation of stem cells or their progeny could cause clinical harm (Anisimov et al., 2010). A recent example of this is where an autologous olfactory stem cell transplant into the spine at a Portuguese hospital had to be removed due to patient pain. On removal the growth was determined to be non-cancerous containing nerve branches, bone and was secreting mucosal material[2]. Therefore the manufacturing process needs to either have a purification stage to separate out just the desired population or be able to reproducibly deliver a defined heterogeneous population with pre-clinical assurances as to its safety.

[1] Geron press release, accessed 11,12,14 http://ir.geron.com/phoenix.zhtml?c=67323&p=irol-newsArticle&ID=1636138

[2] New Scientist, accessed 14,07,14 http://www.newscientist.com/article/dn25859-stem-cell-treatment-causes-nasal-growth-in-womans-back.html#.VJ09XBuQR

1.2.4 Teratomas (PSC Contamination)

A test for the pluripotency of PSC (ability to differentiate into the vast multitude of cell types) is to inject them into an immunodeficient mouse, where they form what is termed teratomas. These teratoma masses are then removed and interrogated for the 3 germ layers that all cells types are derivatives of, thus proving their pluripotency potential. However these PSC derived teratoma like masses do not meet the classic definition of teratomas which contain acquired genetic and epigenetic alterations (Lensch and Ince, 2007). Although benign this ectopic tissue either at the therapeutic site of implantation, or as a result of migration through the body's transport systems may cause harm.

When the FDA first started exploring the potential regulation of PSC therapies in 2008 a meeting with industrial stakeholders was held. Here the view was presented that undifferentiated cells in the final therapy were a safety concern and that the further down the pathway to specialisation and terminal differentiation the lower the risk of "tumour" formation. Thus it is a key part any PSC derived investigational new drug (IND) filing to have accounted for the issue of undifferentiated PSC contamination. In a manufacturing process this could mean the tracking and ultimately confirming the absence of PSC markers in the final product.

1.2.5 Graft overgrowth and karyotype drift

During prolonged cell culture and adaption to new methods PSC can experience Karyotypic drift (chromosomal changes) often resulting in decreased population doubling times which may lead to tumour formation *in vivo* due to uncontrolled proliferation (Mitalipova et al., 2005, Pera, 2004, Draper et al., 2004). But, this has not precluded the use of a karyotypically abnormal cell line being used in therapy for example Carpenter et al. (2009) reported that the FDA approved the use of the human embryonal carcinoma cell line which has between 56 and 61 chromosomes for use in a clinical trial. Yet their inclusion would still be undesirable as they present a significant safety concern. This makes karyotype testing to prove stability over a defined range of passages a likely prerequisite for the working cell bank used in manufacture.

1.2.6 Animal derived reagents

PSCs were traditionally grown in complex ill-defined media containing factors such as foetal bovine serum (FBS) and on inactivated mouse fibroblasts (MEFs). The FDA guidance from the Center for Biologics Evaluation & Research (CBER) considers that PSC/MEF co-culture fit the definition of xenotransplantation, but it does not intend this to preclude the use of PSC in clinical trials. This was demonstrated by the FDA approval for the use of the H1 cell line in clinical trials by the Geron Corporation, which was derived and maintained on mouse feeders. More recently great efforts have been made to move towards a feeder free and Xeno free culture platform, for example Invitrogen's KnockOut™ SR XenoFree product which replaces FBS is formulated with human sourced or human recombinant proteins derived under cGMP conditions. This can be used in combination with other products such as CELLstart also from Invitrogen or flasks coated in Corning's Synthemax (synthetic peptides) that replace the need for a mouse feeder layer. Such advances have enabled the production of cGMP PSC lines for eventual clinical use. Although using animal products presents a risk it has not stopped products reaching the market e.g. Apligraf (Organogenesis) uses bovine serum albumin in manufacture. Even so, the difficulties in sourcing the large amounts of serum from countries who are BSE free, and issues with batch to batch variability, puts significant limitations on the industry as a whole with there potentially only being enough BSA to support only one 'blockbuster' cell therapy (Brindley et al., 2012). This conclusion further necessitates the need to develop economically viable animal alternatives.

1.2.7 Efficacy

The efficacy of a therapy is derived from its target product profile (TPP). This is a set of attributes which can be measured as a predictor of clinical efficacy. Complicating matters is that the current therapeutic action of PSC derived cells is poorly understood exhibiting potentially multifactorial modes of action e.g. it could be both a physical and paracrine interaction, which may or may not require integration of, or be dependent on, the long term survival of the implanted cells. However such predictive assays of potency are vital for clinical success and so will define the targeted critical quality attributes (CQAs) of any

commercial process. For example, is was concluded by some that the Phase 3 trials of Prochymal in the USA failed in part, but was not limited to, a poor understanding of how MSCs work in humans - despite powerful immunosuppressive effects seen in vitro and in animal models, as *"No predictive assays for efficacy exist,"* according to Francesco Dazzi[1] (Allison, 2009).

Such assays are typically refined during later stage clinical development based on previous experience. The current release criteria for the PSC-RPE therapy is based on assessment of the RPE patch for variables such as viability, cell coverage, morphology, pigmentation and patch size. With other markers associated with pluripotency (absence), the RPE phenotype, and PEDF/VEGF secretions recorded on the quality control patch as additional critical quality attributes (CQAs). But, although such markers are linked to the functional RPE phenotype they are not part of a functional assay. The gold standard in vitro test for PSC derived RPE is their ability to process fluorescently labelled rod and cone outer segments. This assay is time consuming and not well suited to lot release criteria; thus validation studies will be needed to link the CQAs to performance in this test should it be used as a predictor of efficacy. Given the poorly defined nature of the variables in the existing lab protocol this thesis will seek to try and explore how possible critical process parameters (CPP) impact these critical quality attributes (CQA) of RPE marker expression with the intention of generating the most efficacious TPP.

1.2.8 Overview of the existing lab protocol

The existing lab based protocol is outlined in **Figure 1.4;** currently all processing is manual and takes place in T25 flasks. In brief, PSC (hESC in the case of the Moorfield's Phase I clinical trial) are expanded on inactivated human fibroblasts and once over-confluent bFGF is removed from the media and the flasks cultured for up to 12 weeks until pigmented foci appear and grow. These foci are then manually excised in a laborious process using the tips of hypodermic needles. The excised RPE are then expanded on matrigel to increase numbers before being detached a final time and seeded onto the permeable structure of

[1] Head of Stem Cell Biology at Imperial College London's Kennedy Institute of Rheumatology

transwell membranes. These RPE coated membranes are cut to size before insertion into the macular region of the eye.

1.3 Thesis aims and objectives

This thesis explores the feasibility of applying methodologies and technologies from traditional biotherapeutic production to cell therapy manufacturing, specifically the creation of a PSC-RPE therapy to treat AMD. The approach was to split the existing lab process into its constituent parts **(Figure 1.5)** and so identify the key manufacturing issues of the current process. Each results chapter is in essence a proof of concept feasibility study for that stage; either applying a new method, approach or technology. The Specific objectives of each chapter are summarised below:

Chapter 2*: Bioreactor culture of pluripotent stem cells using the Quantum Cell Expansion System*

The aim of this chapter was to explore the feasibility of growing PSC at large scale on commercially available machinery that was initially designed for the growth of MSCs.

Chapter 3*: Control of the pluripotent stem cell environment using the Xpansion One System*

The aim of this chapter was to explore the feasibility of growing PSC on the Xpansion One system to determine the platform's suitability for growing PSC prior to scaling up to the industrial scale reactors. Of particular interest was to explore how the online control of environmental conditions such as pH available on the Xpansion system impacted cell growth and the target phenotype.

Chapter 4: *A Design of Experiment (DoE) approach to retinal pigment epithelium differentiation*

The aim of this chapter was to explore the feasibility of the factorial DoE approach for the screening and optimising of the PSC-RPE differentiation. Key process variables that were poorly understood were investigated to determine which had the greatest impact on performance. Key variables were then modelled to predict optimal conditions.

Chapter 5: *Isolation of retinal pigment epithelium from differentiating pluripotent stem cell monolayers*

The aim of this chapter was to assess alternatives to the current manual purification method of excising pigmented RPE foci from the heterogeneous differentiating cell population. An alternate method being a prerequisite for large scale manufacture in the future. The characterisation and performance of a novel filter based separation was explored.

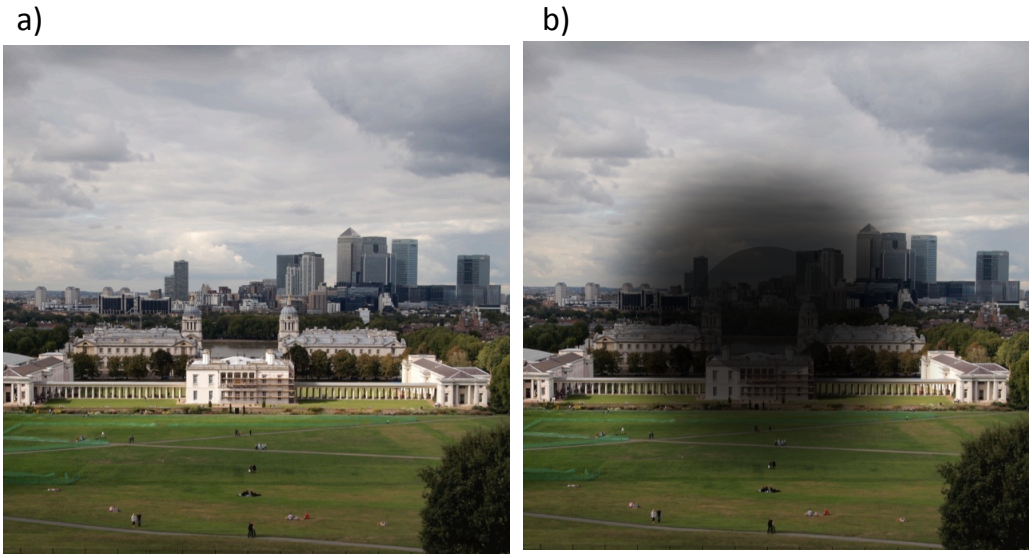

Figure 1.1: Age related macular degeneration. Doctored photos demonstrating the Central Vision Loss AMD Patients Suffer: a) normal visual field, b) and loss of central visual field due to RPE atrophy b).

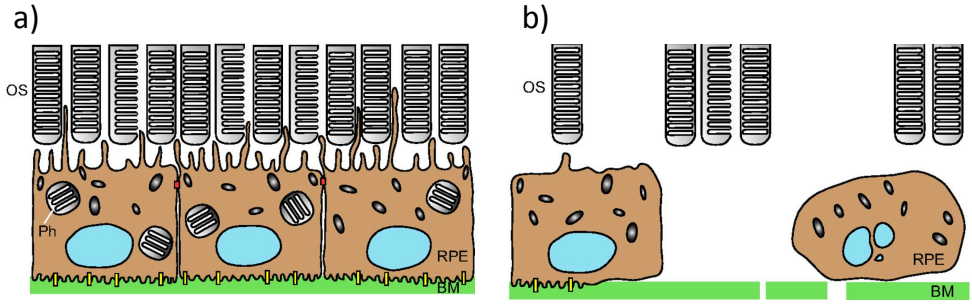

Figure 1.2: RPE death in AMD. a) In a healthy eye, the retinal pigment epithelium (RPE) layer sits upon Bruch's Membrane (BM in green) forming a tight barrier with this membrane whilst interacting with the photoreceptor outer segments (OS); b) In contrast the diseased eye exhibits death and degeneration of the RPE the layer and is discontinuous. Photoreceptor loss also occurs due, in part, to the inability of the degenerated RPE to phagocytose the photoreceptor outer segments, as illustrated by the lack of phagosomes (Ph) within the RPE cells. Cartoon reproduced from (Ramsden et al., 2013).

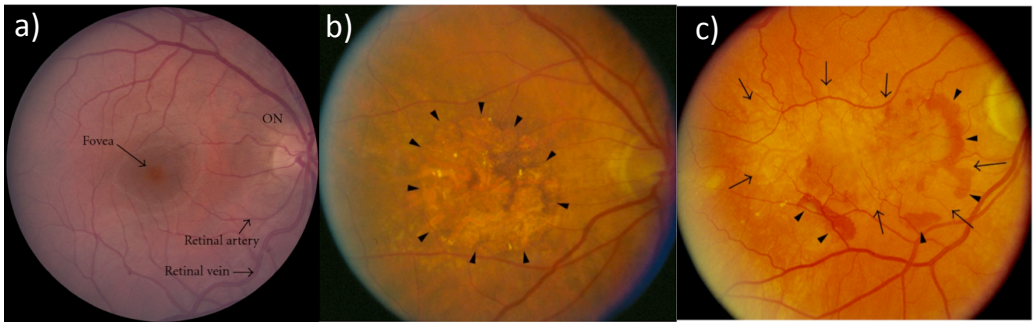

Figure 1.3 Fundus images of the healthy and diseased retina. a) an example of a healthy eye with the fovea, optic nerve (ON) and retinal artry and retinal vein annotated; b) an eye with advanced nonneovascular (dry) AMD (Geographic atrophy). Note area where RPE cells have died from apoptosis (arrowheads; c) an eye with neovascular or wet AMD. Note the subretinal hemorrhage (arrowheads) adjacent to a choroidal neovascular membrane (arrows). Reproduced from (Ebrahimi and Handa, 2011).

1) Expansion of hESC
- hESC expanded on inactivated human fibroblasts in T25 flasks
- Flasks passaged in a 1:2 ratio once per week until target number is reached
- Cells are then cultured for another 2 weeks until superconfluency is reached

2) Differentiation
- Media is changed to differentiation media and changed 3x per week
- 12 weeks

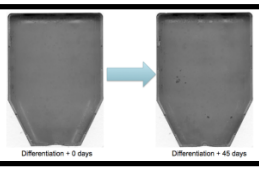

3) Foci excision
- Pigmented areas manually excised and dissociated into single cell suspension

4) hESC-RPE expansion
- Seeding density: 38,000 cells/cm^2
- Coated 48 well plates
- Media change 2x per week
- 7 weeks

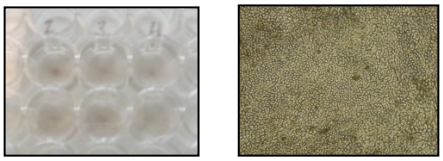

5) Membrane seeding
- Seeding density: 166,000 cells/transwell
- Coated transwell in 48 well plate
- Media change 2x per week
- 3 weeks

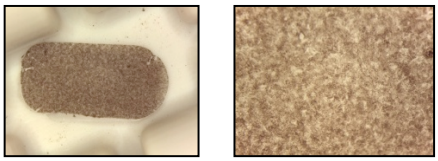

Figure 1.4: Overview of the existing lab process. The existing lab process can be broken down into 5 discrete stages each posing its own challenges to industrial production.

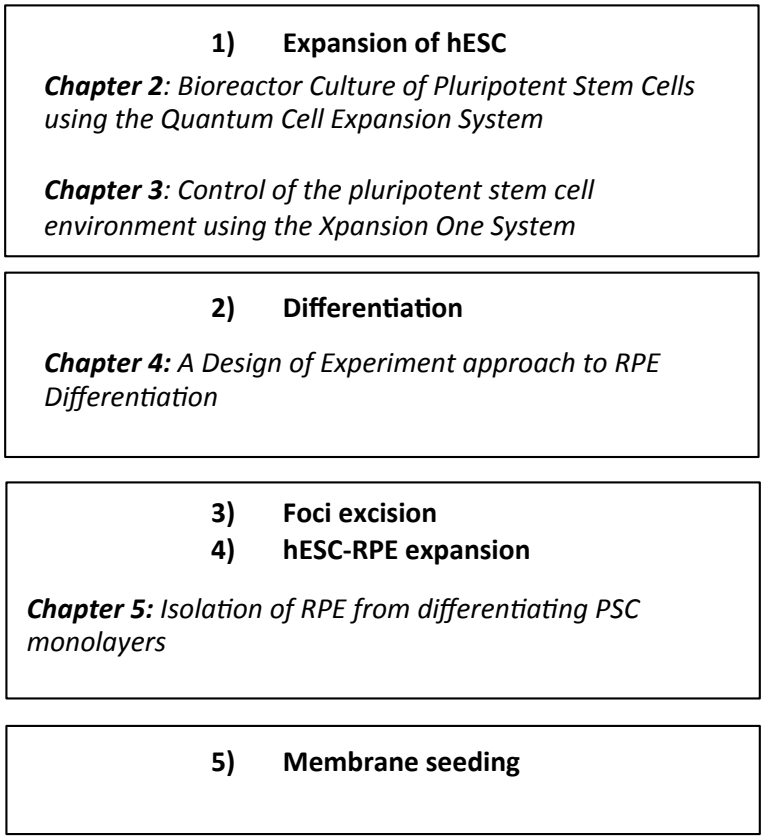

Figure 1.5: Thesis overview. The thesis is broken up into 5 results chapters each addressing a specific processing challenge of the current lab protocol.

Table 1.1: The functions and roles of the RPE to maintain vision, adapted from (Strauss, 2005)

RPE Function	Role in vision
Part of the blood/retina barrier protecting the photoreceptors	Physical barrier
Microvilli on the apical membrane face the photoreceptor outer segments in a structural relationship to necessitate the transfer of nutrients to the photoreceptors and to take waste away. Basal membrane faces Bruch's membrane. The tight junctions between the cells in the RPE monolayer means these species have to pass through the RPE themselves thus under active control.	Control over metabolite transfer
Transport nutrients from the blood such as glucose to the photoreceptors to maintain their high level of metabolic activity.	Metabolite transfer: blood ➔ photoreceptors
Transports ions, water and metabolic end products such as lactic acid from the subretinal space to the blood.	Metabolite transfer: photoreceptors ➔ blood
Re-isomerise *trans*-retinal formed after photon adsorption in the photoreceptors back into 11-*cis*-retinal as part of the retinal cycle, photoreceptors being unable to convert all the *trans*-retinal alone. This isomerisation effectively re-sensitises or refreshes the photoreceptors enabling new visual information to be obtained.	Metabolite recycling
Recycling of the light sensitive photoreceptor outer segments shed by the photoreceptors ensuring the maintenance of excitability. Segments are phagocytised by the RPE and essential compounds such as retinal recycled (see retinal cycle above) and returned to the photoreceptors.	Metabolite recycling
Help to establish the immune privilege of the eye though the excretion of immunosuppressive factors	Excretion of protective agents
Secretes the neuroprotective/antiangiogenic pigment epithelium-derived factor (PEDF) to the neural retina and the vasoprotective/angiogenic vascular endothelial growth factor (VEGF) to the choroid.	Excretion of protective agents
Pigmentation absorbs light energy, reducing light scattering and so improves sight.	Visual acuity

2. Bioreactor culture of pluripotent stem cells using the Quantum Cell Expansion System[1]

2.1 Introduction and aims

2.1.1 Use of bioreactors to scale up stem cell culture

The use of bioreactors that grow cells on fibres or microcarriers as opposed to tissue culture plastic vastly increases the surface area available for cell growth. This enables potential scale-up as it effectively allows cells to be grown in three dimensions, facilitating higher cell densities (i.e., the number of cells grown within a given vessel volume, defined as volumetric productivity). Pluripotent stem cells (PSCs) have been successfully cultured on plates and small scale spinner flask culture on a variety of micro-carrier materials (Fernandes et al., 2009, Phillips et al., 2008, Nie et al., 2009), with optimisation efforts made through control of process variables (Serra et al., 2010). In addition, Steiner et al. (2010) successfully derived and cultured hESC in suspension as aggregates without the use of microcarriers whilst maintaining their pluripotential ability. The use of such bioreactors to scale up cell culture is required to achieve the economies of scale neeed to facilitate the use of cell therapies in routine clinical practice (Mason and Dunnill, 2009).

2.1.2 Design and operation of the Quantum Cell Expansion System

The Quantum cell expansion system **Figure 2.1 a),** and **b)** is a functionally closed and temperature-controlled hollow fibre perfusion bioreactor with a touch screen interface to run either pre-loaded tasks - for example, cell seeding - or custom settings particular to the given cell culture. The bioreactor and its protocols were initially developed for the large-scale commercial culture of mesenchymal stem cells (MSCs), however its use to grow other cell types had been proposed. Two prototype machines were made available on loan from the manufacturer to assess the feasibility of growing hESC on the Quantum cell expansion system in a pilot study.

1 This work is an extended report of the original paper published by the author as: ROBERTS, I., BAILA, S., RICE, R. B., JANSSENS, M. E., NGUYEN, K., MOENS, N., RUBAN, L., HERNANDEZ, D., COFFEY, P. & MASON, C. 2012. Scale-up of human embryonic stem cell culture using a hollow fibre bioreactor. *Biotechnol Lett,* 34**,** 2307-15.

Many of the tasks, such as cell seeding, washes, and harvesting, are fully automated, requiring only that the operator sterile weld reagent bags to the system. This reduction of manual handling and its closed nature should not only reduce the risk of adventitious agents infecting the culture but will also significantly reduce the time demands of the operator in completing tasks such as media changes.

The 3D nature of hollow fibre and other bioreactor designs effectively remove the gas liquid interface required for gas transfer found in flask culture. Additionally, the high cell densities achievable in such 3D environments will likely lead to the rapid depletion of media components and build-up of wastes. To address these issues, the Quantum system is comprised of two semi-independent flow paths, known as the intra capillary (IC) and extra capillary (EC) loops, each of which has access to multiple inlet sources. A flow schematic of the Quantum system is outlined in **Figure 2.2**. The IC loop includes the inside of the hollow fibres, where the cells attach and grow in a low shear environment. The EC loop circulates media around the outside of the fibres and through the gas transfer module (GTM) for continual contact between the media and the pressurized gas supply (5%CO_2, 20% O_2, 75% N_2). Media can be perfused through either loop to facilitate mass transfer of media components and removal of waste, such as lactate. The porous nature of the fibres also acts essentially as a membrane restricting the loss of components larger than 15 kDa. This means expensive growth factors such as bFGF, can be concentrated on the inside of the fibres, whilst smaller molecules such as lactate can be diluted and removed by perfusion on the external loop. Sterile media samples can be taken from the system for off-line analysis as illustrated in **Figure 2.3**, however direct sampling of the cells is not possible. The entire flow path including the bioreactor and gas transfer module are all disposable as highlighted in **Figure 2.4.** Critically, the only environmental variable that is monitored and controlled online is the temperature inside the unit.

The bioreactor module itself is comprised of ~10,000 hollow fibres of diameter ~200 μm, yielding a total area available for growth of 2.1 m^2 (21,000 cm^2). An overview of the hollowfibres shows their physical packing into the bioreactor unit **Figure 2.5 a)** and **b),** and

their structure at the micro scale **Figure 2.5 c)** and attachment of mesenchymal stem cells **Figure 2.5 d)**. The total surface area of 2.1m^2 equates to approximately 840 T25 flasks.

2.1.3 Aims

The aim of this chapter was to explore the feasibility of growing hESC at large scale on commercially available machinery that was initially designed for the growth of MSCs. The specific objectives were:

- To develop a working hESC protocol based on experiences from hESC scoping runs and initial runs with other cell types.
- Determine the ability of the system to replicate the environmental conditions and cell expansion achieved in flask culture.
- Analyse whether maintenance of the target hESC phenotype can be achieved on the bioreactor.
- To generate data as a proof of concept study to inform the future work required to move this process to a defined, optimised, and validatable commercial process.

2.2 Materials and Methods

2.2.1 Cell culture in T25 Flasks

The Shef 3 hESC line was passaged using the TrypLE Express enzyme (Life Technologies) and co-cultured on mitomycin c inactivated mouse embryonic fibroblasts (MEFs). MEFs were originally grown in Dulbecco's Modified Eagle Medium (DMEM, Life Technologies) with 10% v/v heat inactivated fetal bovine serum (FBS, Sera Laboratories International) and 1% v/v 100X MEM non-essential amino acids (NEAA, Life Technologies). hESC were grown in Knockout DMEM, (Life Technologies)(+ 4.5 g D-glucose /L, + sodium pyruvate, – L-glutamine), 20% Knockout Serum Replacement (Life Technologies), GlutaMAX, (Life Technologies), 0.1 mM beta-mercaptoethanol, human basic fibroblast growth factor, 4 ng/ml (bFGF, R&D systems), and 1% 100X MEMNEAA (Life Technologies). Medium was exchanged daily at a ratio of 0.2 ml cm^{-2}. All cell counting and cell viability analysis was

performed on the Vi-Cell (Beckman Coulter), using the trypan blue exclusion viability assessment.

2.2.2 In vitro differentiation

Cell suspensions were allowed to aggregate to form embryoid bodies (EBs) in low attachment plates. These cells were cultured in the hESC media described above excluding bFGF for approximately 1 week before being pelleted, dried and frozen at -80^{o}C for PCR analysis. In addition, a portion of the EBs were transferred to tissue culture vessels coated with 0.1% gelatine and cultured until a monolayer of cells was seen emanating from the attached EB before fixing for immunocytochemistry.

2.2.3 Immunocytochemistry

Cells were fixed in a 1.33 M PFA solution and 0.25% v/v Triton X was used to permeabilise cells. Primary antibodies used were as follows: mouse IgM anti-TRA 1-60 (kind gift from Professor Peter Andrews, Sheffield University), mouse IgG anti-Oct3/4 (Santa Cruz), rabbit IgG anti-Sox 17 (Millipore), mouse IgG anti-brachyury (Millipore), and mouse IgG anti-nestin (Millipore). The following secondary antibodies were used at 1:200 dilutions, Alexa fluor 488 goat anti-mouse IgM, Alexa Fluor 488 goat anti-mouse IgG, Alexa fluor 488 goat anti-rabbit IgG (Life Technologies). Images were taken with an epifluorescence Nikon Eclipse 2000 inverted microscope and the NIS-elements software. Where applicable, isotype controls were run in parallel.

2.2.4 Karyology

Cell karyotyping was carried out by TDL Genetics (London, UK) using standard G banding. A minimum of 20 metaphase spreads were counted per sample.

2.2.5 Reverse transcriptase-polymerase chain reaction (PCR)

Following manufacturer's guidelines, RNA was extracted using the RNeasy mini-kit (Qiagen), and first-strand synthesised using the RetroscriptKit (Ambion). Bio-Taq polymerase (Bioline) was used for the PCR reaction in a Verity cycler (Applied Bio-systems). Primer sequences are outlined in **Table 2.1.**

2.2.6 Lactate dehydrogenase (LDH) assay

0.5% v/v Triton X was used to disrupt any cells remaining on the bioreactor's surfaces after the harvesting protocol. Roche Applied Science Cytotoxicity Detection Kit (LDH) was then used as per the manufacturer's instructions to compare the bioreactor sample against a standard curve of known cell concentrations obtained from the successfully harvested fraction.

2.2.7 Real-time PCR

Following first-strand synthesis with the method described above, quantitative PCR was carried out using the MESA BLUE qPCRMasterMix Plus for SYBR Assay (Eurogentec) in the in the CFX Connect Real-Time System (Bio-Rad). 20 µL reactions were run in triplicate using the following primers from Qiagen: b-ACTIN (QT00095431), UBC (QT00234430), POU5F (QT00210840), NANOG (QT01844808), and SOX2 (QT00237601). Analysis of relative quantification used b-ACTIN and UBC to normalise expression, and primer efficiencies were calculated using a cDNA dilution curve and analysed using Bio-Rad software.

2.2.8 Flow cytometry

The following antibodies were used: mouse anti-SSEA-4 PE conjugate (Millipore) and mouse anti-TRA 1-85 Alexa fluor 488 conjugate (Millipore). A 1% cut-off gate was implemented based on conjugated isotype controls. All samples were analysed using Beckman Coulter Epics XL MCL flow cytometer, and Summit software.

2.2.9 Quantum cell expansion system protocol

100 million MEFs were seeded onto the bioreactor that had been previously coated with 10mg fibronectin (BD bioscience), using automated protocols. Cells were allowed to attach for 48 hours, during which time there was no flow on the intra capillary (IC) loop containing the cells. However, media was perfused through the extra-capillary (EC) loop to refresh media components and remove the waste. Circulation around the EC loop also enabled gas transfer via access to the gas transfer module. After this MEF attachment step,

the MEF media was washed out and replaced with hESC media and 60 million hESC cells (~3000 cells/cm^2) were added to the reactor (Day 0) in the same manner as the MEFs. Cells for Run 1 were seeded at passage 93, and cells for Run 2 were seeded at passage 118. After an additional 52 hours of cell attachment, a low IC inlet rate was initiated to replenish factors such as bFGF, which were too big to be supplied across the fibres from the EC loop. IC circulation was also employed to encourage homogeneity of media components surrounding the cells. Sterile media samples were taken twice daily for measurement of glucose and lactate levels via the YSI 2700 media analyser. Comparisons of these concentrations were made with spent media from flask controls, and inlet rates were increased to the bioreactor in an effort to mimic the environment provided within these control flask cultures.

On day 8 (after 5 days of hESC expansion), cells were harvested by first flushing both the IC and EC loops with three times the total reactor volume of DPBS, followed by an additional two volumes of 0.1 mM (1,085 mL) EDTA (Sigma) and a 15 minute incubation period. A volume of 200 ml of 0.25% trypsin was then added to the IC loop and circulated for 45 minutes. Finally, the cell suspension was flushed into the harvest bag using 20% serum media to quench the trypsin. Cell counts and viability analysis were performed on the cells using the ViCell cell counter (Beckman Coulter).

2.3 Results and discussion

2.3.1 Developing a working pluripotent stem cell protocol based on experiences from 7 trial runs using multiple cell types.

In order to adapt the manufacturers recommended protocols for the culture of MSCs to the working hESC-MEF co-culture protocol described, it was necessary to conduct initial experiments with MSCs, hESC and the ARPE-19 cell line (ATCC). In all 7 runs were conducted at full scale prior to the 2 PSC runs reported here. The ARPE-19 line was chosen to generate additional experience with the machine before moving onto PSC culture due to limited availability of isolated MSCs for use in this project. In addition, it has been previously suggested the ARPE-19 cell line might be of clinical use, as it has reportedly

rescued visual function in the dystrophic royal college of surgeons (RCS) rats (McGill et al., 2004)

In an attempt to reduce costs alternatives to the expensive fibronectin (10mg) coating stage recommended by the manufacturer were investigated under their guidance. Pre-coating the fibres with 10% foetal bovine serum prior to seeding with MSCs resulted in a loss of nearly all the cells seeded after a 5 day expansion protocol. Coating the fibres with 0.1% gelatine proved successful with the ARPE-19 cell line, with 30m cells expanding to 344m cells (93% viability) during a 9 day protocol in the bioreactor. However, when gelatine was used to coat fibres in a MEF-hESC co-culture system there was a net loss of cells. An additional trial run was then conducted using the MEF-hESC co-culture system using 10 mg fibronectin as the coating material, which showed a modest net expansion in cells (21m cells), and maintenance of the hESC phenotype (data not shown). Thus it was concluded that fibronectin was a necessity even in a co-culture environment, but from a cost effectiveness perspective further work is called for to identify an optimum amount of fibronectin material needed, or if other coating materials such as matrigel are computable with the system, which would be required for feeder free culture.

This trial hESC protocol using fibronectin was then further refined to generate the protocol described in this thesis and used to generate the data presented here. The main areas of modification to the manufacturer's existing MSC protocols using data from the 7 trial runs were the following: 1) increasing the volume of the wash used during harvest; 2) the addition of an EDTA incubation stage (to aid cell release); 3) loading of the cells in a more dilute suspension; and 4) to reduce the number of mouse feeder cells used by half. These last two alterations were made in the assumption that cell aggregation during seeding was impacting the ability for the cells to expand, based on observations of large cell masses/clumps during harvest for the first hESC-MEF co-culture run on fibronectin which yielded a net cell expansion of only 21m cells.

2.3.2 Suitability of using a karyotypically abnormal cell line as a model cell line for large-scale experimentation

Prior to the discussion of results from the final two runs using the refined protocol, it is important to discuss the cell line used in this chapter. In particular, these proof of concept studies use a Shef3 hESC line that has been adapted to enzymatic passaging and has been shown to be resilient to low seeding densities. From a practical perspective, both of these characteristics are valuable for large-scale production in a bioreactor. Manual passaging of PSC colonies is not realistic for large surfaces and is impossible in a hollow fibre bioreactor. With respect to seeding density, typical hESC cell lines require seeding densities of ~20,000 cells/cm^2 to establish healthy cultures, whereas the adapted Shef3 hESC line can produce confluent cultures from a low seeding density of ~3,000 cells/cm^2. Therefore, in the context of the limited resources of an academic setting, it becomes possible to produce the number of cells needed to inoculate this large-scale reactor which is only available at a single scale.

Given the advantages of this adapted Shef3 hESC line, it is important to note the karyotypic abnormalities, namely 48,X,+i(12)(p10),+14,+i(17(q10)) (additions to chromosomes 12 and 17), do not make the line unsuitable for use in a study such as this. Such abnormalities are a common occurrence in later passage hESC lines, particularly when enzymatic passaging methods are used (Amps et al., 2011), however these abnormalities have not impacted this line's characteristic hESC pluripotent phenotype and differentiation potential. The pluripotent phenotype was not only present in the stock cell line but it was also retained after expansion on the system as evidenced in **Figure 2.6 a)** and **b)** which show that cells harvested from the Quantum Cell Expansion System still express the pluripotency markers TRA 1-60 and Oct-3/4 after replating. Additionally, once taken through an embryoid body differentiation protocol, the cells expressed markers representative of the three germ layers **Figure 2.6 c), d), e)** and **f)**. Such findings are corroborated by Sun et al. (2008) who previously compared the properties of normal and abnormal hESC lines, concluding that given the similarity in their biological properties abnormal cell lines were useful experimental materials for cell therapy, developmental biology and genetic research.

Crucial practical advantages and phenotypic data validates the use of this adapted line for the purpose of generating important proof of concept data and valuable experience with the large-scale bioreactor. Therefore, a working protocol can be developed before moving to a clinical grade line and a human feeder or feeder-free culture system, examples of which were evaluated by Hernandez et al. (2011). Such systems where considered for this study but the cost implications of using these expensive systems at scale and considerations as to how matrix coatings such as Matrigel (BD bioscience) might impact the porosity of the hollowfibres led to the conclusion to first generate this working protocol using the cheaper MEF-hESC co-culture system.

2.3.3 Perfusion rate rationale

Given the differences in operation between continual perfusion of media into the bioreactor versus daily media changes in a normal flask culture, there are two possible approaches to take regarding the supply of media. The first would be to apply media at a flow rate to the system that exactly matches that used in flasks i.e. 0.2 ml cm^{-2} day^{-1}, which equates to ~4.2 L day^{-1} on the Quantum system. However, based on the earlier preliminary experiments using adult stem cells (described in **2.3.1**), it was believed that such an approach could be an unnecessary waste of media, thus not making best use of the system design. In flask culture, additional media has to be supplied in order to ensure that the base of the flask is covered with media even when cell densities are comparably low, for instance after cell seeding. With a total bioreactor volume of 413 ml, it was thought that the provision of 4.2 L day^{-1} to the bioreactor from the beginning of the run would be an unnecessary waste of resources. It was also considered that this might actually remove key cell-cell signalling components from the system, thus hindering cell growth. Therefore, an alternative approach was deployed: inlet rates were adjusted with the intention of approximating glucose and lactate levels observed in the T25 control flasks. Glucose being used as a proxy measure of other components in the media such as knock out serum replacement (KOSR) which fuel cell growth. In this manner, the usage of expensive media would be minimised, while presumably providing an environment for the cells that was similar to that experienced by the cells in the control flasks. Such a 'reactive' approach i.e. altering the

feeds based on readings as opposed to predicting the cell requirements was recommended by the machines supplier Terumo/BCT based on their success culturing MSCs.

2.3.4 Ability of the Quantum Expansion System to replicate the environmental conditions and cell expansion achieved in flask culture

In Run 1, an initial inlet rate of 0.2 ml/min was used on the extra capillary (EC) loop, with a zero inlet rate on the intracapillary (IC) loop to allow the cells to attach. See **Figure 2.2** for flow schematic of the loops and **Figure 2.7 a)** for the media perfusion rates used and observed glucose and lactate levels for Run 1. At hour 28 of this cell attachment protocol, similar depletion in glucose was seen in both the flask and the Quantum system, with a difference of 0.30 g glucose /L between them (**Figure 2.7 a**). However, by hour 52 of the protocol the difference in glucose levels between the flasks and the Quantum system, had over doubled to 0.77 g glucose/L. Glucose levels remained outside that seen in flasks for the rest of the run, despite incrementally increasing the inlet rate into the IC loop.

Over the 5 day hESC expansion in Run 1, 0.15 ml media cm^{-2} was perfused through the Quantum cell expansion system in total, compared to 1 ml media cm^{-2} supplied to the flasks through daily media changes. **Figure 2.7 e)** shows the accompanying media volumes used during Run 1 each hour per cm^2. It is hypothesised that this undersupply of media resulted in the lower glucose levels seen in the Quantum system, and so the likely explanation for the relatively poor cell yield of the Quantum system compared to the flask culture: 1.8E+4 cells cm^{-2} for the Quantum system and 1.9E+5 cells cm^{-2} or flasks. See **Table 2.2** for a summary of the expansion achieved in Run 1.

A second run (Run 2) sought to feed the cells in a more proactive manner from the start of the run. The initial inlet rate was doubled relative to that in Run 1, namely 0.4 ml/min. Additionally, inlet rates were increased at higher increments throughout the run, **(Figure 2.7 b)** and **e)**, in an effort to maintain higher glucose levels. Total media provision during the 5 day expansion was therefore increased from 0.15 ml cm^{-2} in Run 1 to 0.32 ml cm^{-2} in Run 2. As a result, the expansion in the bioreactor was markedly improved in Run 2,

achieving 708 m cells (3.4E+4 cells cm^{-2}) from 60 m seeded hESC, as compared to the 383 m cells (1.8E+4 cells cm^{-2}) achieved in Run 1 (**Table 2.2**).

The performance of the Quantum system was, however, still not the equivalent to that of the flask culture, which yielded 1.9E+5 cells cm^{-2} (**Table 2.2**). Lactate levels throughout Run 2 may help provide an explanation for the lower yields per surface area. **Figure 2.7 b)** illustrates the disparity between flask and Quantum system concentrations of glucose and lactate for Run 2. It can be seen that glucose and lactate levels differed significantly between the flask and the Quantum system for much of the expansion. Though higher inlet rates relative to Run 1 were used, a rapid rise in lactate levels was also observed over the first 52 hours, perhaps indicating comparatively increased cell expansion. Although levels of lactate and glucose were brought to within levels observed in flask culture by the end of the run by increasing the inlet rates, the long period of exposure to high lactate levels may have inhibited growth. The detrimental impact of high lactate levels on hESC growth has been described by Chen et al. (2010) who reported that supplementing hESC cultures with 1–5 g lactate/L for 3 days resulted in 15%–50% reduction in cell growth. Thus a combination of high lactate levels and low glucose levels recorded in Run 2 is the likely cause of expansion on the Quantum System not matching the flask controls.

Readings for pH were also taken 'off-line' on the sampled media (**Figure 2.7 c** and **d**) and follows a inverse correlation to that of lactate (**Figure 2.7 a** and **b**), the pH remaining lower than the flask controls for the majority of the runs. Unfortunately with no online measurement of CO_2 or ability to control the gas mix, to reduce the supplied CO_2 below 5%, it is not possible to have the required control over pH which might be critical to obtain and maintain higher cell densities.

The manufacturer reported that such a decrease in pH had not been seen with the other cell lines previously tested on the machine and that this was part of the reason that no online measurement is available. It is critical in any bioreactor that the gas transfer rate (GTR) achievable is not less than the oxygen uptake rate (OUR) that the cells have become adapted to in flask culture. A failure to achieve a GTR equal or greater to the OUR would force the

cells to respire anaerobically likely impacting both growth and phenotype given these are pluripotent cells that have not been adapted to hypoxia. The component parts of the GTR are described in Equation 1 below- where C* represents the solubility of oxygen in the medium, C_L is the oxygen concentration in the medium; thus (C^*-C_L) is known as the concentration-difference driving force of the mass transfer. Due to the low solubility of oxygen, it being only a value of about 10ppm under ambient temperature and pressure, makes it vital that the contribution of K_La in the equation is as large as possible to overcome this limitation to increase the OTR. K_La represents the volumetric mass transfer coefficient for oxygen transfer and describes the ability for a bioreactor and its operation to deliver oxygen into the liquid medium. K_La is split into two parts, K_L (ms^{-1}) is the liquid-phase mass-transfer coefficient and "a" (m^2m^{-3}) is the gas-liquid interfacial area per unit volume of fluid. Considering the design of the hollowfibre perfusion bioreactor there are 3 possible courses of action to maximise OTR: 1) increase the surface area available for gas and mass transfer, by increasing the number, or length of the fibres in the gas transfer module and bioreactor; 2) increase the O_2 concentration in the supplied gas mix above 20%; 3) increase the circulation rate of the media to the gas transfer module. As it was not possible to impact either 1) or 2) due to the fixed design of the bioreactor, a high circulatory flow rate of 200 ml/min was used on the extracapillary side of the bioreactor to maximise the OTR (the standard protocol used 30mL/min). With 200 ml/min being the maximum value recommended by the manufacturer for the system with assurances made that the residence times in the gas transfer module and the bioreactor itself were such that equilibration between the gas and liquid phases (in the gas transfer module) and the two loops (in the bioreactor) could take place.

However with no online O_2 measurement it was not possible to ascertain whether the GTR rate became growth limiting, particularly at the higher cell densities later in the runs. In addition ,values of K_La for the bioreactor were not available from the manufacture which would have made useful comparisons with other bioreactor designs. The addition of a retrofitted O_2 probe to the bioreactor for tracking dissolved oxygen during culture and determination of K_La was discussed with the manufacturer, however difficulties regarding

the maintenance of sterility and time pressures rendered this avenue of investigation impractical.

Equation 1:

$$OTR = K_L A(C^* - C_L)$$

2.3.5 Maintenance of the target PSC phenotype on the Quantum Cell Expansion system

In both Runs, there was a net expansion of hESC and atrophy of nearly all MEFs by the time of harvest, as evidenced by high expression of the human specific marker TRA 1-85. **Table 2.3** displays a summary of marker expression in the seeded and harvested cells showing similarities in TRA 1-85 between these populations. The harvested cells also maintained high levels of pluripotency marker expression, with 96.2% and 97.7% of cells expressing SSEA-4 in Runs 1 and 2, respectively, compared to 99.9% in flask controls (**Table 2.3**). PCR analysis of pluripotency markers appear to show decreased *Nanog* expression in both runs; however, both *Pou5f* and *Sox2* normalised fold expression were comparable to the range seen in the triplicate flask controls of the same seeding density (**Figure 2.8**). It is believed that this data demonstrates not only that the Quantum system can maintain cells in a pluripotent state but also that minimum optimisation of the protocol could maintain a healthier cell population, thus proving equivalence to traditional flask culture in maintaining the target phenotype.

2.3.6 Cell attachment and release from the hollowfibres

All waste bags containing the perfused media from the runs had their contents spun down to check for cells/cell debris. However, no discernible cell pellet was produced, suggesting a high seeding efficiency and cell strong attachment to the fibres throughout the runs and wash stages at the flow rates used. Viability was slightly reduced in the runs, but still greater than 93% (**Table 2.2**). This is a likely result of the harsh conditions used to harvest the cells from the hollow fibres, 0.25% Trypsin for 45 minutes on the reactor, compared to TrypLE enzyme for 10 minutes in the T25 Flasks. The suboptimal media provision may also

have impacted cell viability and their susceptibility to the harvest protocol used. Some cells did remain attached to the reactor after harvest, as evidenced by lactate dehydrogenase assay (**Table 2.2**). The remaining cells could have been released using different dissociating agents such as higher percentage concentration trypsin, collagenase or accutase mixtures with a higher concentration of EDTA. Wash volumes and incubation times could also be optimised. Such optimisation has been done with success by the manufacture using other cell types on the machine such as mesenchymal stem cells (source: communication with manufacturer).

2.4 Conclusions

2.4.1 Areas for optimisation

The data presented in this chapter from this initial proof of concept study using the Quantum Cell Expansion System demonstrates that hESC cultures can be scaled up significantly through use of a hollow fibre bioreactor whilst maintaining their pluripotent phenotype and differentiation potential. Yet is clear that in order to maximise hESC expansion on the system to achieve the cell densities obtained in flasks, 1.9E+5 cells cm^{-2} (~4 billion cells in the Quantum system), several aspects of the current protocol would need to be optimised and aspects of the machine developed.

Optimisation of media perfusion rates is likely to be the key to realising the potential cell yields. Although the Initial cell attachment to the fibres did not appear to be impacted by the resultant shear at the flow rates used; further work is required to determine what the optimum perfusion and circulation rates are to provide an environment for the cells which enables optimum growth. For instance from the results presented here it would be assumed higher flow rates would be needed to maintain an environment akin to flask culture; thus it would need to be determined whether there is a trade-off due to shear or dilution effects at higher perfusion and circulation rates. For example, Titmarsh et al. (2011) investigated hESC growth in a perfusion microbioreactor and identified significant correlation between flow rate and growth. Optimisation of media use could also improve the process economics by concentrating larger (>15kDa) expensive media components on the loop surrounding

the cells, such as bFGF, and not supplying media in unnecessary excess. Optimisation efforts could be made through further iterative experiments using the approach outlined here. Alternatively, a more effective approach would be to link the Quantum system to an online media monitoring and control system such as those offered by YSI Life Sciences (Ohio, USA) with minimal modifications. This would provide far better 'real time' control over the system then the empirical operator-driven method used here. For example Chen et al. (2010) concluded that reducing the concentration of glucose in the later stages of high cell density hESC cultures with online control of pH could reduce the high lactate levels and low pH which detrimentally impact cell growth and pluripotency. Other variables such as seeding densities would need to be optimised, as explored by Hewitt et al. (2011) who found the seeding density of mesenchymal stem cells onto microcarriers had a critical impact on expansion

2.4.2 Monitoring of more variables noninvasively

In addition, given that it is not possible to sample the cells directly during culture, if long differentiation experiments were to be conducted on the machine it would be of interest to explore a wider number of components in the media sample to track the process. For instance, factors such as of α-fetoprotein (AFP), β-human chorionic gonadotropin (ß-hCG) and activin A, were tracked in the paper by Stachelscheid et al. (2012) where hESC were differentiated in bioreactors. Additionally the work by Csaszar et al. (2013) sort to control the concentration of TGF-β1 in a bioreactor culture of umbilical cord cells though use of quantum dot microbeads and a fed batch system.

2.4.3 More information is needed on Quantum Cell Expansion System's fluid flow characteristics

Regrettably, there is a remaining concern that the environment within the Quantum Cell Expansion System's bioreactor is not homogenous and so creates microenvironments which could be impacting cell growth and phenotype. The manufacturer was unable to provide either experimental data or computational fluid dynamic data to validate that the gas and mass transfer was uniform between the two loops in both axial and longitudinal

directions in the bioreactor to back up their claims of homogeneity. Conversely given the manufacturers protocols call on ~3 full bioreactor volumes of wash to both loops when changing from one media to another the likelihood of the bioreactor being truly homogeneous is assumed to be low. Furthermore, as the gas and mass transfer of the system is reliant on unimpeded flow along the intracapillary side of the fibres where the cells attach and grow it would also be desirable to have more information on how cell expansion impedes this flow. For example, when harvested the cells often appear to be released as large 'clumps' of cells and given the width of the hollowfibres is only 200 μm it could be very possible that fibres are 'fouled' with cells as a function of cell growth. Efforts were made to stain fibres to identify whether cell growth was homogeneous across the bioreactor, yet due to autofluorescence of the fibres this was not possible. Although scanning electron microscopy had been shown by the manufacturer as a successful method to image cells due to practical and time limitations this approach was not attempted and it was believed it would not answer the question of whether flow was impeded. What would be of use is a way to measure the pressure drop across individual fibres or sections of the bioreactor online to determine if fouling was taking place, but requires significant re-design of the machine. Pressure readings were available for the whole bioreactor unit; but these fluctuated widely and so were not of use for the purpose of determining cell build-up on the fibres.

2.5 Summary

Based on this feasibility study using this novel large-scale bioreactor to grow hESC two general issues of paramount importance can be identified for a successful transition from standard flask culture to successful scale-up in bioreactors.

2.5.1 The need for small scale bioreactor mimics, and flexibility of reactor sizes

The number of experiments required to generate a truly optimised protocol is simply not feasible as the scale used here. The generation of the cell numbers needed to seed such a large-scale reactor, and the media required to maintain their culture on the reactor would

not be resource or time efficient. Small-scale mimics and micro scale mimics are widely used in biopharmaceutical process development and design. They enable a number of experiments to be carried out in parallel producing results which can predict large scale performance. Ideally the mimic would exhibit the same shear and gas and mass transfer properties as the large scale, with the attachment surface having the same physicochemical properties. For example to take the work forward towards clinical trials manufacture it would be important to determine the seeding efficiency of the cells under a xeno free/feeder free alternatives for hESC culture such as CELLstart (Life Technologies). Furthermore, due to the correlation between seeding densities and cell proliferation a bioreactor technology needs to be available at a number of scales and so a 'seed train' can be used to expand the cells up to the required production scale whilst making best use of the reduction in manual handling and additional process control bioreactors provide. The Quantum Expansion System being only available in one size is extremely limited in this respect.

2.5.2 The need for online monitoring and control

Due to the aforementioned lack of the gas liquid interface in bioreactors that is present in flask culture, bioreactors require alternate methods of aeration necessitating mixing. Furthermore, in perfusion, or fed systems, mixing is also required to facilitate mass transfer. Thus it is critical that the important environmental processing variables such as pH, CO_2 and O_2 are both monitored and controlled to optimise expansion and maintenance of the target phenotype. The ability to link such online data to the phenotype required for the target product profile and, therby clinical outcome will be key in the validation of such processes.

Investigations exploring the importance of these issues, in particular the need for online control of the process environment, will be addressed in the next chapter using an alternate bioreactor design.

a)

b)

Figure 2.1: Overview of the Quantum Cell Expansion System. a) Closed unit displaying the touch screen interface, b) open unit showing a loaded disposable bioreactor kit.

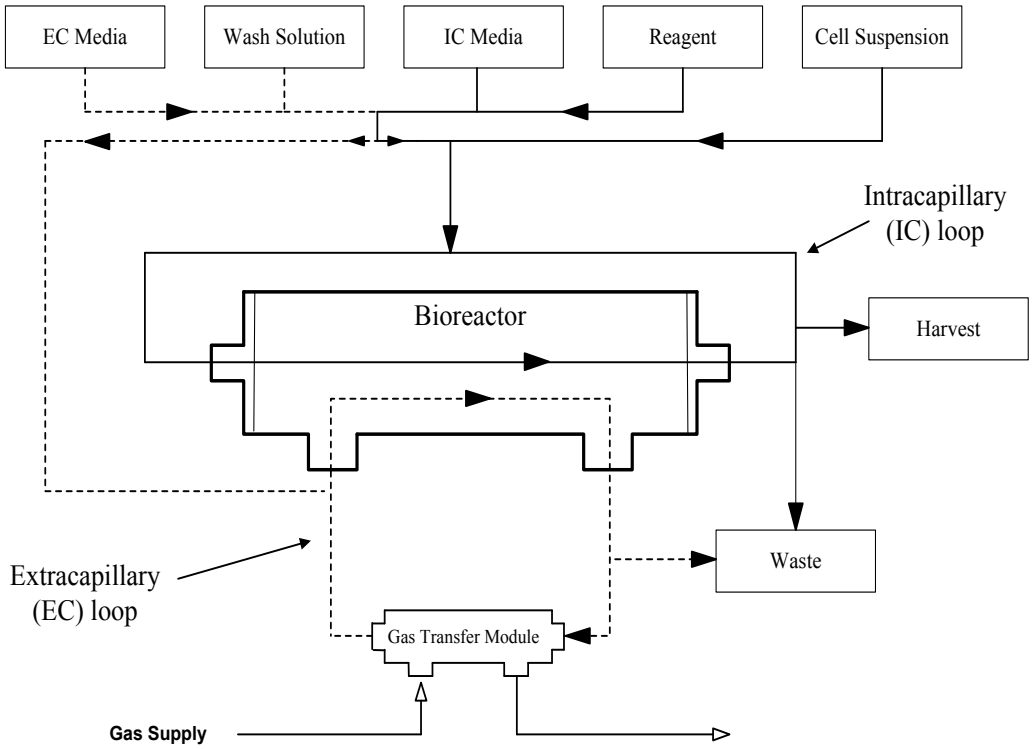

Figure 2.2: Simplified Quantum Cell Expansion System flow diagram. The Intracapillary (IC) loop flows on the inside of the hollowfibres where the adherent cells are attached. Fresh media is added to this loop from the IC media bag. Both the IC circulation rate and IC media addition rate can be set separately. The extracapillary (EC) circulates on the outside of the hollowfibres and so is not in direct contact with the cells. This loop includes the gas transfer modules which is itself another hollowfibre unit containing pressurised gas on one side and the growth media on the other. The circulation rate of the EC loop is set higher than the IC loop and can also be set independently of the EC media inlet.

Figure 2.3: Taking sterile media samples from the bioreactor. Samples are drawn from the IC loop through a 0.22µm filter into a Luer Lock syringe.

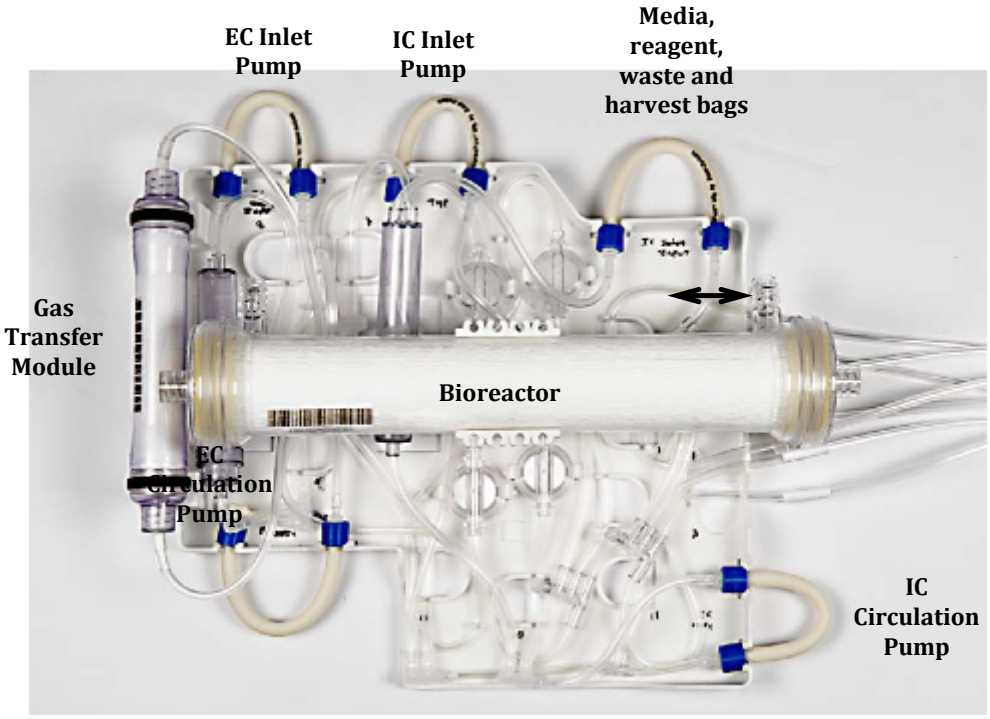

Figure 2.4: Disposable flow paths of the Quantum Expansion System. The entire flowpath of the system is disposable and is supplied pre-sterilised. The kit sits on a plastic plate which slots onto the reactor requiring the operator to secure the system with inbuilt clips and to run the tubes round the pump heads. Missing from the image are the pre-attached media and waste bags.

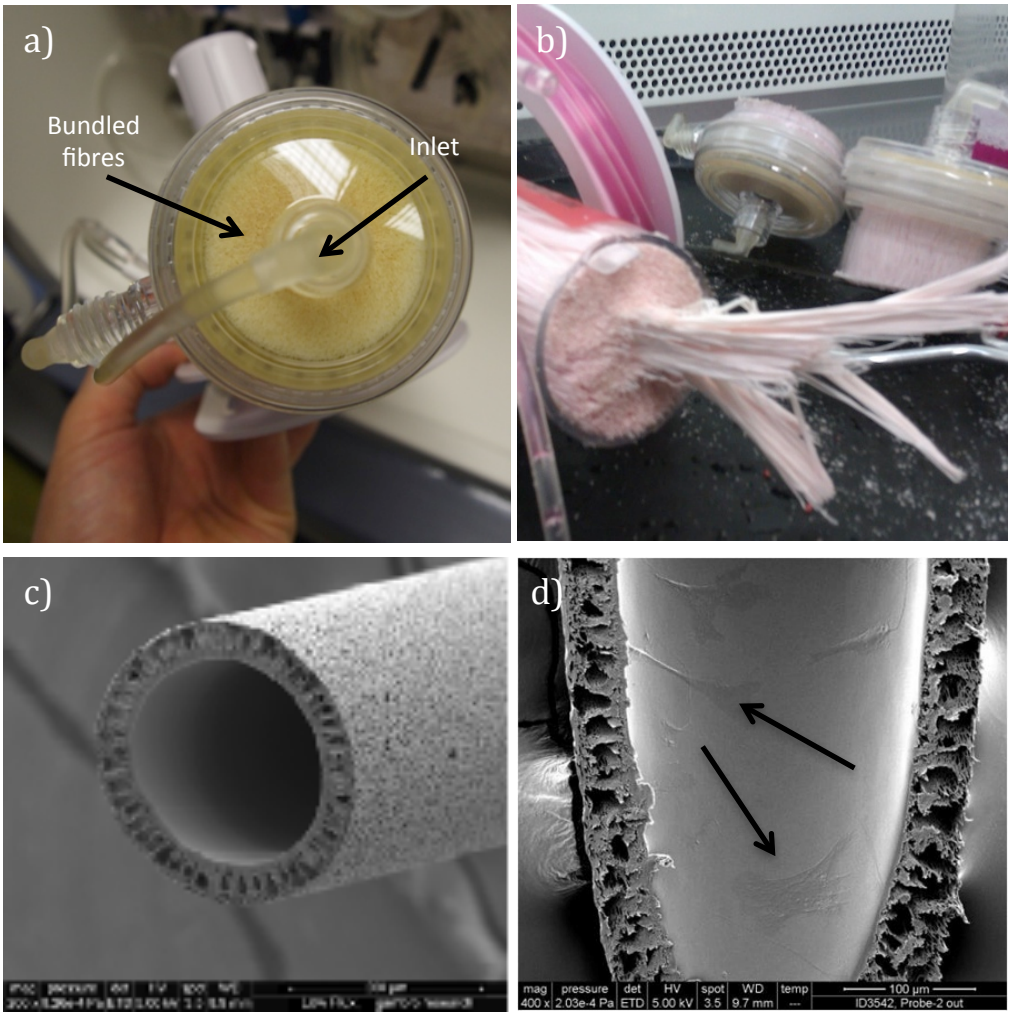

Figure 2.5: Overview of the hollowfibres in the Quantum Cell Expansion System. Approximately 10,000 hollowfibres make up the bioreactor. a) The intracapillary flow is distributed axially across the bundled fibres from a single inlet as is shown in this end view of the reactor unit. b) The fibres are tightly packed into the bioreactor capsule with little interstic space. c) Scanning electron microscope (SEM) images courtesy of (Terumo BCT) show the porous nature of the fibre wall d) and mesenchymal stem cells attached to the intracapillary surface.

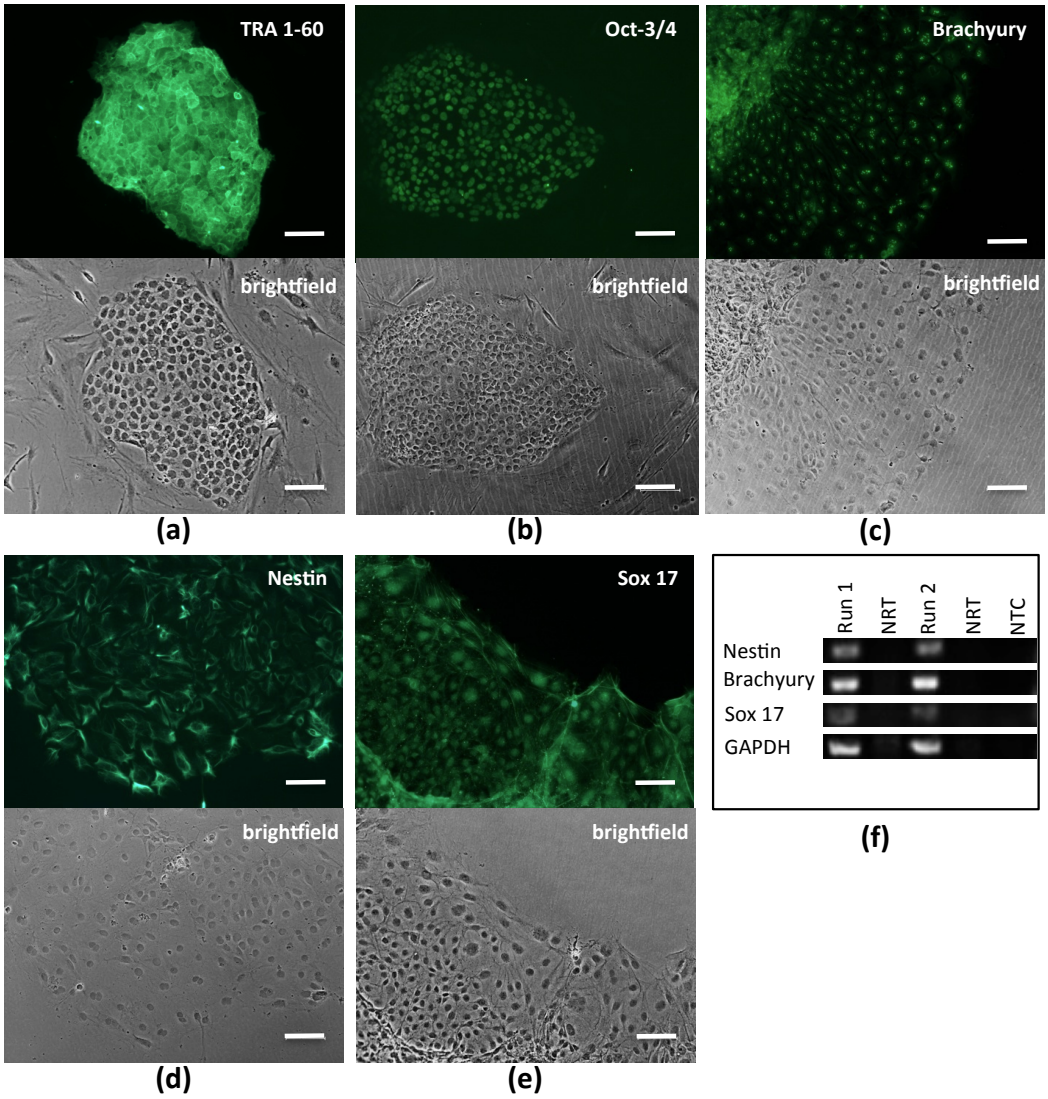

Figure 2.6: Maintenance of the pluripotent phenotype after expansion on the Quantum Cell Expansion System. Sample images demonstrating that expansion did not impact expression of the pluripotency markers TRA 1-60 and Oct-3/4 when the harvested cells were re-plated a) and b). In addition, replated embryoid bodies from the harvested cells expressed markers representative of the three germ layers (c) Brachyury (mesoderm), (d) Nestin (ectoderm), (e) SOX 17 (endoderm), illustrating that the differentiation potential of the hESC was not lost. (Scale bar = 100μm). Expression of these germ layer genes was also confirmed using PCR on the embryoid bodies at day 7 (f). The no reverse transcription (NRT) lane lacked reverse transcriptase during cDNA synthesis. PCR products were absent from the no template control (NTC) lane. Housekeeping gene is GAPDH.

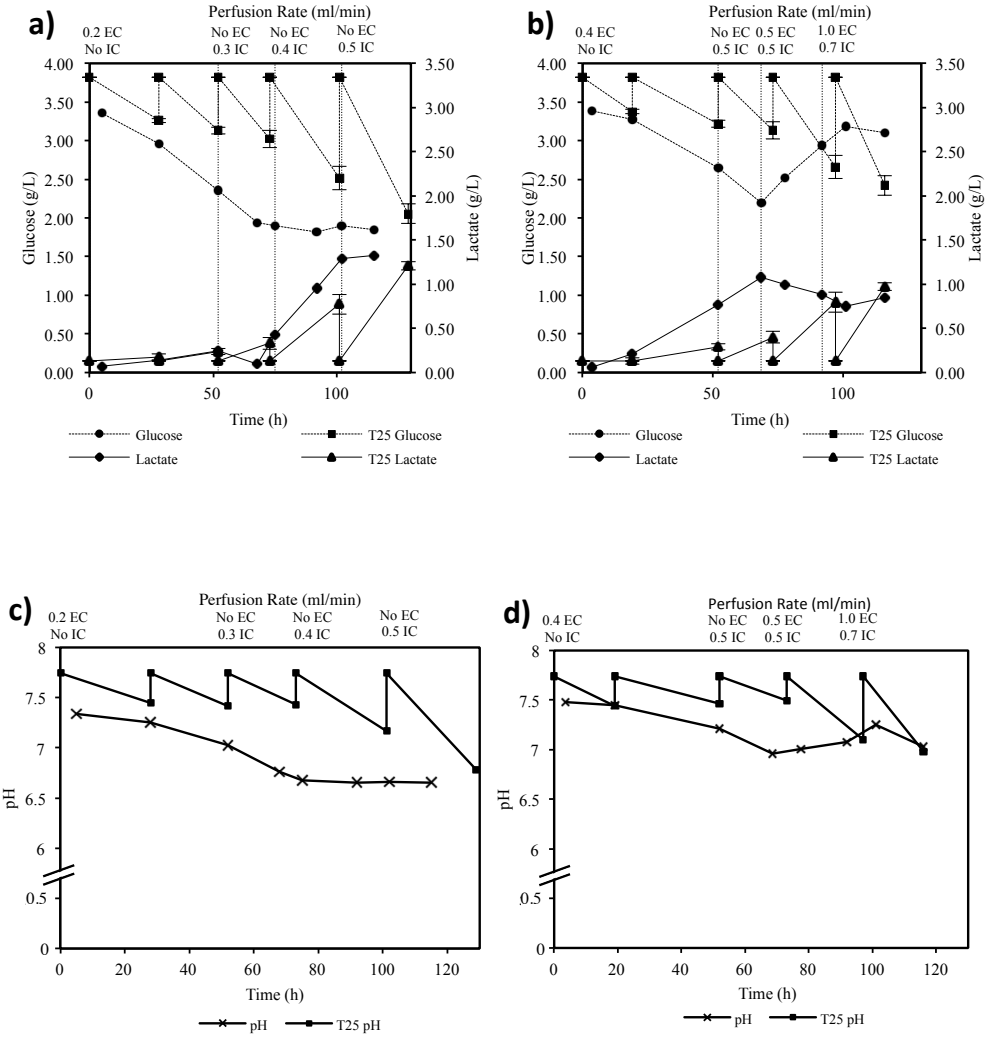

Figure 2.7: Ability of the Quantum Expansion System to replicate the environmental conditions found in flask culture. Changes in glucose and lactate with time for Run 1 (a) and Run 2 (b). Error bars represent 1 standard deviation (SD). Changes in pH with time for Run 1 (c) and Run 2 (d). T25 flasks were seeded alongside the bioreactor at an equivalent seeding density of 3000 cells cm^{-2}. The amount of media used per hour, per cm^2, is shown in e). Note for the T25 all media is removed from the flask every day and replaced thus the line represents an average for comparison with media perfusion in the bioreactors. Where there is both IC and EC inlet used at the same time the actual inputs were automatically switched every 5 minutes and run at twice the inlet rate to provide the averages quoted for each loop.

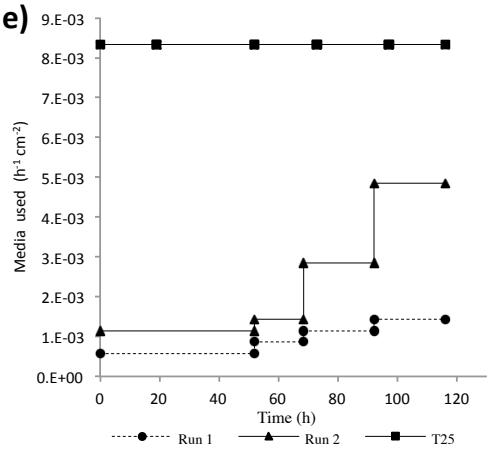

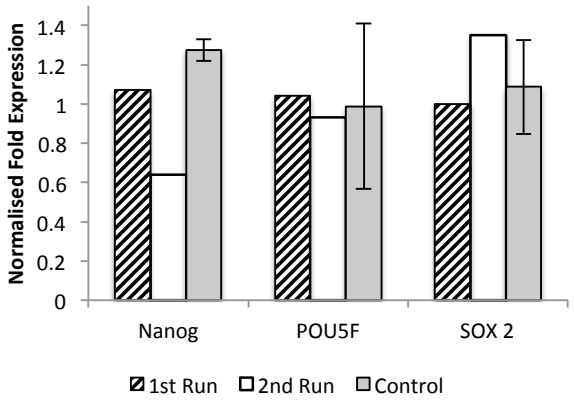

Figure 2.8: Gene expression of the pluripotency markers nanog, POU5F and SOX 2 when harvested at day 5. Comparison against triplicate T25 flask controls seeded at the same density (3000 cells cm^{-2}) and harvested at day 5. Error bars represent standard deviation of triplicate flasks.

Table 2.1: **PCR Primer sequences reproduced from (Hernandez et al. 2011)**

Gene	Amplicon Size	Forward	Backwards
GAPDH	277	CGA CCA CTT TGT CAA GCT CA	AGG GGT CTA CAT GGC AAC TG
Nestin	156	TGC GGG CTA CTG AAA AGT TC	AGG AGG GTC CTG TAC GTG G
Brachyury	279	GTC CAC CTG CAA ATC CTC AT	GGGTACTGACTG GAGCTGGT
Sox17	472	AAG ATG CTG GGC AAG TCG T	AGA CCT GCG CGT AGC TGT AG

Table 2.2: **Expansion performance of the Quantum Cell Expansion System**. Cells were cultured in a combination of T25 and T75 flasks for 3 days prior to seeding into triplicate control flasks or the Quantum Cell Expansion System. Errors are represented as 1 standard deviation.

	Run 1	Run 2	T25
Number of cells harvested	270 m	540 m	4.7 m ±0.13
Viability	94.0%	93.0%	99.3%±0.4
Cells remaining on the reactor	113 m	168 m	
Total cells grown	383 m	708 m	
Cell density achieved (cells cm^{-2})	1.8E+4	3.4E+4	1.9E+5
Media used over 5 days (ml cm^{-2})	0.15	0.32	1.00

Table 2.3: **Percentage of cells expressing the pluripotency marker SSEA-4 and the human specific marker TRA 1-85 when harvested at day 5**. Cells were also seeded at the same density of 3000 cells cm^{-2} into triplicate T25 flasks and harvested after 5 days, errors represented as 1 standard deviation.

	Run 1		Run 2		T25
	Seeded	Harvest	Seeded	Harvest	Harvest
SSEA-4	97.5%	96.2%	99.7%	97.7%	99.9%±0.06
TRA 1-85	98.1%	97.4%		97.7%	

3. Control of the pluripotent stem cell environment using the Xpansion One System

3.1 Introduction and aims

3.1.1 The Integrity Xpansion Multiplate bioreactor

The Xpansion bioreactor system (**Figure 3.1 a and b**) is designed by ATMI to scale-up adherent culture into large-scale bioreactors with minimal process development. As illustrated in the previous chapter there are a large number of complex issues that need to be addressed when moving from a well-understood protocol in flasks to a novel system such as hollowfibres or suspension culture. For example, if cells cannot be directly sampled or imaged (an important tool to visualise differentiation), different analytical methods to track cell growth and phenotype will be needed, such as tracking cell metabolites or cytokines in the media. Also a great concern of regulatory bodies is the ability to prove that cells grown in these 3D, shear inducing, dynamic environments, are clinically equivalent to those produced in flask culture. There might be the requirement to repeat clinical work if the culture system is changed to accommodate larger scale, later stage, clinical trials. Thereby making the decision point of when to change production systems and the associated development time/costs required critical. It was this requirement to facilitate a move to large-scale cell culture whilst making as little change as possible to the existing flask based paradigm that defined ATMI's[1] development of the Integrity Xpansion system after requests by customers.

The approach of the Xpansion system to scale-up cell culture involves increasing the volumetric productivity of 2D adherent culture by removing the large dead spaces of air above the media and then stacking a large numbers of alternating liquid and plastic layers in a single unit see **Figure 3.2**. This reduces the gaps between each plastic culture layer to

[1] The work with the Xpansion system was conducted with Artelis, who were then bought by ATMI during the project who subsequently sold the technology to the Pall Corporation.

1.6mm, vastly increasing the volumetric productivity compared to other multilayer systems. For instance the potential volumetric productivity of a 40 layer CellSTACK (Corning) is 0.56 cm^2 available for adherent growth per cm^3 of vessel volume, whereas the Xpansion system increases volumetric productivity over 10 fold to 5.59 cm^2/cm^3 by removing the stagnant gas layer. This approach makes it still possible to grow the cells using the same adherent based protocols developed in flasks whilst gaining productivity advantages of bioreactor culture. Furthermore, visualisation of the cells is achievable through use of a holographic microscope (also supplied by ATMI). But, the trade-off in such a simplistic layered approach to minimise process development for scale up is that the theoretical volumetric productivity of the bioreactor is reduced when compared to suspension systems. For example using typical flask harvest densities as a guide the Xpansion system could only yield 0.56m cells/cm^3 whereas Kehoe et al. (2010) reported yields of 3.4m PSCs per ml for cells grown in suspension.

Without a gas layer above the media, the gas exchange to the media is driven via a system located within the central column of the reactor (**Figure 3.3 a**). Gas mix is circulated through a coil of gas permeable silicon tubing in this central column where it equilibrates with the media. When values of pH or O_2 drop below set points the mixing system is initiated which forces liquid through the gaps between each layer of plates **(Figure 3.3 b**) to circulate around the reactor. The aim of this discontinuous system is to cause a minimal amount of shear stress to the cells.

The sizing of each of the Xpansion plates is equivalent to a single layer in a CellSTACK (Corning); so the Xpansion MPB-10 which contains 10-layers has approximately the same growth surface area as a 10 layer CellSTACK. The various scales the Xpansion system is currently available in are outlined in **Table 3.1**. The reactors are designed to sit inside a temperature-controlled incubator.

3.1.2 Description of Xpansion One

As discussed in the previous chapter experimentation at large-scale to develop an optimised protocol is prohibitively expensive and wastes resources, thus ATMI have

designed a small-scale mimic of their system named the Xpansion One **(Figure 3.4)**. The Xpansion One has a growth area of 128cm^2 and mimics the fluid dynamics and gas exchange control system exhibited on the far larger 0.6m^2, 3.m^2 and 11.m^2 Integrity Xpansion bioreactors. The resin sealed polystyrene Xpansion plate (XP) includes optical sensors for pH and DO measurements and sits on a docking station (**Figure 3.4 a**). Gas transfer is driven by a pump that circulates the media through a gas permeable silicon tube to equilibrate with the gasses in the incubator (**Figure 3.4b**) – in essence this is the same method employed at the large scale, the difference being there that the media is circulated around the outside of the tubing. Thus, the Xpansion one exhibits the same physicochemical properties as the large scale system as well as the same linear velocities and discontinuous mixing system to control environmental variables. The drawback of the simplified method employed in this small-scale mimic is that the gas mix cannot be altered/controlled as it is set to the set-points of the incubator in which the unit is situated, typically 5% CO_2, 18.5% O_2.

3.1.3 Description of Xpansion One regulatory mechanism

An example plot illustrating how the pump action is used to control pH in the Xpansion One system is outlined in **Figure 3.5**. In brief, as cells respire and grow the CO_2 produced reduces the pH below the chosen set-point pH. When the recorded value falls more than 0.05 pH units below the set-point (the alarm setting) this change is picked up by the optical sensor measurement system which initiates the pump system. The pump causes the circulation of media through the plate and around a section of gas permeable silicon tubing, allowing the gas in the liquid phase to equilibrate with that of the incubator and so raises the pH. Once the pH reaches a value of set-point -0.03 (Hyst) the pump action stops.

3.1.4 Aims

As with the Quantum Cell Expansion system the Xpansion systems were not developed using PSCs. For example, much of the development work used mesenchymal stem cells. Unlike many other cell types, PSCs require daily media changes and when these cultures become confluent they have a significant impact on the pH of the media causing phenol red

indicators to turn yellow. Thus, PSCs have would appear to put higher mass and gas transfer requirements on a bioreactor system than other cell types.

The aim of this chapter was to explore both the feasibility of growing hESC on the Xpansion One system to access the possibility of using the large scale machines for clinical/commercial production. Of particular interest was to build on the experience generated in the previous chapter using the Quantum Cell Expansion System to explore how the online control of environmental conditions, such as pH available on the Xpansion system impacts cell growth and the target phenotype. The specific objectives were:

- Determine if the Xpansion One system is compatible with hESC culture, e.g. will the cells attach to the plastic used and not be washed out by the flow regime?
- Maximise cell growth with respect to flask culture whilst maintaining the target PSC phenotype.

It was not the goal to generate a detailed understanding of the impact of experimental variables e.g. explore a multitude of pH setpoints, seeding densities, and flowrates in combination due to the limited number of bioreactor plates available. Rather, the goal was to perform select experiments altering these variables to try and generate a semi-optimised working protocol for future optimisation.

3.2 Materials and methods

3.2.1 Cell culture in T25 Flasks

The Shef 3 hESC line was passaged using the TrypLE Express enzyme (Life Technologies) and co-cultured on mitomycin c inactivated mouse embryonic fibroblasts (MEFs). MEFs were originally grown in Dulbecco's Modified Eagle Medium (DMEM, Life Technologies) with 10% v/v heat inactivated fetal bovine serum (FBS, Sera Laboratories International) and 1% v/v 100X MEM non-essential amino acids (NEAA, Life Technologies). hESC were grown in Knockout DMEM, (Life Technologies)(+ 4.5 g D-glucose /L, + sodium pyruvate, – L-glutamine), 20% Knockout Serum Replacement (Life Technologies), GlutaMAX, (Life

Technologies), 0.1 mM beta-mercaptoethanol, human basic fibroblast growth factor, 4 ng/ml (bFGF, R&D systems), and 1% 100X MEMNEAA (Life Technologies). Medium was exchanged daily at a ratio of 0.2 ml cm^{-2}. All cell counting and cell viability analysis was performed on the Vi-Cell (Beckman Coulter), using the trypan blue exclusion viability assessment.

3.2.2 Reverse transcriptase-polymerase chain reaction (PCR)

Following manufacturers guidelines RNA was extracted using the RNeasy mini-kit (Qiagen), and first-strand synthesised using the RetroscriptKit (Ambion). Bio-Taq polymerase (Bioline) was used for the PCR reaction in a Verity cycler (Applied Bio-systems).

Following first-strand synthesis with the method described above, quantitative PCR was carried out using the MESA BLUE qPCRMasterMix Plus for SYBR Assay (Eurogentec) in the CFX Connect Real-Time System (Bio-Rad). 20 µL reactions were run in triplicate using the following primers from Qiagen: b-ACTIN, UBC, POU5F, NANOG, EPAS1, HIF1 alpha and VEGF alpha. Analysis of relative quantification used b-ACTIN and UBC to normalise expression, and primer efficiencies were calculated using a cDNA dilution curve and analysed using Bio-Rad software.

3.2.3 Flow cytometry

The following antibodies were used: mouse anti-SSEA-4 PE conjugate (Millipore) and mouse IgM anti-TRA 1-60 (kind gift from Prof. Peter Andrews, Sheffield University) with Alexa fluor 488 goat anti-mouse (Life Technologies). A 1% cut-off gate was implemented based on conjugated isotype controls. All samples were analysed using Beckman Coulter Epics XL MCL flow cytometer, and Summit software.

3.2.4 Matching Xpansion One culture to flask culture

As far as was feasible the culture of hESC on the Xpansion Plates was matched to flask culture so as to be able to make direct comparisons between the two systems. For instance, instead of operating the plate in perfusion mode it was decided to replace the entire media volume daily in a single change, as is the case with flask culture. Furthermore the volumes

of media and reagents such as TrypLE Express (Invitrogen) for cell detachment were used at the same ml/cm^2 ratio in both systems, and other culture variables such as incubation times were also kept the same. Online measurements of pH and O_2 were taken every 30 s from optical patches attached to the plate (**Figure 3.6 a**). The Polestar unit only displays the most recent reading with historic readings saved to a USB stick (**Figure 3.6 b**). The system was calibrated following manufacturers instructions and recommendations via a one-point calibration based on an offline pH reading (Mettler Toledo Seven Easy) taken from excess seeded cell suspension run through the plate. Flask controls were also run in triplicates in the same incubator as the Xpansion plates (XP) for comparison. An outline of the experimental protocol can be seen in **Table 3.2**.

3.3 Results and Discussion

3.3.1 pH Monitoring

Following the manufacturer's guidance a one-point calibration was performed on the system on day 0 using run-through media from the seeding stage. Based on the manufacturer's experience this one-point calibration gives accurate pH readings when the experimental pH remains near this calibration point. However, due to the large falls in pH seen in hESC cultures as the experiments progressed over time there was a larger disparity between the readings given via the online patches to those recorded offline on spent media using the bench top pH probe. Therefore, both offline and online pH readings were recorded for all experiments to allow the Xpansion plates (XP) to be directly compared to the flasks using offline measurements and using the online measurements to compare XP run with XP run.

3.3.2 Limited resources of the feasibility study

The prototype equipment used in this chapter was made available under agreement with ATMI to determine the feasibility of their using bioreactor platform to grow PSC. Therefore, the utilisation of the prototype bioreactor Xpansion Plates (XPs) was at a premium, this limited the number of experiments possible. However, the overriding aim of this study was

to maximise cell growth to get as close to the flask controls as possible, whilst maintaining the target PSC phenotype, as opposed to generating a detailed understanding of the impact of experimental variables such as shear.

When scoping the study it was the intention to eventually move the work from the Xpansion One on to the larger scale Integrity Xpansion bioreactor. With this large-scale experimentation in mind the same karyotypically abnormal hESC line from the previous chapter was used under the same rationale i.e. it being best suited to large-scale experimentation. But, due to time constraints a move to large scale experimentation was not made.

3.3.3. Impacts of a constant flow regime (experiment XP1)

In order to determine whether increasing flow rate detrimentally impacted growth, 3 Xpansion Plates (XP) were run in parallel over a range of constant flow rates, i.e. as opposed to the discontinuous flow regime applied during regulation mode. The following flow rates were used 0.2 mm/s (XP1.1), 1.0mm/s (XP1.2) and 5mm/s (XP1.3), representing a 25 fold change in linear velocities. In this experiment a low seeding density of 4500 cells/cm^2 was used in an attempt to ensure that oxygen uptake rate (OUR) of the cells would not be greater than the gas transfer rate (GTR) or the reactor (see previous **Chapter 2, Equation 1** for definitions). By ensuring that the GTR is not limiting at any of the flow rates used it was predicted that the liquid phase should be fully equilibrated with the incubator gasses and thus maintain a pH of ~7.32 throughout all flasks and plates allowing the impact of the flow rate to be separated from the other variables. The pH value of 7.32 is the pH of hESC media when left to equilibrate in the 5% CO_2, 18.5% O_2 and 37°C environment of our lab's incubators.

From **Figure 3.7 a)** it can be seen that the online pH across all 3 flow rates was maintained at ~7.32 as expected. There is a slight discrepancy in pH readings between the XPs from D0 to D2, which was due to poorly calibrated pH sensors. This was remedied by recalibration using spent media, when the media was exchanged on D2, after which there was closer agreement between the online pH readings. In addition the pH level maintained in the XPs

closely matched that seen in flasks based on spent media analysis (**Figure 3.7 b**). Even so, despite the pH levels being very similar between the XPs and the flasks it can be seen that a far lower cell density was achieved on the XPs than on the flasks at harvest (**Figure 3.8 a**), with the cell growth on the plates being between 42% and 33% of that seen in flasks (**Figure 3.8 b**). The media analysis data (**Figure 3.8 c**) shows that the flask culture has slightly lower glucose levels and slightly higher lactate levels at harvest when compared to the XPs which correlates with the higher cell densities achieved. Increasing flowrate across a 25 fold range (0.2mm/s to 5mm/s) did not appear to impact cell growth, given there was a larger standard deviation across the 3 control flasks (technical repeats) than between the 3 Xpansion plates running at different speeds (**Figure 3.8 a**).

However the highest flowrate of 5.0mm/s (XP1.3) did correspond with a large reduction in viability (**Figure 3.8 d**). There were also clear visible differences seen on this plate as illustrated in **Figure 3.9**. The area denoted by A) shows a large amount of precipitated protein accumulating in the centre of the plate and the area denoted by B) shows a steady stream of bubbles focusing on the edge of the flow distributor element. So, it was decided not to run the XP at this highest flowrate again in future experiments.

Unfortunately, online DO readings from this experiment were inconclusive due to the practical limitations of needing to run 3 plates simultaneously but with only 4 channels available on the Polestar equipment for optical readings. Therefore, 3 of the channels were used for constant online pH monitoring with the final fibre optic channel being devoted to DO. This meant that instead of a constant DO reading the probe had to be manually moved between all 3 plates to take readings at different time-points. The consequence of this manual moving of the probe between plates was erratic and inconclusive DO data. This was believed to be due to calibration errors as it was not possible to calibrate each optical patch independently**.** Subsequent experiments did not involve running more than two XPs in parallel to enable both pH and DO to be recorded continuously online.

3.3.4 Regulation through discontinuous mixing (experiment XP2)

From the constant flow experiments (XP1.1, XP1.2, XP1.3) it was seen even when pH was maintained to the same level in flasks that cell densities achieved on the XP were lower than in flasks (**Figure 3.8 b**). It was first hypothesised that this could be due to one of two causes: either the differing chemistry of the plastic between the XPs and the flasks was adversely effecting growth; or that that any flow rate on the XPs no matter how low negatively impacted growth.

The first hypothesis was tested by comparing growth in Nunc branded T25 plastic versus Corning branded T25 plastic. The latter being plasma treated, as opposed to electric current treated, and so according to the XP manufacturer (ATMI) the Corning plastic flasks should have the same characteristics as the Xpansion plates. Under this direct growth comparison there was no significant difference in growth (data not shown) and so the reduced growth observed on the XPs was not believed to be down to incompatible surface chemistry.

To test the second hypothesis i.e. that is was the very effect of having any flow at all which reduces cell growth, it was decided to change operation from one of constant flow to one of regulation using discontinuous mixing. In this regime flow is only initiated to regulate pH when it is away from the target set point described in **Figure 3.5.** A pH set point of 7.32 was chosen as this matches the pH of hESC media that has been allowed to equilibrate in a 5% CO_2 incubator environment overnight. A linear flow rate of 2.9mm/s was chosen based on outcomes from the constant flow experiment and advice from the manufacturer on what had been used successfully with other cell types. The seeding density was also increased to 13,000 cells/cm^2 in this experiment to increase the number of cells available at harvest for analysis. The regulation loop which includes the gas permeable silicon tube was added on D2 to allow the hESC to attach for a full 24h before flow was initiated.

From **Figure 3.10 a)** it can be seen that the system operated under regulation during the D3-D4 period, as evidenced by the fluctuations in DO and pH during this period. An enlarged plot of this time period with a caption explaining the pump operation is shown in **Figure 3.10 b)**. The regulation system managed to maintain pH at or around the setpoint of

7.32 until the latter stages of D4, with a final online pH before harvest of 7.24. When the offline readings of pH of the control flask culture (7.08) and the XP2 (7.16) are compared directly **(Figure 3.11)** it can be seen that although the XP regulation system failed to keep the system at the desired setpoint of 7.32, the harvest pH was still higher than that seen in the control flasks. The differences between the online DO patch readings and the offline spent media analysis was a result of only using a 1-point calibration method (as opposed to 2 or 3 points). As described earlier this required the logging of both online and spent media pH for all experiments and as such both readings are plotted in spate charts in the Figures to allow direct comparisons to be made between the XPs and the control plates.

Again, it can be seen that despite the similarities in pH levels the cell density achieved in flasks was still considerably higher than that achieved on the XPs (**Figure 3.12 a**). However, the introduction of the discontinuous mixing regime to control the pH has improved the respective performance of the XP, with the XP2 regulation experiment achieving 52.50% of the flask cell density (**Figure 3.12 b**) compared to the best result of 42.16% achieved in the XP1 constant flow experiment **Figure 3.8 b)**. As before, the higher cell density achieved in the flasks resulted in lower levels of glucose and higher levels of lactate in the flasks when compared to the XP (**Figure 3.12 c**). In addition the viability at this flowrate (2.9mm/s) remained high at 97.0% (**Figure 3.12 d**).

3.3.5 Initiating regulation earlier (experiment XP3)

With regulation producing better results than constant flow it was decided to explore the impact of adding the regulation loop earlier than the 24h time point used in the previous experiment (experiment XP2). Therefore, 2 plates were run in parallel one with no regulation (XP3.1) and one in which regulation would be started at 6h post seeding of PSC XP3.2, with both flasks being harvested at 24h post seeding. Furthermore, the seeding density was increased to 20,000 cells to try and ensure that cell metabolism would bring the pH down to the setpoint within this 24 hour time period to trigger the regulation and so flow/mixing. This higher seeding density also matches that used when using karyotypically

normal cell lines in our lab. The linear flowrate was also reduced to 1 mm/s to try and reduce the likelihood of the recently attached cells being lifted.

From **Figure 3.13 a)** it can be seen that the regulated plate (XP3.2) maintained a higher pH at harvest of 7.28, and so closer to the setpoint of 7.32, compared to the non-regulated plate (XP3.1) which had a harvest pH of 7.09. When compared to the offline pH of the control flask culture (**Figure 3.13 b**) it can be seen that the regulated plate (XP3.2) maintained a pH far closer to the pH of the flask controls than the unregulated plate (XP3.1) did. In addition, from microscope analysis during the run the flowrates did not appear to cause the cells to lift (data not shown).

From **Figure 3.14 a)** it can be seen that the plate undergoing regulation (XP3.2) yielded a higher density (82% relative to the control) than that under no regulation (XP3.1, 72.74% relative to the control). The viability of the regulated plate was also higher (**Figure 3.14 b**), thus for all future optimisation experiments the regulation was initiated 6 h post seeding and a seeding density of 20,000 cells/cm^2 was used.

3.3.6 Increasing the expansion time (experiment XP4)

Given the improvements in cell density achieved by implementing regulation and applying it early it was decided to extend the culture period by a day to determine whether there was a lag effect on the growth on the Xpansion plates which could be overcome. So, again two plates were run in parallel, both against separate triplicate controls: PSC were expanded for 3 days (experiment day D4) on XP4.1; and expanded for 4 days (experiment day D5) on XP4.2.

From **Figure 3.15 a)** it can be observed that both plates struggled to maintain the pH at the desired set point of 7.32 during the interval between the media changes on D3 and D4. This is despite the CO_2 in the incubator being reduced from 5% to 1% during this period in an effort to raise the pH (see **Figure 3.15 b)** caption for timings). At harvest XP4.1 on which hESC were cultured for 3 days (4 day total protocol length) the online pH was 7.10 (**Figure 3.15 a**) and offline pH 6.89, which was close to that of the offline pH for the control flasks of

6.96 (**Figure 3.16 a**). Critically during the final 24 hour period from D4 to D5 (XP4.2) the system only matches the set point for a fleeting period of time. Thus when harvested the online reading for XP4.2 was 6.54 (**Figure 3.15 a**) and the offline reading was 6.27; these are both considerably lower than the flask controls whose harvest pH was 6.71 (**Figure 3.16 a**). Interestingly, an alternative trend with respect to glucose and lactate was observed for XP4.2 compared to previous XP experiments. Despite there being far fewer cells per cm^2 in XP4.2 than the control flasks the depletion in glucose and increases in lactate are far larger **(**see **Figure 3.16 b)**. This is suggestive of alternative metabolic processes taking place on the XP compared to the flask culture due to the differing environmental conditions.

The conclusion from this experiment was that culturing the XP for an additional day did not improve the density achieved when compared to flask culture grown for an equivalent amount of time. With XP4.1 yielding 54.3% of controls and XP4.2 yielding 47.3% (**Figure 3.17**).

3.3.7 Increasing the regulatory flowrate (experiment XP5)

Due to the inability of the XP system to maintain the pH at the set point value at the higher cell densities achieved in XP4 on D4 and D5 it was decided to increase the flow rate from 1mm/s to 2.9 mm/s for XP5.1 to try and improve the gas transfer rate.

From the online pH readings for XP5.1 (**Figure 3.18**) it can be seen that despite the higher flow rate the pH still dropped significantly below the set point towards the end of D4. For XP5.1 it was decided not to reduce the CO_2 in the incubator as was attempted in XP4 as this crude approach meant it was very hard to control the outcome and actually generated great pH peaks when fresh media was added during the trial and error approach. The cell density achieved in XP5.1 was equivalent to that of XP4.1 which was run at the lower flow rate of 1mm/s, however XP5.1's performance relative to controls was better in XP5.1 (62.15%) than for XP4.1 (54.30%) as can be seen in **Figure 3.17**. This apparent improvement could be attributed to a lower cell density achieved in the XP5.1 control condition (**Figure 3.14 a**)

which makes the percentage performance appear better. Thus, it is unclear whether the higher flow rate had a positive effect or not, but what is clear is that any effect is minimal.

3.3.8 Determining whether oxygen supply is growth limiting (experiment XP6)

From the previous experiments (XP1-5) it could be seen that growth performance of the XPs was significantly lower than controls, with the best XP harvest densities being around 50-60% of controls (**Figure 3.17**). This is somewhat surprising given that although the control of the environment was not ideal in these experiments the observed differences in the pH and glucose and lactate levels were relatively small. It was considered that a lack of oxygen supply that caused the poor performance on the XPs. The hypothesis being that when the system reaches the pH setpoint the pumping stops and there is a corresponding drop in DO. A good example of this can be seen in the online plot of **Figure 3.10 b**. To determine whether such a drop in DO retarded cell growth triplicate control flasks were run in an incubator in hypoxic conditions alongside two Xpansion plates namely XP6.1 1mm/s and XP6.2 2.9mm/s. The O_2 supply was manually reduced using the incubator controller settings (13% O_2 setpoint) to produce a DO on the XP of 60% under pumping which corresponded to the reduced DO when there was no pump action observed in previous experiments.

From **Figure 3.19 a)** it can be seen that the regulation achieved at both the 1 mm/s and the 2.9 mm/s flow rate yielded similar results with the harvest pH's being 7.17 and 7.08 respectively. The DO was maintained at approximately 60% when the pump was initiated. From the offline pH it can be seen that the pH on the XPs was maintained at a slightly higher pH than the control flasks **Figure 3.19 b)**. Glucose levels in the controls were also slightly lower, and lactate levels slightly higher, when compared to the XPs **Figure 3.19 c)**.

The lowering of the DO in the incubator to 13% to reduce the online DO of the XP to 60% did not negatively impact growth in the control flasks, with the control flasks for XP6 performing similar to XP5 and XP 4.1 controls (**Figure 3.14 a**). These results of the control flasks would suggest that growing hESC under a lower oxygen condition for a single passage

does not adversely impact growth. However, the low O_2 did seem to have an adverse impact on the XPs, with the 1mm/s flowrate (XP6.1) and the 2.9 mm\s flowrates (XP6.2) having relative performance to controls of 52% and 42% (**Figure 3.17)**. The cell densities achieved under reduced O_2 on the XPs were also slightly lower than the equivalent conditions grown under atmospheric O_2, namely XP4.1 1mm/s and XP5.1 2.9 mm/s (see **Figure 3.14 a**). Therefore, the lack of pumping when the setpoint is reached on the XPs and accompanying drop in DO does not explain the large 40-50% reduction in cell density when compared to flask controls.

3.3.9 Further analysis of the metabolic activity of the cells

What was intriguing when looking at all the experimental data as a whole is that although glucose and lactate concentrations were very similar at harvest throughout all the experiments (both the controls and XPs), these levels were corresponding to very different cell densities. When these cell densities are plotted against glucose and lactate concentrations (**Figure 3.20 a) and b**), it can be seen that as cell density increases there is a clear difference in trends between the Xpansion plates and the control flasks. As cell density increases in the Xpansion plate there is a clear liner relationship between glucose consumption and lactate production at increasing cell density. But, this relationship does not hold true in the control flasks, where at higher cell densities far less glucose is consumed and lactate is produced per million cells per cm^2.

Two possible explanations for this could be that the control flasks utilise alternative carbon sources at higher densities such as glutamine, or that the KL_a of the Xpansion Plate is not greater than the oxygen uptake rate (OUR) of the cells and so the XP becomes hypoxic and the culture anaerobic, relying more on glycolysis and so producing more lactic acid.

To explore the first hypothesis glutamine consumption would ideally be measured. Unfortunately, a stabilised form of glutamine was used in these experiments (Glutamax, Invitrogen) which due to its stabilisation readings could not be obtained using the glutamine capable analyser available (Nova Biomedical). Furthermore, Glutamax

degradation over time actually causes glutamine concentrations to rise as noted by Chen et al. (2010).

To test the second hypothesis that oxygen provision to the cells is rate limiting, it would be assumed that the online DO levels are inaccurate given the results of XP6. In fact this could be due to the positioning of the optical patches as they record the DO in the bulk media and not the close vicinity of the growing cells; this means the cellular oxygen partial pressure can be very different. The cellular oxygen partial pressure is impacted by high cell densities, high cellular oxygen consumption rates, and large medium heights, and it can be calculated mathematically as described by Millman et al. (2009). However, the data for the mathematical model requires significant additional experimentation, growing cells on a highly gas permeable surface so that there is minimal disparity between the oxygen levels (Powers et al., 2010). As an alternative to completing such work and modelling the XP system (which was beyond the scope of this feasibility study) a number of hypoxia related genes were explored via qPCR for the XP4 experiment (see **Figure 3.21**). These genes chosen cover a wide range of hypoxia pathways for instance HIF-1α is the initiator of the cellular response to low oxygen conditions whereas EPAS1 (HIF-2α) regulates hES cell pluripotency as well as proliferation under hypoxic conditions (Forristal et al., 2010). Under hypoxic conditions HIF-1α subunits translocate to the nucleus and activate transcription of target genes such as VEGF that promotes angiogenesis.

From the chart **(Figure 3.21)** it can be seen that there are roughly similar expression levels of the hypoxia related genes between the flasks and the XPs for XP4. Additionally, ANNOVA analysis between triplicate flasks also showed no significance difference from allowing the cells to become more confluent through allowing them to grow another day. This would suggest that the cellular oxygen partial pressure environment is highly similar between the XPs and the controls, and that oxygen supply is not significantly growth limiting as was also shown experimentally in XP6.

3.3.10 Maintenance of the pluripotent phenotype

Despite greatly reduced growth in the XPs, the impact on pluripotency marker expression was relatively minor. From **Figure 3.22 a)** it can be seen that SSEA-4 protein expression was only slightly reduced when compared to the flask controls and **Figure 3.22 b)** shows that TRA 1-60 expression either matched or was greater than the controls in most of the experiments. It was considered that the use of these markers and flow cytometry might not be sensitive enough to pick up changes in pluripotency, So, qPCR analysis was run on the XP4.1 and XP4.2 experiments for the pluripotency markers Nanog and Pou5F **(Figure 3.23)** which showed a greater difference between the XP and the controls. What would be critical in determining whether the Xpansion One system has a negative impact on pluripotency marker expression would be to culture hESC on the XPs over a number of passages to allow time for pluripotency marker expression to change. In addition, the running of multiple plates over a number of passages would produce statistical certainty in the result.

3.4 Conclusions

3.4.1 Establishment of a working protocol to take forward to large-scale experimentation

Although experiments were limited by the number of XP bioreactors available, it is believed that the work detailed here utilising the Xpansion One system enabled the exploration of key variables using this small-scale mimic. Such work being vital before committing to large-scale process development using the Integrity Xpansion systems (**Table 3.1**). Key conclusions from this work are as follows. At lower cell densities increasing the flowrate did not appear to adversely impact cell growth and the pH could be maintained equivalent to flask culture (experiment XP1); the introduction of discontinuous flow to achieve regulation further improved growth (experiment XP2). Moreover, adding the regulation loop after 6.5 hours instead of 24h increased cell growth (experiment XP3). However, in using higher seeding densities which better match those used for karyotypically normal cell lines the system struggled to maintain the set point pH and increasing the culture period did not increase performance relative to controls (experiment XP4). Finally, increasing

flowrate at the higher densities did not appear to improve either regulation of importance (experiment XP5).

3.4.2 Is the design of the Xpansion One system suitable for high density PSC culture?

The XPs have a clear linear relationship between cell density and glucose consumption, whereas in flask culture less glucose is consumed and lactate produced at increasing cell density **(Figure 3.20).** It was hypothesised that this was a result of anaerobic conditions being produced in the Xpansion One system due to either drops in DO when the pH set point was reached, or that the oxygen provision directly around the cells was low and not being picked up due to the positioning of the sensors. By running plates at reduced incubator O_2 (13%) to yield a DO max of 60%, which matched the minimum DO during normal culture, it was seen that low O_2 only appeared to have a minimal negative impact on XPs and no impact on the control flasks (experiment XP6). Furthermore, hypoxia gene expression was largely similar between the XPs and flask controls suggesting that there is similar oxygen provision in the flasks and the XPs (**Figure 3.21**). From this, it would be the conclusion that gas transfer in the XP system is not growth rate limiting.

More experiments would be needed at various cell densities and oxygen tensions to determine that the K_La of the XPs is greater than the OUR. For instance, there are ways to measure the K_La of bioreactors using the 'gassing in' method in this case would require the entire incubator to be filled with nitrogen and the XP run to remove all oxygen. The K_La would be determined via the DO response of the XP when the incubator is re-filled with O_2 gas mix, this rapid refilling would be technically difficult in practice. In traditional bioreactors the gassing in approach utilises a built in sparger.

The other main issue when growing these-high density PSC cultures in the XP system was the poor ability to maintain pH at the setpoint. Increasing the linear flow rate between 1mm/s to 2.9mm/s showed no obvious benefit and raising the flowrate significantly to 5mm/s caused protein precipitation and bubbles. Options for improving pH regulation and

thereby performance, are better addressed using the larger scale Integrity Xpansion systems due to their more complex regulatory systems.

3.4.3 Options to improve performance when scaling-up

What is clear from this feasibility study is that the MEF-hESC co-culture system is compatible with the XP system. Although the best growth performance relative to controls was only 62% the work described here narrows the discrepancy down to two causes: a) either growing PSCs under a fluid shear/dynamic environment; b) or inability to control pH accurately.

In terms of a) it may be that any flow in a PSC system reduces growth. Titmarsh et al. (2011) reported work using a continuously perfused microbioreactor that PSCs under shear stresses between $5x10^{-4}$ to $7.5x10^{-4}$ Pa matched static controls in terms of growth. However, the paper also reports that low perfusion rates caused the culture to become limited by mass transfer (with only 11% yield compared to static controls at a shear stress $8.5x10^{-5}$ Pa). In addition, 'high' perfusion rates resulted in performance of only 18% of static controls, with cells appearing to detach and wash out (shear stress 1.1 $x10^{-3}$ Pa). Computational fluid dynamics studies and experimental validations by ATMI report at all their scales that at a linear velocity of 2mm/s that 90% of the culture experiences a shear stress of 6 $x10^{-3}$ Pa, with a maximum shear stress at the walls of 10 $x10^{-3}$ Pa i.e. a shear stress of over 5 times higher than the 'high' flowrates used by Titmarsh et al. (2011). Even so, despite these shear rates in the XP being far higher than those reported by Titmarsh et al. (2011) the performance in relation to its static controls was over 3 times better (62% yield compared to 18%). It is hypothesised that it might be the discontinuous mixing system, or the different geometry of the XPs that is the reason for the improved performance even though the shear rates are higher.

In terms of b) (see above) that it was poor control of pH or gas transfer that caused the reductions in growth it would be anticipated that the yields would be increased when scaling up to the larger Xpansion systems as they have more complex control systems. The previously described regulation system in the Xpansion One (**Figure 3.5)** works by

equilibrating the dissolved gasses in the silicon tubing to the background gas mix of the incubator. This severely limits the ability to control pH by altering the gas mix. For instance, CO_2 was manually reduced using the incubator settings in XP4 (**Figure 3.15)**, but the results were a very crude and did not allow proper regulation of pH. Advantageously, the regulatory system of the full sized Xpansion systems allows control over the gas mix to control both pH and DO (**Figure 3.24)** and so it is believed the best performance of 62% in the Xpansion One could be greatly improved on by moving to the larger scale bioreactors. An alternate way to improve pH control would be to perfuse in fresh media. However this would increase the amount of media needed to grow each cell and so any improvements in yield would need to be balanced with the increased costs of media.

Finally one aspect which could significantly improve results is one of repeat passaging. Cells and PSCs in particular often take a few passages to adapt to a new culture method. While it was not tried here sequential passaging of cells using the Xpansion system may aid cell adaption and so improve growth performance.

3.5 Summary

3.5.1 The importance of environmental control

Good environmental control of pH is vital, it is clear that small variations in environmental conditions such as pH has a major impact on performance, with growth being reduced greater than 40%. Comparatively little is known about the ideal environmental conditions for PSC cultures in dynamic conditions and it is highly likely that the conditions used in static flask culture non-ideal. From this feasibility study using the Xpansion One system it can be seen that an understanding of a broad range of environmental conditions such as pH, fluid mixing, shear and nutrient and waste mass transfer will be vital if a successful translation of PSC culture to bioreactors is to be made.

3.5.2 Future work

If the Xpansion One system was being used in a commercial setting a greater number of experiments would have been conducted using this small-scale mimic. These results would

be used to add statistical certainty to the conclusions made here regarding flow rate, maintenance of the pluripotent phenotype and the gas transfer capacities of the system. Furthermore, a range of set point pH values would be explored to see if the pH of 7.32 (the value of PSC media equilibrated with the temperature and 5% CO_2 of a standard incubator) is indeed ideal. Future work would also use a 2 point calibration on the online patches to solve the discrepancy issues between online and offline readings, such a two point system is used on the large scale bioreactors. Also, a more detailed metabolite analysis would be useful, particularly tracking glutamine (not possible here due to the use of Glutamax), to try and understand the differing trends of glucose consumption and lactate production between the XPs and the flasks at increasing density. Calculation of the yield coefficients of these metabolites would also be useful for comparing environmental conditions with other systems as described by Chen et al. (2010), but this would require accurate measurements of cell density during culture.

What would be really interesting would be to conduct differentiation experiments using the Xpansion system as it could well be that the environmental conditions that are optimum for the maintenance of the PSC pluripotent phenotype are not the optimum for PSC differentiation. Finally given the large numbers of potential variables which can impact performance a statistically led, multifactorial screening, and optimisation approach would be beneficial. Such an approach is applied to PSC differentiation to RPE in **Chapter 4**.

a)

b)

Figure 3.1: Overview of the Integrity Xpansion Multiplate bioreactor (Pall). a) The Xpansion system will its control unit. b) A computer model of the multilayer system within the reactor b)

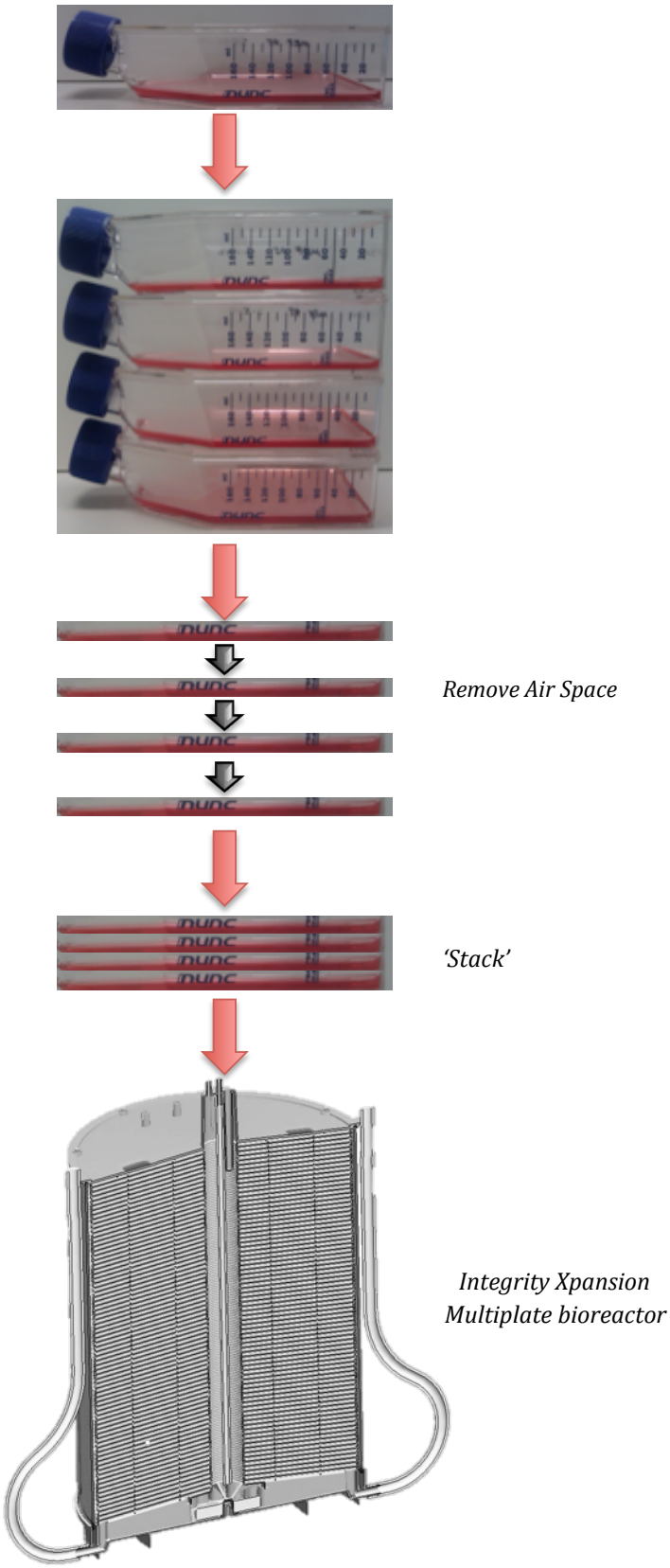

Figure 3.2: Removal of the Airspace to Increase Volumetric productivity. Volumetric productivity is increased by removing the air space between the liquid layer and the next plastic layer which is normally found in flask or CellSTACK (Corning) culture systems.

a)

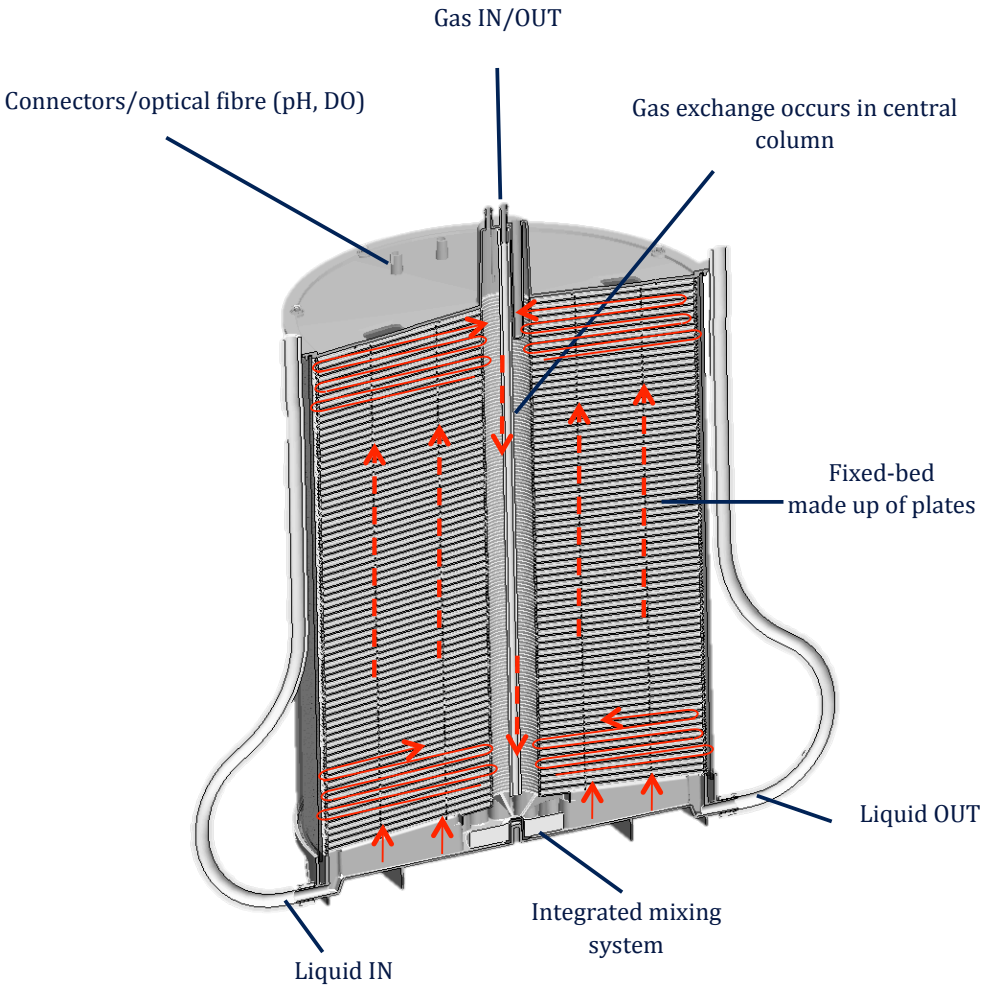

b)

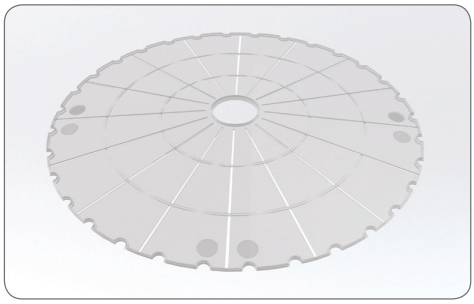

Figure 3.3: The Flow Regime for Gas Transfer in the Xpansion System. a) the arrows depict how the integrated mixing system (impeller) drives the flow of fluid through and around the stacked plates. This fluid is then bought back down the central column in which is located gas permeable silicon tubing across which gas transfer occurs. The inlet and outlet tubing allows the addition and removal of liquids during loading and harvesting. These could also potentially allow the system to be run in a perfusion mode of operation. b) An image showing a single plate allowing the "slits" in the plates to be seen which allow fluid flow.

a)

b)

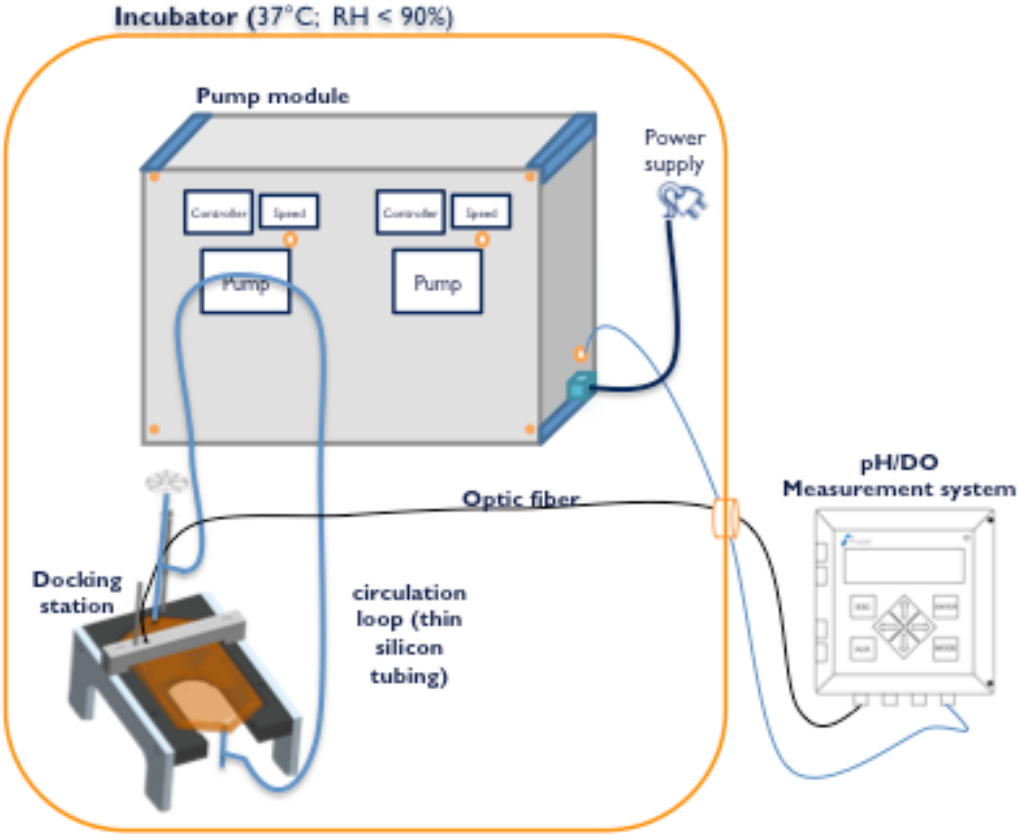

Figure 3.4: Overview of the Xpansion One System. a) The control unit allows simultaneous control and operation of two Xpansion One plates at one time. b) The experimental set-up of the Xpansion One system b)

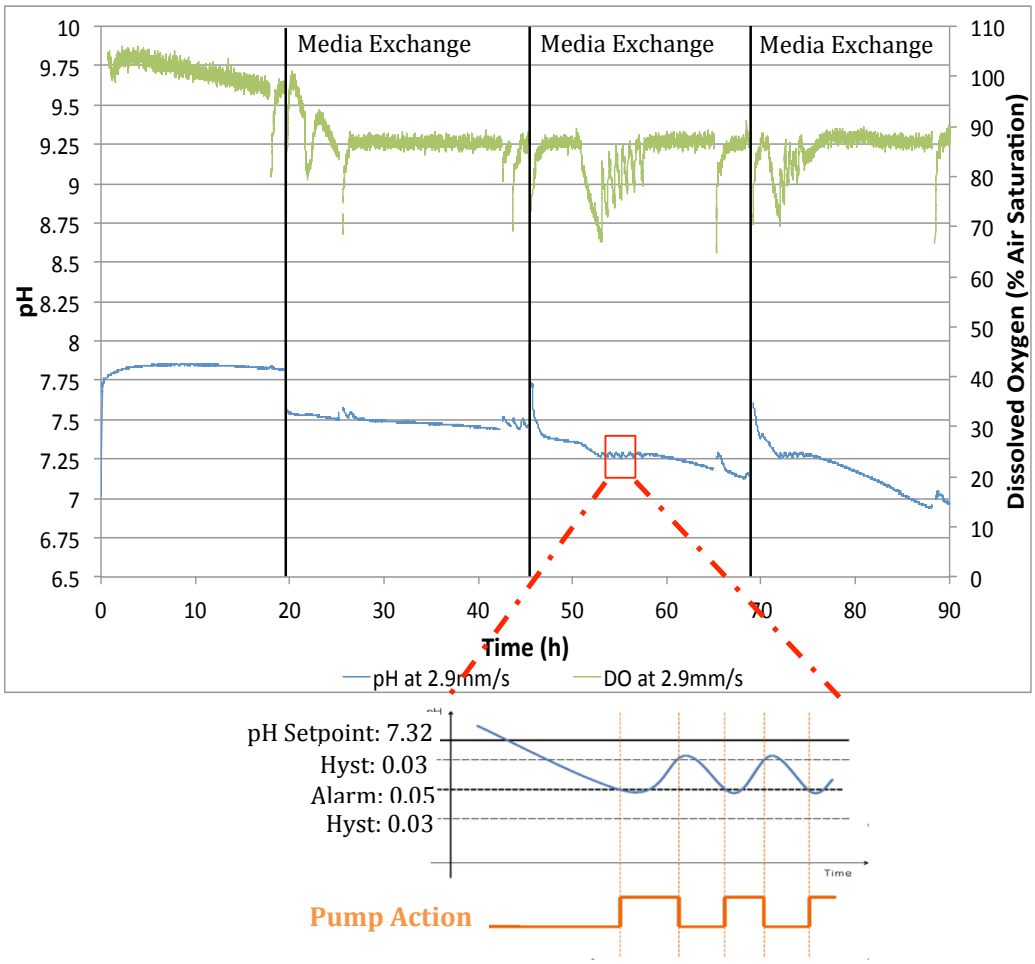

Figure 3.5: An example plot illustrating the regulation control in the Xpansion One system. The system pump is only started when the pH reading deviates a certain amount from the set-point and stops when it is brought back within the desired margin (hysteresis or hyst. vale).

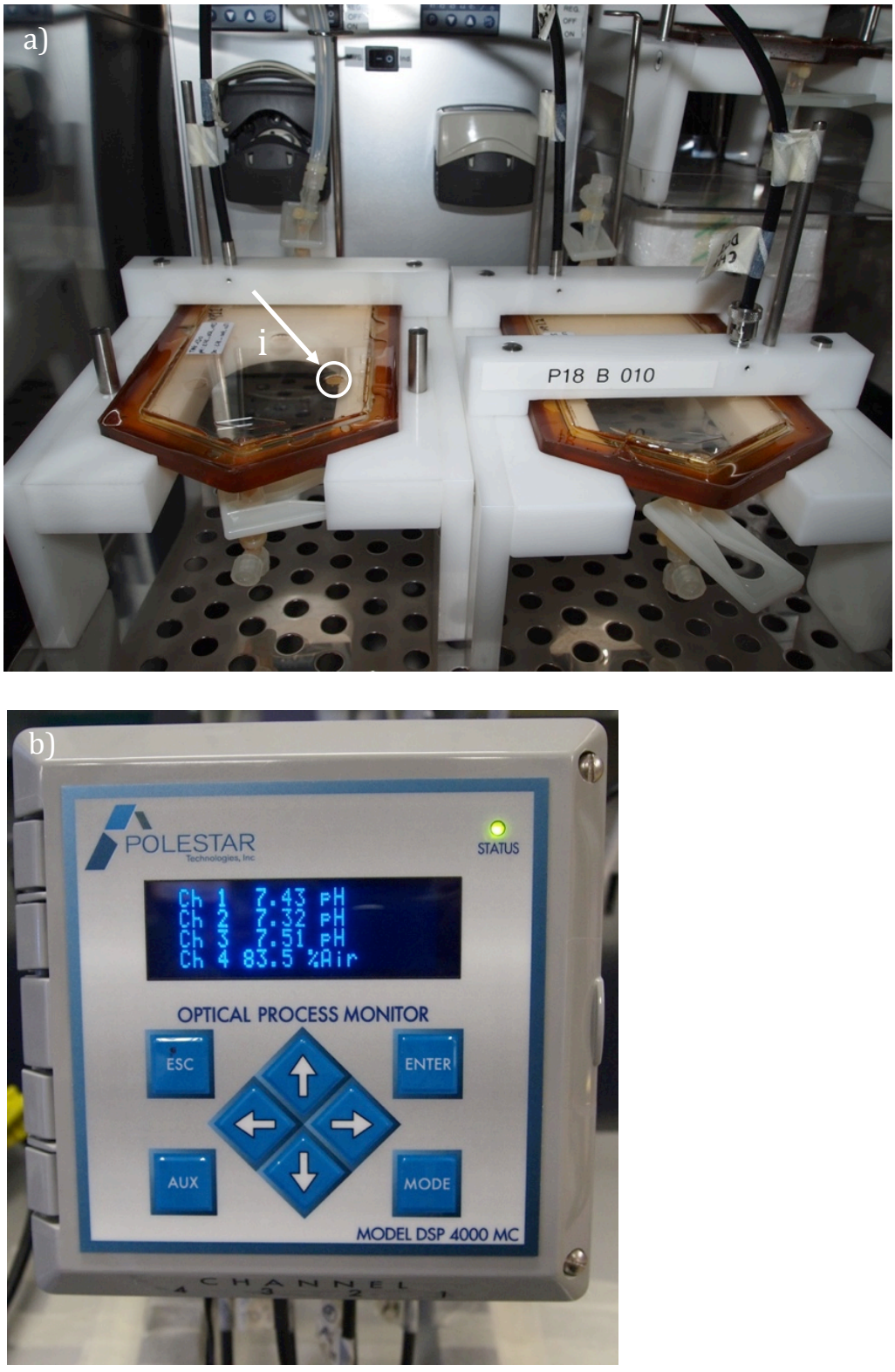

Figure 3.6: Connection and monitoring using optical sensors. a) The fibreoptic sensors are held in place whilst in the doc system), optical sensors are preinstalled onto the inside of plate and highlighted by i). b) The fibre optic is connected to the polestar unit which displays the most recent reading and logs previous readings to a USB stick.

a)

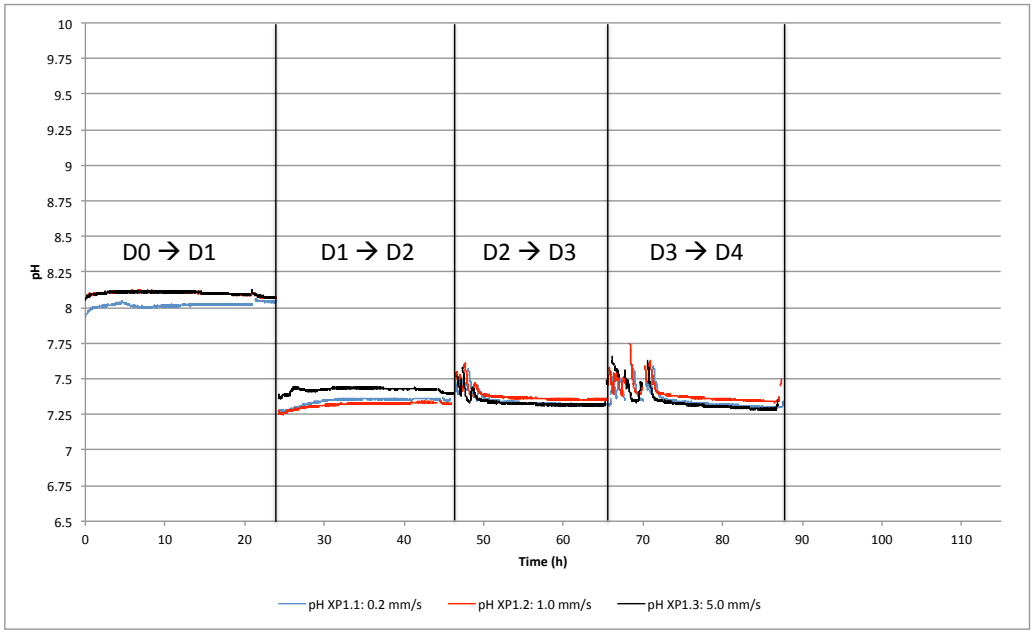

b)

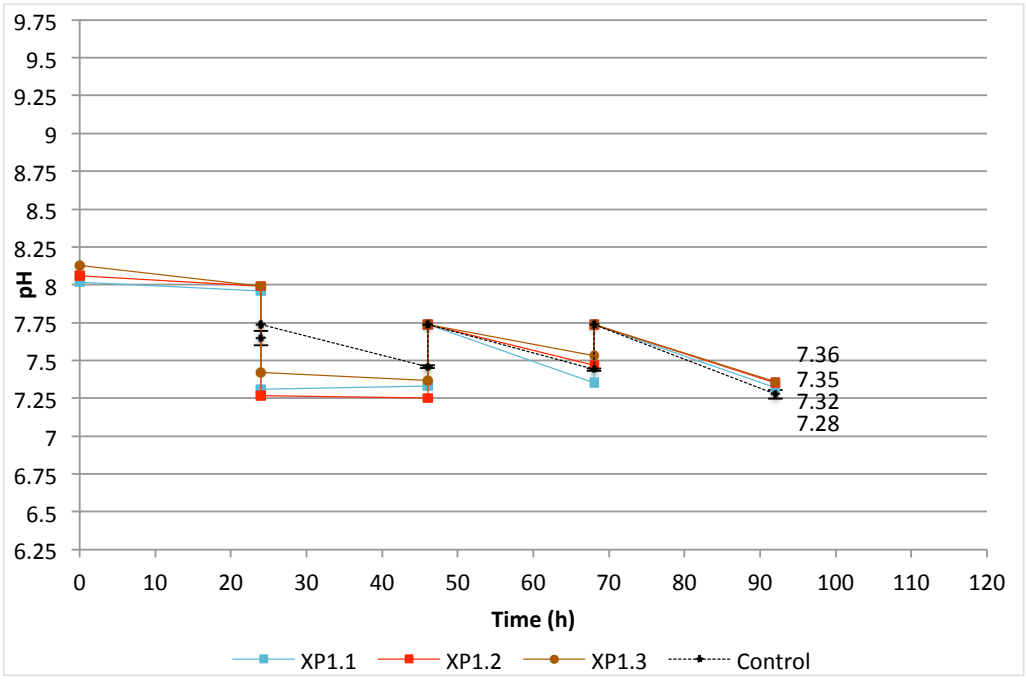

Figure 3.7: Constant flow regime (XP1) pH readings. Online pH data a), offline pH data on spent media b).

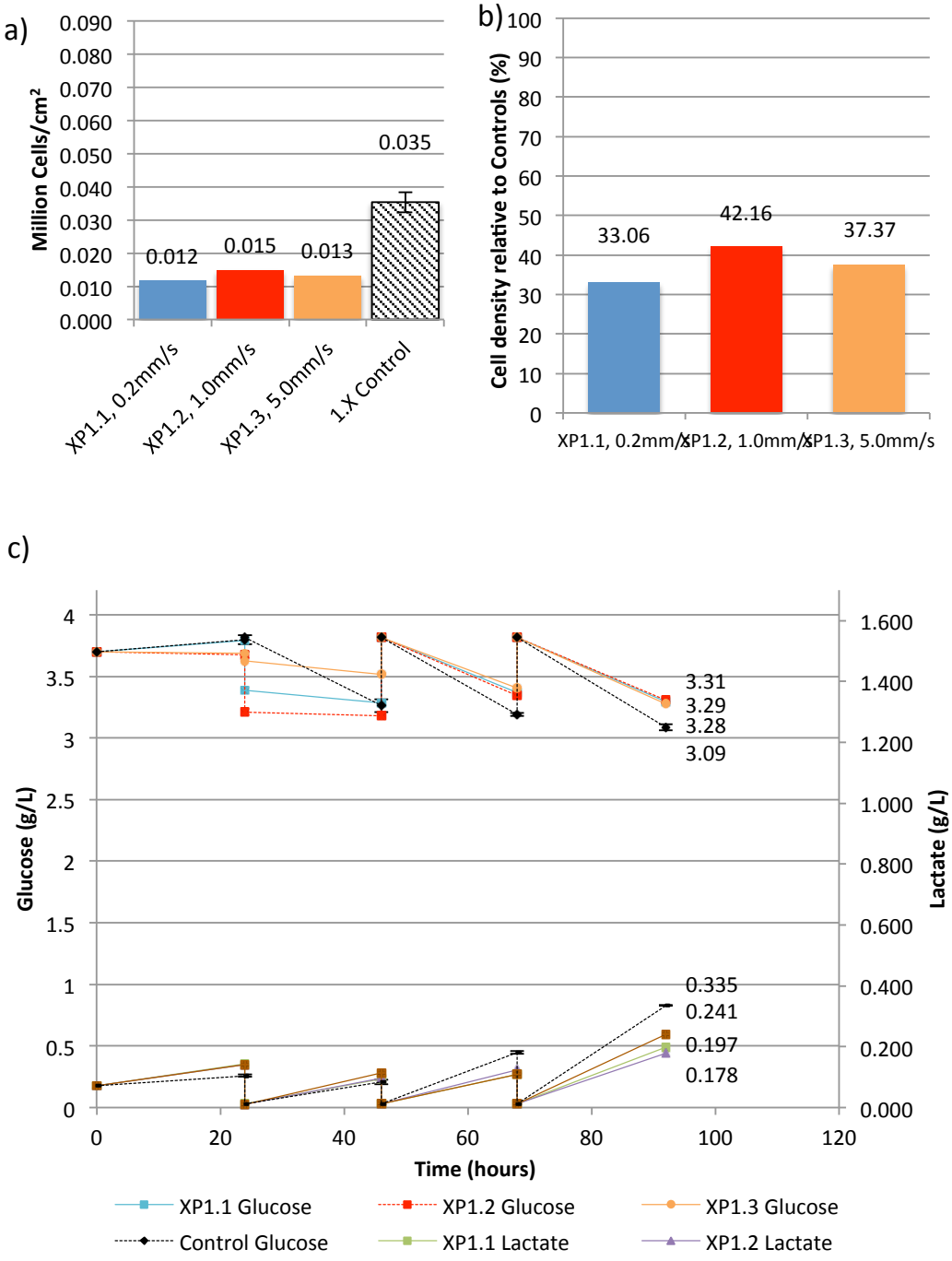

Figure 3.8: **Results for constant flow regime experiments (XP1)**. Density of viable cells at harvest a), and Xpansion plate performance relative to controls b), glucose and lactate levels c) and viability at harvest d).

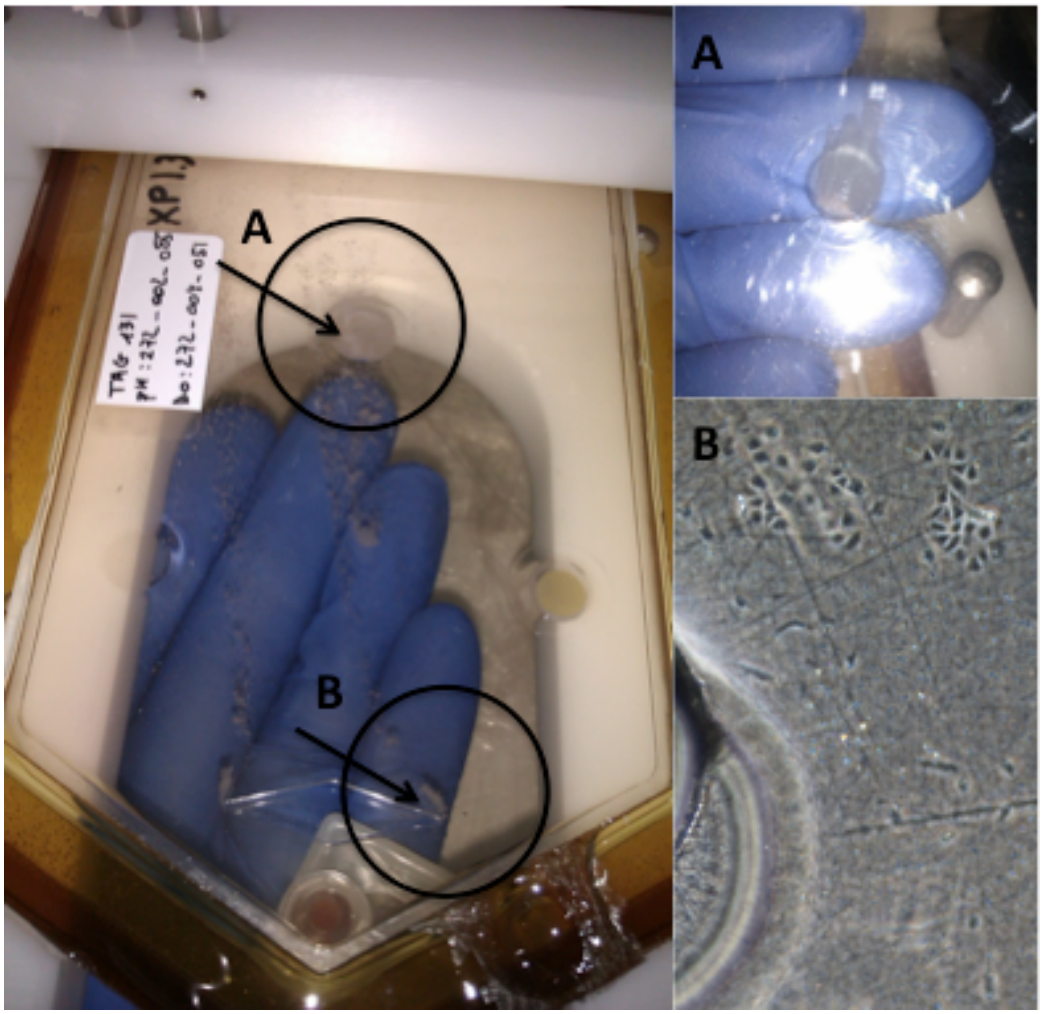

Figure 3.9: Visual differences of running a plate at a high flowrate of 5.0mm/s. Area denoted by A) shows protein precipitation accumulating in the centre of the plate. Area denoted by B) shows considerable bubble formation around the flow distributor not seen at other flowrates, although this did not appear to impact cell attachment when viewed under a microscope.

a)

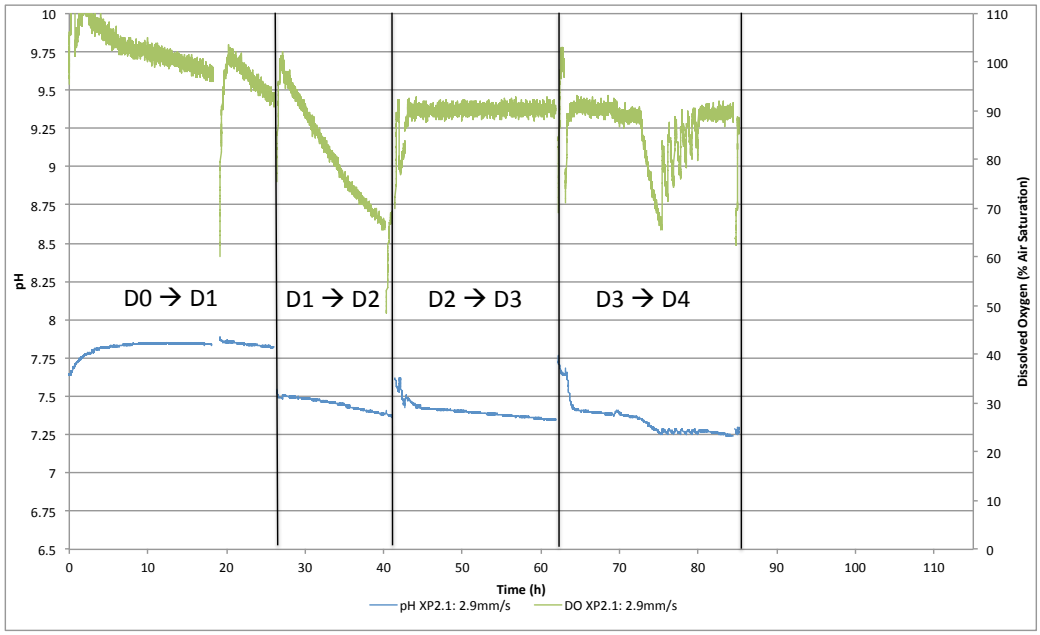

b)

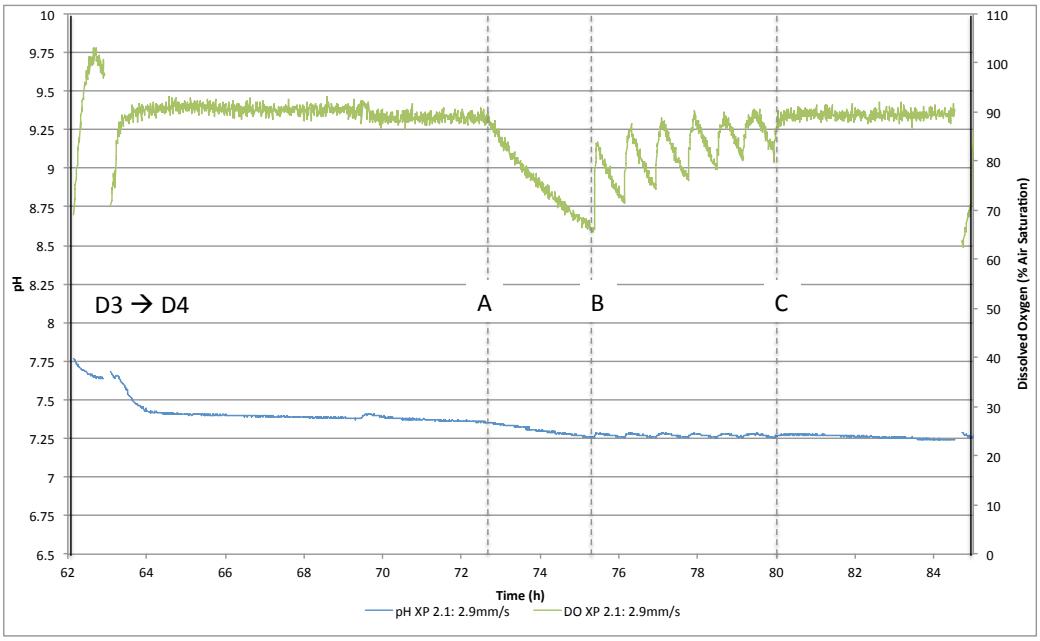

Figure 3.10: Regulation through discontinuous mixing (XP2) online pH and DO readings. Measurements over the full time course of the experiment a). An enlarged plot covering just the period from D3 → D4 to illustrate the regulation effect b). At A) the pH setpoint is reached (blue line) and so the pump stops and flow ceases. This lack of flow between A) and B) corresponds with a significant decrease in DO (green line). At point B the pH reaches the alarm value of 7.27 (setpoint minus 0.05) and the pump is restarted until the pH reaches the hyst value of 7.29 (setpoint minus 0.03). This regulation effect continues to point C) where the pumping action to equilibriate the dissolved gasses media with the gasses in the incubator is not sufficient to reach the hyst value of hyst value of 7.29 and so the pump remains constantly on for the duration.

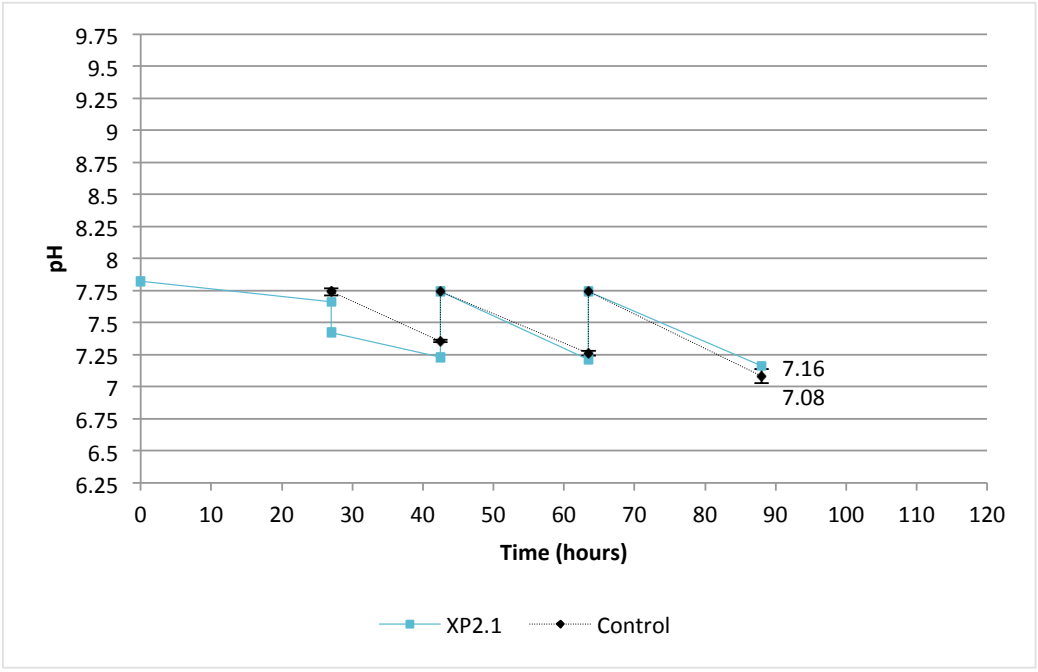

Figure 3.11: Regulation through discontinuous mixing (XP2) offline pH readings

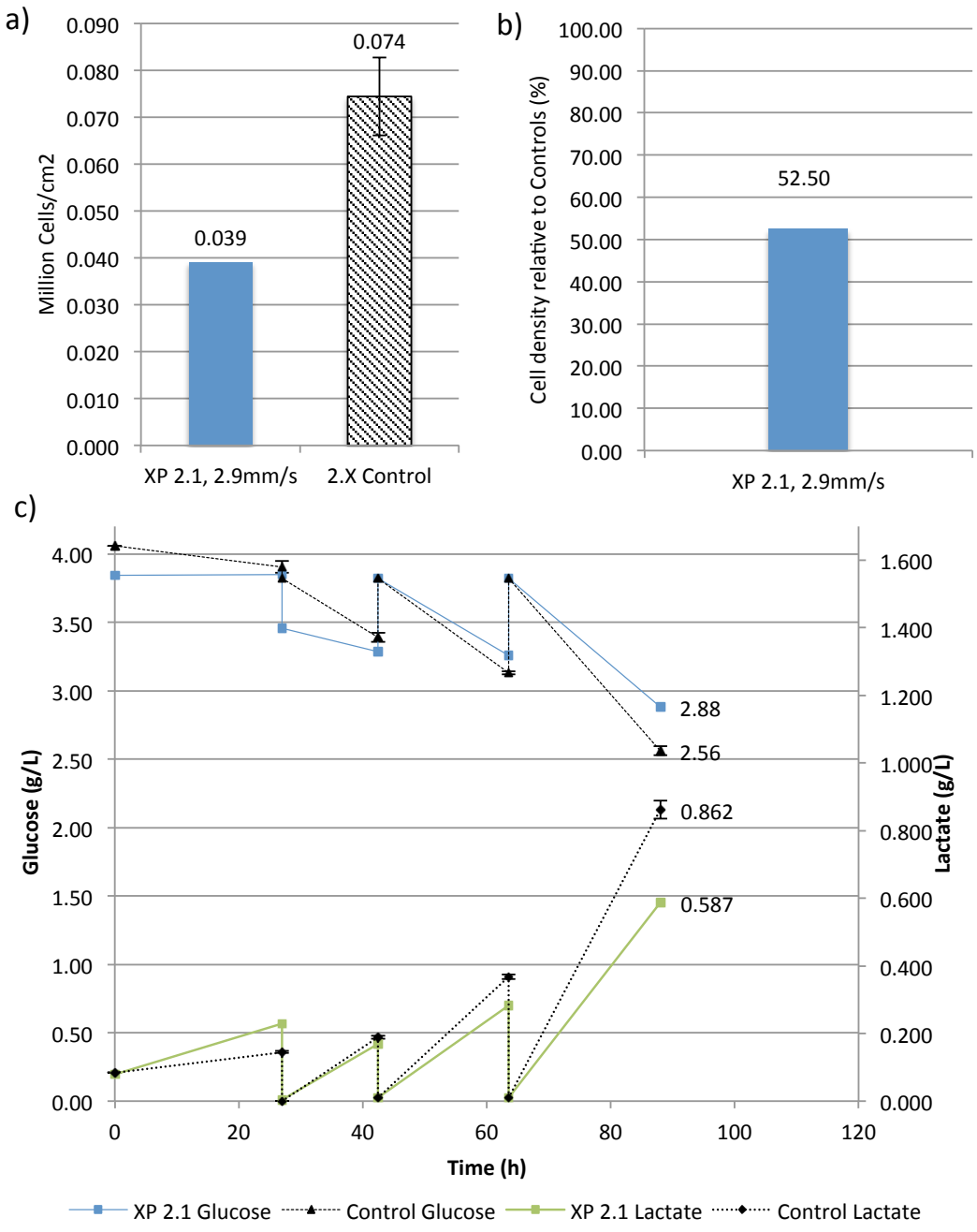

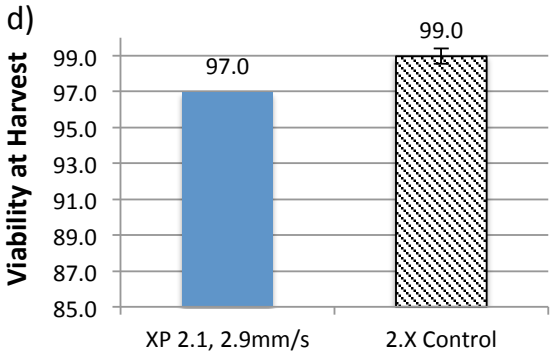

Figure 3.12: Results for regulation through discontinuous mixing (XP2). Harvest density a), performance relative to controls b) Glucose and lactate levels' c) and viability at harvest d).

a)

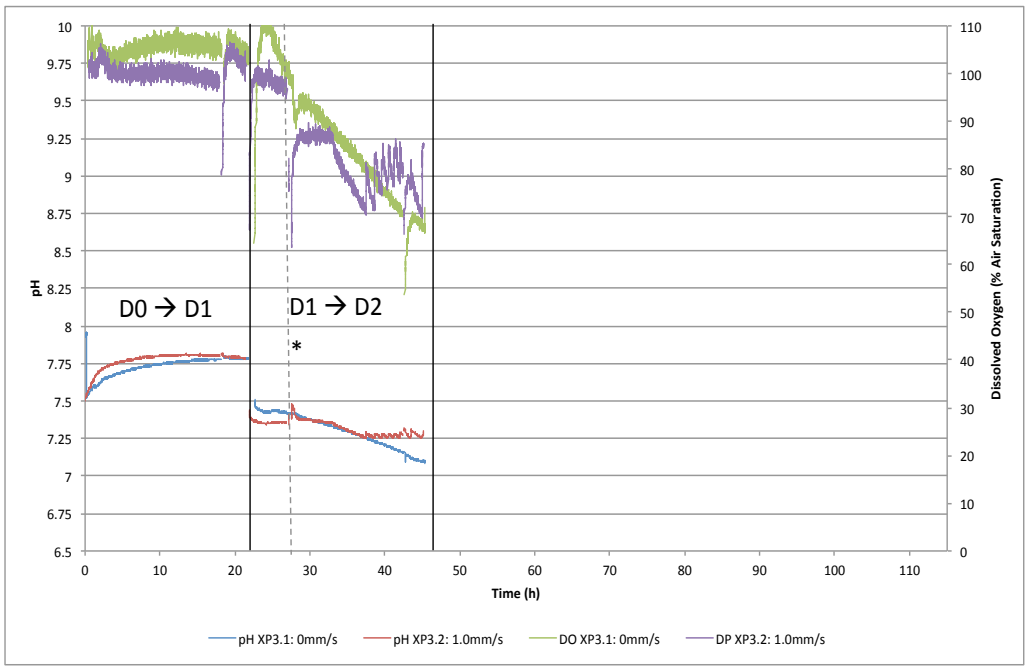

b)

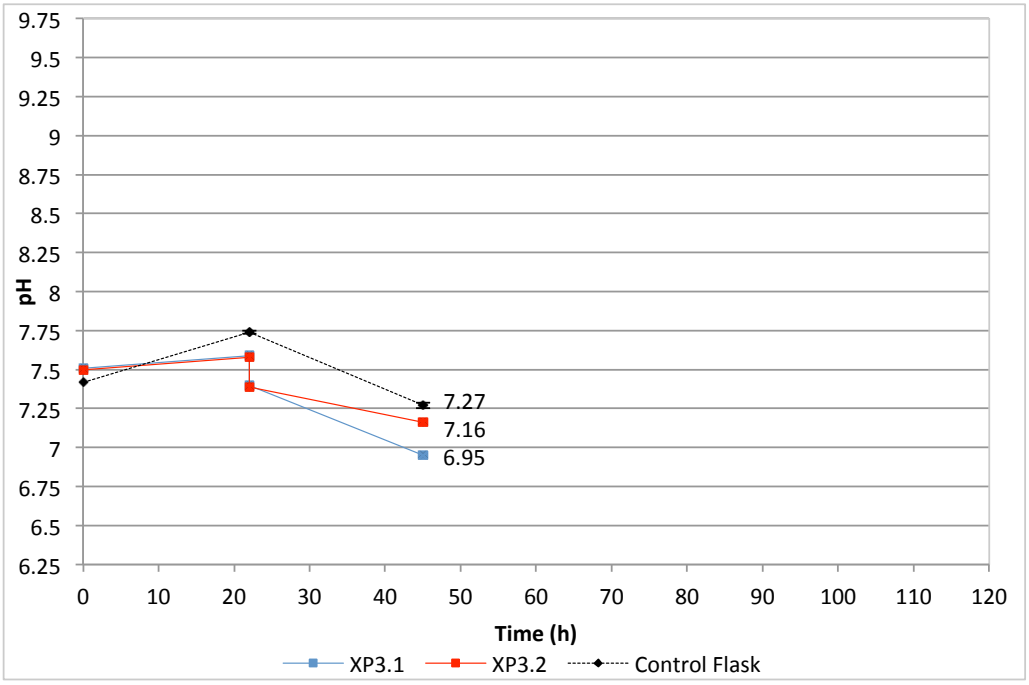

Figure 3.13: Initiating regulation earlier (XP3) pH and DO readings. Online readings a) offline pH readings b)

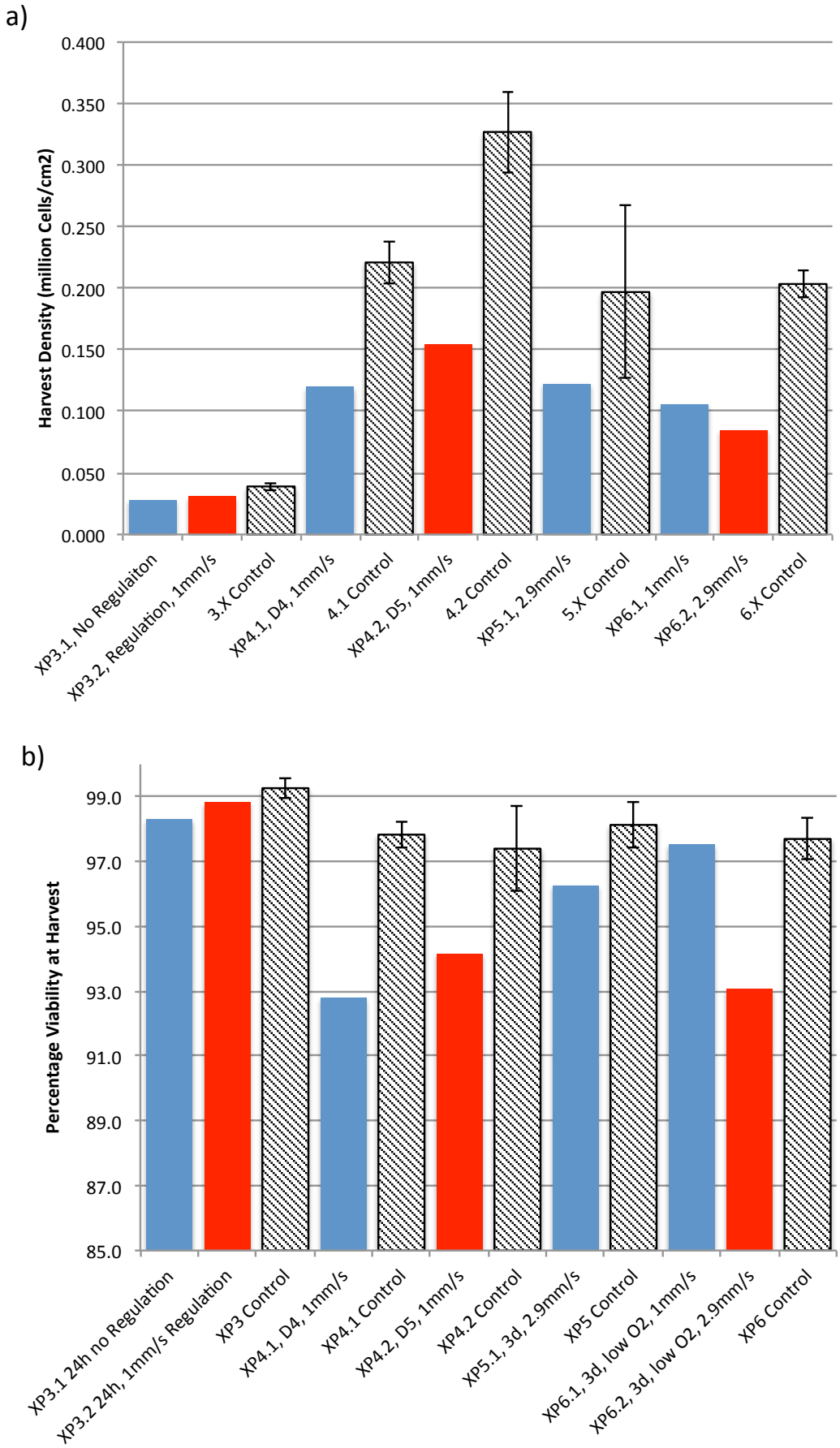

Figure 3.14: Harvest densities and viabilities for all experiments seeded at 20,000 cells/ cm^2. Harvest densities a), harvest viabilities b).

a)

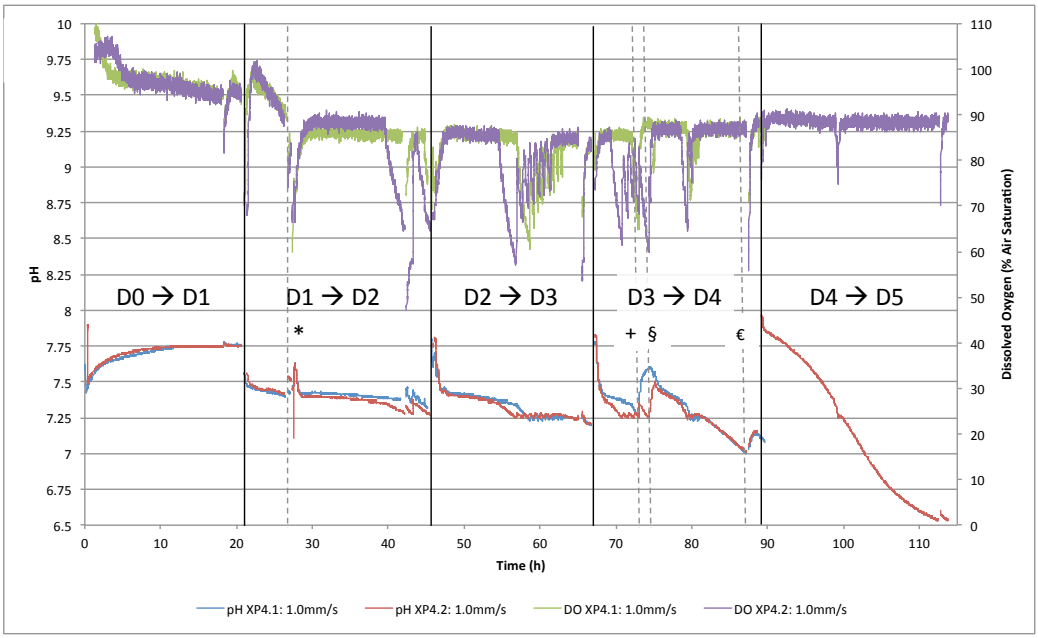

b)

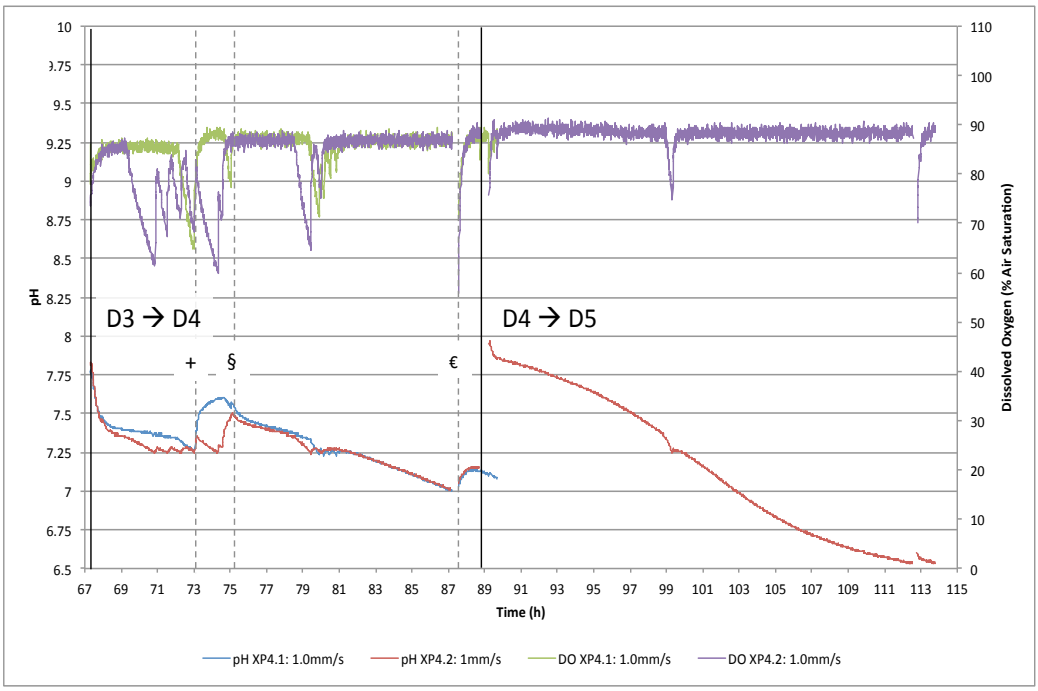

Figure 3.15: Increasing the expansion time (XP4) online pH and DO readings. Readings over the entire time course a), the dotted line marked with * denotes when regulation was started. An enlarged plot of the last 48 hours during which incubator $C0_2$ was reduced b). The dotted line marked + is the time at which the CO_2 was reduced from 5% to 2%. The dotted line marked § is where the CO_2 was raised to 3% out of concerns the pH was rising to far above the set point. The final dotted line marked € represents where the CO_2 in the incubator was reduced to 1%.

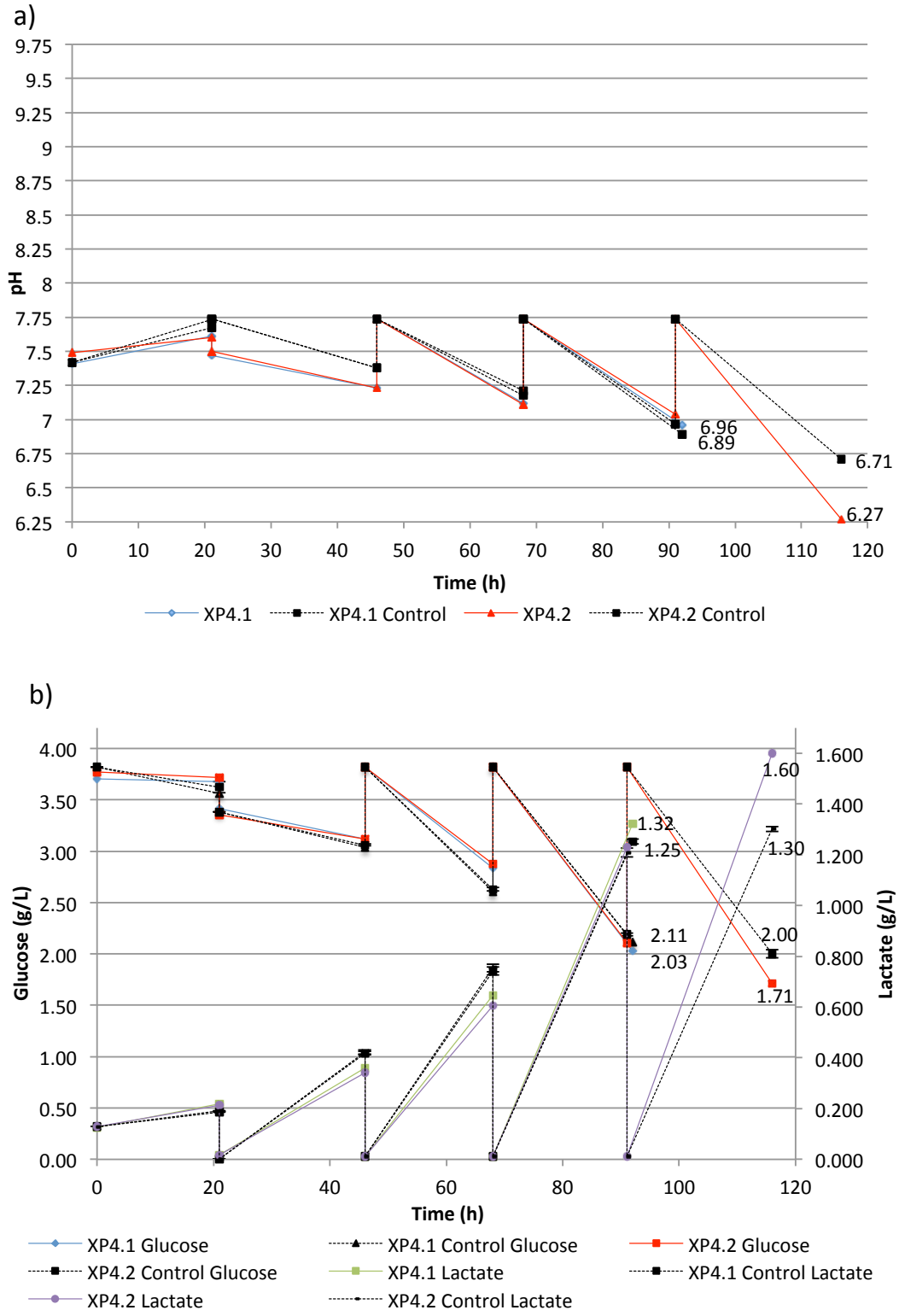

Figure 3.16: Offline pH and media analysis of readings from Increasing the expansion time (XP4). Offline pH a), glucose and lactate levels b).

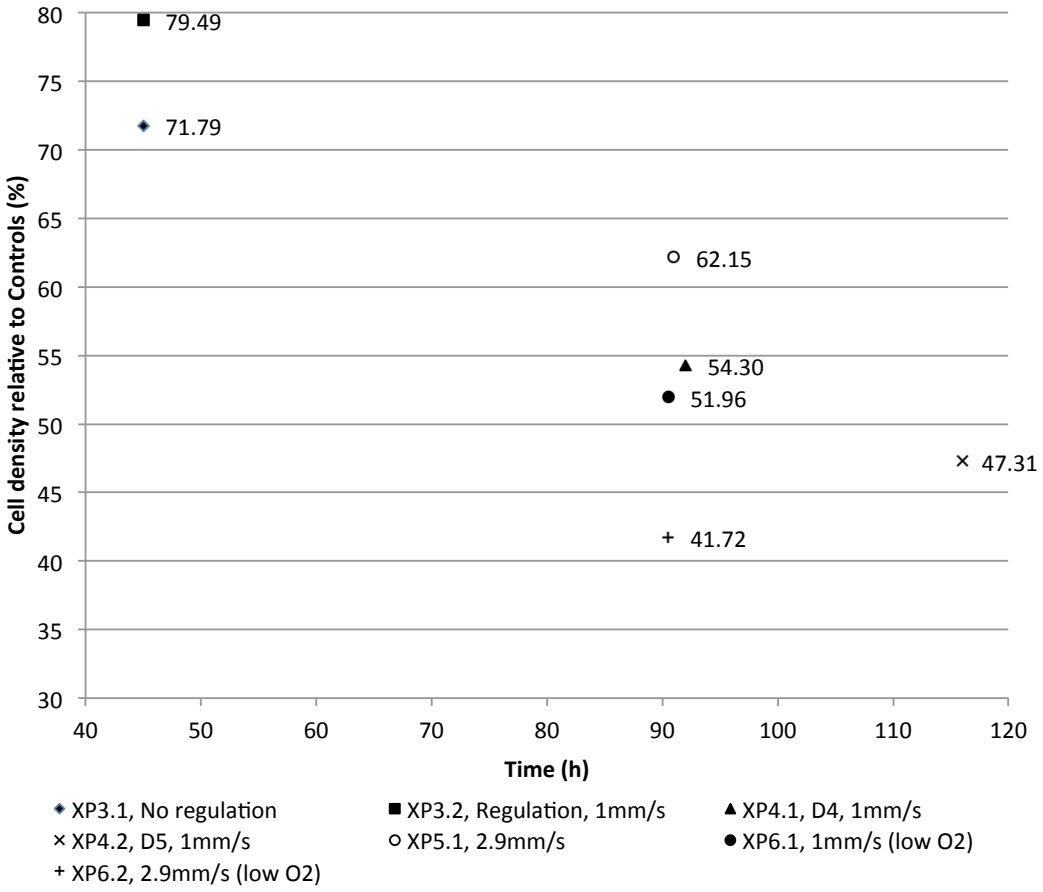

Figure 3.17: XP cell density relative to controls against time for all experiments seeded at 20,000 cells / cm^2

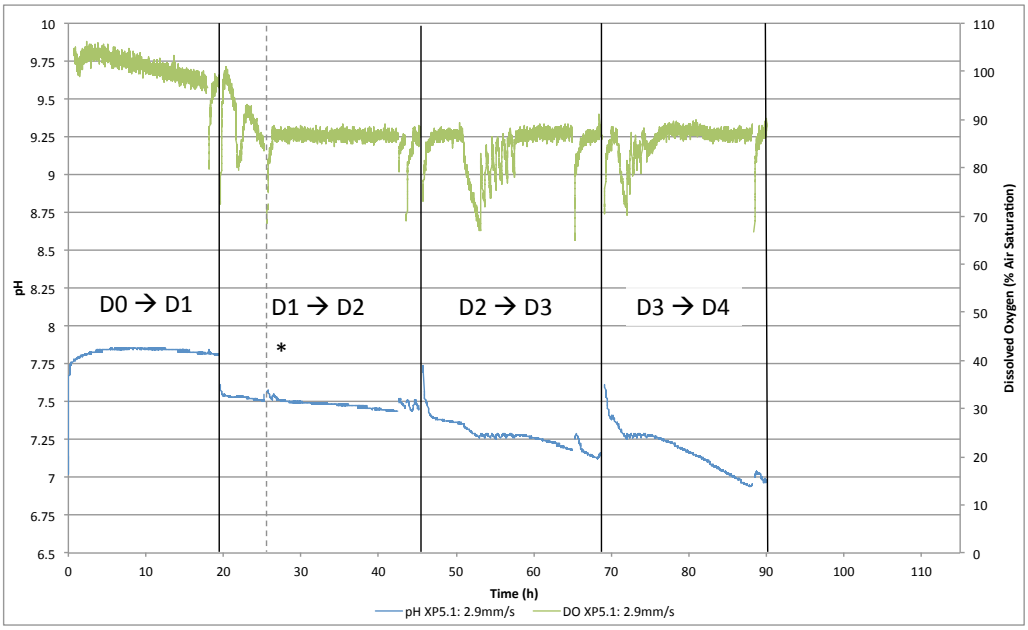

Figure 3.18: **Increasing the regulatory flowrate (XP 5) online DO and pH readings**

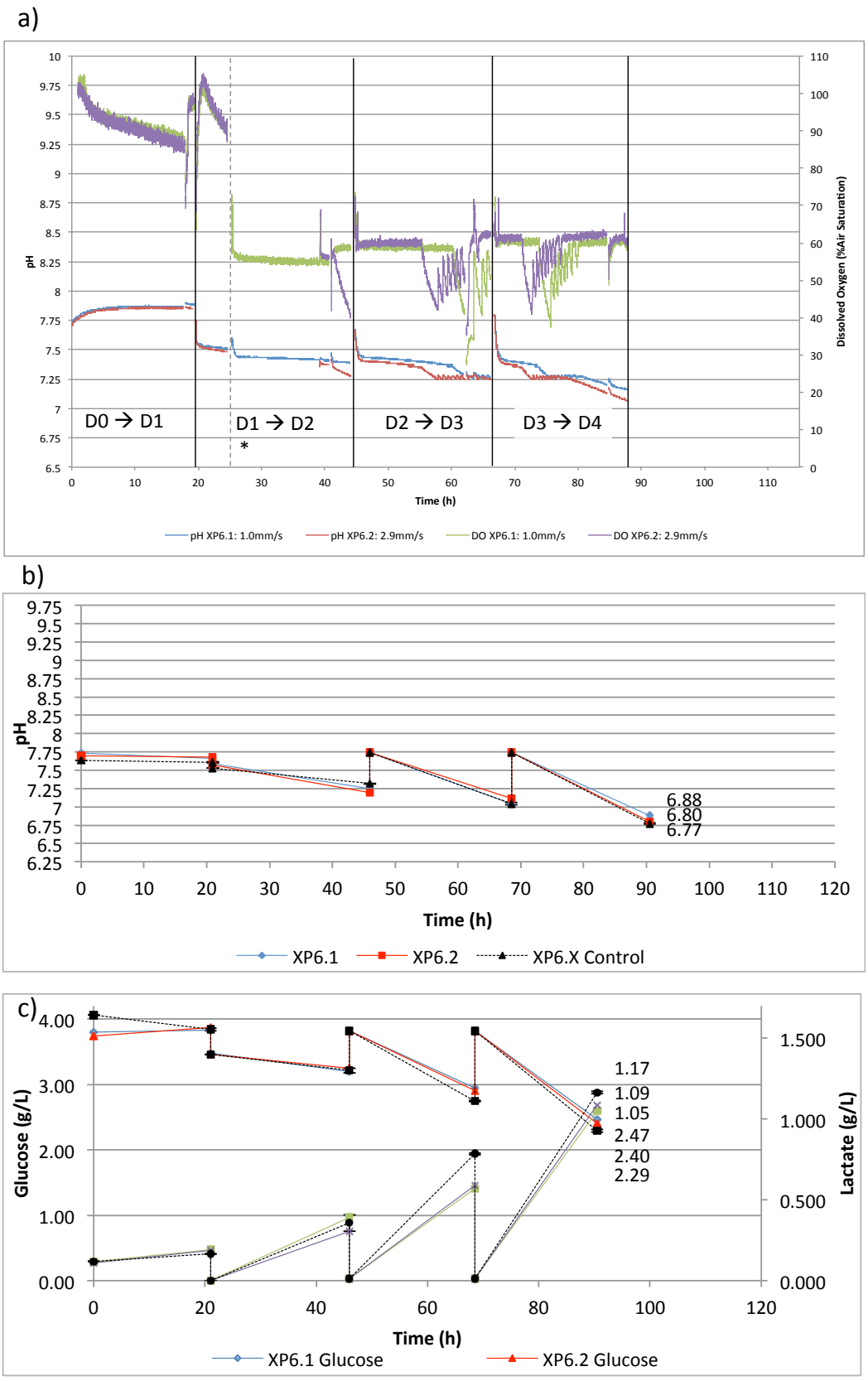

Figure 3.19: Results from determining whether oxygen supply is growth limiting (XP 6). Online pH and DO a), Offline pH readings on spent media b), and glucose and lactate levels c).

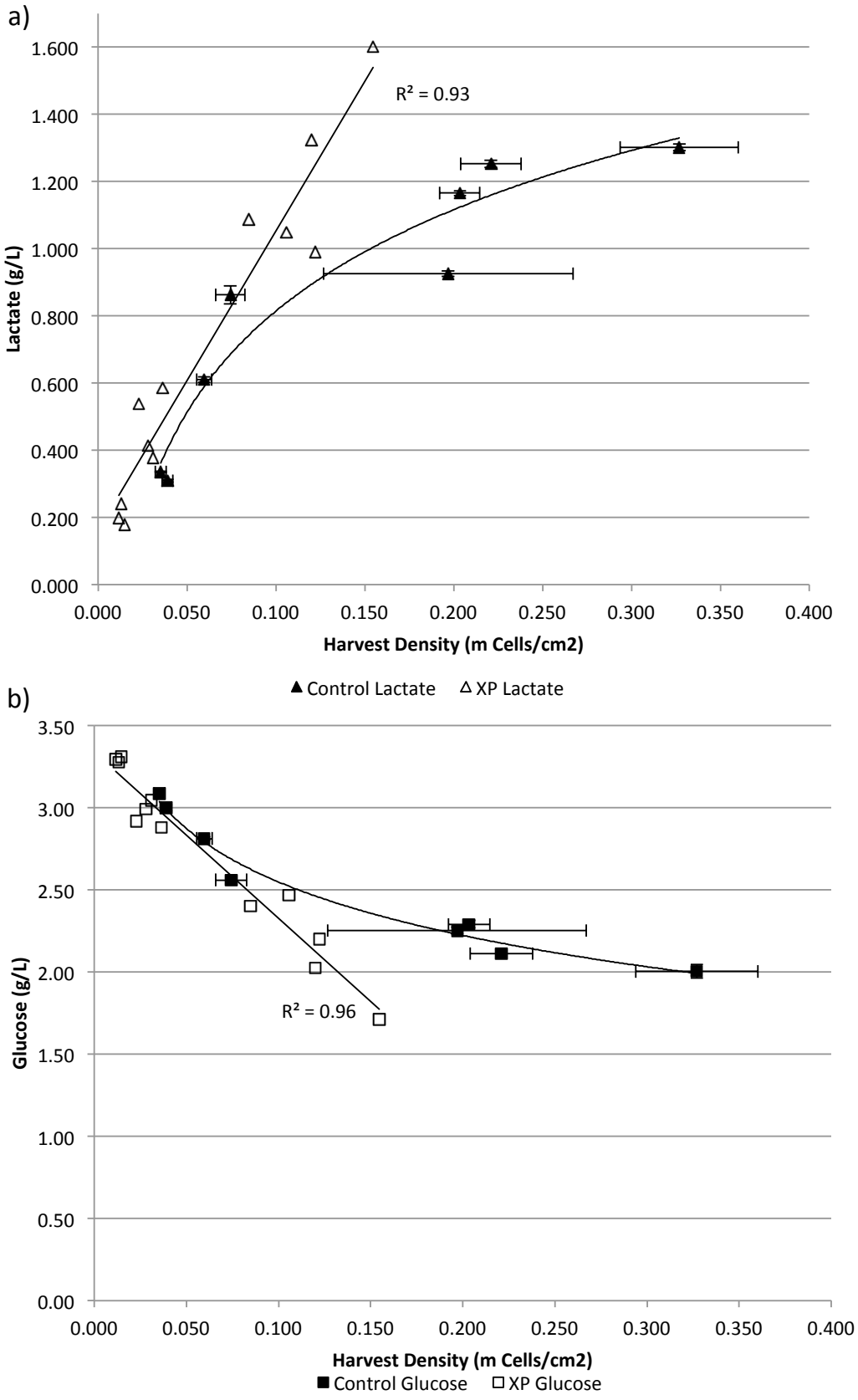

Figure 3.20: Further analysis of the metabolic activity of the cells. lactate a) and glucose b) concentrations at harvest against harvest cell density for all experiments seeded at 20,000 cells / cm^2

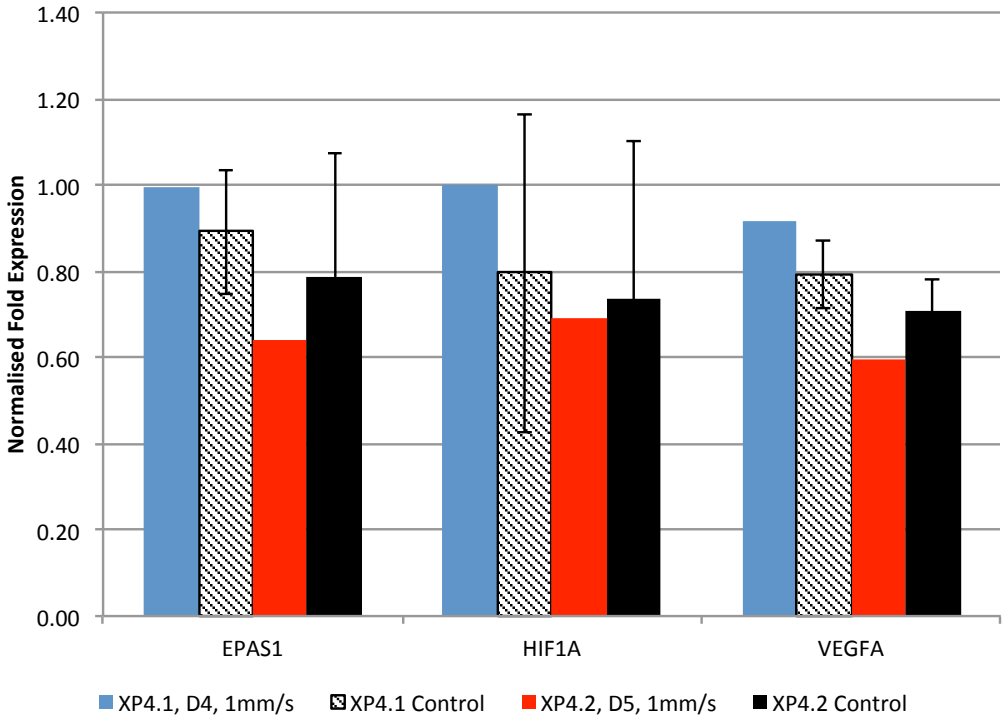

Figure 3.21: **Expression of the hypoxia related markers *EPAS1*, *HIF1A* and *VEGFA* on cells harvested from XP4.** XP4.1 (D4) and XP4.2 (D5) compared to triplicate T25 flask controls seeded at the same density (20,000 cells / cm^2. Error bars represent standard deviation of triplicate flasks. NB no significant difference between XP4.1 and XP4.2 for any of the genes using 1-way ANOVA.

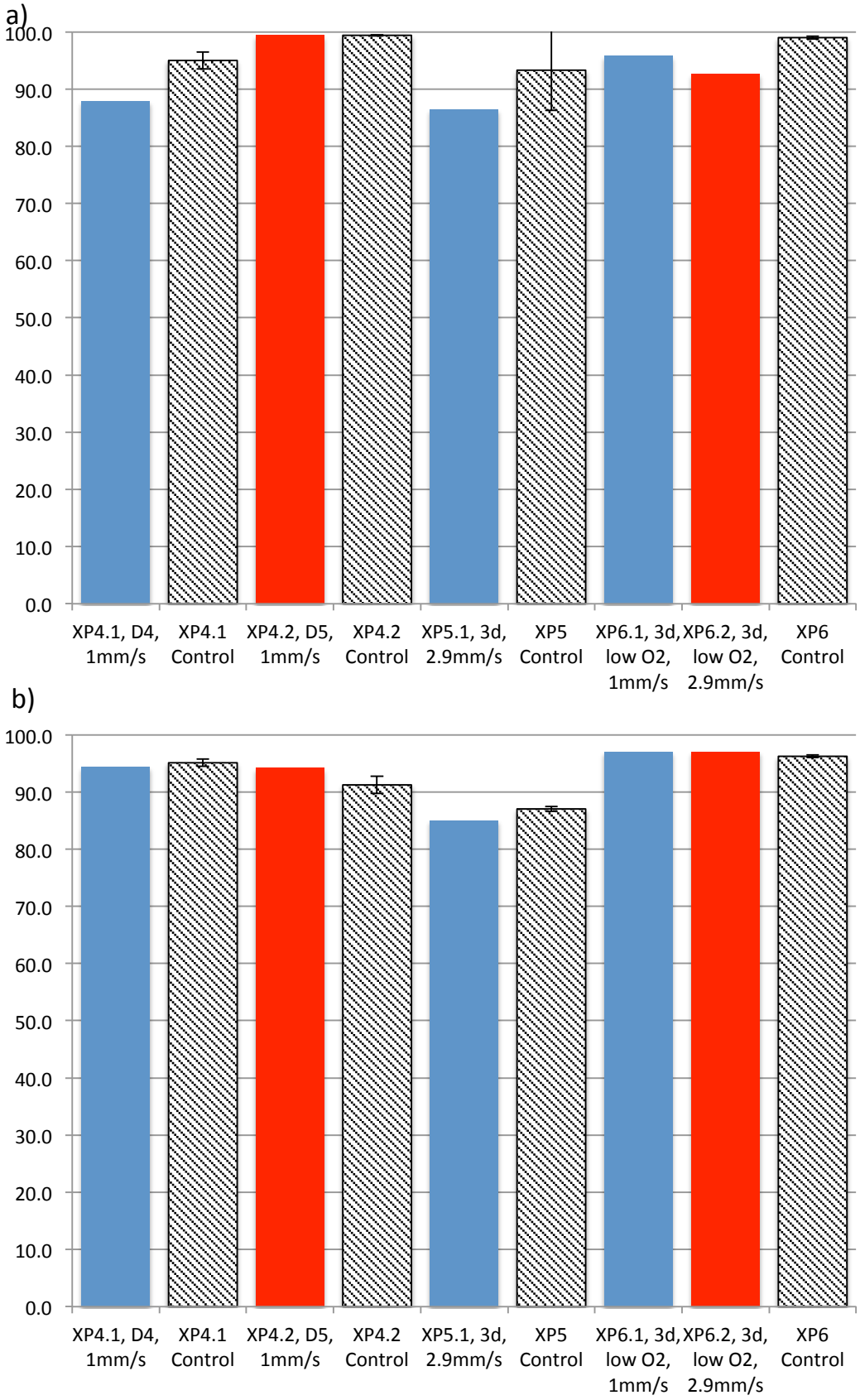

Figure 3.22: **Expression of the pluripotency markers as determined via flow cytometry at harvest for all experiments seeded at 20,000 cells / cm2**. SSEA-4 a) and TRA 1-60 B)

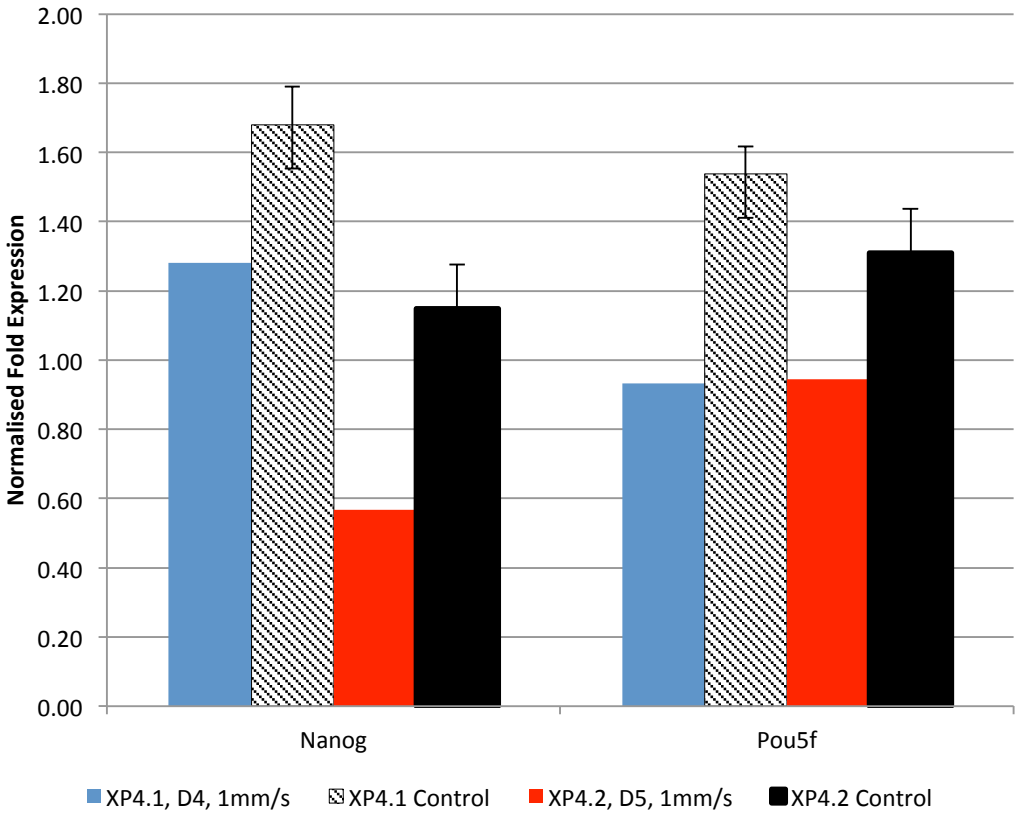

Figure 3.23: Gene expression of the pluripotency markers *nanog* and *POU5F* on cells harvested from XP4.1 (D4) and XP4.2 (D5) compared to triplicate T25 flask controls seeded at the same density (20,000 cells / cm²). Error bars represent standard deviation of triplicate flasks

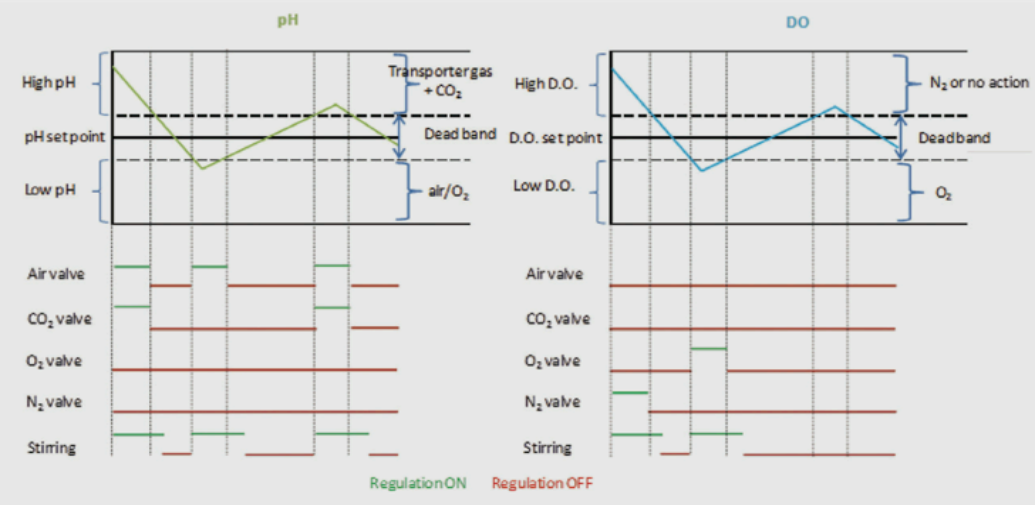

Figure 3.24: Illustration of pH and DO regulation using the Integrity Xpansion system. The following is replicated from the Xpansion User manual. *Regulating the pH value*: when the pH value is high the controller has to inject CO_2 in order to decrease the pH value. The controller injects a mix of two gasses a transporter gas (which may be O_2, air or N_2 depending on the DO value) and CO_2. When pH is low the controller injects air or O_2 (depending on the O_2 value) in order to strip excess CO_2. Regulation stops once the pH value returns to the dead band. *Regulating the DO value:* when the DO value is high the controller can either decrease it by injecting N_2, or let it fall without action until the DO value rests in the dead band. When DO value is low O_2 is then required. Regulation stops once the DO value returns to the dead band.

Table 3.1: Xpansion bioreactor sizes

Scale	Number of Plates	Growth Surface Area	Size (diameter x height)	Media Working Volume
Xpansion MPB-10	10	6350 cm^2	33 x 16 cm	1.7 L
Xpansion MPB-50	50	3,1800 cm^2	35 x 26 cm	6 L
Xpansion MPB-180	180	11,5000 cm^2	35 x 60 cm	18 L

Table 3.2: Experimental protocol for the Xpansion One system.

Day 0	• Plate coated with 0.1% gelatine for 30min • Mitomycin C inactivated MEFs seeded at 10,000 cells cm^{-2} • Optical sensors calibrated based on offline readings from excess cell suspension run through plate • Online pH and dissolved oxygen (DO) readings taken every 30 s
Day 1	• Spent MEF media analysed* • hESC Seeded at 20,000 cells cm^{-2} • Seeded hESC media analysed • 6.5h post seeding control loop added and regulation started
Day 2	• Media exchanged at a ratio of 0.18ml/cm^2 • Spent hESC media analysed*
Day 3	• Media exchanged at a ratio of 0.18ml/cm^2 • Spent hESC media analysed*
Day 4	• Spent hESC media analysed*

4. A design of experiment (DoE) approach to retinal pigment epithelium differentiation

4.1 Introduction and aims

4.1.1 Limitations of the one factor at a time (OFAT) approach

Development of current differentiation protocols for stem cells are driven by a 'best guess' approach as to what factor should be explored and varied to try and optimise the process to deliver the target phenotype. These choices are normally informed by previous experiences of the research group or an understanding of *in-vivo* embryonic development combined with reviews of protocols published in literature. This often results in an experimental design that draws in on a limited amount of what are believed to be key factors which are varied over minimal ranges. However, very little of the design space is explored using this OFAT (one factor at a time) methodology **(Figure 4.1 a)**, and it does little to elucidate the impact of multiple variables impacting on one another. Thus OFAT design can be seen as an inefficient use of resources and prone to miss the true optimum.

4.1.2 The statistical design of experiments (DoE) approach

The alternative is to use a statisticaldesign of experiments (DoE) approach **(Figure 4.1 b)**. Here experiments are conducted around the possible design space changing multiple factors at the same time. Different DoE designs vary the number and position of these points allowing compromises between the coverage of the design space and the number of experiments required. The use of statistical packages such as Design-Expert (Stat-Ease) can determine the significance of a factor's impact on the desired response from these multiplexed conditions or 'runs'. In addition such packages can then model the interactions of factors over their ranges to produce a computer model to fit the experimental data. Such models can then be used to give an indication as to where the optimum combinations of factors lie and so positioning of the design/operation space. This is often represented as a 'heat map' or contour plot, which is then verified experimentally.

This statistical approach to experimental design has been employed for many decades in biotechnology, for instance, Haaland (1989) and Adrion (1984) used a computer assisted approach to optimise *in vivo* monoclonal antibody production. DoE is now a widely adopted tool in bioprocess development being used in combination with high throughput screening technologies. However, application of DoE to optimise processes in the field of stem cell research is at its relative infancy with minimal, but diverse, uses in the literature. For instance Ratcliffe et al. (2013) and Hunt et al. (2013) applied DoE to stem cell bioreactor operation, and Knospel et al. (2010) used the approach for the serum-free culture medium for mouse embryonic stem cells, whilst Li et al. (2012) explored matrix environment impact on neuronal differentiation of embryonic carcinoma cells and Decaris and Leach (2011) explored cell-secreted matrices for directing osteogenic differentiation in mesenchymal stem cells.

When attempting to scale up a lab protocol for clinical trials or commercial production there is often a poor understanding of factors that could have an impact on the performance and economics of the differentiation. For example, initial seeding densities, media volumes and regularity of media changes are seldom reported in the literature with little evidence of any attempts to optimise or understand their impact. Although such variables may seem trivial, at the research scale they are very important when exploring the cost economics of the large-scale process. For instance, initial seeding densities not only determine the seed chain requirements per batch but it can also impact the differentiation process itself, for example in neural differentiation of PSCs (Chambers et al., 2009).

4.1.3 Aims

The aim of this chapter was to explore the feasibility of applying the DoE approach to the screening and optimising of the PSC-RPE differentiation protocol. The specific objectives in applying the sequential DoE approach were:

- Conduct a "screening" experiment to determine which out of a large number of poorly understood variables had a significant impact on the differentiation efficiency.

- Use knowledge gained from the screening experiment to pick the most significant variables and conduct a second "optimisation" experiment of higher statistical resolution in an attempt to model the data so as to predict where the optimum differentiation conditions lay.

4.2 Materials and methods

4.2.1 Design of experiments software

Design-Expert 6 (Stat-Ease) was used set up the runs based on the chosen factors and resolution of the design. The software was also used to generate the models to fit the experimental data and determine its statistical fit as well as generating all the plots.

4.2.2 Flow cytometry

The anti-SSEA-4 PE conjugate (Millipore) antibody was used to determine pluripotency expression prior to seeding cells in the experiments. A 1% cut-off gate was implemented based on conjugated isotype controls. All samples where analysed using a Beckman Coulter Epics XL MCL flow cytometer, and Summit software.

4.2.3 qPCR

Following manufacturer's guidelines (all reagents used were from Qiagen), RNA was extracted using the RNeasy mini-kit and first-strand synthesised using the QuantiTect Reverse Transcription Kit. Quantitative PCR was carried out using the SYBR Green master mix in the CFX Connect Real-Time System (Bio-Rad). Reactions were run using the following QuantiTect Primer Assays, OTX2 (QT00213129), RAX (QT00212667), MITF (QT00037737), PMEL (QT00016149), RPE65 (QT00001351), BEST1 (QT00023282), TYR (QT00080815). Analysis of relative quantification used b-ACTIN (QT0000 95431), and UBC (QT00234430) to normalise expression against internal controls. Primer efficiencies were calculated using a cDNA dilution curve and analysed using Bio-Rad software.

4.2.4 Cell Culture

Two different iPS lines were made available for study. The BJ line used was created by the Moorefield's group (University College London) using the StemGent mRNA reprogramming method utilising Oct4, Klf4, Sox2, Lin28 and c-Myc to reprogram StemGent's BJ human fibroblast cell line created from human foreskin. The second line 'MSUH001' was derived in xeno-free conditions from 16 week gestation age foetal fibroblast cells (originally from ATCC) using the reprogramming factors Oct4, Sox2, Nanog and Lin28 and published as Ross et al. (2010). The line was created by the Cellular Reprogramming Laboratory at Michigan State University (USA) and deposited in the Banco Nacional De Lineas Celulares (Troncales), which is the Spanish stem cell bank. The MSUH001 was kindly supplied by Professor Jose B. Cibelli's group.

Both BJ and MSUH001 lines were maintained on matrigel (BD bioscience) using mTeSR 1 media (Stem Cell Technologies) and mechanically passaged according to manufacturer's guidelines. For the differentiation experiment cells were enzymatically detached using TrypLE Express (Life Technologies) and counted using a haemocytometer. Cells were seeded in mTeSR 1 media supplemented with 10μM ROCKi (Cambridge Bioscience) to aid cell attachment. The base differentiation media contained Knockout DMEM, (Life Technologies)(4.5 g D-glucose/L, + sodium pyruvate, -L-glutamine), 20 % Knockout Serum Replacement (Life Technologies), GlutaMAX, (Life Technologies), 0.1 mM b-mercaptoethanol, and 1 % 100 9 MEMNEAA (Life Technologies). This base media was supplemented with combinations and concentrations of the following based on the experimental design: human basic fibroblast growth factor (bFGF, R&D systems), IWP-2 (Sigma) and nicotinamide (Sigma). All media combinations were made in bulk and stored at -80^{o}C. Individual aliquots were then thawed on day of use to ensure there was no variation between different media used on different days due to any degradation of media components.

4.2.5 Image J analysis of percentage pigmentation

The tissue culture plates were imaged using an Epson Perfection V750 Photo Scanner. To account for heterogeneity in contrast across the wells images were taken in two different orientations. These images were then imported to Image J (National Institutes of Health) and converted to binary images based on a chosen threshold to select only the pigmented areas. This allows the determination of percentage coverage of pigmentation in a well. The method is similar to that reported by and validated against manual counts by Lane et al. (2014).

4.3 Results and discussion

4.3.1 Screening design

The application of the DoE approach to bioprocess optimisation normally follows two stages. First, a large number of potential variables are screened in a minimal set of experiments to determine which factors have the largest impact. Then, the interaction of factors is explored using a response surface design that produces a visual statistical model that can be used to determine the optimal operation space.

The number of factors chosen for the screen has a significant impact on the number of runs to be completed and so greatly impact the costs and practicalities of the experiment. For two level designs, i.e. where each variable is explored at it's maxima and minima the Stat-Ease software visualises the runs required in a table **(Figure 4.2)**. For example if 4 factors were to be explored at two levels 16 runs would be needed (2^4) or for 8 factors 256 runs would be needed (2^8), such designs are termed full factorial designs. The advantage of using DoE to screen variables is that these run numbers can be vastly reduced by decreasing the resolution of the design and so lowering the experimental effort. However, reducing the number of runs from the full factorial number also decreases the resolution which means that factors become aliased together. The lower the resolution the greater amount of aliasing. An example of aliasing for factors [A], [B] and [C] would be that the software would be able to say that either factors [A] and [B] have a significant impact on the result or

factors [A] and [C] do, but it would be unable to discriminate which combination is having the effect. Therefore either past experience or further experimentation can be used to decide on which alias is correct. In lower resolution designs only 2 factor interactions will be aliased e.g. [A] with [B] or it could be [A] with [C] having the effect. However, in higher resolution designs only 3 or more factor interactions will be aliased (2 factor interactions being fully resolved) e.g. [A] with [B] with [C] or it could be [A] with [B] with [D] having the effect. Such 3 factor combinations are rarely the biggest effectors on the result and so deemed acceptable in most screening designs.

Using the Stat-Ease Software it was decided that an 8 factor screening experiment at resolution IV would be a good test of the applying a DoE approach to PSC differentiation as this would explore a greater number of factors than normally published in the literature. From **Figure 4.2,** it can be seen that this requires 16 unique runs. In addition to this 4 centre points were used which are essentially 4 replicates of the middle values used for each factor. These centre points are used to determine the signal to noise ratio in the experiment and also determine curvature, i.e. where there is a non-liner relation between a factor and the desired response. Each run was also completed in duplicate and averaged before inputting into the software meaning 40 runs were required in total for the screening experiment. The aliases of the resolution IV design chosen are replicated below showing single factors only aliased with 3 factors interactions, and 2 factor interactions are only aliased with other 2 factor interactions. As the purpose of screening experiments is to determine the key single factor impacts on the differentiation before a subsequent optimisation experiment this resolution IV design was decided to be the best approach.

[A] = A + BCE + BDH + BFG + CDG + CFH + DEF + EGH

[B] = B + ACE + ADH + AFG + CDF + CGH + DEG + EFH

[C] = C + ABE + ADG + AFH + BDF + BGH + DEH + EFG

[D] = D + ABH + ACG + AEF + BCF + BEG + CEH + FGH

[E] = E + ABC + ADF + AGH + BDG + BFH + CDH + CFG

[F] = F + ABG + ACH + ADE + BCD + BEH + CEG + DGH

[G] = G + ABF + ACD + AEH + BCH + BDE + CEF + DFH

[H] = H + ABD + ACF + AEG + BCG + BEF + CDE + DFG

[AB] = AB + CE + DH + FG

[AC] = AC + BE + DG + FH

[AD] = AD + BH + CG + EF

[AE] = AE + BC + DF + GH

[AF] = AF + BG + CH + DE

[AG] = AG + BF + CD + EH

[AH] = AH + BD + CF + EG

4.3.2 The two common methods of PSC to RPE differentiation

There are a large number of published protocols for the differentiation of PSC to RPE as summarised in the literature reviews of Ramsden et al. (2013) and Rowland et al. (2012). These are split into two main methodologies, the first being the spontaneous adherent based method where hESC colonies are allowed to become super-confluent and then bFGF is removed, with the cultures then being maintained for a number of weeks before pigmented foci of RPE are observed (Klimanskaya et al., 2004, Lund et al., 2006, Vugler et al., 2008). This is the methodology followed by the London Project to Cure Blindness that this thesis is in collaboration with and so is the basis of the protocol used in this Chapter. The alternate method involves allowing dissociated hESC colonies to form aggregates in suspension which are then maintained for similar time periods prior to re-plating (Meyer et al., 2009).

4.3.3 Choosing factors for the PSC to RPE screening experiment

There are a large number of potential factors that could impact the efficiency of the differentiation. A common tool to visually represent and categorise factors likely to impact on a system is the Ishikawa diagram (see **Figure 4.3**). For the PSC-RPE differentiation the main categories impacting differentiation were chosen to be media components, timings (e.g. differentiation periods), materials (e.g. feeder free systems), the cells (e.g. cell line), the environment (e.g. DO) and media volumes (e.g. amount of media fed to the cells). Further consideration of these broad categories yields tens of potential factors that could impact the

differentiation, all of which could be varied over a number of levels in combination with each other. Therefore a search of the literature and past experience was used to select the 8 factors used in the screening experiment. Some of the factors were also chosen due to their impact on the economics of the process.

There have been a number of media components that have been supplemented or removed from the media to try and increase the differentiation efficiency. For instance Vugler et al. (2008) found that there was no significant improvement in the differentiation through the removal of bFGF. This is despite evidence in the embryology that the absence of FGF in development results in poor regionalisation between RPE and neural retina, a result that can be reversed with exogenous application of FGFs in mouse eye development (Nguyen and Arnheiter, 2000). Given the expense of bFGF and that its removal is the only media component changed in the current clinical protocol of the Moorfields group (to save costs), it was decided to chose bFGF for the screening experiment to validate this decision. An upper concentration of 8ng/ml of bFGF was used **(Figure 4.4),** as this is the same used in the expansion media.

Other signalling molecules such as DKK-1 (Wnt inhibitor) and lefty-A (Nodal inhibitor) have been added at the start of differentiation protocols (~first 20 days) to drive the differentiation towards eye field development, increasing expression of retinal progenitor markers such as RAX and MITF which is an RPE progenitor cell marker (Osakada et al., 2009a, Hirami et al., 2009, Nistor et al., 2010). However, these factors are very expensive and so not desirable when scaling up the process. Interestingly, the use of cheaper small molecules has also shown to increase RPE differentiation efficiency, for example Osakada et al. (2009b) used the casein kinase I inhibitor CKI-7, the ALK4 inhibitor SB-431542 - to inhibit Wnt and Nodal signalling respectively. With this in mind, another Wnt inhibitor IWP-2 was selected as a factor for this screening experiment, as this has not been used in RPE differentiation before but has been used in cardiomyocyte differentiation from PSCs (Lian et al., 2012). IWP-2 Inhibits both Wnt processing and secretion by inactivating Porcn, a membrane-bound O-acyltransferase (MBOAT) which selectively inhibits palmitoylation of Wnt. A concentration of 10μM IWP-2 was chosen as this would mean the centre point of the

design would be 5μM which matches published levels **(Figure 4.4).** IWP-2 was only added for the first 20 days of the differentiation to match the protocols using DKK-1 and the casein kinase I inhibitor. The timing of the addition of these factors being critical as Nakano et al. (2012) showed that only the addition of CHIR99021 (GSK3β inhibitor and Wnt agonist) later in differentiation from days 18-21 increased MITF expression. Nicotinamide is the amide of nicotinic acid (vitamin B3/niacin) and us a PARP-1 inhibitor. It is another inexpensive small molecule that was shown to significantly increase RPE gene expression (Idelson et al., 2009), yet its use had produced variable results by this research group in the past and so was chosen as another factor to include in the media **(Figure 4.4)**.

Seeding density has been reported to have a significant impact on differentiation efficiency for instance, Chambers et al. (2009) reported that the initial seeding density of PSC onto matrigel determined the ratio of central nervous system and neural crest progeny with an ideal cell density being 18,000 cells/cm^2. For the screening experiment a range between 10,000 and 25,000 cells/cm^2 **(Figure 4.4)** was chosen based on past experience.

From initial work on the RPE-PSC differentiation there appeared to be a relationship between the confluence of the culture at the time of switching to the differentiation media and the differentiation efficiency. The protocol published by Vugler et al. (2008) making the switch when the cultures had become "super" confluent, whereas Lane et al. (2014) made the switch uniformly at day 10. As the degree of confluence is a function of both time and seeding density, it was decided to also vary the time at which this switch was made to see if there was indeed an interaction. High and low values were chosen of 14 and 7 days **(Figure 4.4).**

Factors which are often poorly reported in the literature but have a significant impact on the economics of the process, are the volumes and regularities of media changes; media being a significant cost of goods component in these therapies. Furthermore, discussion with those working on the PSC-RPE protocol led to the discovery that various researchers at the London project were using a wide variation in media volumes and regularity of media changing. A common rationale was that when differentiating the PSC culture the media

should be changed infrequently to stress the cells into differentiating, and to concentrate any signalling factors. To explore whether media volume or frequency of media changes had an impact these were also varied in the screening experiment. The volume of media per change was varied between 4 and 3 mL in a single well of a 6 well plate, and the frequency varied between every day feeding and every third day feeding **(Figure 4.4).**

Finally, two separate cell lines were used to see if the same factors had a significant impact for both lines. The lines used were both iPS lines, namely BJ and MSUH001. They were maintained in a feeder free culture using the mTeSR material system in an attempt to reduce potential variation from the MEF-PSC co-culture system used elsewhere in this thesis. The total protocol was run for 49 days to allow sufficient time for pigmented RPE foci to appear even in conditions where efficiency might be low or subject to an initial lag phase due to a later switch to differentiation media.

To complete the screening experiment as described 20 runs were conducted in experimental duplicate (40 runs in total) and inputted into the Design Expert software **(Figure 4.5).** Triplicate data points were considered but this was not considered to be practically feasible. This design was on the limits of what was practically possible to handle as a single individual working in a lab. It required 14 different types of media to be made and delivered to different wells, on different 6 well plates, in different volumes on different days, over a 49 day protocol. The well plan for the experimental protocol is represented in **Figure 4.6.**

4.3.4 Results and discussion of the PSC to RPE screening experiment

Both the BJ and MSUH001 lines were tested for the SSEA-4 pluripotency marker via flow cytometry when seeded and were found to have expression levels of 95% and 94% respectively, demonstrating a high degree of pluripotency. Both lines had been previously maintained using manual colony dissection but showed good replating efficiency after enzymatic dissociation with the TrypLE Express (life technologies) enzyme and supplementing the media with ROCK inhibitor. The earliest point at which the switch was made from the mTeSR pluripotency media to the differentiation media was 7 days. From

Figure 4.7 a) and **b)** it can be seen that both lines were highly confluent at the D7 time point, however the BJ line appeared to have slightly quicker growth judging by the D4 time point.

A large amount of data was obtained for the 20 duplicate runs (40 experimental runs in total). Gene analysis focused on the RPE related genes *BEST-1, MIT F, PMEL 17, TYR, RPE 65* and the eye field related genes *OTX 2 and RAX*. This data was inputted into the Design Expert software and initially tested using the Half Normal Plot and Pareto Charts. The Half Normal Plot involves selecting factors which have the greatest impact on the response gene e.g. *OTX 2* (See **Figure 4.8**) to leave those which do not have a significant impact on the response clustered along the remaining straight line (which is a representation of experimental noise). The Pareto Chart (See **Figure 4.9**) is an alternate representation of this same selection process to confirm the factors chosen are above the statistical limits of significance. Unfortunately, despite obtaining data for all 7 genes in the 20 duplicate runs (40 in total) only *OTX 2* and *TYR* passed these first tests in the Design Expert software. There was no describable expression for *RPE 65* gene response to be entered into the screening model. The F values for these genes which passed the significance levels from the Pareto Chart are displayed in **Figure 4.10.** The F values are colour coded depending on whether they were greater than the t-limit or greater than the Bonferroni limit. The Bonferroni limits controls for family wise error rate which is an issue when multiple hypothesis are in a single test. From a desired outcome perspective, *TYR* expression is more important than *OTX 2* as it represents a gene involved in melanin synthesis and so indicative of RPE formation. Whereas, *OTX 2* is an eye field marker involved in RPE development but is also expressed in a number of forebrain derivatives and so not as specific for RPE (Larsen et al., 2009). Eye filed genes such as *OTX 2* and *RAX* had been included in the analysis to see if any inverse trends with the RPE specific genes could be determined.

From **Figure 4.10** it would appear that seeding density has a positive impact on both *OTX 2* and *TYR*, and that nicotinamide could potentially have a positive impact on *TYR*. There also appears to be some support for the hypothesis that feeding cells less often increases the

differentiation efficiency, judging by the response for differentiation media volume and regularity of media change on *TYR* expression. Spent media was analysed for pH, glucose and lactate at several time points (using a YSI 2700 media analyser) and fed into the Design Expert software to see if any other information with respect to media volumes and regularity of media volume could be elucidated, however all this data also failed the statistical tests. The use of IWP-2 had a negative impact on *OTX 2* and *TYR*, with these cultures also producing a large amount of spontaneously beating cardiomyocytes suggesting the cultures had not been efficiently driven down the neuroectoderm lineage. The growth of cardiomyocytes was understandable as IWP-2 has been shown previously to optimize cardiomyocyte differentiation in PSCs (Lian et al., 2012). It could therefore be that this small molecule has other effects in addition to being a Wnt inhibitor which makes it an unsuitable replacement for expensive factors such as DKK-1 in RPE differentiation protocols.

The results of the percentage pigmentation analysis are shown in **(Figure 4.11).** When this data was imported into the Design Expert software it could be seen that increasing both seeding density and increasing bFGF both had a negative impact on percentage pigmentation (analysis performed using Software's user guides). This is an important result as it was previously unclear whether the removal of bFGF had any clear impact on the differentiation efficiency, it being removed from the differentiation media on primarily cost grounds. With bFGF being the most expensive part of the culture media showing that its inclusion has a deleterious impact on differentiation could mean significant savings as the process is scaled up.

The chosen factors for each specific response were then imported into the ANOVA analysis section of the software analysis tool. The aim of this part of the tool is to match the data with a computational model. Unfortunately for the data highlighted in **Figure 4.10,** none of the proposed models passed the software's tests for significance. The only response which did pass the tests and could be modelled was the *OTX 2* response. However as this gene is not-RPE specific to the desired mature RPE phenotype the results are not discussed here.

As only the 3 responses of i) percentage pigmentation, ii) *OTX 2* and iii) *TYR* were compatible with the DoE software the raw data for all responses was also plotted (see **Figures 4.11**, **4.12, 4.13**). From these plots it is clear that Run/condition 4 was clearly the superior condition with high expression of the RPE markers particularly those markers representative of the mature RPE phenotype such as BEST-1. The condition for Run 4 used the MSUH001 line, without bFGF, and differentiation was started at the shortest time point of 7 days but at the highest seeding density of 25,000 cells/cm^2. The condition was also supplemented with the highest amount of nicatinamide (20μM) and without IWP-2. Interestingly, if only the Design Expert software had been relied upon in isolation this Run 4 condition, which showed the best result, would not have been flagged for further investigation. This is because the software takes a holistic approach to analysing the data looking for trends, this means single point outliers are not immediately obvious. Especially if the response was excluded from the analysis as it failed to meet expectance criteria for to be modelled. For instance the response could be very low and so fail the signal noise ratio in most of the runs, yet due to serendipity of the conditions chosen a very high response might be seen in just one condition.

4.3.5 Lessons learned from the PSC to RPE screening experiment

Applying the DoE approach to screen a large amount of variables for the PSC-RPE differentiation proved to be problematic, not just in generating data that passed the software's statistical tests but also the practicalities of completing the experiment. The complexity of using 14 different types of media in 40 different conditions, being fed on different days, different volumes of media over a 49 day protocol was perhaps underestimated. It was disappointing that a large amount of the data could not be used in the analysis software, this included not only the majority of the RPE genes of interest but also the spent media analysis. However, considerable insight was gleaned into factors influencing the differentiation process.

The inability of the data to satisfy the requirements for a statistical model could be due to a number of reasons. The most probable reason is the signal noise ratio of the experiment

was too low. The centrepoints are essentially technical repeats of the same condition to access the "noise" of the experiment. This noise is then compared to the "signal" obtained from one of the experimental conditions. If the noise is high for example due to the high amounts of variability in PSC differentiation or if the signal is low e.g. the gene expression varies little, there will be a low signal noise ratio and the data will therefore fail the significance tests.

It was the original intention to use the screening experiment to select the factors of greatest impact on the PSC-RPE differentiation to inform the design of the optimisation experiment. Even though the data generated from the screen could not be used to create a statistically valid model to fit the data it did confirm that the seeding density, time to differentiation and nicotinamide may have an impact on differentiation efficiency. Therefore, these were the 3 factors chosen and taken forward to the optimization experiment as planned.

4.3.6 Central composite design for the PSC-RPE differentiation experiment

For the optimization experiment a central composite design (see **Figure 4.1 b**) was chosen to carry out a full factorial experiment to allow the estimation of second order relationships between the factors and target result as part of response surface methodology (RSM). This is similar in many ways to the screening design used in that a number of centre points are used to determine the noise of the experiment, then each factor is varied at both high and low iterations. However, axial points are also used. These points essentially sit outside the box (**Figure 4.1 b**) and are identical to the centre points except for 1 of the factors that is varied to a value sitting outside of the high to low range. This high/low range is visually represented as the sides of the box, and the axial points sitting off these faces (**Figure 4.1 b**). For this response surface design, a full factorial experiment was used which means that every combination of factor is experimentally tested meaning there is no aliasing of the data.

For the optimisation experiment Run 4 from the screening experiment was used as a baseline. Also to reduce the experimental effort only the MSUH001 line was used. It was

decided to feed the cells 3mL of media every third day as the screen showed this did not have a negative impact on the differentiation (compared to feeding cells 4mL every day). Such a feeding regime would lead to savings if the process was scaled up. Further decreasing media volumes, or decreasing feeding regularity in the optimisation experiment was not explored as there was already a very high amount of cell death and very low pH's produced in the screen (as low as 6.5). Thus reducing the amount of media fed to the cultures any further could lead to total cell death in the Run(s) which would lead to missing data points.

In the screening experiment, nicotinamide was varied between 0-20 mM which appeared to have some positive impact on *OTX 2* and *TYR* **(Figure 4.10)**. It was thought that greater concentration of nicotinamide could increase this further and so in the optimisation experiment a range of 10-30mM nicotinamide was used **(Figure 4.14 a).** Altering seeding density also impacted the expression of *OTX* and *TYR.* Yet, somewhat counter intuitively, it appeared to have a negative impact on percentage pigmentation (**Figure 4.10**). The paper by Lane et al. (2014) reports findings based on single cell seeding of PSCs at various densities for the PSC-PRE differentiation in a feeder free system. They reported not only that single cell seeding produced better yields than traditional manual passaging of colony clumps, but in addition increasing seeding density from 17,000 cells/cm^2 to 35,000 cells/cm^2 increased the pigmented surface area five-fold. However, at seeding densities greater than 35,000 cells/cm^2 RPE differentiation was arrested. Therefore, for the optimisation experiment the seeding density range was widened from the 13,000 cells/cm^2 to 25,000 cells/cm^2 used in the screen (**Figure 4.5**) to 13,000 cells to 37,000 cells/cm^2 for the optimisation experiment **(Figure 4.14 a).** Finally, the range of time passed prior to the switch to differentiation media was also changed for the optimisation experiment. In the original screening experiment the earliest change to differentiation media was day 7, at which point all the conditions were fully confluent **(Figure 4.7).** Based on previous work (data not shown) interesting results had been obtained when the switch was made prior to confluency. Therefore, the range was changed from the high and low values of 7 and 15 used in the screen (**Figure 4.4)** to 3 days (72 hours) and 11 days (264 hours) in the

optimisation experiment (**Figure 4.14 a**). The upper limit was reduced from 15 to 11 as from looking at the raw data the 15 day cultures had no clear improvement over the others and 11 days is closer to the standard protocol used with success in the Moorfields group.

Using the Stat Ease software the 3 factors of i) time to differentiation, ii) nicotinamide concentration and iii) seeding density were inputted into the Central Composite design builder (**Figure 4.14**). As the alpha values sit below the lower and upper range of the values chosen the true range of the experiment is actually larger. For instance the chosen range of seeding density was 13,000 cells to 37,000 cells/cm^2, however, due to the alpha values the lowest seeding density to be experimented with was 4,819 (-alpha) and highest 45,182 (+alpha). For the time to differentiation factor the –alpha was only 6.55 hours, this meant that the media mTeSR media containing ROCK inhibitor in which the cells were seeded in was swapped for the differentiation media after only 6.55 hours. Each experimental condition was repeated twice as technical repeats **(Figure 4.14 b).** Through consultation of the Design Expert help function tutorials a total of 5 centre points were used and a "rotatable" alpha applied **(Figure 4.14 b).** Finally by selecting a full factorial design (to remove aliasing) a total of 33 runs were required **(Figure 4.14 c).** The description of each of these Runs is presented in **Figure 4.15**.

4.3.7 Results and discussion of the central composite PSC-RPE differentiation experiment

As for the screening experiment, the pluripotency of the seeded population of the MSUH001 was tested for the SSEA-4 market via flow cytometry with 93% of cells proving positive (for the screening experiment 94% of the cells were positive). The growth of the cells at the 13,000 and 25,000 cells/cm^2 were also very similar to that seen in the screening experiment (**Figure 4.16** compared to **Figure 4.7 b**). Even at the lowest density of 4,818 cells/cm^2 a good degree of confluency was achieved (**Figure 4.16**). In addition, changing the media only 6.55 hours after seeding (as was required in some of the conditions) did not negatively impact this conditions ability to achieve good confluence by day 7.

One clearly observable difference from the screening experiment was the high degree of pigmentation seen in the cultures, with a maximum pigmentation of 8.2% compared to a maximal value of only 0.32% in the screening experiment. A range of pigmentations from 0.4% to 6.9% is shown in **Figure 4.17,** to illustrate this difference and the raw pigmentation data at D49 is presented in the chart of **Figure 4.18**. The improved performance was assumed to be a result of taking the best performing run from the screen (Run 4) as a baseline for conditions to be used in the optimization experiment. When the percentage pigmentation data was imported into the Design Expert software the data passed the various inbuilt validation tests, such as the normal plot of residues all sitting on the same line (data not shown), this allowed the data to be successfully modelled. The F value for the model was 40.62 which meant that there was only a 0.01% chance that this could be due to noise. The F value being used as a measure of whether the expected values of a quantitative variable within several pre-defined groups differ from each other. The significant model terms at a 5% confidence interval were A, B, C, AB, AC, BC, B^2, C^2, where A = Seeding Density, B = Time to differentiation, C = nicotinamide concentration. This meant that not only do the factors chosen have a significant impact on percentage pigmentation but that there are a number of two factor interactions involved. These would have been very hard to elucidate using traditional experimental approaches as can been seen from the model's equation below.

Percentage Pigmentation	=
2.48	
-8.44E-05	* Seeding Density
-0.00086	* Time to differentiation
0.16	* Nicotinamide
1.6E-07	* Seeding Density * Time to differentiation
1.36E-06	* Seeding Density * Nicotinamide
0.00025	* Time to differentiation * Nicotinamide
2.02E-10	* Seeding Density^2
-3.30E-05	* Time to differentiation^2
-0.0064	* Nicotinamide^2

The model created using the significant terms is then employed to create contour plots to analyse trends in the data. Plots of seeding density versus time to differentiation at varying

concentrations of nicotinamide are represented in **Figure 4.19.** From these plots, its clear that an increase from 10mM nicotinamide to 20mM increases the percentage pigmentation across the ranges chosen for seeding density and time to differentiation. Visually this is seen as a "warming" of the plots and the percentage pigmentation values on the contour lines. However, an increase to 30mM nicotinamide has a deleterious impact **(Figure 4.19 c)**. An alternate way of representing this same data is to plot seeding density Vs nicotinamide concentration and then generate unique plots for the range of values chosen for time to differentiation **(Figure 4.20).** From these contour plots, it can be seen that increasing the time before the swap to differentiation media is made from 72 to 120h, the optimum operating space is reduced **(Figure 4.20 a)** and **b).** Further increasing the time period to 168h has a further negative effect on percentage pigmentation **Figure 4.20 c).** In addition from these plots (**Figure 4.19 and Figure 4.20**) it can be observed that the optimum condition for the differentiation to optimise percentage pigmentation occurs at lower values of time to differentiation and seeding density, than that were used in the design. Using the built in optimisation algorithm of the Design Expert software the best conditions to maximise percentage pigmentation were found to be a nicotinamide concentration of 15mM, seeding density and 13,000 cells/cm^2 and time to differentiation of 75 hours (**Figure 4.21**). Such settings are predicted by the model to yield an optimum percentage pigmentation of 7.82%. The seeding density value is right on the edge of the plot which further suggests that the lower seeding densities would produce even better results and so that the design space has missed the optimum.

As with the screening experiment, the data for gene expression mostly failed the significance tests of the Design Expert software and so could not be used to generate models and contour plots which would allow the optimisation algorithm to be run and visualised. The exception was *PMEL* that did pass these tests. This was fortuitous as *PMEL-17* is a key RPE associated gene involved in the melanosome and is controlled by another highly RPE associated gene MIT F (Baxter and Pavan, 2003). *MIT F* was also included in the analysis but failed data validation tests. This could be due to the *PMEL17* transcript being expressed highly in absolute numbers (copies of mRNA) therefore the fold changes or

signal are larger compared to the experimental noise. Whereas *MITF* as a transcription factor only varies over a small range in mRNA numbers but has a big impact on downstream transcripts. To fit the validation requirements of the data, the software recommended the data underwent a square root transformation hence the label sqrt(PMEL) in the Figures. This also means that the values from the contour plots require squaring for them to be transformed back to normalized fold expression data. As with the percentage pigmentation data, the F value (21.01) for the pigmentation data was significant with there being only a 0.01% chance that this was due to noise. The "lack of fit" of the model was also determined by the software to be insignificant. The significant factors having an impact on the *PMEL* expression at the 5% confidence interval were slightly narrower than that were found for the percentage pigmentation response with only the terms A, B, C, AB, AC, C^2 having an impact. As these terms are significant the software includes them as part of the *PMEL* response model, for which the equation is below.

Sqrt(PMEL)	=
1.59	
-3.85E-05	* Seeding Density
-0.0065	* Time to differentiation
0.079	* Nicotinamide
9.78E-08	* Seeding Density * Time to differentiation
9.54E-07	* Seeding Density * Nicotinamide
7.17E-05	* Time to differentiation * Nicotinamide
-2.045E-10	* Seeding Density^2
2.56E-06	* Time to differentiation^2
-0.0031	* Nicotinamide^2

Using these terms the Design Expert software outputs the contour plots in **Figure 4.22** and **4.23**. For plots of seeding density Vs time to differentiation at increasing nicotinamide concentration (**Figure 4.22 a)** 10mM, **b)** 20mM**, c)** 30mM) the trend for PMEL expression is very similar as that which was seen for percentage pigmentation **(Figure 4.19)**. The *PMEL* plots of seeding density Vs nicotinamide concentration at different time points prior to the swap to differentiation media are also highly similar to those observed for percentage pigmentation (comparison of **Figure 4.23** to **4.20**). These correlations are understandable due to the link between the *PMEL* gene and the pigmented phenotype. Using the software to predict the optimum condition based on PMEL alone produced a slightly different result than when an optimisation was performed on percentage pigmentation alone (comparison

of **Figure 4.24** to **Figure 4.21**). The difference being for PMEL optimization a slightly higher nicotinamide concentration of 15.13mM is required (compared to 15mM) and the seeding density and time to differentiation parameters sit in the bottom corner at 72 hours (compared to 75h), and 13,000 cells/cm^2. This PMEL optimization data further suggests the optimum conditions lay outside the design space. The Design Expert software also allows optimization based on more than one response, and a weighting to be given to the preferred response. Based on an equal rating of PMEL and percentage pigmentation the plot in **Figure 4.25,** was generated which essentially recommends the same parameters as for the PMEL expression optimization, again confirming the actual optimum is likely to be outside the design space.

The gene expression data which failed to produce significant models in the Design Expert software was plotted against *PMEL* to see if any clustering could be observed (**Figure 4.26**). Understandably, *PMEL*, *MIT F* and *TYR* all showed similar clustering as they are all involved in pigmentation pathways. Interestingly two key RPE genes which are representative of the most mature phenotype *BEST* and *RPE 65* (Idelson et al., 2009) show slightly different trends . These genes are not directly part of the pigmentation pathways with the bestrophin protein being present on the basolateral plasma membrane of mature RPE cells and *RPE 65* being involved in the vision cycle (Marmorstein et al., 2000). In particular *RPE 65* shows some strong expression at some of the very lower concentrations of nicotinamide (3.18mM) where all the other pigmentation genes show weak expression (**Figure 4.26**). This is confirmed when plots are made of gene expression Vs nicotinamide concentrations (**Figure 4.27** and **Figure 4.28**) which shows *RPE 65* expression is unique in that it is highest at the lowest nicotinamide concentration. Furthermore, *RPE 65* displays the opposite relationship to seeding density when plots of gene expression Vs seeding density are made (**Figure 4.29**, **Figure 4.30**), with a higher seeding density producing a higher RPE 65 expression. This could be suggestive of there being two subtypes of RPE being present e.g. an immature and a more mature phenotype, it also indicates that perhaps nicotinamide should only be supplemented to the media during a particular window if there is an inhibitory effect.

4.4 Conclusions

4.3.8 The feasibility of applying DoE methodology to the PSC-RPE differentiation

The aim of this chapter was to explore the feasibility of applying the DoE approach to the PSC-RPE differentiation, as it was the hope that the methodology would not only identify new significant factors but also generate an understanding of any complex interactions. By first completing a screening experiment of a large number of factors it was hoped that using this approach the factors with the largest impact could be easily identified with minimal effort through use of a rationalised design involving aliasing. In practice, due to the large number of experimental conditions and variations of media it was practically complex to complete the experiment as planed over the 49 day protocol. The experiment did however give good confidence that seeding density, time before switching to differentiation media, and nicotinamide concentration were important to improving the differentiation efficiency, even if the effects could not be quantitatively modelled. The screen also showed that reducing media feeding from every day to every 3rd day and reducing the media volumes by 25% actually had a positive impact. At the extreme this means a reduction in total media used of 75% and so would have a significant impact on the process economics as this process scales.

Using the key factors identified from the screen the central composite design was used to better understand the interactions between the key factors so as to be able to predict an optimum. From the raw data points plotted in **Figure 4.25** to **Figure 4.28** it can be seen just how noisy some of the raw data is for what are technical repeats. Such variation is common issue in PSC differentiation where protocols are highly manual, and given the long length of this protocol in particular (49 days) there is plenty of time for any small differences to be magnified. So, although qPCR is a very sensitive analytical test in determining small differences in gene expression between similar conditions perhaps the "signal" of the test is not sufficient to be used in a robust manner in software packages such as Design Expert as part of DoE approaches. It should also be noted that gene expression does not equal protein expression, and there are likely to be a number of post-

transcriptional processes as well as post translational processes involved in the differentiation. The good correlation between PMEL and percentage pigmentation does give confidence that such factors are not having a significant impact in this differentiation .The ANNOVA analysis tests this using a term called "adequate precision" which measures the signal to noise ratio where a ratio of greater than 4 is described as "desirable". For the optimisation experiment, the two responses which passed all the tests had adequate precision ratio of 22 for percentage pigmentation and for *PMEL* it was over 16.

The question then has to be asked what marker/output should be optimised for? For this stage of the process the aim is to gain as much pigmentation in the cultures as possible so that they can be visually identified and dissected. Therefore, using percentage pigmentation as the critical quality attribute is probably most desirable. Even though the gene expression for *RPE 65* and *BEST* might not directly correlate with the conditions that provide maximum percentage pigmentation at this stage in the process, it could be hypothesized that once these pigmented areas are successfully replated and allowed to mature a positive correlation would occur.

From a feasibility perspective, where the DoE approach was particularly successful was in the identification and modelling of a particularly complex interaction between seeding density, time to differentiation and nicotinamide concentration. One issue was that the predicted optimum lay at the very lowest position of the seeding density and time to differentiation time points used, and so there is a high likelihood that the true optimum was missed. It is not believed that this could have been anticipated when planning the experiment as the finding was contrary to the past experience of the research team. The current protocol involves prolonged feeding of PSC cultures to allow them to become "super confluent" before the switch to differentiation media is made (Vugler et al., 2008). Therefore making the switch after only 6.55 hours in the –alpha condition was considered to be a high risk in the planning stage, as it was feared that all the cells could be washed away if they had not successfully seeded or that growth would be so poor no RPE would be produced. For future work it would be interesting to see what the impact of seeding straight into differentiation media would be.

With regards to the optimisation plots showing that lowest seeding densities produce the best differentiation conditions, this was a good result in that it confirmed what was seen from the screening experiment F values (**Figure 4.10**). However, these results are very different from the conclusions drawn from Lane et al. (2014) who reported that an increase of seeding density from 17,000 cells/cm^2 to 35,000 cells/cm^2 increased the pigmented surface area five-fold. This data was the reason why the upper seeding density used in the screen (25,000 cells/cm^2) was increased for the optimisation experiment to 37,000 cells /cm^2. There are a number of factors that could explain this observed discrepancy. The first is that not only that different PSC lines were used, which often lead to discrepancies, but also that the cells used in this work were iPS cells were rather than hESC lines used by Lane et al. (2014). But, perhaps more importantly was the use of ROCK inhibitor in this study which increases PSC survival during replating (Claassen et al., 2009) and supplementing the various conditions with nicotinamide has also been reported to improve neural stem cell survival in vitro (Li et al., 2006, Shen et al., 2004). Therefore both these agents could be responsible in part for a shift in the location of the optimum seeding density below the range chosen for optimisation design.

It would also be normal to confirm the optimum predicted from the data with a final experiment. However, in this case as appears that the true optimum was slightly missed due to the ranges used, and that the protocol takes several months from start to finish, it was believed this was not the best use of time and resources. A large amount of other data was also recorded for the optimization experiment such as percentage pigmentation image analysis at other time points and also analysing spent media. A number of these tests did produce data that did pass the validation requirements of the software to produce models, but were not discussed here for the sake of brevity as they were not directly related to the RPE phenotype. It would be hoped that if this non-destructive and quick to obtain data was collected over a number of experiments it could be used as proxy measurements to predict quality attributes such as gene expression.

4.3.9 Summary

Where there is a need to understand a complex relationship of a limited number of factors which impact a differentiation processes' critical attributes the DoE approach is a feasible and powerful tool to give real insights. For example, the data here has shown evidence that the media consumption can be reduced by 75% without any adverse effect on the differentiation, the lowest seeding densities give the best results which will improve economics by reducing the seed chain requirements. Furthermore, differentiation efficiency was shown to be improved by the addition of a very cheap small molecule (nicotinamide) but that there is an optimum that needs to be understood which is impacted by a combination of seeding density and time to differentiation. This might explain the mixed results this lab has achieved with nicotinamide before. However, the application of DoE as a screening tool for PSC differentiation really requires high throughput automation methods to both culture the cells but also mix the media components. Combining such methods with technologies that allow close control of the environment should not only reduce variation, and so solve the signal to noise ratio issues, but also allow conditions such as hypoxia during differentiation to be explored. For example, hypoxia has been found to increase RPE related pathways such as PEDF secretion in Müller cells (Yang et al., 2012). Ideally, if this could be coupled up to online image analysis of percentage pigmentation the process would not only be better understood but interventions could be made to both optimize the end result and increase process robustness.

a)

b)

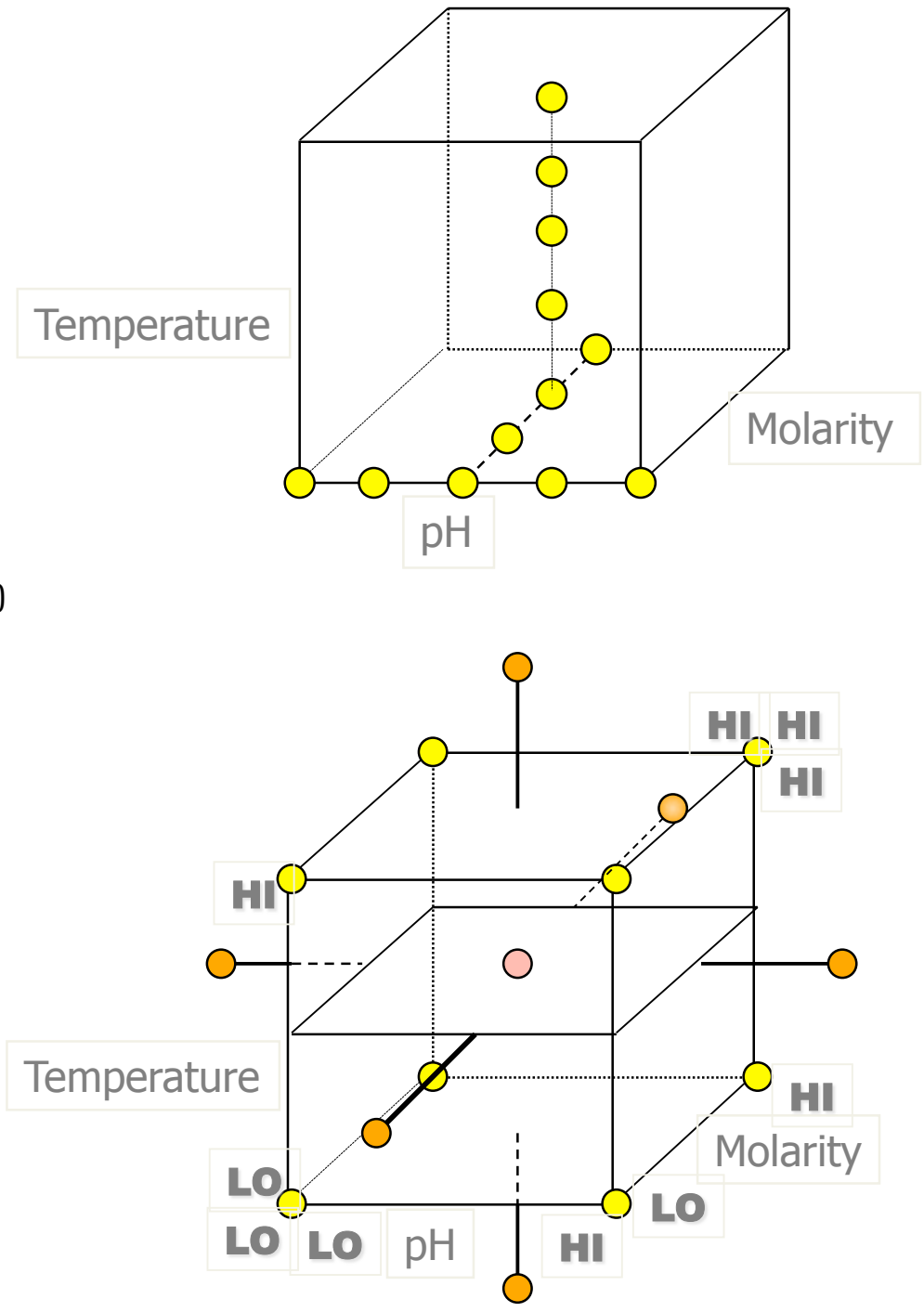

Figure 4.1: Comparison between a one factor at a time approach (OFAT) and a design of experiment approach (DoE). a) An example of the OFAT approach would be to first vary pH at a constant temperature and molarity, then morality is varied at the 'optimum' pH at a set temperature, finally the temperature is varied at the 'optimum' values of pH and Molarity. Such an approach only explores a minimal area of the experimental space. b) Alternatively, using the DoE approach all factors are varied at the same time at both the high and low extremes of the design space, outside the design space and at its centre – allowing the understanding of the relationship between factors to allow the prediction where the optimum area lies in this multidimensional environment.

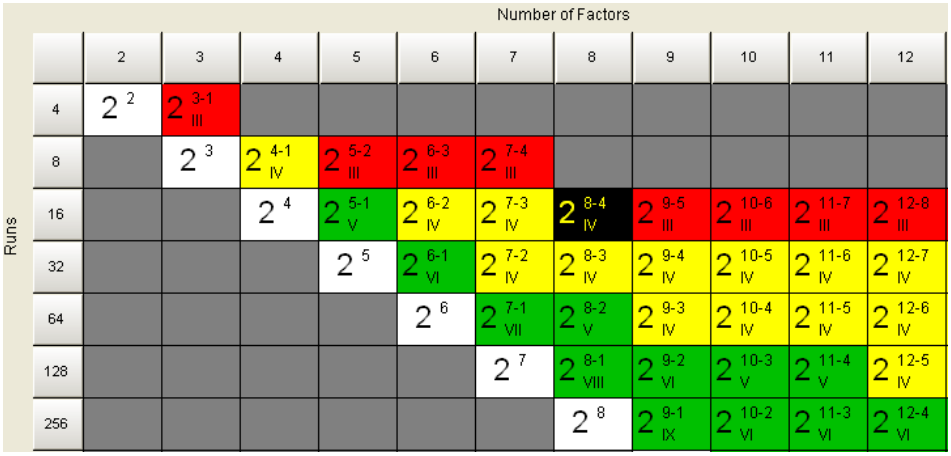

Figure 4.2: Design Expert visual representation of number of runs required for 2 level designs. As the number of factors are increased for a 2-level design the number of runs required also increases in a 2^n fashion. Reducing the number of runs for a given number of factors reduces the resolution of the design, as indicated by the Roman numerals and colours. The lower the Roman numeral the lower the resolution and so the greater the risk of misidentifying a factor (or combination of) as having a particular impact. The black square highlights the design chosen for the screening experiment an 8 factor resolution IV design.

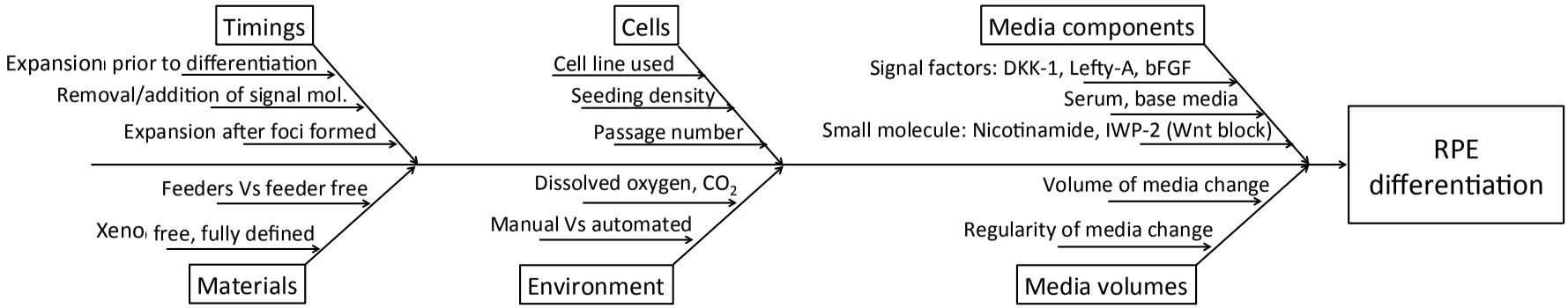

Figure 4.3: Ishikawa diagram for PSC-RPE differentiation: The Ishikawa diagram has been used to identify and visually represent what are believed to be the key factors impacting the PSC-RPE differentiation system.

Name	Units	Type	Low	Med	High
Cell line [CL]		Categoric	MSUH001		BJ iPS
Seeding Density [SD]	cell/cm²	Numeric	13,000	19,000	25,000
bFGF	ng/ml	Numeric	0	4	8
Time to differentiation [diff time]	days	Numeric	7	11	15
Differentiation media volume	ml	Numeric	3	3.5	4
Time between media changes [med. time]	days	Numeric	1	2	3
Nicotinamide [nic]	mM	Numeric	0	10	20
IWP-2	µM	Numeric	0	5	10

Figure 4.4: Factors chosen for the PSC-RPE screening experiment: Factors were chosen based on past experience, published differentiation protocols and other factors which are interesting with respect to scaling the process.

A: Cell line [CL]	B: Seeding Density [SD] (cell/cm2)	D: Switch to differentiation media[exp] (days)	F: Time between media changes [med. time] (days)	E: Differentiation media volume (ml)	C: bFGF (ng/ml)	G: Nicotinamide [nic] (mM)	H:IWP-2 (µ/M)
MSUH001	13,000	15	1	3	8	20	0
MSUH001	25,000	15	1	3	0	0	10
MSUH001	25,000	15	3	4	8	20	10
MSUH001	13,000	15	3	4	0	0	0
MSUH001	19,000	11	2	3.5	4	10	5
MSUH001	19,000	11	2	3.5	4	10	5
MSUH001	13,000	7	3	3	8	0	10
MSUH001	25,000	7	1	4	8	0	0
MSUH001	13,000	7	1	4	0	20	10
MSUH001	25,000	7	3	3	0	20	0
BJ	25,000	15	1	4	0	20	0
BJ	13,000	15	1	4	8	0	10
BJ	25,000	15	3	3	8	0	0
BJ	13,000	15	3	3	0	20	10
BJ	19,000	11	2	3.5	4	10	5
BJ	19,000	11	2	3.5	4	10	5
BJ	13,000	7	1	3	0	0	0
BJ	25,000	7	1	3	8	20	10
BJ	15,000	7	3	4	8	20	0
BJ	25,000	7	3	4	0	0	10

Figure 4.5: Run descriptions for the PSC-RPE screening experiment: To complete the DoE screening experiment as designed, 20 runs were completed in experimental duplicate which required the use of 14 different types of media.

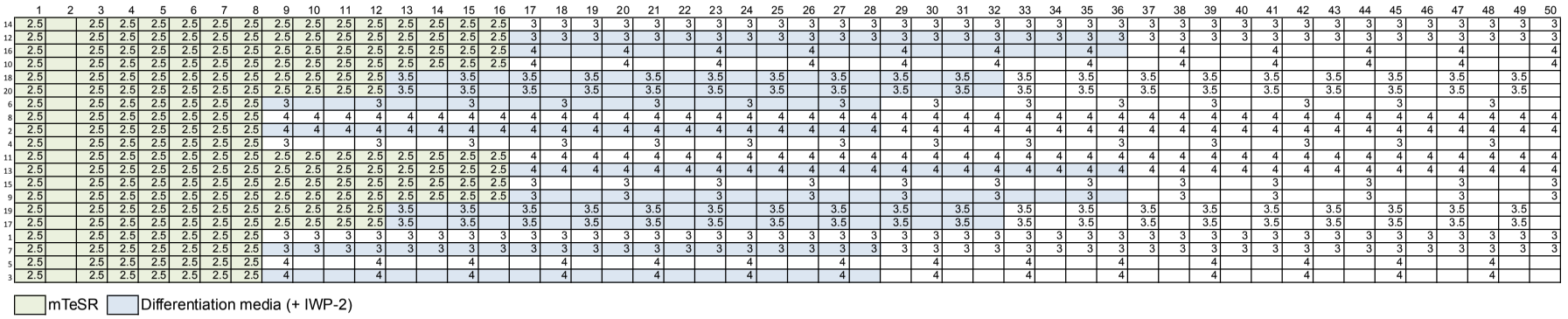

Figure 4.6: PSC-RPE Screening Experiment protocol: Each well was given a run number from 1-20 and run on duplicate plates. The numbers on the top row indicate the protocol day. The numbers in the cells denote the volume of media to be fed that day. The green background cells were fed mTeSR media. The white background cells were fed the prescribed differentiation media cross referenced to the run number. The blue background cells also had IWP-2 supplemented for the first 20 days of the differentiation.

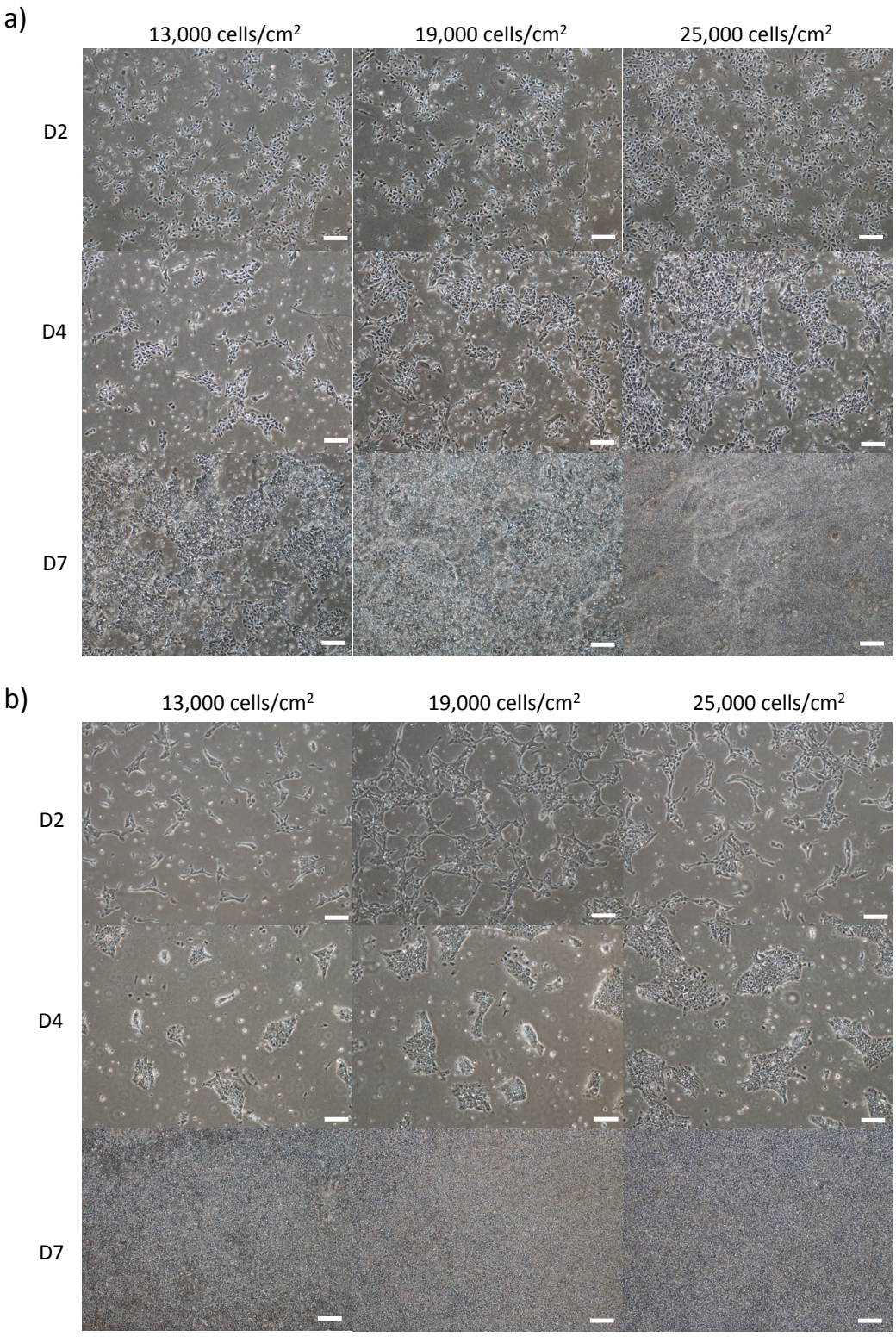

Figure 4.7: Expansion of the BJ and MSUH001 after single cell dissociation. a) The expansion of the BJ line at densities of 13,000, 19,000 and 25,000 cells/cm^2 at timepoints D2, D4 and D7. b) The expansion of the MSUH001 line at densities of 13,000, 19,000 and 25,000 cells/ cm^2 at timepoints D2, D4 and D7. Scale bar is 50µm.

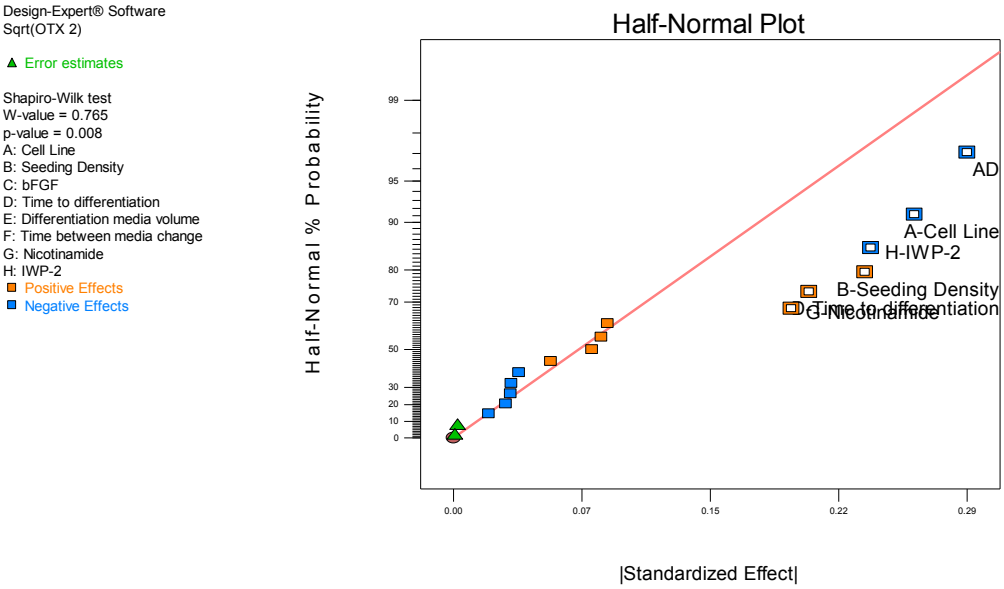

Figure 4.8: Half normal plot for the OTX 2 response in the PSC-RPE screening experiment. Factors which are selected for inclusion in the model and ANNOVA analysis sit off the red line.

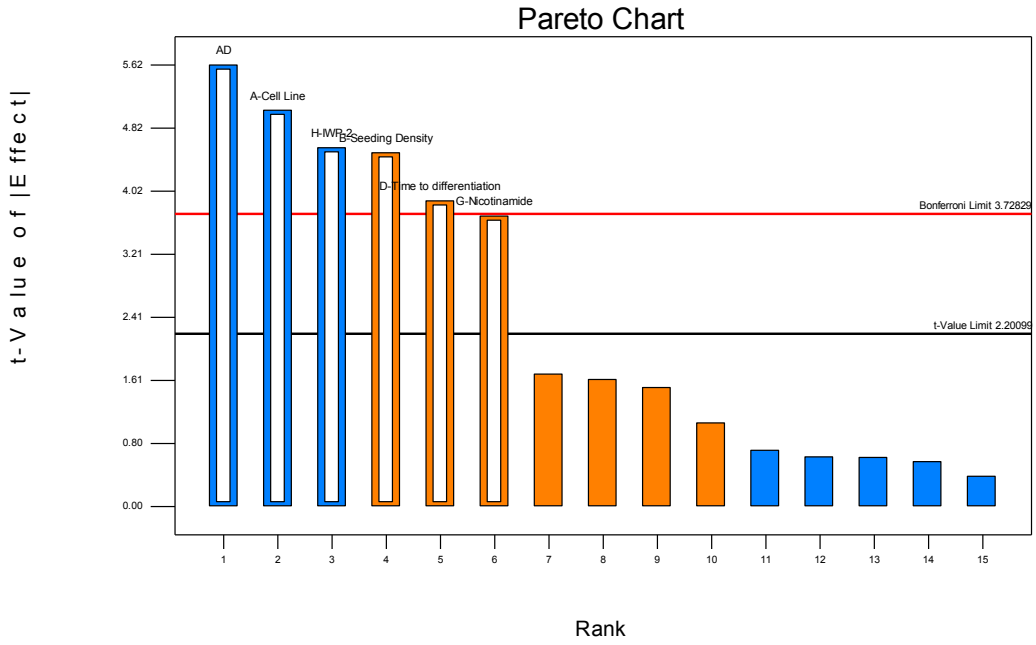

Figure 4.9: Pareto Chart for the OTX 2 response in the PSC-RPE screening experiment Factors which are selected for the model have a white centre to the bar.

	F-Values		
	% Pigmentation	OTX 2	TYR
A-Cell Line		0.0000	
B-Seeding Density	0.0483	0.0005	0.0105
C-bFGF	0.0357		
D-Time to differentiation		0.0015	
E-Differentiation media volume			0.0060
F-Time between media change			0.0053
G-Nicotinamide		0.0021	0.0372
H-IWP-2	0.0347	0.0004	0.0061
AB			
AC, BE, DG, FH	0.0267		0.0082
AD		0.0001	0.0068
AE			
AF, BG, CH, DE			
AG, BF, CD, EH			0.0058
AH			

Prob>F: The probabilities of getting an F Value of this size if the term did not have an effect on the response

Colour shading key overlayed from Pareto Chart	
Negative impact t> Bon. F limit	
Negative impact t> t limit	
Positive impact t> Bon. F limit	
Positive impact t> t limit	

Figure 4.10: F-values from the PSC to RPE screening experiment. F-values were obtained from the Pareto chart for the factors which has the largest impact on the responses of: percentage pigmentation, OTX 2 and TYR. But, only when these factors were above either the t-limit or Bonferroni limit.

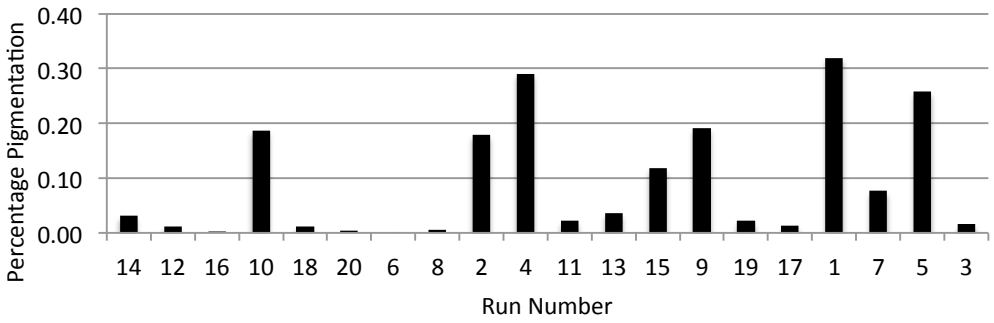

Figure 4.11: Percentage pigmentation for the screening experiment . Well plates were scanned using a flat bed scanner from two orientations and then image analysed at 2 different threshold values for percentage pigmentation using the Image J software analysis tools. These 4 values were than averaged.

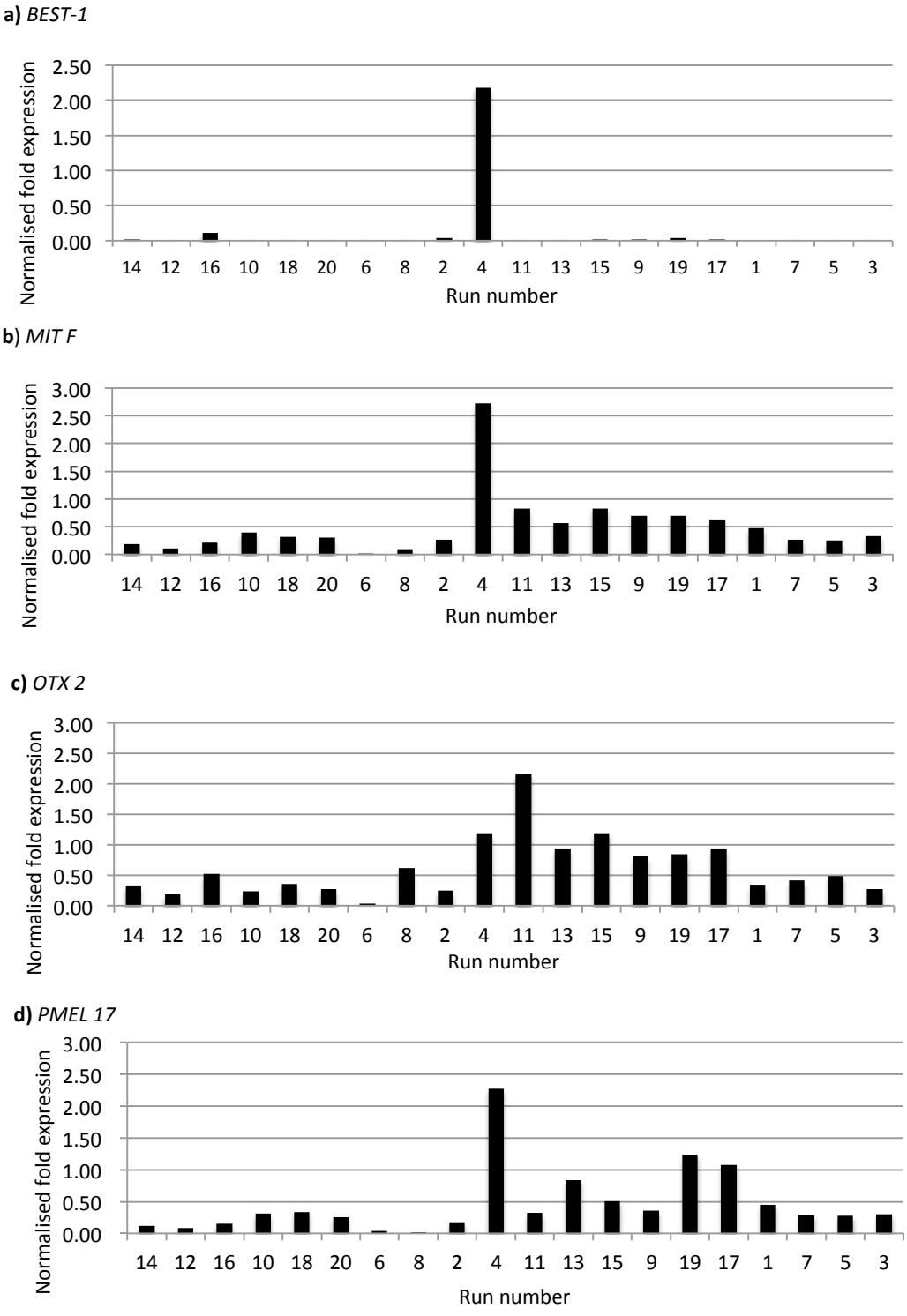

Figure 4.12: Gene expression of eye field and RPE markers: It is clear from the normalised gene expression that Run 4 has superior expression of the RPE markers *BEST-1* a), *MIT F* b) and *PMEL -17* d) whilst having high expression of other eye field related markers such as *OTX 2* c).

e) *RAX*

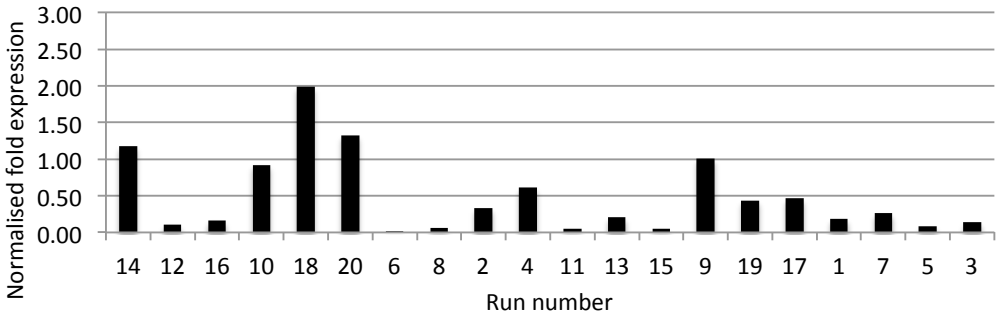

e) *TYR*

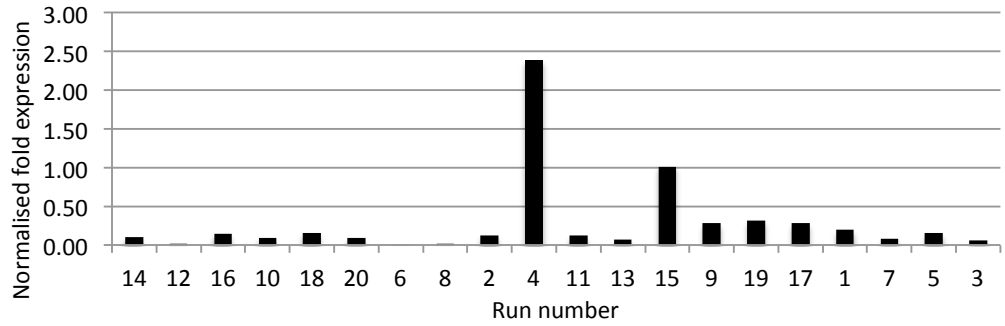

Figure 4.13: Gene expression of eye field and RPE markers continued: Run 4 showed low level expression of the eye field marker *RAX* a) but a high level of the RPE marker *TYR* e).

a)

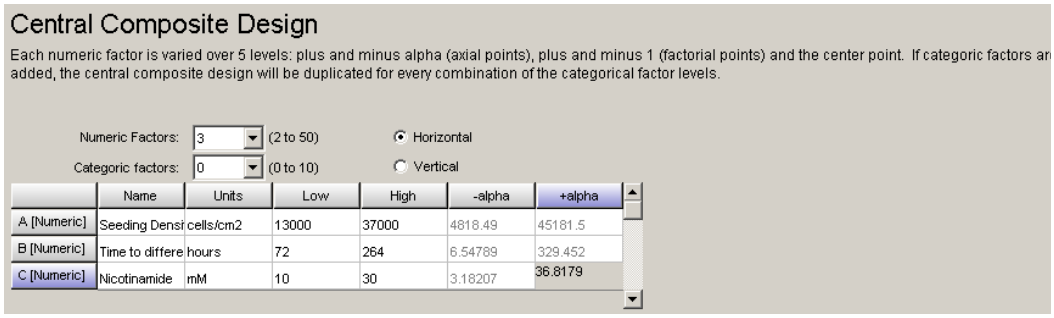

b)

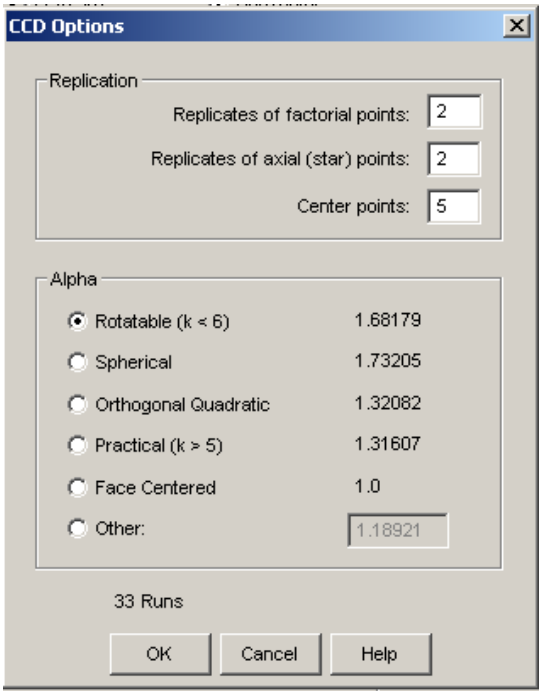

c)

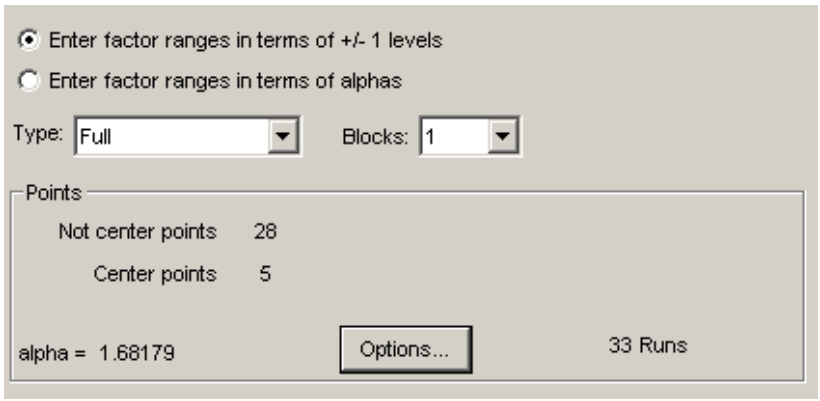

Figure 4.14: Screen shots of the Design Expert software for the central composite design: a) seeding density, time to differentiation and nicotinamide were used as the 3 factors. b) each data point was replicated twice, 5 centre points were used and a rotatable alpha was used as per the software's guidance. c) By selecting a full factorial design 33 runs were required to populate the design space.

Run	Type	Seeding Density (cells/cm^2)	Time to differentiation (d)	Nicotinamide (mM)
1	Axial	25000.00	7.00	36.82
2	Factorial	37000.00	3.00	10.00
3	Factorial	37000.00	3.00	30.00
4	Factorial	13000.00	3.00	10.00
5	Center	25000.00	7.00	20.00
6	Axial	45181.51	7.00	20.00
7	Axial	25000.00	7.00	36.82
8	Factorial	13000.00	3.00	30.00
9	Factorial	13000.00	11.00	10.00
10	Factorial	13000.00	11.00	30.00
11	Factorial	13000.00	3.00	30.00
12	Factorial	37000.00	11.00	10.00
13	Factorial	13000.00	11.00	10.00
14	Center	25000.00	7.00	20.00
15	Center	25000.00	7.00	20.00
16	Factorial	37000.00	11.00	10.00
17	Factorial	37000.00	11.00	30.00
18	Axial	25000.00	7.00	3.18
19	Factorial	37000.00	3.00	10.00
20	Factorial	37000.00	3.00	30.00
21	Center	25000.00	7.00	20.00
22	Axial	4818.49	7.00	20.00
23	Axial	25000.00	0.27	20.00
24	Axial	25000.00	7.00	3.18
25	Factorial	13000.00	11.00	30.00
26	Axial	4818.49	7.00	20.00
27	Factorial	13000.00	3.00	10.00
28	Axial	45181.51	7.00	20.00
29	Factorial	37000.00	11.00	30.00
30	Axial	25000.00	0.27	20.00
31	Axial	25000.00	13.73	20.00
32	Axial	25000.00	13.73	20.00
33	Center	25000.00	7.00	20.00

Figure 4.15: Run descriptions of the optimisation experiment: In all 33 Runs were needed to generate data for the Central Composite design. Where timings were a fraction of a day these were converted to hours post seeding to follow the design precisely.

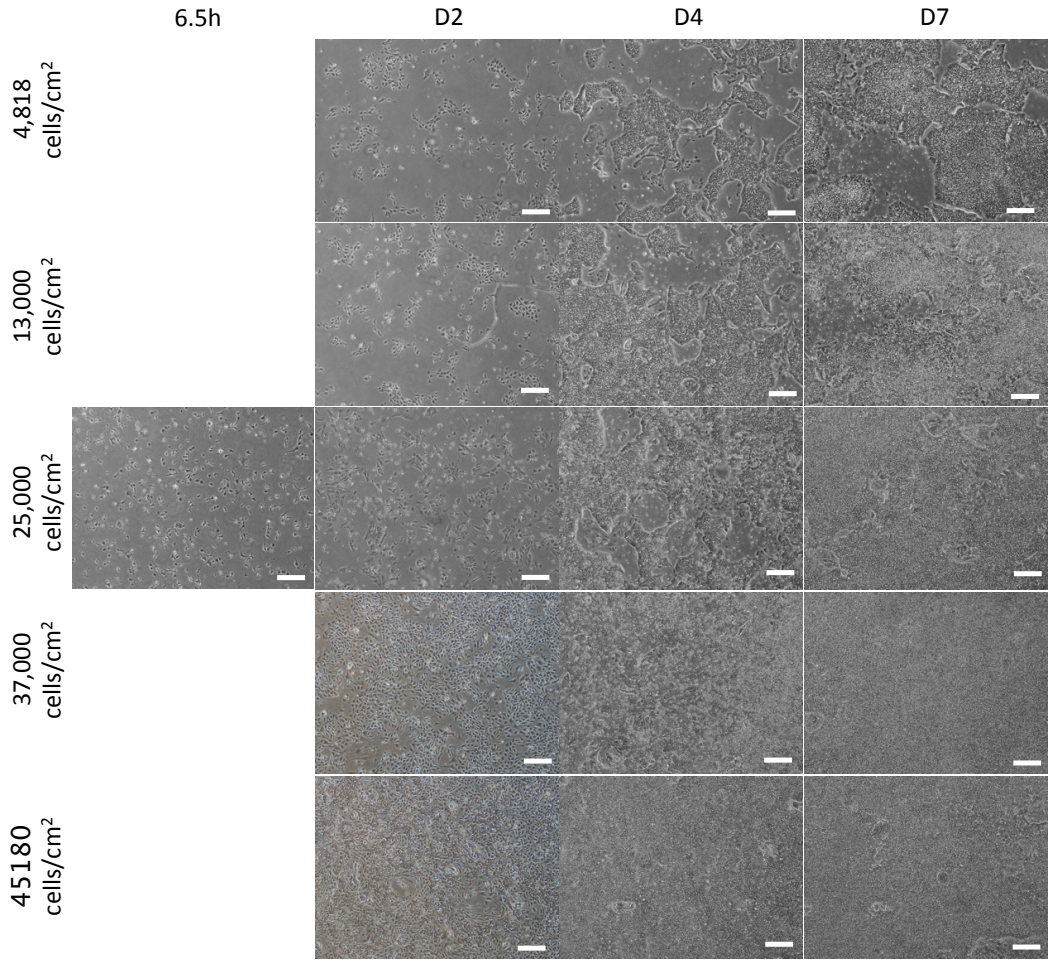

Figure 4.16: Microscopy images of cell growth in the optimisation experiment. Comparison of growth of the MSH001 line at different seeding densities during the DoE optimisation experiment. Scale bars are 50μm.

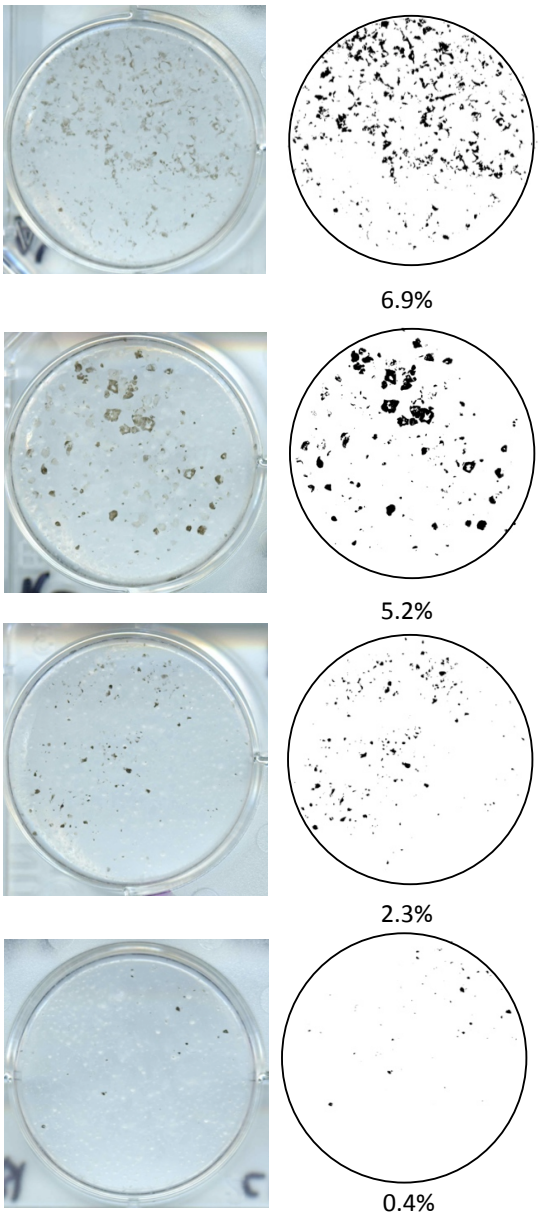

Figure 4.17: Images and corresponding percentage pigmentation for the Optimisation experiment . Each well is scanned using a flat bed scanner and converted to a binary image to determine the percentage pigmentation based on surface area.

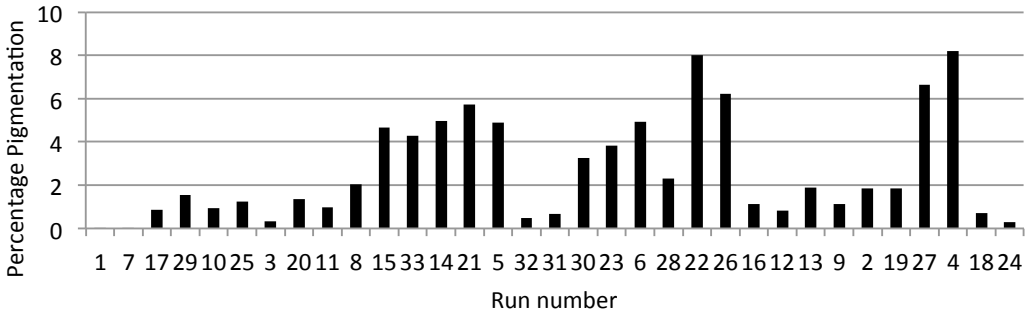

Figure 4.18: Chart of percentage pigmentation at D49 for the optimisation experiment. There was a considerable range in the percentage pigmentation data. All conditions achieved some level of pigmentation and were not below the detection level of the analytical method.

a) 10mM Nicotinamide

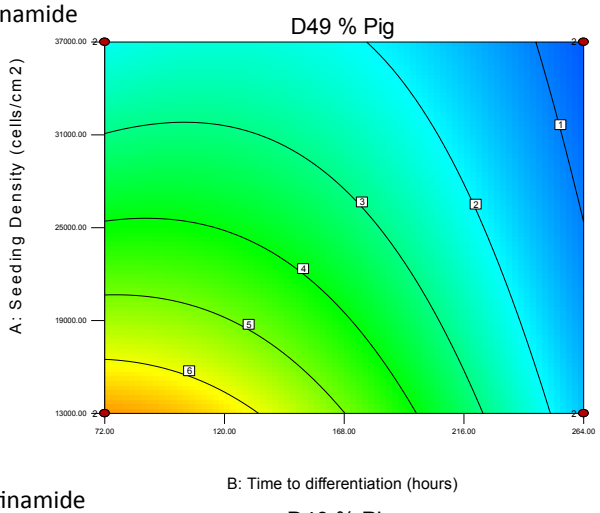

b) 20mM Nicotinamide

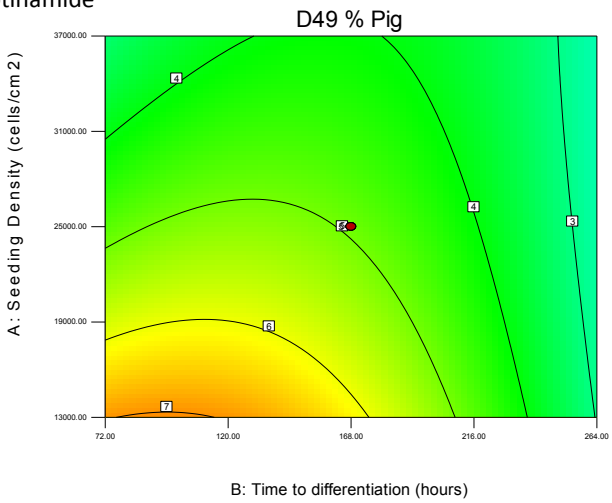

c) 30mM Nicotinamide

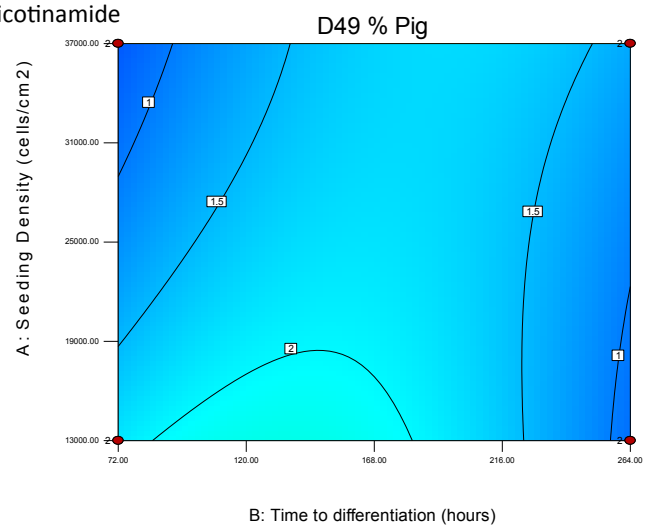

Figure 4.19: Contour plots of seeding density versus time to differentiation at different nicotinamide concentrations, with pigmentation as the output. Each plot a-c) is a plot of seeding density versus time to differentiation with the contour lines representing the percentage pigmentation with warmer colours indicating a higher percentage. It can be seen that percentage pigmentation is improved from a move from 10mM nicotinamide a) to 20 mM in b). However, an increase to 30mM has a detrimental impact, c).

a) 72h before switch to differentiation media

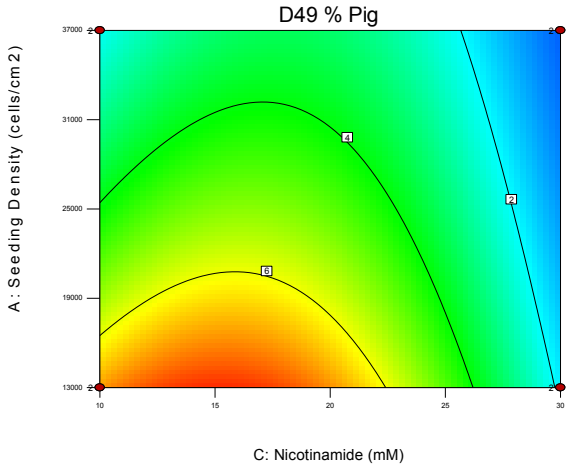

b) 120h before switch to differentiation media

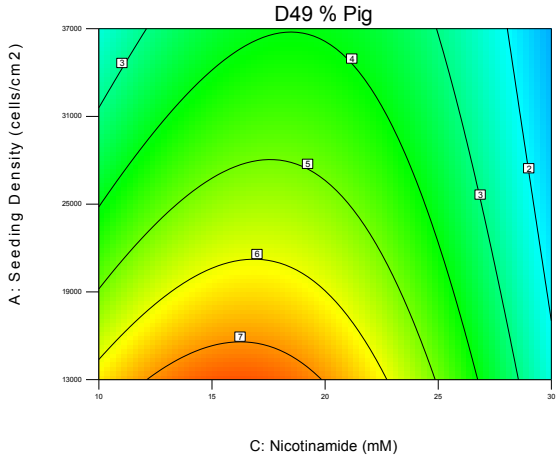

c) 168h before switch to differentiation media

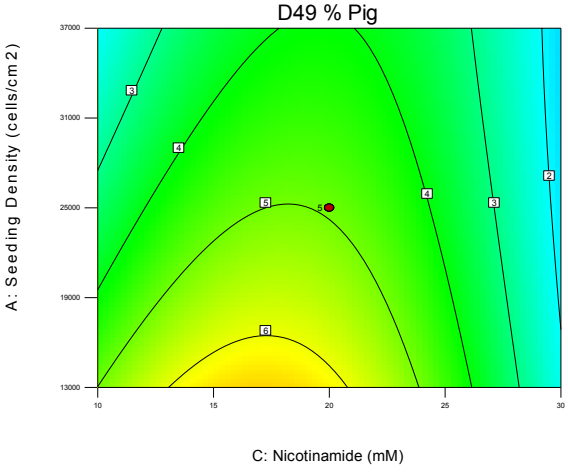

Figure 4.20: Contour plots of seeding density versus nicotinamide at various time points before the switch to differentiation media is made, with percentage pigmentation as the output. Each plot a-c) is a plot of seeding density versus nicotinamide concentration with the contour lines representing the percentage pigmentation. Warmer colours indicating a higher percentage pigmentation. It can be seen that percentage pigmentation is reduced for the chosen ranges as the time is increased from 72 to 168h a-c).

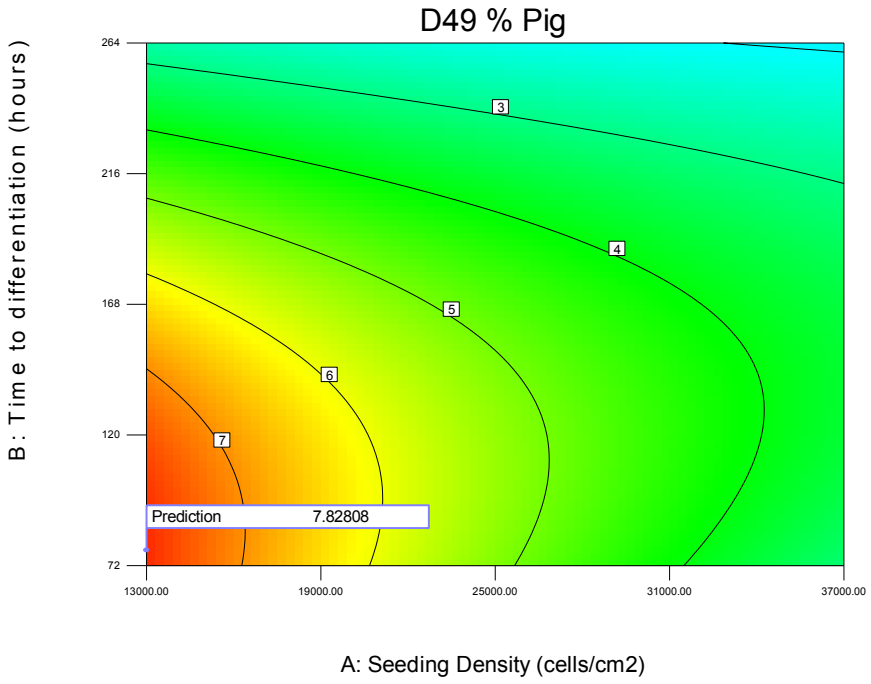

Figure 4.21: Contour plot displaying the optimum condition to maximise percentage pigmentation. Using the optimisation algorithms built into the Design Expert software, the optimal nicotinamide concentration was 15mM, the optimal seeding density 13,000 cells/cm^2 and time to differentiation 75 hours. Such settings are predicted to yield an optimise percentage pigmentation of 7.82%.

a) 10mM Nicotinamide

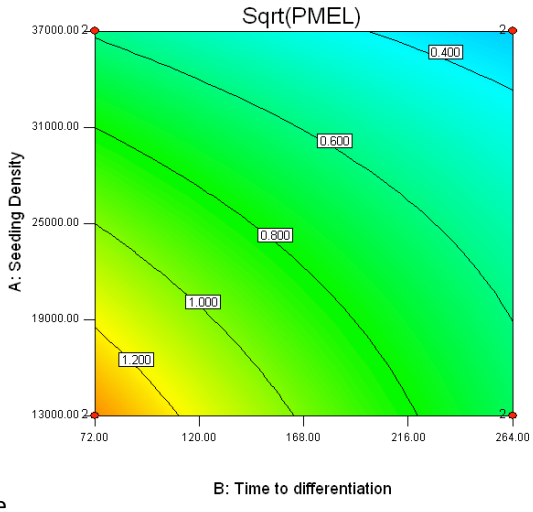

b) 20mM Nicotinamide

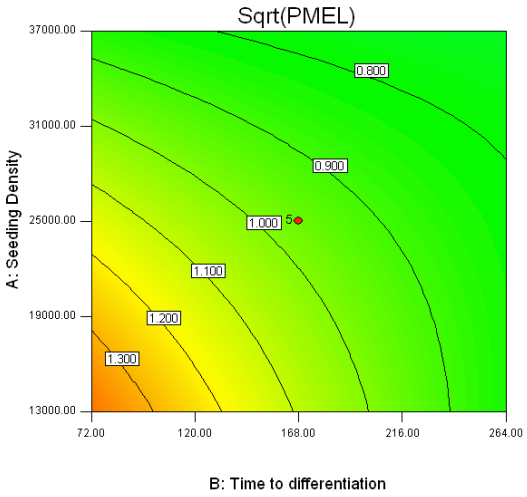

c) 30mM Nicotinamide

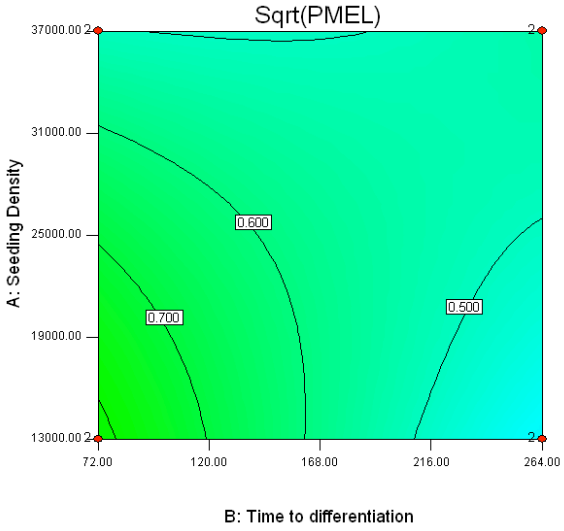

Figure 4.22: Contour plots of seeding density versus time to differentiation at different nicotinamide concentrations, with *PMEL* fold expression as the output. Each plot a-c) is a plot of seeding density versus nicotinamide concentration with the contour lines representing *PMEL* gene expression with warmer colours indicating a higher fold expression.

a) 72h before switch to differentiation media

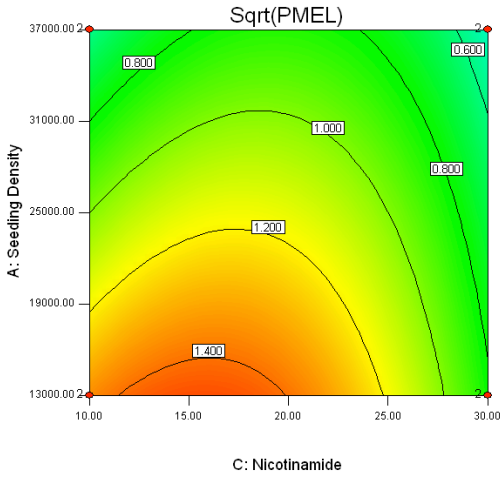

b) 120h before switch to differentiation media

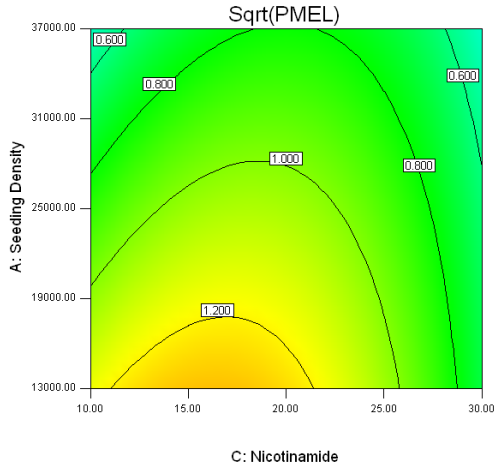

c) 168h before switch to differentiation media

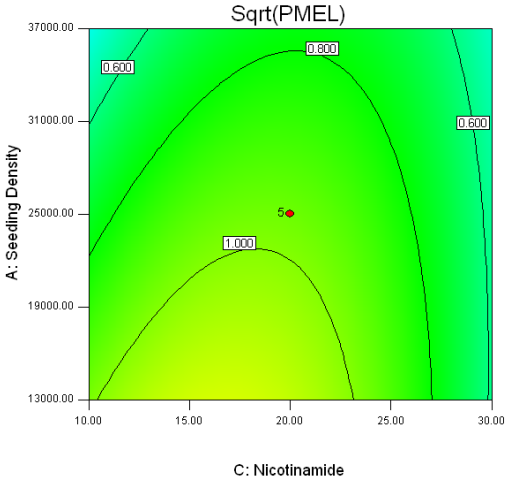

Figure 4.23: Contour plots of seeding density versus nicotinamide at various times before switch to differentiation media, with *PMEL* expression as the output. Each plot a-c) is a plot of seeding density versus nicotinamide concentration with the contour lines representing the *PMEL* expression with warmer colours indicating a higher fold expression. As was found for percentage pigmentation it can be seen that the fold expression of PMEL is reduced for the chosen ranges at the time before swapping to differentiation media is increased from a-c).

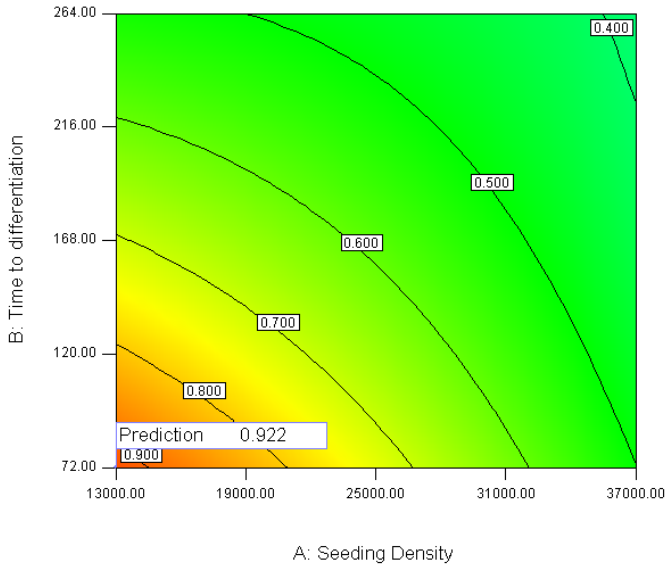

Figure 4.24: Contour plot displaying the optimum condition to maximise *PMEL* expression. Using the optimisation algorithms built into the Design Expert software the optimal nicotinamide concentration was 15.13mM, the optimal seeding density 13,000 cells/cm^2 and time to differentiation 72 hours. Such settings are predicted to yield an optimised PMEL expression of $0.922^{-(1/2)}$

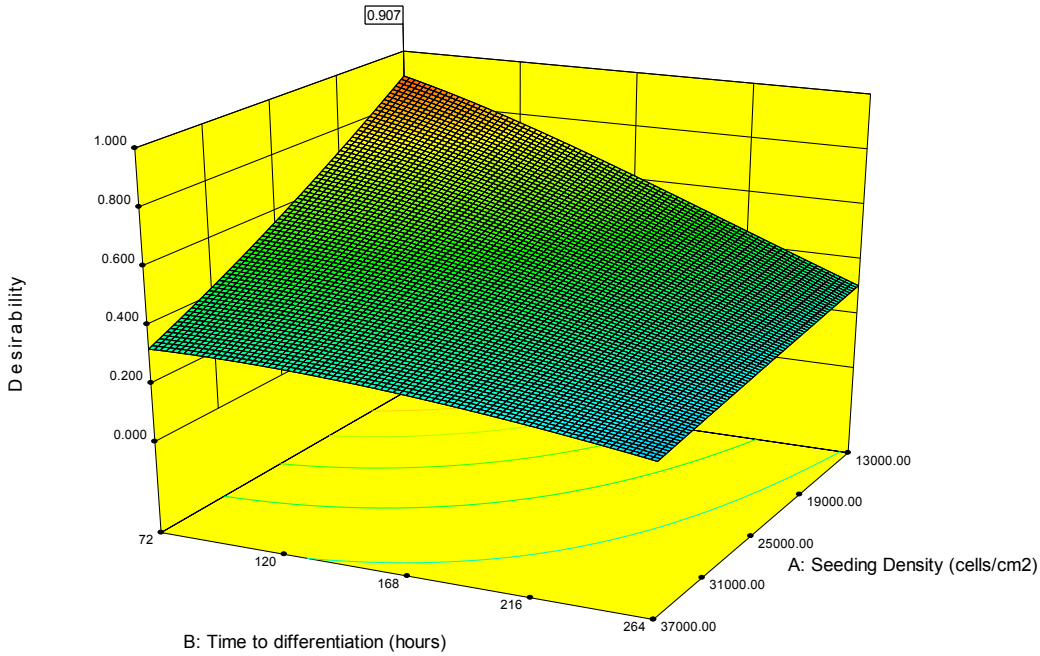

Figure 4.25: Optimisation plot to maximise both percentage pigmentation and *PMEL* expression. The optimal conditions were found to be the same as for Figure 4.24 when the output was optimised for *PMEL* alone. Desirability being a unitless measure to be able to combine the responses of PMEL and percentage pigmentation.

Run number	Seeding Density (cells/cm2)	Time to differentiation (days)	Nicatinamide (mM)	BEST	MITF	OTX 2	PMEL	RAX	RPE 65	TYR
1	25,000	7.00	36.82	0.0004	0.0361	0.0048	0.0003	0.0147	0.1531	0.0002
7	25,000	7.00	36.82	0.0001	0.0407	0.0058	0.0004	0.0131	0.1537	0.0003
17	37,000	11.00	30.00	0.1412	0.2395	0.2888	0.0935	0.1452	0.2845	0.2068
29	37,000	11.00	30.00	0.2280	0.2463	0.2337	0.2734	0.1118	0.3529	0.1962
10	13,000	11.00	30.00	0.3478	0.3004	0.3346	0.1395	0.2111	0.2018	0.3302
25	13,000	11.00	30.00	0.1899	0.1626	0.1872	0.2241	0.2305	0.1865	0.0759
3	37,000	3.00	30.00	0.3453	0.3379	0.3344	0.1886	0.1097	0.2590	0.2561
20	37,000	3.00	30.00	0.7559	0.4535	0.5014	0.4112	0.2213	0.3537	0.5149
11	13,000	3.00	30.00	0.7573	0.4898	0.3435	0.3660	0.1238	0.2562	0.3337
8	13,000	3.00	30.00	0.7056	0.5860	0.3920	0.6174	0.2537	0.3291	0.4539
15	25,000	7.00	20.00	0.4504	0.7757	1.1331	0.9113	0.1562	0.5139	1.2779
33	25,000	7.00	20.00	0.4767	0.9919	1.4448	1.7543	0.1342	0.8676	1.3210
14	25,000	7.00	20.00	0.6778	0.7091	0.9997	0.7076	0.1204	0.8406	1.0099
21	25,000	7.00	20.00	0.8804	0.5542	0.9708	0.5789	0.2049	0.6586	1.0938
5	25,000	7.00	20.00	0.9764	0.6887	1.0466	0.7920	0.1545	0.8409	0.9668
32	25,000	13.73	20.00	0.1653	0.5242	0.8021	0.5625	0.1318	0.5070	1.0022
31	25,000	13.73	20.00	0.2457	0.6002	1.0194	0.7444	0.1075	0.5404	1.2122
30	25,000	0.27	20.00	2.4810	1.4691	1.8821	2.4810	2.4810	1.2907	1.6081
23	25,000	0.27	20.00	3.9831	1.0854	1.7209	1.3733	0.6310	1.3005	1.4612
6	45,182	7.00	20.00	0.3399	0.7230	1.1073	0.3601	0.1575	0.8553	0.9967
28	45,182	7.00	20.00	0.2433	0.5386	1.0441	0.5326	0.1466	0.7811	0.5408
22	4,818	7.00	20.00	1.1299	1.6511	2.4044	1.6968	0.4248	0.4052	2.2720
26	4,818	7.00	20.00	0.6529	1.6895	1.6320	1.2694	0.1764	0.5721	1.8000
16	37,000	11.00	10.00	0.1063	0.4317	0.6372	0.2110	0.1031	0.5100	0.2523
12	37,000	11.00	10.00	0.0547	0.6531	0.9064	0.0842	0.1731	0.4915	0.5259
13	13,000	11.00	10.00	0.1711	0.4480	0.8371	0.2965	0.1280	0.3264	0.4170
9	13,000	11.00	10.00	0.1026	0.4209	0.7208	0.2864	0.0942	0.3617	0.4438
2	37,000	3.00	10.00	0.0605	0.8628	1.2520	0.1827	0.0777	1.5244	0.4329
19	37,000	3.00	10.00	0.0522	0.9938	1.4292	0.2660	0.0933	1.3558	0.4282
27	13,000	3.00	10.00	0.1735	2.0380	2.6379	1.9874	0.6534	0.8094	2.3347
4	13,000	3.00	10.00	0.2672	2.1464	2.1464	1.8738	0.4039	0.7245	2.1464
18	25,000	7.00	3.18	0.0282	0.5755	0.9362	0.1026	0.0653	1.2895	0.1590
24	25,000	7.00	3.18	0.0130	0.6810	0.9659	0.0636	0.0651	1.3020	0.1312

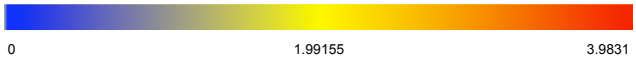

Figure 4.26: Gene Expression data for the optimisation experiment. The normalised expression data for all the genes investigated in the central composite design were plotted to see if any clustering could be observed. The colour coding is based on the key at the bottom which displays the range of data obtained for gene expression data normalised on *UBC* and *B-ACTIN* internal housekeeping gene controls.

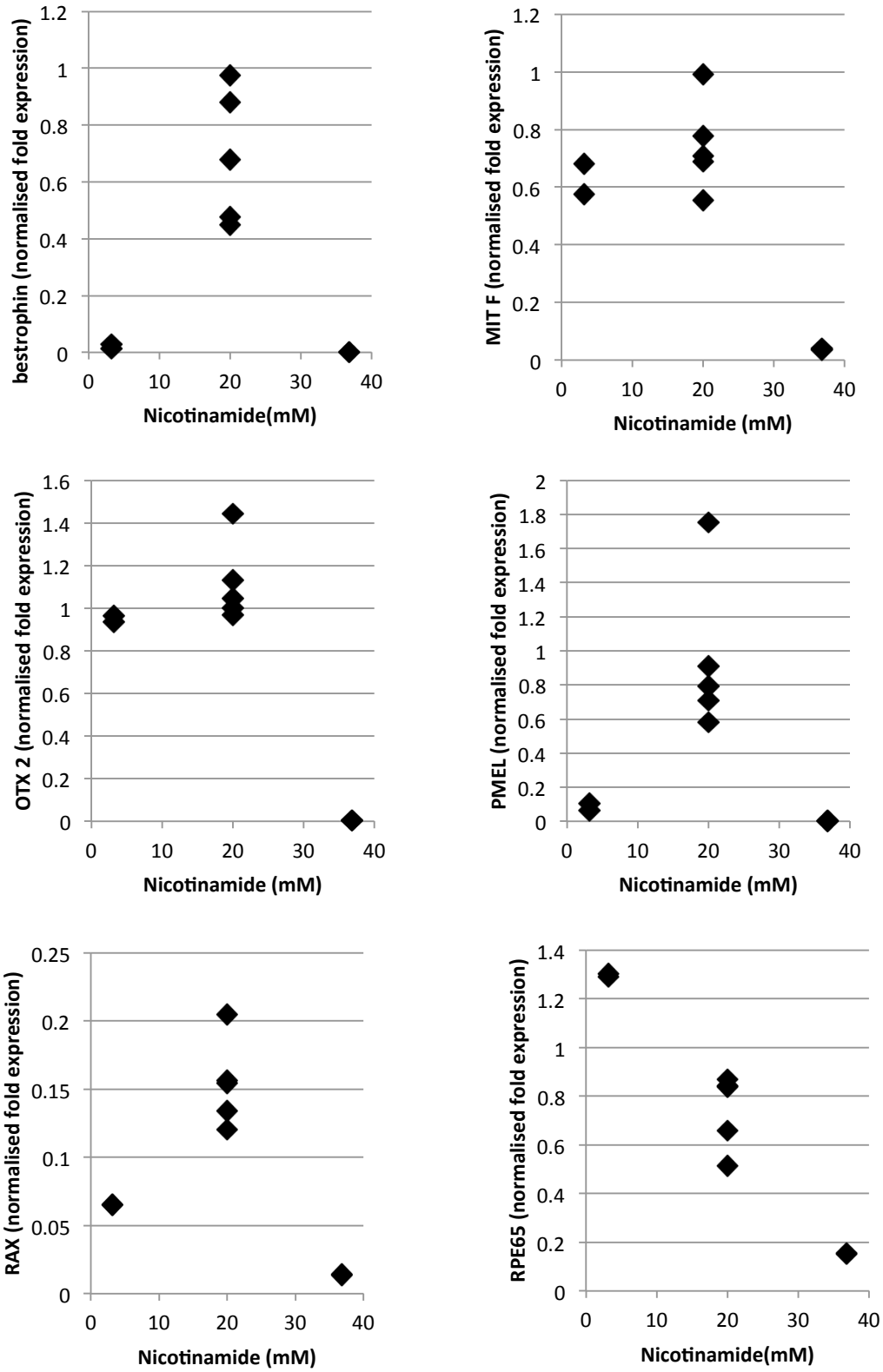

Figure 4.27: Plots of gene expression and percentage pigmentation Vs nicotinamide concentration for the optimisation experiment

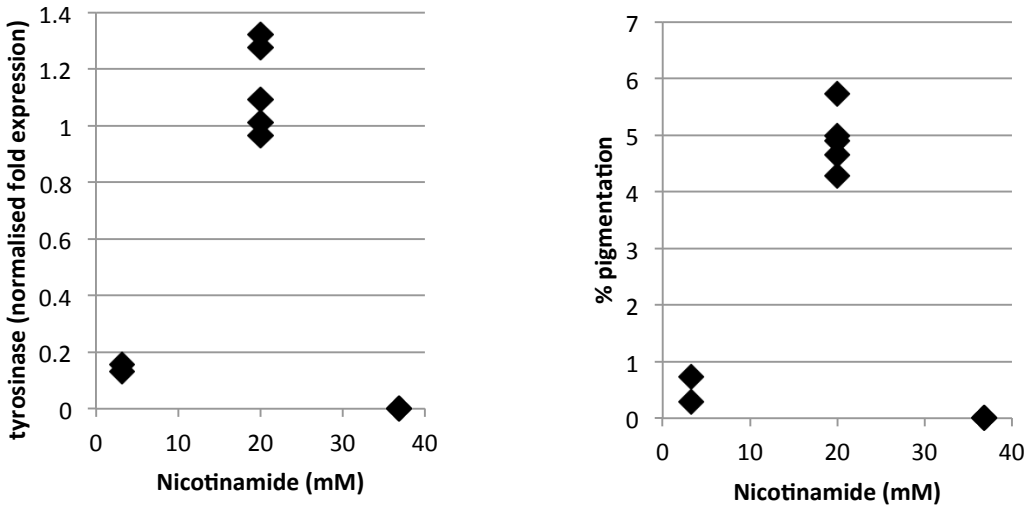

Figure 4.28: Plots of gene expression and percentage pigmentation Vs nicotinamide concentration for the optimisation experiment– continued.

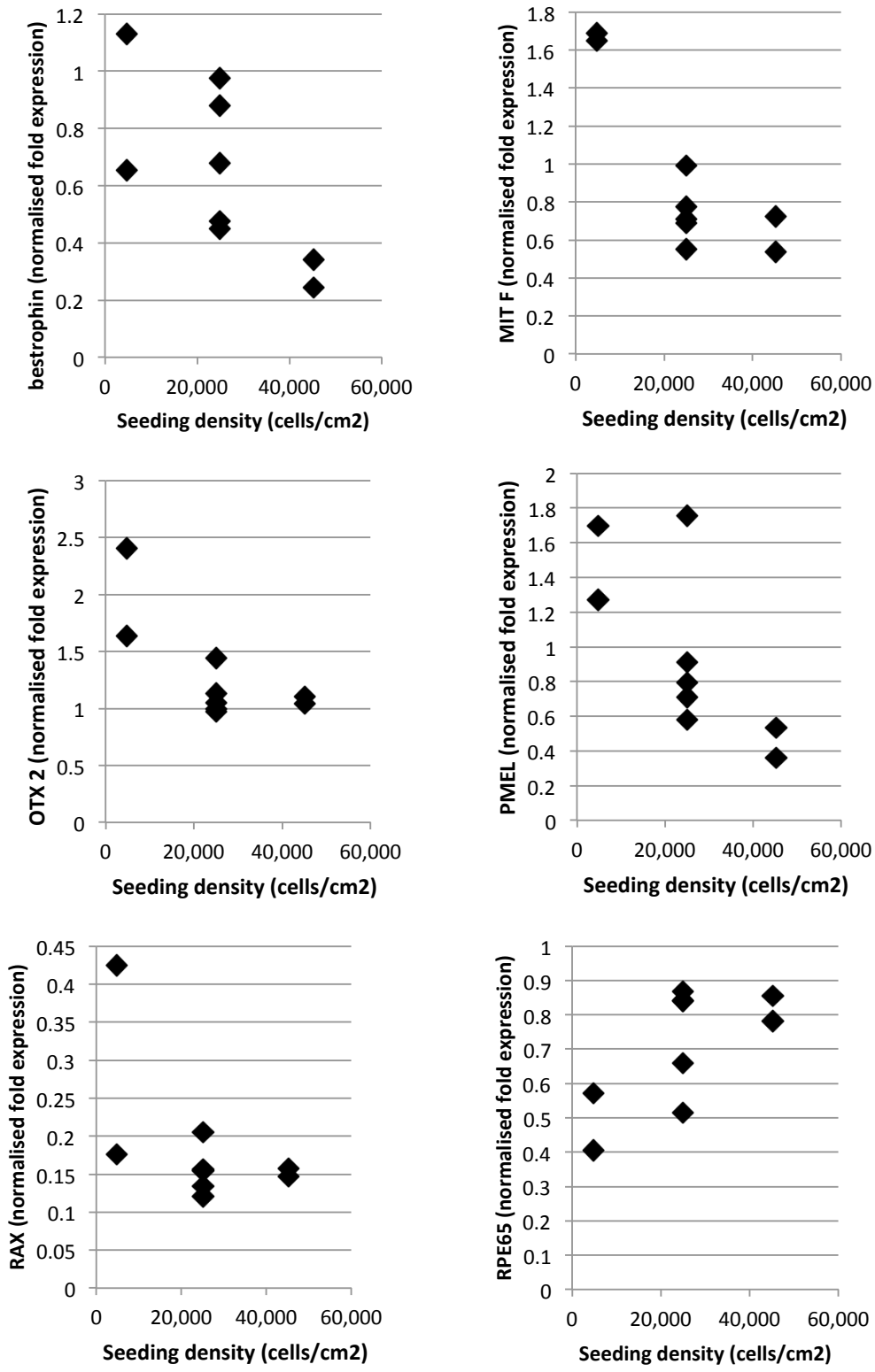

Figure 4.29: Plots of gene expression and percentage pigmentation versus seeding density for the optimisation experiment outlined Figure 4.15.

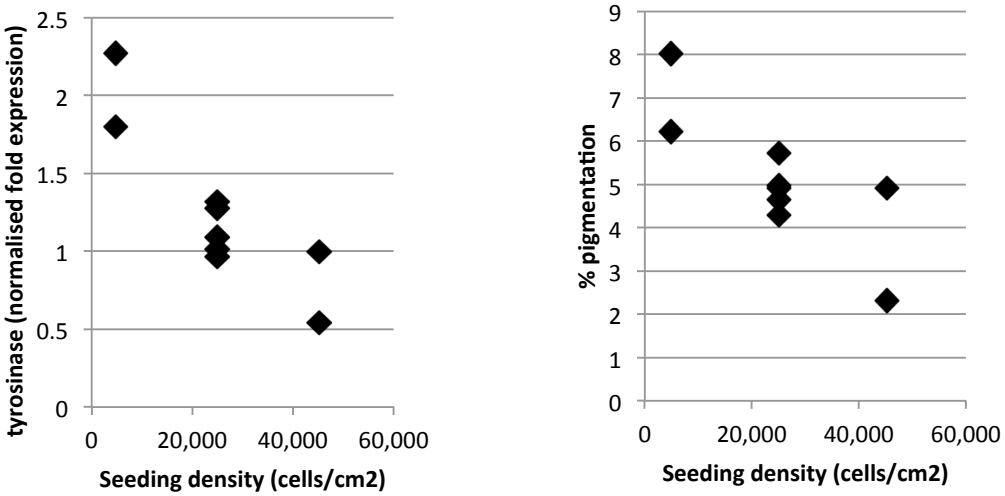

Figure 4.30: Plots of gene expression and percentage pigmentation versus seeding density for the optimisation experiment Figure 4.15.

5. Isolation of retinal pigment epithelium cells from differentiating pluripotent stem cell monolayers

5.1 Introduction and aims

5.1.1 The bottleneck of manual pigmented foci separation

Key to transforming the current lab based protocol to a commercialisable bioprocess is addressing the separation bottleneck of removing the pigmented RPE from the other non-RPE contaminants in the differentiating monolayer. The current method is described as follows and is replicated from Vugler et al. (2008) "*pigmented foci are excised mechanically using the tip of a glass Pasteur pipette and microsurgical blades – this only being practical when foci had reached at least 1 mm in diameter. Efforts are made to dissect away surrounding, non-pigmented material. The excised foci are then directly plated onto matrigel coated plates to expand as a monolayer".* Clearly this method is undesirable because it is highly manual and operator dependent. The purity and quality of the excised foci is also subjective as the protocol prescribes that "best efforts" are made to dissect away contaminant material. Thus determining any critical quality attributes or achieving reproducibility in commercial production is very unlikely. It is also exceptionally hard to do in practice taking around 30 min for a single T25 flask. Consequently, alternative approaches need to be explored.

5.1.2 Technologies for the separation of live cells

There are a number of technologies for the identification and separation of sub populations of cells that could be used as alternatives to the manual method currently employed. Such methods have traditionally been utilised for analytical purposes e.g. disease diagnosis. Apheresis machines and other technologies, such as density based centrifugation are commonly used to enrich blood for a particular sub population, for instance, monocytes, based on the differing physical characteristics of the cells. However, such systems are not well suited to the purification of PSC derived differentiation products where the differences

between the cells are more nuanced and higher purities are a requirement. Here the most common methods suggested are fluorescence-activated cell sorting (FACs) and magnetic-activated cell sorting (MACs) which are currently applied in single patient therapies for instance the separation of CD34+ cells for hematopoietic stem cell transplants after radiotherapy.

5.1.3 Fluorescence-activated cell sorting (FACs)

Flow Cytometry (**Figure 5.1 a**) involves the passing of a single cell suspension through a small capillary where it is interrogated with a laser. Analysis of the cells is based on computational identification from the relative light-scattering and colour-discriminated fluorescence. Typically cells are labelled to aid identification by using primary antibodies raised against specific cell markers in or/on target cells. Then a fluorophore labelled secondary antibody attaches to the primary antibody, labelling the cell. FACs sorts cells by putting the stream of cells into droplets of liquid with each drop containing only one cell. Target cells which are identified and 'gated' by the computer software have their droplets labelled with an electric charge, this physically alters their trajectory as they pass deflector plates, causing the cell to be deposited in a specific collection tube **(Figure 5.1 a)**.

Although capable of highly selective separations the capacity of the technology as a commercial purification system for allogeneic therapies is limited. For instance the manufacturers data for the BD FACSAria III reports a throughput of 70,000 events for cell sorting can be achieved without affecting purity, however, this 'high' speed greatly affects yield. This is because in order for the system to achieve high purity a compromise needs to be made against yield. When the machine detects two drops as being too close together to be physically separated as determined by the software a separation attempt is not made and so both drops go to waste. Experimental analysis and modelling of this trade-off using PSCs could not be found on the manufacturer's site or in the literature. The performance robustness of FACS in a commercial bioprocess also represents something of an unknown as key performance indicators such as purity, viability and yield are highly dependent on the cell type used, the population being isolated, and the protocols applied as discussed in

depth in the review by Weil and Veraitch (2014). Overall the inherent problem in scaling up FACs technology in that it only interrogates one cell at a time, and with the high costs of each machine 'scale out' is not an option. This limited throughput also means very long processing times if FACS was applied to the separation of pigmented RPE at commercial scale where it is likely many billions of cells would need to be processed as part of an allogeneic bioprocess. However it remains a highly powerful tool for the specific isolation of cells prior to expansion at the start of a process.

As the RPE cells are highly pigmented it was expected that the cells would have a greater side scatter and lower forward scatter on a flow cytometry dot plot than the other non-pigmented cells in the heterogeneous differentiating culture, as is the case with pigmented melanocytes (Dupin et al., 2000). In fact Shi and Clegg (2008) used FACS on the expanding PSC-RPE monolayer (after manual separation and re-plating) to enrich what they termed as "darkly pigmented" cells from 30.4% before the sort to 90.6% after the sort. Some initial work was undertaken in pursuit of this thesis to determine if a pigmented population within the differentiating monolayer could be identified using flow cytometer (data not shown), however without a second fluorescence marker to compare against it was virtually impossible to define a subpopulation on pigmentation alone, particularly given the low efficiency of the differentiation protocol used (a few per cent).

5.1.4 Magnetic activated cell sorting (MACs)

Magnetic activated cell sorted MACs has far better prospects from a viewpoint of scale-up with the throughput being limited to the size of the column and the number of labelled magnetic beads available for binding, an overview of its operation is reproduced in **Figure 5.1 b)**. This affinity chromatography system could also benefit from knowledge transferred from the scale-up of traditional biopharmaceuticals in which chromatography is a key purification technology. The autoMACS platform which is the trade name of the electronically controlled automatic MACS systems from Miltenyi has a column capacity to bind up to 2×10^8 magnetically labelled cells from a total cell population of 4×10^9 cells (50ml tubes) "in about 5 minutes" (personal communication). Throughputs in the technical

specification (based on 1ml) is 10^7 cells/sec with a total program time of 2-15mins (dependent on the separation program selected), so even at this small scale MACs would appear to have a far higher throughput than FACs. In addition the MACs technology has already been used in the clinic with the 'cliniMACs' machine used in the isolation of CD34+ cells from blood.

Unfortunately no papers were found in the literature that adequately compared the purity and throughput achieved with the two different technologies where multiple variables were investigated for an optimised system. If would be assumed that as the MACs system scales by increasing the column size that this is inherently more scalable. Importantly both systems make use of the antibody labelling of the cells, which is both highly expensive, and a regulatory concern. The latter is due to the safety considerations of introducing antibodies raised in a different species (typically rabbit, goat or mouse) into therapeutic process as they present the risk of zoonoses. The alternative would be to produce the antibodies through recombinant technologies, for example, using a CHO (Chinese hamster ovary) expression system. However this would be far from trivial and likely to be expensive. Additionally, the work needed to prove no transmissible agents were introduced and that the antibodies and their attached fluorophores/magnetic beads were absent from the end product would be considerable. But perhaps the main criticism of using antibody labelling in a therapeutic bioprocess in this PSC-RPE application is that no definitive RPE marker was available to this project.

5.1.5 Dielectrophoresis

An alternative to MACs and FACs postulated in the literature, which does not involve antibody labelling is dielectrophoresis (DEP). Here, electrical stimulation induces a frequency-dependent dipole in the cells which traps/migrates them towards or away from the electrodes. The effect is dependent on the cells' composition, morphology and phenotype (Doh and Cho, 2005). For example, Flanagan et al. (2008) showed that populations of mouse neural stem/precursor cells (NSPCs) harvested from mice at different stages of embryonic development displayed different differentiation propensities, the

NSPCs from different stages could not be characterized using FACs but could be by using a DEP device. This demonstrates the DEP technology as a useful characterization tool where suitable markers are unavailable. At the microfluidic scale such devices have been modified to operate under a continuous flow regime to separate viable and dead yeast cells at a flowrate of 4.8million cells an hour (Doh and Cho, 2005) this compares favourably to the separation of PSC from PSC derived neurons using a FACS machine, operating at a throughput of 3.6-10.8 million cells and hour (1K-3K per second) (Pruszak et al., 2007). There are examples of many other DEP sorting devices in the literature (Korohoda and Wilk, 2008, Wang et al., 2009, Alazzam et al., 2008). The low cost of these microfluidic devices mean they can be a disposable technology which helps with batch-to-batch validation and thereby making them cost effective for 'scale out'. It would be assumed the technology would be readily applicable to the RPE separation due to the high concentration of charged melanosomes in the RPE (Testorf et al., 2001). The expectation being that the melanosome charge would result in a vastly different experience of the RPE to the DEP effect compared to the non-pigmented contaminates, thereby creating a basis for separation. However, without a commercially available device the technology is unlikely to be applied to any cell therapy in the immediate future and so not pursued in this thesis.

5.1.6 Laser-enabled analysis and processing system

Due to the pigmented nature of the cells allowing the identification of the RPE phenotype via bright field imaging, some preliminary work was conducted using the laser-enabled analysis and processing system (LEAP), from a company called Cyntellect which is no longer in existence. The system combines a rapid whole well imaging system with a selective laser to purify colonies based ablation of contaminants. The device was marketed as a method to passage PSC colonies or to remove cells which had failed to reprogram in iPS protocols. A number wells containing pigmented foci were tested on the system (**Figure 5.1 c**), which allowed pigmented areas to be manually "circled" using the software. The laser then ablated the surrounding cells with the aim that the pigmented foci would be released. The early results from the system demonstrated it might have some promise if applied earlier in the differentiation protocol, but as with the aforementioned build up of extra

cellular matrix the laser cutting was inconsistent across the well. A hypothesised protocol would involve repeated removal of non-pigmented cells surrounding the foci allowing room for the foci to expand into a monolayer without the need for replating. However, due to circumstances beyond the control of this thesis further work on the machine to test his protocol on the machine was not possible (the company is now no longer in existence).

5.1.7 The required purity of a separation technology

As discussed in the Introduction to this thesis the final therapy could be contaminated with undifferentiated PSCs, cells with abnormal karyotype, or non-RPE contaminant cells. Thus, when evaluating and eventually deciding on a separation technology the required purity needs to be considered.

Crucially when considering PSCs in the final therapy it is unknown whether all contaminant PSCs need be removed from a therapy or whether a certain amount is acceptable. For instance Lawrenz et al. (2004) found that injections of as few as 2 mouse embryonic stem cells (mESC) into BALB/c nude (inhibited immune system) mice produced teratomas yet the study of Shih et al. (2007) showed it took a minimum of 5000 PSC injected into engrafted human foetal tissue (lung and thymus) into severe combined immunodeficient mice (SCID) mice, to cause teratomas, yet a level of 50 PSC contaminants did not. The site of implantation of the cells also seems to play an important role, when PSC were engrafted into the liver of nude mice large tumours (teratomas) formed containing a majority of 'immature' cells, yet masses from subcutaneous implantations grew slower eventually containing differentiated cells (Cooke et al., 2006). The result being an unclear view into the amount of PSC which would be considered safe in a therapy.

Using the findings of Lawrenz et al. (2004) where only 2 mESC caused tumours a paper by Schriebl et al. (2010) experimentally characterised a MACs sort based the separation of mouse stem cells. Applying a model calculation they estimated the number of separation stages needed to achieve a purity of less than 10^{-1} stem cells per 10^{9} cells in a single treatment. With an initial purity of 60% they equated it would take 31 stages to achieve this tolerance. This lead them to conclude that with a target log clearance rate of 10 for a

hypothetical clinical product that the MACs technology as it stands was not suitable. However, the situation is far more complex than this as the Lawrenz et al. (2004) data is based on putting mESC into immunosupressed mice rather than human PSCs as xenografts into immunosupressed mice. So these papers present a poor model for a human therapy, and thus requirements of a separation technology.

Fortuitously, with respect to the PSC-RPE clinical protocol PSC contamination in the final product does not seem to be an issue. The rationale being the length of the differentiation protocol is so long that the pluripotent phenotype is lost completely as determined by QPCR analysis (data not shown). This is also seen in the literature with Anisimov et al. (2010) reporting that in animal studies long differentiation protocols removed the risk of tumor formation for stem cell transplants.

Of other importance is contamination from non PSC-RPE cells in the final therapy. The current crude manual separation which involves best efforts to remove non-pigmented cells has actually been shown to be highly robust in animal studies as part of pre-clinical development (personal communication with Professor Pete Coffey, data not publically available). With no graft overgrowth of contaminant cells on the implanted patches. Therefore for the planned initial human trials the patches for implantation are released based on viability, cell coverage, morphology and pigmentation. With a QC patched interrogated for TRA-1-60 (pluripotency marker), Ki67 (a proliferation marker, RPE being post mitotic), PMEL-17 (RPE marker) and MERTK (RPE marker).

5.1.8 Aims

With the potential cell separation methods described above not well suited to a commercial PSC RPE purification it was important to explore alternate approaches. During experimental work on the cells it was noticed that the in the spontaneously differentiating monolayers that the RPE cells and bulk monolayer have a differing susceptibility to dissociation agents. This observation became the basis of developing a novel filter based separation method. Specifically the aims were:

- Characterise the spontaneous formation of pigmented RPE foci in monolayer culture and evaluate the current manual method of isolation and subsequent expansion.

- Exploration of a novel alternate enzymatic and filter based separation method which was discovered serendipitously through working with the cultures.

5.2 Materials and methods

5.2.1 Cell culture and differentiation into PSC-RPE

The Shef 3 hESC line was passaged manually twice weekly using the tip of a Pasteur pipette and co-cultured on mitomycin c inactivated mouse embryonic fibroblasts (MEFs). MEFs were originally grown in Dulbecco's Modified Eagle Medium (DMEM, Life Technologies) with 10 % (v/v) heat inactivated fetal bovine serum (FBS, Sera Laboratories International) and 1 % (v/v) 100x alpha MEM non-essential amino acids (NEAA, Life Technologies). PSC were grown in Knockout DMEM, (Life Technologies)(4.5 g D-glucose/L, sodium pyruvate, -L-glutamine), 20 % Knockout Serum Replacement (Life Technologies), GlutaMAX, (Life Technologies), 0.1 mM b-mercaptoethanol, human basic fibroblast growth factor, 4 ng/ml (bFGF, R&D systems), and 1 % 100 alpha MEMNEAA (Life Technologies).

5.2.2 Filter separation method

T-25 flasks which had been left to differentiate for at least 8 weeks to the point which pigmented foci were observed were rinsed 3x with dPBS and 2 mg/ml Collagenase IV was added. These flasks were left overnight on a shaker platform set to its highest setting in an incubator (5% CO_2, 37^0C). These cultures were than pelleted at 300 rcf for 3 min, and re-suspended in PBS and passed through a 70μM filter. The non-pigmented run though was also pelleted to determine if any pigmented clusters had made it though the filter or if the pellet itself was discoloured.

The pigmented foci retained on the surface of the 70μM filter were rinsed from the filter using 0.25% trypsin (Invitrogen). This foci-trypsin suspension was then incubated for 30-

45m until the foci visually 'fell apart'. Repeat pipetting of the solution was then used to try and obtain a single cell suspension. This suspension was then transferred to a fresh 70μM filter and inactivation media (PSC media -bFGF) was used to rinse the filter into a collection tube. The resultant suspension was then pelleted at 300 rcf for 3 min and re-suspended in PSC media –bFGF and counted using a haemocytometer.

5.2.3 PSC-RPE expansion

After the PSC-RPE were separated from the contaminant cells they were replated onto wells coated with Matrigel (BD bioscience) and the media was changed twice weekly using PSC media as previously described but without bFGF.

5.2.4 Image J analysis

The percentage of pigmented cells in the seeded population was determined via manual counting of the pigmented cells. Images from 3 fields of view taken using the Nikon Eclipse 2000 inverted microscope and the NIS-elements software. These images were then imported into Image J (National Institute of Health) and the software's cell counting and annotating tools were used.

The relative coverage of pigmented area for the expanded RPE was also determined via Image J analysis. Images taken using the Nikon Eclipse 2000 inverted microscope and the NIS-elements software were first cropped to remove any areas of shadow and then imported into Image J and converted to binary form via setting of a threshold value where all pigmented cells were accounted for. The percentage area covered was measured using Image J's built in analysis tool.

5.2.5 Immunocytochemistry

Cells were fixed in a 1.33 M PFA solution and 0.25 %v/v Triton X was used to permeabilise cells. Primary antibodies used were as follows Bestrophin (1:1000 dilution, Millipore), OTX 2 (1:500 dilution, Millipore), ZO1 (1:50 dilution, Zymed). The following secondary antibodies were used at 1:200 dilutions: Alexa fluor 488 goat anti-mouse IgG, Alexa fluor 488 goat anti-rabbit IgG and Alexa fluor 594 goat anti-rabbit IgG (all from Life

Technologies). Images were taken with an epifluorescence Nikon Eclipse 2000 inverted microscope and the NIS-elements software. Where applicable, isotype controls were run in parallel.

5.3 Results and discussion

5.3.1 RPE form spontaneously in differentiating RPE monolayers

The pigmented foci which form spontaneously in differentiating monolayers are very heterogonous in both shape and subsequent expansion within the culture. An example of two common morphologies is highlighted in **Figure 5.2. a)** which shows areas of foci which have clear boundaries and others which appear to be 'smeared'. Interestingly these 'smeared' areas increase in pigmentation overtime and become more defined as illustrated in **Figure 5.2. b)**. It is important to note that the other dark areas not highlighted by the arrow or asterisk in **Figure 5.2. b)** are not pigmented RPE and rather represent areas of monolayer build-up. Distinction between true pigmentation and this build-up is easier to discern with by eye then using a microscope.

5.3.2 Evaluation of the manual excision method

Over the prolonged differentiation period, which can be up to up to 12 weeks, large amounts of extra cellular matrix (ECM) build-up in the cultures. Therefore when the RPE are to be excised the whole culture can be pulled out as a single sheet that curls up into a 'slimy' ball **Figure 5.2. c).** This ball is highly elastic and hard to dissect making the release of the pigmented RPE harder, however foci are typically released as a distinct cluster of cells. Particular difficulties arise when the foci are very small and so cannot be easily dissected from contaminants and so are lost. Once transferred to fresh matrigel coated plates the expansion of the RPE monolayer was also seen to be highly variable. In some instances there was clear expansion of a pigmented monolayer from the explant **Figure 5.2. d)**. However, in other cases the foci appeared to just attach and not expand, it being unclear whether this was due to a lack of viability or other cause **Figure 5.2. e)**.

5.3.3 Immunocytochemistry determination of the RPE phenotype

The expanding RPE monolayers were interrogated for markers representative of the RPE phenotype. Bestrophin is found on the basolateral plasma membrane of differentiated RPE cells in vivo (Marmorstein et al., 2000) **Figure 5.3. a)**, OTX 2 is involved in RPE cell development and is localised to the nucleus **Figure 5.3. b)**, and Z01 is located on the cytoplasmic membranes surface of intracellular tight functions, found in both developing and mature RPE cells (Vugler et al., 2008) (see **Figure 5.4).** This immunocytochemistry of the explanted foci shows a clear correlation between the pigmented foci in the differentiating cultures **Figure 5.2 a), b)** and the characteristic pigmented cobblestone morphology and the expression of RPE markers (**Figure 5.3 and Figure 5.4**). The inference from this correlation being that the pigmented foci which spontaneously form will (if excised and replated on matrigel) expand into an RPE monolayer. Thus these spontaneously forming pigmented foci are RPE and not another pigmented cell type such as dopaminergic neurons of the substantia nigra. The ultimate way to confirm these cells are true RPE cells would be to determine their ability to rescue sight in the royal college of surgeons rat model of RPE (Sauve et al., 1998), or to test their ability to internalise fluorescently labelled rod and cone outer segments (Carr et al., 2009). However, such additional confirmatory testing was considered to be beyond the scope of this thesis, especially given the well-reported and clear correlation between pigmented foci and the RPE phenotype.

5.3.4 Single cell seeding improves RPE monolayer expansion post replating

As previously described and illustrated the subsequent expansion from the explanted foci isolated through the manual excision method was variable to the eye (**Figure 5.2 d)** and **e)**. These differences were further explored over a time course using microscopy **Figure 5.5 a)** and **c)**. The series of pictures shown in **Figure 5.5 a)** shows a mixed morphology expanded from the explant foci; initially one cell type expands from the boundary and becomes confluent and then a second more pigmented cell type emanates/matures in spikes or tubes with defined boundary like those displayed previously in **Figure 5.2 b).** In contrast the

series of images of **Figure 5.5 b)** show what appears to be the explanting foci reducing in size and pigmentation as time progresses and non-pigmented cells expand. It is unclear that if the experiment was run for longer whether this culture will re-pigment as described by Vugler et al. (2008). Finally the third series of images (**Figure 5.5 c**) shows clear expansion of a pigmented cobblestone morphology. Critically maintaining this cobblestone morphology has a clear relationship with the expression of markers representative of the target RPE phenotype. In **Figure 5.6** it can be seen that in areas where this target morphology is lost during expansion that the RPE marker Bestrophin is also lost.

To improve the expansion of the excised foci instead of plating whole foci onto matrigel the manually excised foci were first enzymatically dissociated using 0.25% trypsin (Invitrogen). When this single cell suspension was replated the expansion characteristics where vastly improved (see **Figure 5.7 a), b),** and **C).** Furthermore the seeding efficiency was very high and the cells quickly expanded to form a monolayer, which as it matured over a number of weeks became highly pigmented. What was of particular interest was that these qualities were not adversely impacted by very long incubation times (up to 45 minutes) with 0.25% trypsin to obtain the single cell suspension. An examination of the whole well scan (**Figure 5.8**) demonstrates a heterogeneous spread of pigmentation, a likely result of PSC-RPE colonies expanding to meet each other at different rates. Images **i)** and **ii)** in **Figure 5.8** show areas of very good RPE morphology but poor pigmentation, whether these areas will eventually pigment or if they are not optimal for use in a therapy is an unknown. Images **iii)** and **iv)** in **Figure 5.8** depict what could be described as the opposite to the former images i.e. poor cobblestone morphology yet high amounts of pigmentation. Whereas images **v)** and **vi)** shows cells which have high amounts of pigmentation and what could be good cobblestone morphology but it is hard to visualise due to the pigmentation. It was hypothesised that a more heterogeneous expansion could be achieved by varying the seeding density as from the whole well image it appears that a number of individual colonies have expanded and collided and then pigmented at differing rate. Such experimentation on the seeding density is explored later in this Chapter.

5.3.5 A novel enzymatic PSC-RPE purification method

While attempting to dissociate the spontaneously differentiating PSC monolayer it was noted that the pigmented foci were preferentially released from the thick monolayer when collagenase was used rather than trypsin. These foci remained whole and intact and would not further dissociate using longer incubation periods with collagenase (see **Figure 5.9**). After some initial experimentation it was determined that the foci could be successfully removed from the contaminant monolayer by overnight incubation in 2 mg/ml collagenase on a shaker platform set at its highest setting. The foci could then be separated from the resultant suspension via filtration through a 70µm filter that retained the foci. The non-pigmented contaminant filtrate was then centrifuged to identify if any pigmented cells had passed through the filter. From visual observation there was no discernable pigmentation suggesting yield is high, however further experimentation would be needed to quantify this. PCR might be a useful assay to quantify this. As described in the methods section the retained foci where then dissociated into a single cell suspension through extended incubation with 0.25% trypsin (up to 45 minutes) and pipetting of the same and filtered again through a 70µm filter. When these cells were replated and compared to manually excised foci which were plated onto matrigel without dissociation there was a clear improvement in RPE expansion after 4 weeks (**Figure 5.9 b**). Additionally it can be seen in **Figure 5.9 b** that in the wells where the foci were manually excised that a non-pigmented cell type has proliferated across the well and caused the cell sheet to peel at the edges (as denoted by arrows). Although it is unclear where this second type is a contaminant of not, such peeling is undesirable in culture.

Using this enzymatic and filtration method as described above it was then explored to see if there was an optimum seeding density which would allow expansion of the PSC-RPE whilst maintaining the RPE phenotype **(Figure 5.10)**. It can be seen that the best result from a morphology perspective were achieved at the highest seeding density of 67,000 cells per cm^2. This culture was fully confluent at only 3 days post seeding and at D22 had the highest percentage of pigmentation at 69%. At the lower seeding densities more swirl-like morphology was observed and the resultant pigmentation was lower. When the whole

wells were scanned using a flat bead scanner at the highest density of 67,000 cells per cm^2 **(Figure 5.11 a)** there were a couple of areas in which aggregates had been transferred to the well, possibly a result of over-pipetting the sample after it was passed through the final filter. Yet overall the well had clear homogeneity of pigmentation. For 50,000 cells per cm^2 **(Figure 5.11 b)** there was a denser 'streak' of cells at the centre of the well where the cells had accumulated. Such a distribution has been seen using other cell types in smaller well formats (e.g. 48 well), it would be assumed this phenomenon could be avoided by moving up to a larger well format. Further work is needed to characterise this successful proof of concept separation method quantitatively using a range of phenotypic markers to explore purity, yield and devise a way to scope the target morphology.

5.4 Conclusions

RPE adopt a number of morphologies as they appear as foci in PSC monolayer differentiation experiments, why exactly there is heterogeneity is an unknown but for the current manual excision method foci less than 1mm cannot be successfully harvested. The manual method is very hard to perform and time consuming and without subsequent dissociation of the foci poor expansion of the PSC-RPE culture is seen. As has been widely reported in the literature these pigmented foci once replated quickly expand and adopt a highly distinct pigmented monolayer which is positive for RPE specific markers (where the morphology is maintained), this validates the approach of tracking percentage pigmentation - to track the differentiation in a non-invasive way. In addition this adds to the confidence that it is not another pigmented cell type that has been obtained.

There are a number of separation technologies that could be used to replace the manual method, such as FACs, MACs, and potentially dielectrophoresis. As these technologies currently stand they are not well suited to the mass manufacture of an allogeneic cell therapy. The exception being MACs where there is precedent for the scaling of affinity chromatography in recombinant protein purification. However, without a definitive surface marker to base the sort on, the costs involved, and validation effort involved in sorting using antibodies the approach is not without significant issues.

Although the current manual separation approach makes best efforts to only take pigmented cells the approach clearly cannot produce 100% purity, however in numerous animal studies there has been no issue arising from a contaminant cell type causing graft overgrowth etc. Thus without a need for a high purity separation stage the antibody based separation methods of MACs and FACs are probably not required to ensure the safety of this particular PSC-RPE therapy.

In fact, it would appear that there is no requirement for a separation stage at all. After the work reported in this Chapter was completed, a paper was published by Maruotti et al. (2013) which serially passaged the entire differentiating sheet to produce the target RPE monolayer. The difference to the method described in this Chapter is the Maruotti et al. (2013) method does not have the first filtration step to separate away the dissociated non-pigmented cells from the non-dissociated foci, but instead it passages the whole culture. Specifically in the Maruotti et al. (2013) approach the differentiating culture is incubated for 4 hours under collagenase, then under Accumax (Sigma-Aldrich) for 45mins, and through the use of "vigorous" pipetting and passing the suspension through a 40μm filter, a single cell suspension was obtained and seeded at 100,000 cells/cm^2. This is a far higher seeding density than that explored here (67,000 cells cm^2), however based on the trend observed it would be assumed that the higher density would result in an improved morphology and in the current clinical protocol a seeding density of 116,000 cells/cm^2 at the final stage onto the membrane for implantation.

5.5 Summary

The current manual separation method is totally unsuited to commercial manufacture and needs to be replaced. The enzymatic based method described here and the similar one described by Maruotti et al. (2013) demonstrate there are enzymatic alternatives which provide a proof of concept for further optimisation for adoption into a commercial bioprocess.

5.5.1 Future work

Ideally the method described here would be compared to the method described by Maruotti et al. (2013), however due to a lack of clinical understanding there is no quantifiable target product profile to optimise either method and compare them. For instance although the cobblestone morphology with tight junctions is the target attribute of the monolayer there is no easy way to quantifiably score it for a whole well, here some kind of automated imaging combined with algorithmic analyses of the morphology like that described in Vugler et al. (2008) and Boatright et al. (2015) could be useful. Another way to test the integrity of the PSC-RPE sheet in transwell plates is to test for impedance and permeability, with the sheets with the highest impedance and lowest permeability representing the more mature phenotype (Savolainen et al., 2011). Both tests are non-destructive and so would be ideal lot release tests if they could be validated to relate to functional tests such as rod and code phagocytosis *in vitro* and expected clinical efficacy. Finally, no matter which enzymatic method is pursued the method needs to be scaled up so that the changes between dissociation agents, wash media and inactivation media can be completed in an automated fashion. There are a large number of filtration units and purification rigs currently applied to whole cell separation and protein purification that could be modified to the task to create a robust, controllable and so validatable separation solution.

a)

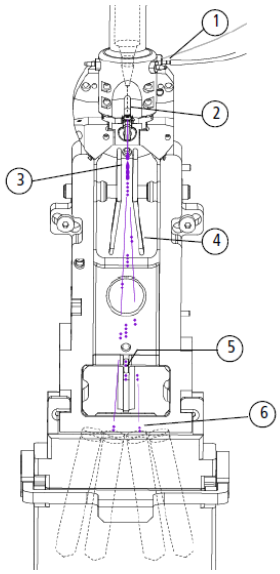

1. Charge is applied via the stream-charging wire in the barb.
2. The sample generates light scatter and fluorescence signal. The signal is analyzed.
3. The charged droplet breaks off.
4. Deflection plates attract or repel the charged droplet.
5. Uncharged droplets pass to waste.
6. Charged drops containing particles of interest are collected.

b)

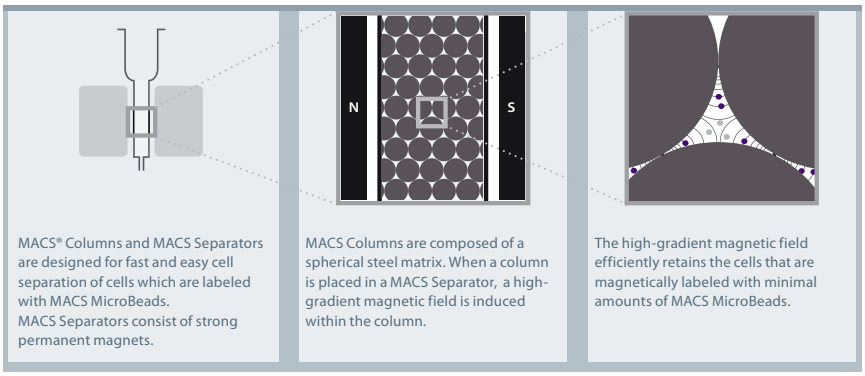

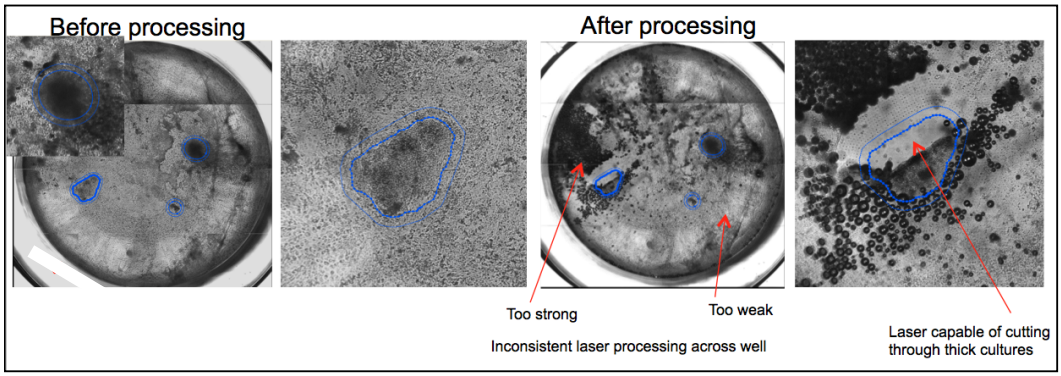

Figure 5.1: Antibody and laser based cell sorting methods. a) Schematic of the Aria II FACs machine (BD Biosciences), b) operation principal of the MACs system (Miltenyi) and c) results from using the LEAP system (Cyntellect).

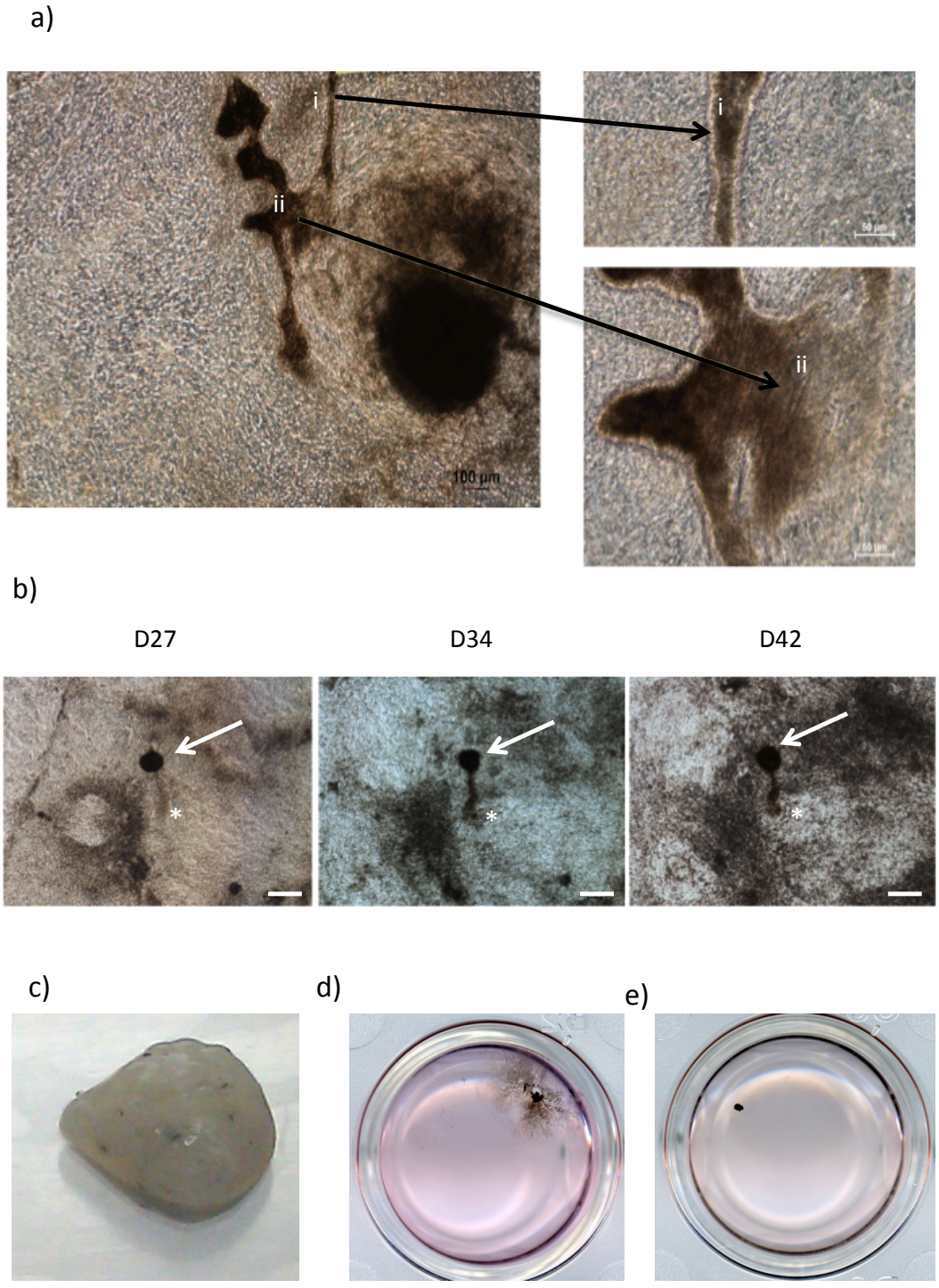

Figure 5.2: Characterisation of the spontaneous formation of pigmented RPE foci and their replating after manual excision. a) An example of two common types of foci morphology those with clearly defined boundaries i) and those with hard to define boundaries and appear 'smeared' ii). b) Overtime foci areas with clear boundaries do not increase in size (denoted by the white arrow), however areas which appear 'smeared' (denoted by *) increase in pigmentation and achieve clearer boarders, scale bar 200µm. c) A differentiated cell 'sheet' curled up into a ball. Examples of post dissection expansion d) and e).

a)

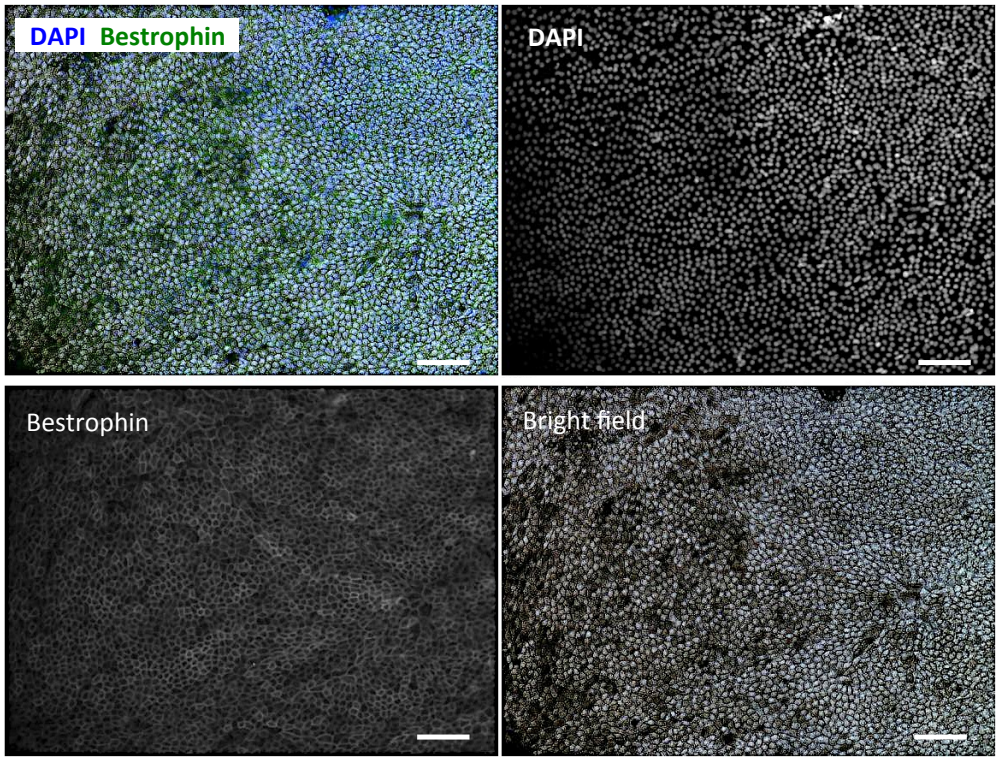

b)

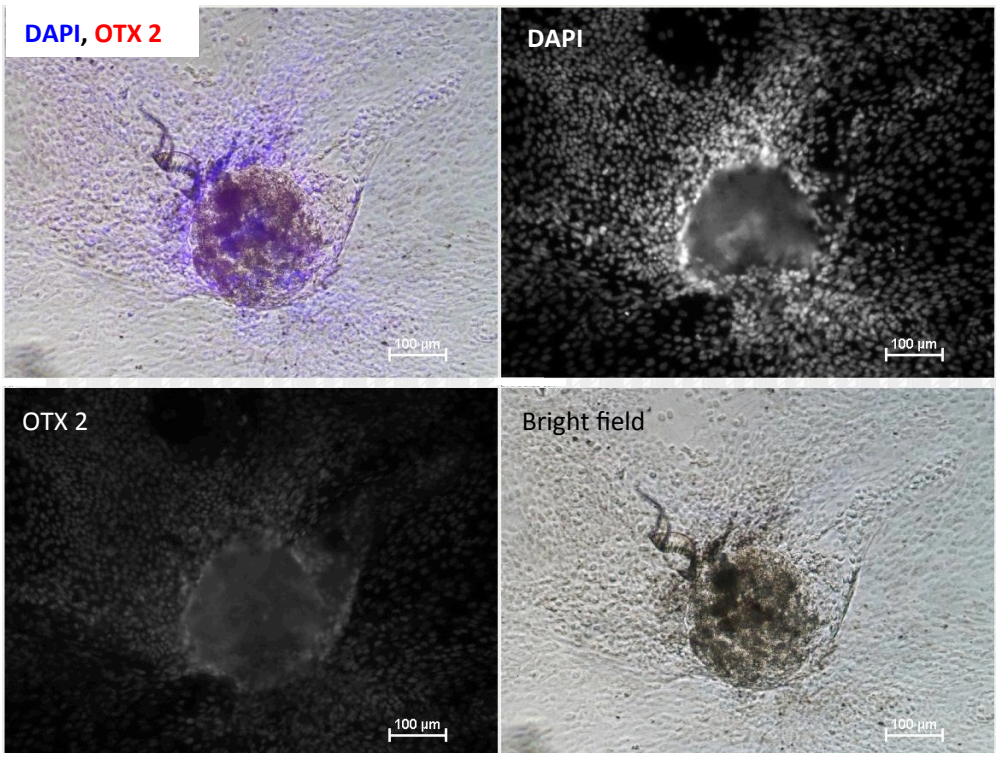

Figure 5.3: Expanding RPE monolayer stained positive for bestrophin a) and OTX 2 b). scale bar 100µm

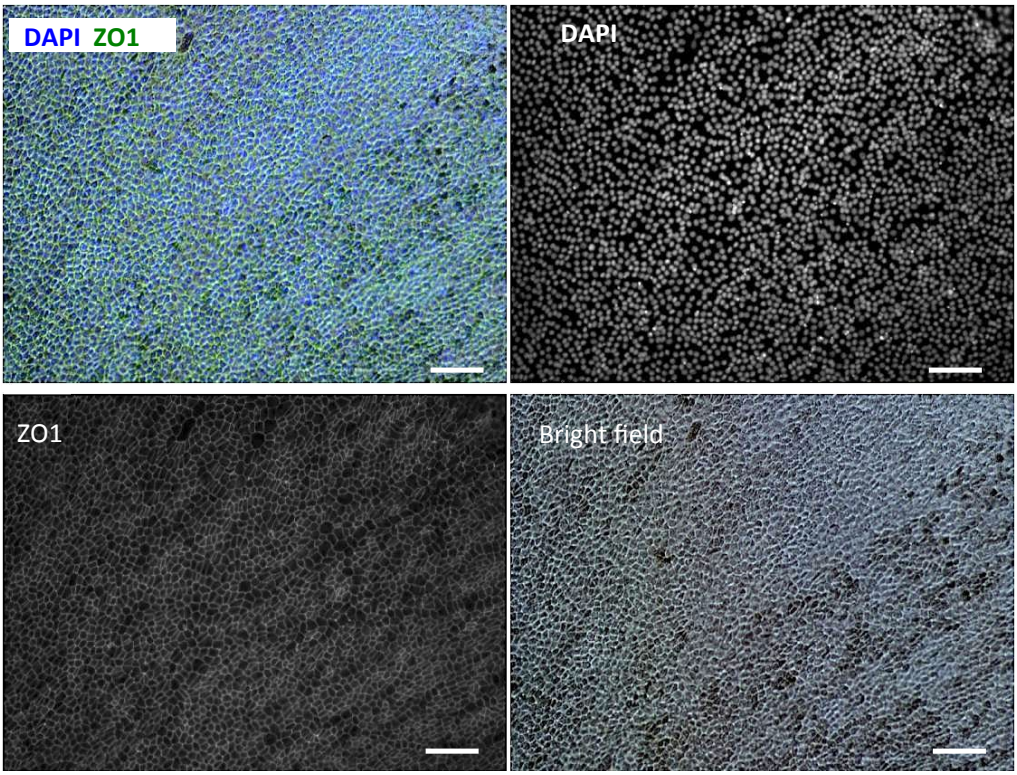

Figure 5.4: Expanding RPE monolayer stained positive for ZO1. Scale bar 100µm

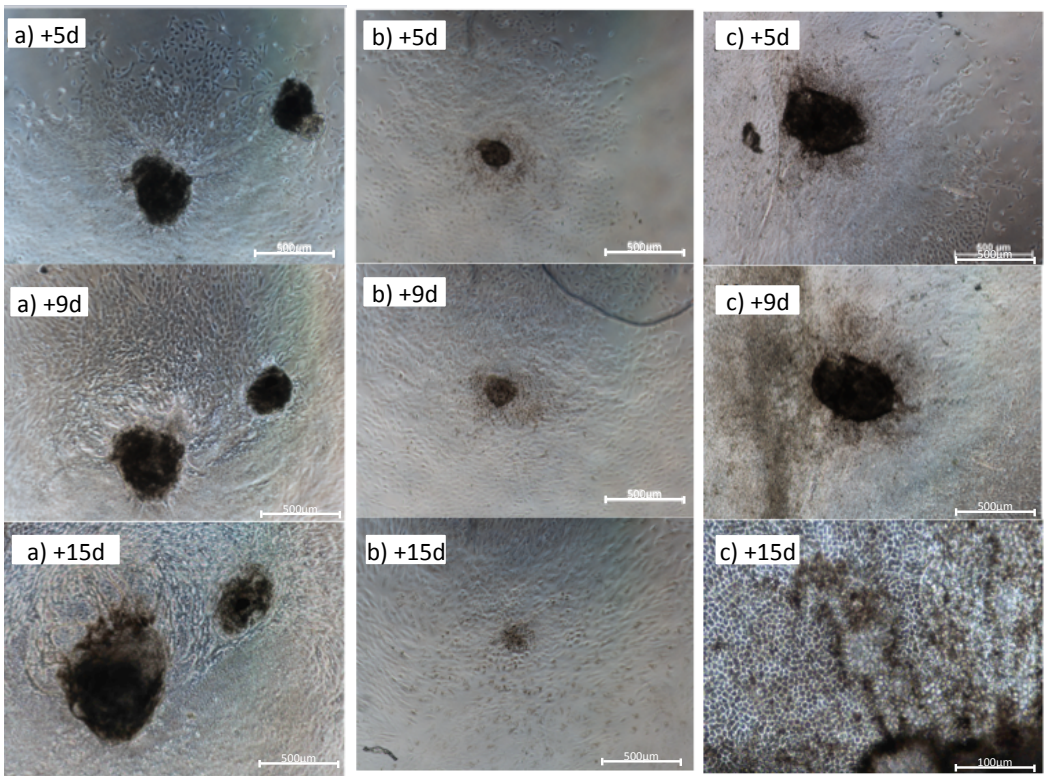

Figure 5.5: Time course of three expanding explanted foci. Explanted foci expand in a multitude of ways once replated onto matrigel

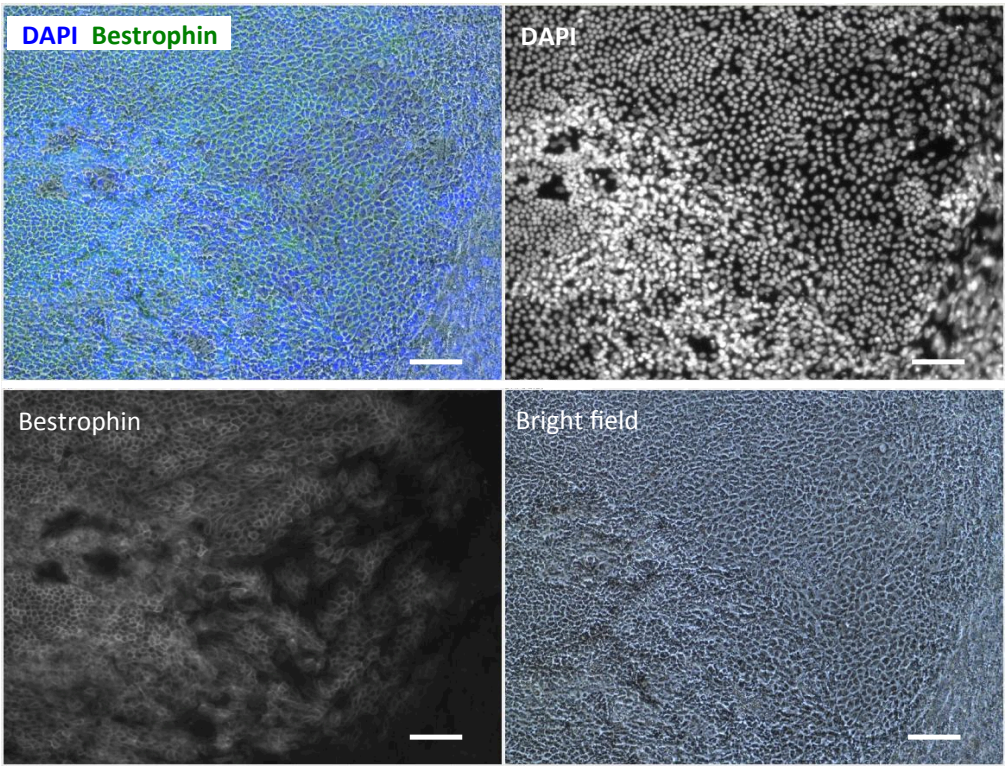

Figure 5.6: RPE related protein expression is related to morphology. Areas of cobblestone RPE morphology correspond to the expression of the RPE related marker Bestrophin.

a)

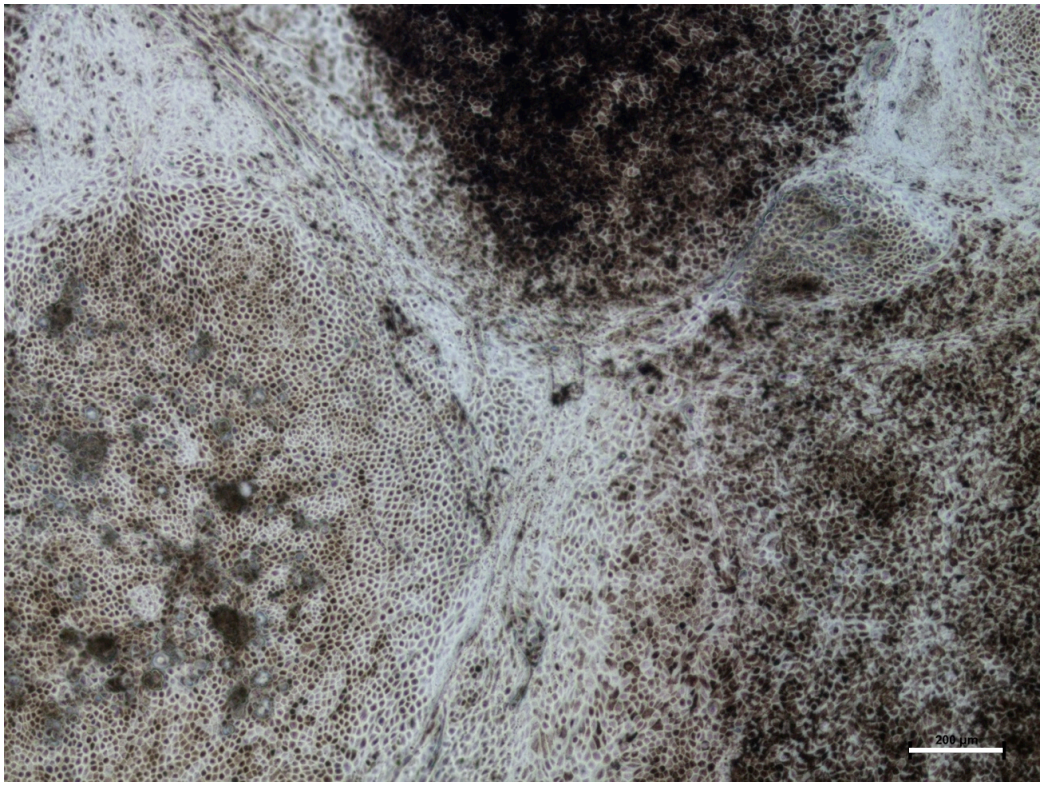

b)

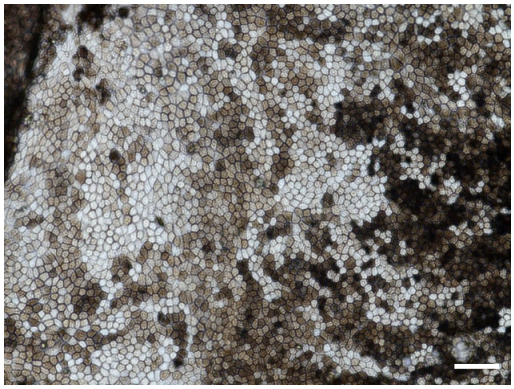

c)

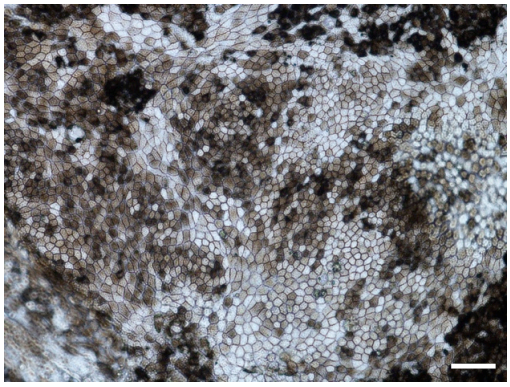

Figure 5.7: Representative images of manually excised foci replaced after single cell dissociation. Large areas of expanding cobble stone colliding a), scale bar 200µm. Higher magnification images show a homogeneity of morphology and a variation in pigmentation b) and c), scale bar 100µm.

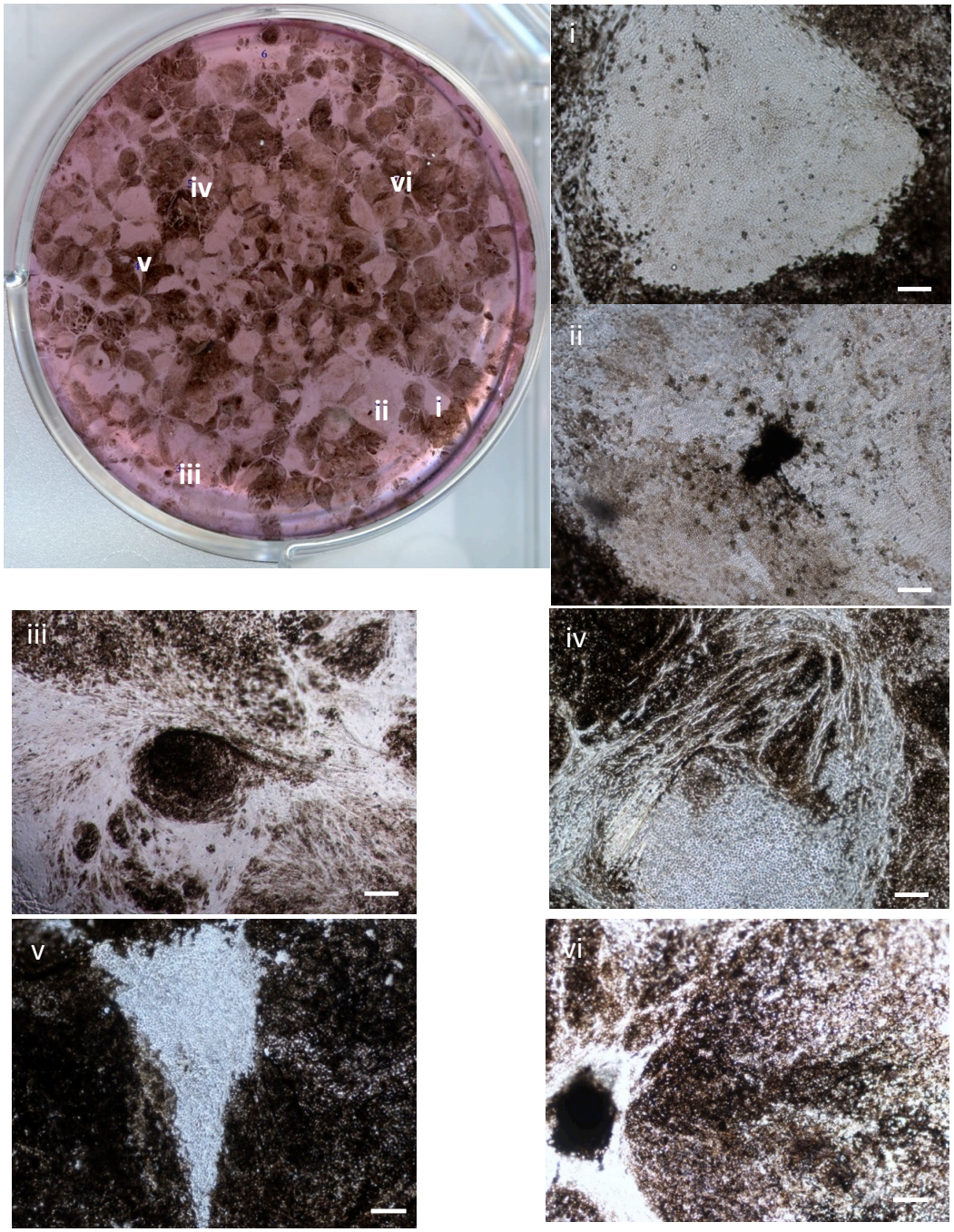

Figure 5.8: Examination of mixed morphology after single cell plating of PSC-RPE. Images i-vii are microscope images taken in the corresponding locations of the scanned well. Scale bar 200μM.

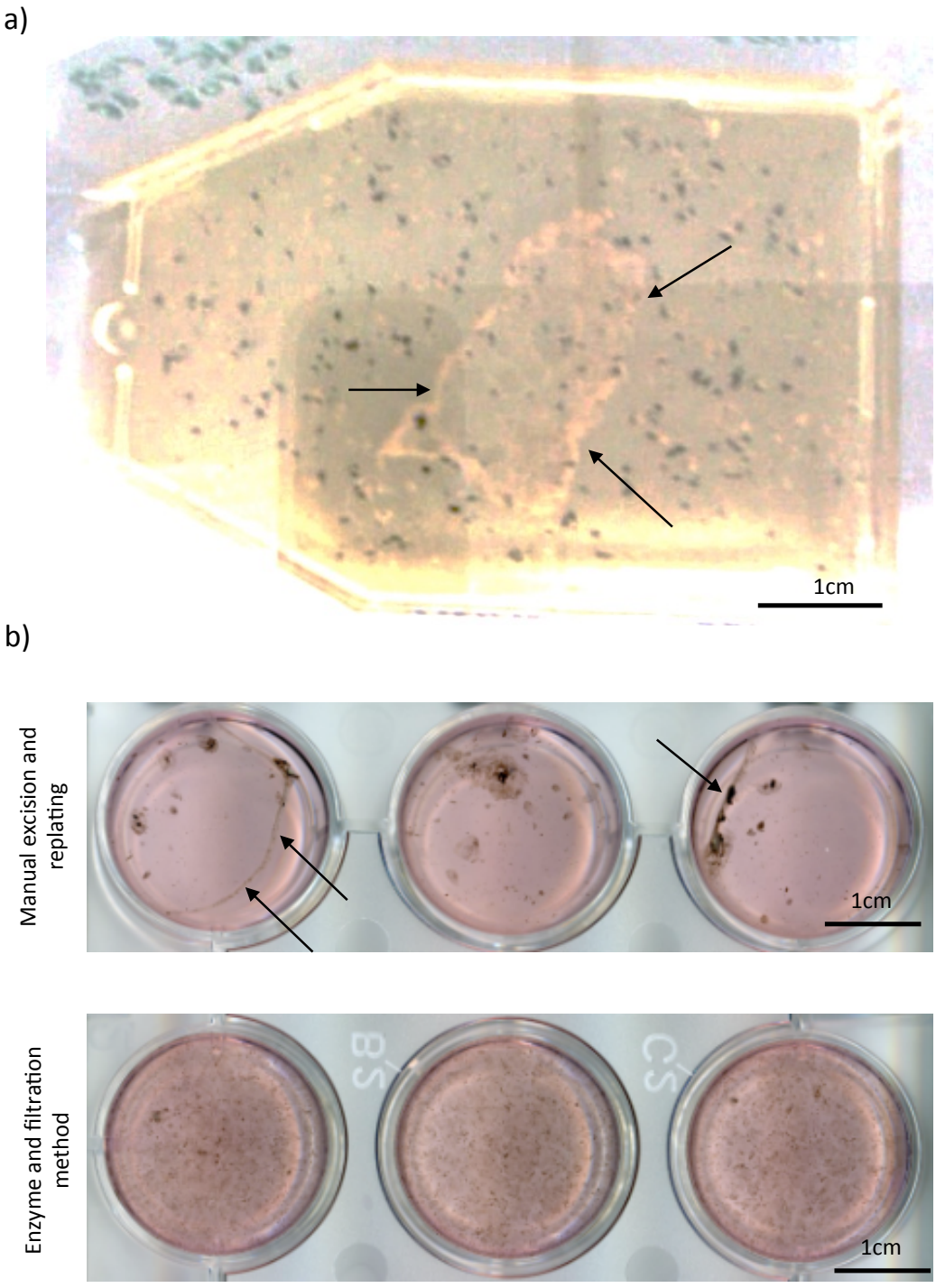

F**igure 5.9: Characterisation of a novel enzymatic hESC-RPE purification method**. a) The foci are preferentially dissociated from the differentiating cultures, the free RPE foci can be seen as black spots, with the remaining monolayer highlighted by arrows. b) The filter method using the enzymatic digestion stages shows clear improvements over the manual excision method. The arrows for the manual method highlight where the cell sheet containing non-pigmented contaminant cells has come away from the plate.

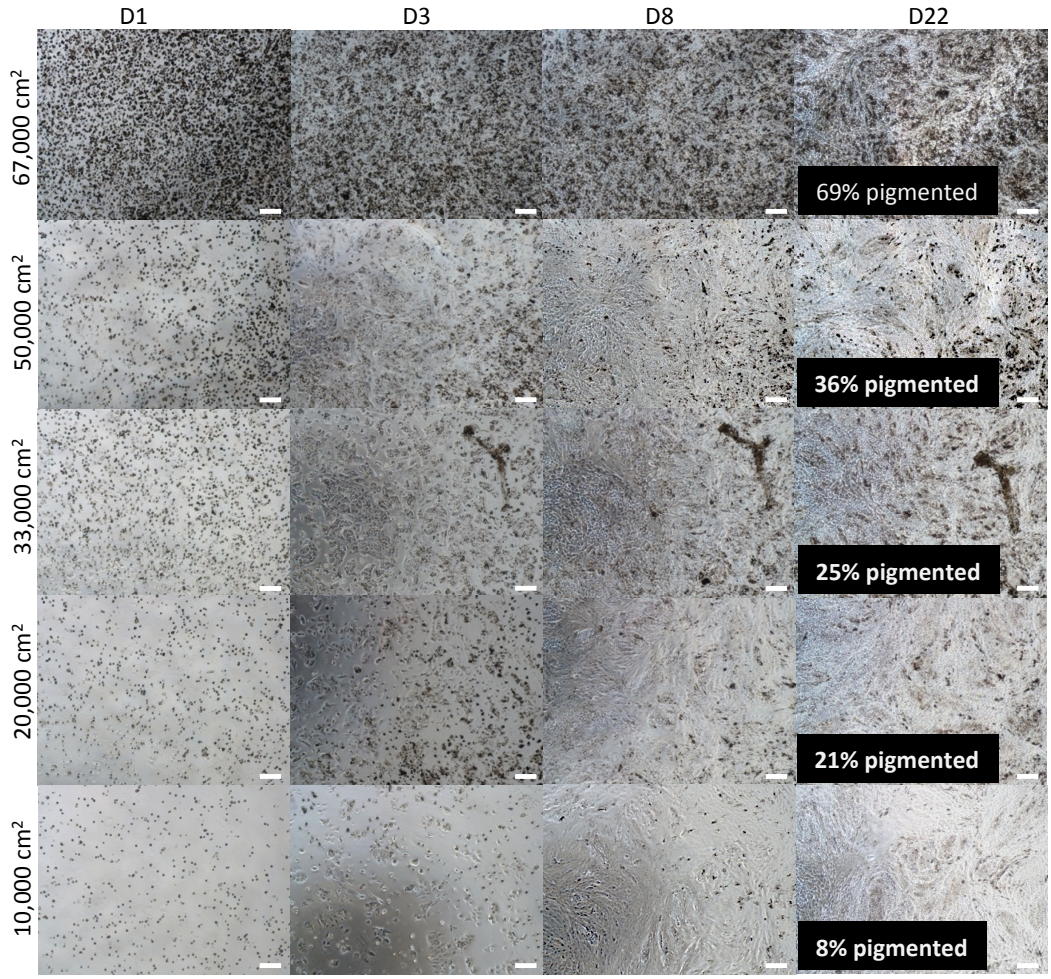

Figure 5.10: Exploring seeding after an enzymatic hESC-RPE purification method. Microscopy images of the replated PSC-RPE indicate a high seeding efficiency and that the higher the seeding density the more compact and pigmented the resultant PSC-RPE monolayer is. Scale bar 200µM.

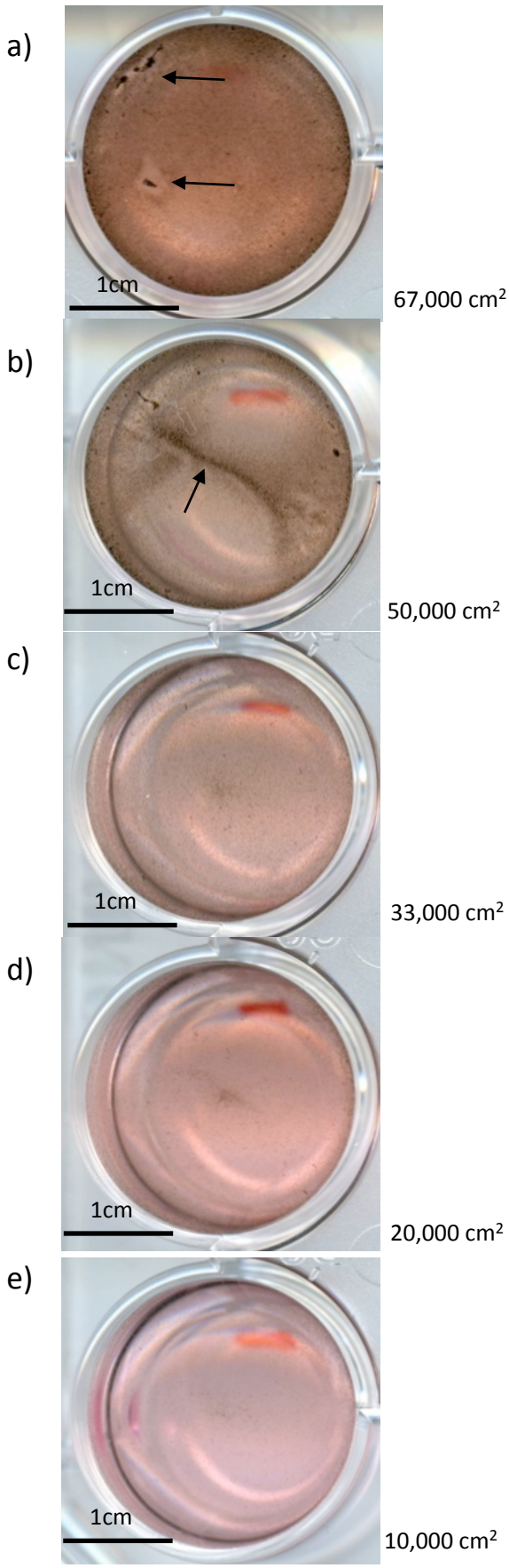

Figure 5.11:. Whole well scans of PSC-RPE wells at different densities. By imaging the whole wells the differing degrees of pigmentation between the seeding densities are clear, but also is the homogeneity across the wells which could have clinical implications.

6. Conclusions and future work

6.1 Summary and overall conclusions

6.1.1 Meeting of thesis aims and objectives

The aim of this thesis was to explore the feasibility of applying methodologies and technologies from traditional biotherapeutic production to cell therapy manufacturing, specifically the creation of a PSC-RPE therapy to treat AMD. The overall focus of the thesis being the development of a scalable and robust cell therapy manufacturing process to treat blindness

Key to the scaling of any cell culture process is to realise economies of scale and to do this in a robust and predictable manner. This traditionally involves either automation (common in a "scale out" approach) or the use of larger production units (in a "scale out") approach. In **Chapter 2** the Quantum Cell Expansion system was used to scale up cell culture. Using the system 60 million human embryonic stem cells were expanded to 708 million cells over 5 days. High levels of pluripotency marker expression were maintained on the bioreactor, with 97.7% of cells expressing SSEA-4 when harvested. However, the cell density achieved per cm^2 was 18% of traditional 2D flask controls. The likely source of this variation was the inability to control the provision of an ideal environment for cell growth in this perfusion system as there was a lack of online monitoring or control.

As the Quantum System lacks the following: i) a small-scale mimic for process development ii) a range of product sizes to be used in a seed chain and iii) and no online monitoring or control besides temperature, in its current state it is not suitable for use in an allogeneic PSC derived RPE therapy. It is important to note that this conclusion is specific for the PSC application as the Quantum system clearly has a number of key processing advantages when it is used with mesenchymal stem cells and similar cell types, for which it was originally designed. A particularly interesting application is the expansion of adherent cells from whole bone marrow aspirate. As the device is a functionally closed unit with a large

amount of automated functions for the isolation and expansion of bone marrow aspirate, it could potentially be used as a "point of care" device.

From the work with the Quantum Cell Expansion System it was clear that for a mass-produced allogeneic PSC-RPE therapy online monitoring and control were needed to optimise production and realise economies of scale. The collaboration with Artelis (who became part of ATMI and now Pall) gave access to the Xpansion One system, a 128cm^2 mimic of their larger production reactors (**Chapter 3**). This device allowed the investigation of online monitoring and control of pH and dissolved oxygen. The best performance relative to flask controls was 62%. It was observed that even small changes in pH had a large impact on growth and that the highly metabolic nature of PSCs at high density put great demands on systems originally developed for mesenchymal stem cell culture. Better results would be expected if the gas mix of the system could be controlled, i.e. increase of O_2 and reduction of CO_2 at these higher cell densities. Control of gas mix is achievable on the production scale units but not the Xpansion One development scale used in this thesis.

What was particularly interesting about the Xpansion system is that the manufacturer had intentionally tried to intensify traditional 2D culture systems rather than move to a fully 3D environment. The aim being to minimise the process development required to scale the process and minimise any impact on the target phenotype that might necessitate the replication of pre-clinical or clinical work. Through the removal of the gas headspace in the Xpansion systems a greater volumetric productivity can be achieved when compared to flasks (cm^2 available per cm^3 of bioreactor volume). However, by removing this headspace the gas transfer needs to be driven in a dynamic manner. This can cause issues due shear or other effects on the cells or if the rector design can not match the oxygen uptake rate of the cells, as described in the K_La equation. A comparison of a number of metrics for various flask/stack based methods to adherent bioreactor culture are replicated in **Figures 6.1** and **6.2** (these were originally presented as part of a poster at the Engineering Conferences International conference on Cell Therapy Manufacturing in 2013). As can be seen in **Figure 6.1** a traditional T-flask has a volumetric productivity of 0.26 (cm^2/cm^3), and a HYPERStack

has a ratio of 4.62, the Xpansion system improves on the latter slightly to 5.59 **(Figure 6.2).** The Xpansion system is limited to any further increases in volumetric productivity as the media volume per cm^2 was chosen to match traditional flask culture as close as possible and so the vessel volume can not be reduced any further. With experience of using the Xpansion system and using the data from **Figure 6.1** and **6.2** it would be interesting to run a comparison of the larger Xpansion reactors against the HYPER system to see which is better suited to commercial production of a PSC-RPE therapy. Key to this would be to determine how the highly metabolic nature of the PSC impacts the gas and mass transfer capabilities of the respective systems.

In summary, the work with the Quantum Cell Xpansion System and Xpansion One bioreactors meant that the feasibility of growing PSCs in very different dynamic environments for the first time. Clearly, the work conducted in the thesis did not produce optimised protocols to take into clinical manufacturing but the work was successful in identifying a number of technical and practical questions which need to be asked when scaling such systems. The results of this work were fed back to the manufacturers and it is hoped that they will inform the design of their respective product ranges if they seek to grow PSCs for allogeneic therapies.

No evidence could be found in the literature of applying the DoE approach to PSC differentiation in either a screening design or an optimisation design. So, given the heavy use of the approach in biotherapeutic production it was seen as a key tool to attempt to apply to PSC differentiation to develop a scalable and robust PSC-RPE process **(Chapter 4)**. Initially a screening run of 8 factors was completed to identify key variables. From this it was identified that reducing media changes from every day to once every 3 days, and reducing media volume by half did not have an adverse impact on pigmentation yield - this is vital when considering process economics. The screen also suggested that the outputs of percentage pigmentation and the RPE related gene *TYR* were significantly impacted by seeding density, the time to differentiation and nicotinamide concentration. However, the validity of the data recorded was such that Stat Ease software could not create a statistically

valid model of these inputs to be able to quantifiably predict the outcomes for the screening experiment.

This screening experiment was followed by a central composite design in a full factorial experiment to determine the process optimum with replicates of each of the 33 chosen data points for the 49 day protocol. The outputs measured for each data point included quantitative PCR of 7 RPE related genes, pH, media composition (glucose and lactate), and percentage pigmentation (a proxy measurement of RPE differentiation) all at several time points. For the optimisation experiment the factors explored were: i) time prior to switch to differentiation media, ii) nicotinamide concentration and iii) initial seeding density. Due to the variability of manual PSC culture many of the observations from these measurements were not significant when analysed in the Design Expert software (Stat-Ease). However, Pmel17 (a key RPE development marker) and percentage pigmentation allowed the creation of a computational model that statistically matched the experimental data. Exploration of this experimental space identified optimum conditions of: 15.3mM nicotinamide, an initial seeding density 13,000 cells/cm^2 and allowing 72 hours post seeding before making a change to differentiation media from PSC media. But, the contour plots suggested that the range explored in the design laid outside of the true optimal conditions. The model indicating that yet better results achievable at lower seeding densities and shorter periods before a switch to differentiation media is made.

There were clear practical issues in applying the DoE approach to PSC differentiation, due to the highly manual nature of the protocols and variability of the results from long differentiation protocols. Yet, the approach did yield interesting and useful results and has given a far better understanding of complex interactions of processing variables, such as seeding density, time to differentiation and nicotinamide concentration. It is expected as new technological methods and automated platforms are developed which allow high throughput screening of culture parameters that the DoE approach will be become standard practice.

The key limiting step of the current protocol is clearly the manual separation of the pigmented RPE from the rest of the differentiation culture. A novel separation stage using two different types of enzyme and a number of filtration stages was found to produce RPE monolayers of the target morphology **(Chapter 5)**. This method is inherently more scalable than the manual method and it would be relatively simple through the use of commercially available filtration units, pumps and values to build a proof of concept device that would remove much of the manual handling. What halts the progression of such work is a lack of understanding what the target product profile of the final monolayer actually is. From analysis of the expanding monolayer there is clear variation in the cell size and cobblestone morphology, and that this has an impact on RPE protein expression. There are a number of ways in which this and other metrics such as trans-membrane electrical potential, or protein secretions could be scored non-destructively, yet without an understanding of how these impact the potency of the final product the exercise would essentially be fruitless. What was critical in deciding not to take this work further, which would entail characterising and optimising the process, is that it appeared it might not be necessary to sort the cells at all. The manual method of using "best efforts" to remove any contaminant cells obviously does not create a pure population of cells, yet this has not caused any adverse incidents of graft overgrowth in any of the animal models. Furthermore, a new protocol published by Maruotti et al. (2013) obtains a high yield of RPE in a short timeframe by dissociating the entire differentiating culture, and then serially passaging the culture and so making no effort to "purify" the cells at all. If such an enzymatic method can show safety to the regulators from a cell contaminant perspective it would be a very simple method to scale successfully, negating the need for the current manual dissection method.

6.1.2 Practical and resource issues

Attempting to apply standard biomanufacturing technologies, such as bioreactors and approaches like DoE to PSC culture and differentiation, produced a large number of practical and resourcing issues. These presented a significant challenge in trying to develop a scalable and robust manufacturing process.

A key issue from the start of the work was the need for single cell passaging methods of PSCs. Typically PSCs are manually passaging through the selection of PSC colonies via a plastic pipette under a dissecting microscope. Such methods are extremely time consuming and insufficient to produce the number of cells required to complete the work with the bioreactors used in this thesis (60million cells were needed to seed each run of the Quantum system, and the Xpansion One unit has a 128cm^2 growth area). A number of attempts were made within the research group at UCL to adapt cell lines to enzymatic passaging methods however these always yielded cell line with stable, yet abnormal, karyotypes. Such a line was used in **Chapters 2** and **3**, which although deemed suitable for these feasibility studies when developing a new process it would have been better to have used karyotypically normal lines to ensure the data produced was directly transferable to the clinical work. The DoE work (**Chapter 4**) used karyotypically normal iPS lines and the (Stem Cell Technologies) feeder free system which through use of rock inhibitor could remain kayotypically stable after passaging with enzymatic methods. But, such systems are far too expensive for an academic lab to be used in process development work in the Quantum System or the Xpansion One system.

Even using the cheaper mouse feeder based system the Quantum Cell Expansion System was very expensive. Each run involved the coating of the 21,000 cm^2 of the bioreactor with fibronectin. Additionally, if media consumption had of been matched to the same mL per cm^2 ratio as used in flasks 4.2L of media would have been required per day. So, even though the poorer growth in the Quantum System compared to flask culture is believed to be in part because of an undersupply in media, to “oversupply” media at the start of the culture when the cell number is comparably low was simply unaffordable in an academic setting. In all 7 runs were completed on Quantum System using a variety of cell lines before the runs described in **Chapter 2** were performed (each run taking weeks to months to complete and analyse). Experimenting at such a large scale proved to not just be highly expensive, but also impractical in having to grow up 10’s millions of cells per run to conduct a simple experiment such as seeding efficiency. Therefore it is clear that any bioreactor system

needs to be available in a full range of small scale testing forms and large-scale production units.

Variability was also a constant issue with the work. Among other factors the RPE differentiation is adversely effected by passage number Lane et al. (2014) which causes reproducibility issues. To address this experiments were always set up at the same time and from the same passage. However, this creates significant labour demands for a single operator as it requires the culturing of a large number of cells before starting any experimental work. The differentiation protocol used in this thesis was also extremely long. After the first PSC expansion phase the differentiation stage to produce the pigmented foci can be run for 12 weeks. The excised foci are then expanded for up to another 7 weeks in well plates, before a further 3 week expansion on transwell plates. These very long culture periods made it not only very had to generate data but also give a very long time period on which any variation to take place.

6.2 Recommendations for future research

6.2.1 Expansion of the Work Started in this Thesis

The bioreactor work reported here focused on adherent based PSC culture. Similarly, the PSC to RPE differentiation protocols also used adherent cultures as this is the protocol followed by the Moorfields group. However, far higher volumetric productivities can be achieved by scaling cell culture in suspension methods as opposed to adherent methods. For example the maximum theoretical yield of the Xpansion system is 0.56m cells/cm^3 **(Figure 6.2)** yet in suspension cultures PSC aggregates have been grown to 3.4m cells/ml spinner flasks (Kehoe et al., 2010). As a number of PSC-RPE protocols already use suspension methods (Meyer et al., 2009) this would be an interesting avenue of research to explore the technical challenges of scale-up.

As the therapeutic dose of the PSC-RPE is likely to be as low as 50,000 cells per eye the scale up of the process to achieve economies of scale is probably less of a concern than the control and robustness of the process. Although the use of bioreactors and their control

systems usually yields a greater amount of process control, it could be argued that automation would be a very interesting avenue for investigation. An automated machine would not necessarily be a highly complex machine. For instance, during the long differentiation protocols that last several weeks the only operation performed is to change media every few days, therefore a simple automated media exchanger would free up a lot of time and labour costs in the GMP culture facilities.

6.2.2 Economic and resource modelling

The question of where resources would be best committed to remove both bottlenecks and costs from the process became critically apparent during work on this thesis. This is because there are a vast amount of potential issues that need to be addressed in the creation of a totally new manufacturing process to produce a new class of therapeutic. To this end work was initiated to model the existing process used by the clinical team at Moorfields as accurately as possible in a way which would allow the prediction of how key aspects such as cost per patient would change as the current process scales. The eventual goal was to then make suggestions of alternative approaches making use of new technologies such as automation platforms, and then to compare the scenarios. Unfortunately due to time limitations this work was not completed in time for inclusion in this thesis, however, preliminary results of the model are discussed below in brief as they represent a key area of future work.

The current lab scale process was modelled through use of Excel macros to create a tool that could take in inputs, such as number of patients to be treated a week, or the differentiation efficiency, and from this generate data such as cost per treatment or capacity utilisation of the facility. An overview of the model is displayed in **Figure 6.3** which shows the model inputs and outputs. Using the model an initial scenario was run based on a requirement to treat 3 patients per week from a single batch (with an additional patch for QC). After a 5 week expansion phase the production of each batch takes 24 weeks, and from this data the charts in **Figure 6.4** were produced. The media requirements are dominant for the stages prior to the separation of the pigmented foci (**Figure 6.4 a).** The reason being

during the "expansion" and "differentiation" stages both the target cell type and the contaminate cells are being fed media in the heterogeneous culture. Changing the differentiation efficiency of the process had by far the biggest impact on the process economics due to this relationship. Even though the later stages of the process "hESC-RPE expansion" and "Seeding onto membrane" take up a significant amount of time (**Figure 6.4 b**) from a resourcing standpoint little is needed for the stages. This is due to the culture moving from T-25 flasks in the expansion and differentiation phases into only a few well plates for the PSC-RPE expansion (as the differentiation efficiencies are relatively low with every cm^2 of PSC producing 3,800 PSC-RPE). Due to low resource requirements of the process after the separation of the foci, if the model was further developed the resourcing requirements of these stages could be considered to be either negligible or not impacting on any capacity constraints used in the equations. Finally, it was interesting to see how many media changes were needed to create 3 patches, with 1,340 needed in total (**Figure 6.4 c**). Future work would explore at what scale a simple automated media changing system would be cost effective in the removal of this manual effort to change media.

The overheads and running costs for the lab that was modelled included 2 FTEs, and were estimated to be £1.7m for a 5 year lifespan of the facility (based on personal communication, and the figure excludes admin and associated costs). The cell line used is validated to produce clinical material over 43 passages, therefore after this number a new vial from the working cell bank needs to be thawed and expanded. The Excel macros written were designed to display this information visually as shown in **Figure 6.5**. This allowed a simple scenario analysis to be run: the first scenario i) expands cells from the working cell bank and produces clinical material until the 43 passage limit, whereas the second scenario ii) involves initiation the thaw of the next working cell bank before the last final cultures of the previous lot were complete. The main difference being that with scenario ii) capacity utilisation can be maximised and so more patches produced over the 5 year facility lifetime. Based on the limitation in the current facility, being that 2 operators cannot handle more than 360 T25 flasks at any one time (180 flasks being passaged at a 1:2 ratio in a single day being the throughput bottleneck), the plots in **Figure 6.6** were

generated. From the plots, it can be observed that for scenario ii) the plants capacity is at peak (from a number of flasks perspective) for nearly the entire lifetime. In scenario i) 444 patches can be produced in the 5 years, using 102,000 litres of hESC media, with a cost per patch of £4,526. Conversely, for scenario ii) 684 patches could be produced in the same period with a cost per patch of £3,184 which represents a saving of 30%.

If more time was available more scenarios would have been run on the model and it would have been expanded to include more variables such as the size of the facility and number of operators. Ultimately a decisional tool would have been developed into which could have been tested the feasibility of investment into automation and bioreactor platforms.




	T-Flask	10 Layer CS	40 Layer CS	HYPERflask	HYPERStack 36 layer
Growth Area (cm^2)	225	6,320	25,440	1,720	18,000
volumetric productivity (cm^2/cm^3) (growth area/ reactor volume)	0.26	0.46	0.56	3.07	4.62
Cost/growth area (£/cm^2)	0.031	0.042	0.038	0.030	0.074
Potential Harvest*	34m (0.038m /cm^3)	954m (0.069m/ cm^3)	3,816m (0.083m/ cm^3)	258m (0.378m/ cm^3)	2,700m (0.692m/ cm^3)
Comments		• Less labour than dishes/flasks per cell grown • Easy scale-up, adding more layers • 40 layer manipulator costs £4,230 • Heavy when filled, more difficult to manipulate • Hard to check cell growth by microscopy		• Removal of gas-liquid interface (vessel fully filled with liquid) • Gas transfer limited by diffusion and transfer though gas permeable plastic layers • Issues with homogeneity?	

Figure 6.1: Comparison of 2D adherent flask and stacked flasks. The easiest way to scale up flask culture with minimal process development is to stack the plastic layers. However, this is not without drawbacks. *PSC harvest density of 1.5E5 cells cm^{-2}.

			
	100 layer CellCube	**Integrity Xpansion 200 layer**	**Quantum Cell Expansion System**
Growth Area (cm^2)	85,000	122,400	21,000
Available Scales (cm^2)	8,500; 21,250; 85,000	6,120; 30,600; 61,200; 122,400	21,000
volumetric productivity (cm^2/ cm^3) (growth area/ reactor volume)	14.16	5.59	38.71
Potential Harvest*	8,500m (1.42m/cm^3)	12,240m (0.56m/ cm^3)	2,100m (3.87m/cm^3)
Comments	• Gas transfer via oxygenator module at large scale (external silicon tube at small scale) • Perfused system	• Gas transfer via internal silicon tube • Gas mix and media circulation used to control pH and dissolved oxygen • Media volume per cm^2 maintained to be the same as flasks ~0.2ml/ cm^2 (no perfusion)	• Cells grown in perfused hollowfibres • Gas transfer via 2nd hollowfibre unit • Built in incubation • Highly automated from cell seeding to harvest

Figure 6.2: Comparison of adherent bioreactors. Further intensification of 2D culture through increasing volumetric productivity involves removal of the gas headspace in the reactor which causes gas transfer issues which need to be addressed. *PSC harvest density of 1.5E5 cells cm^{-2}.

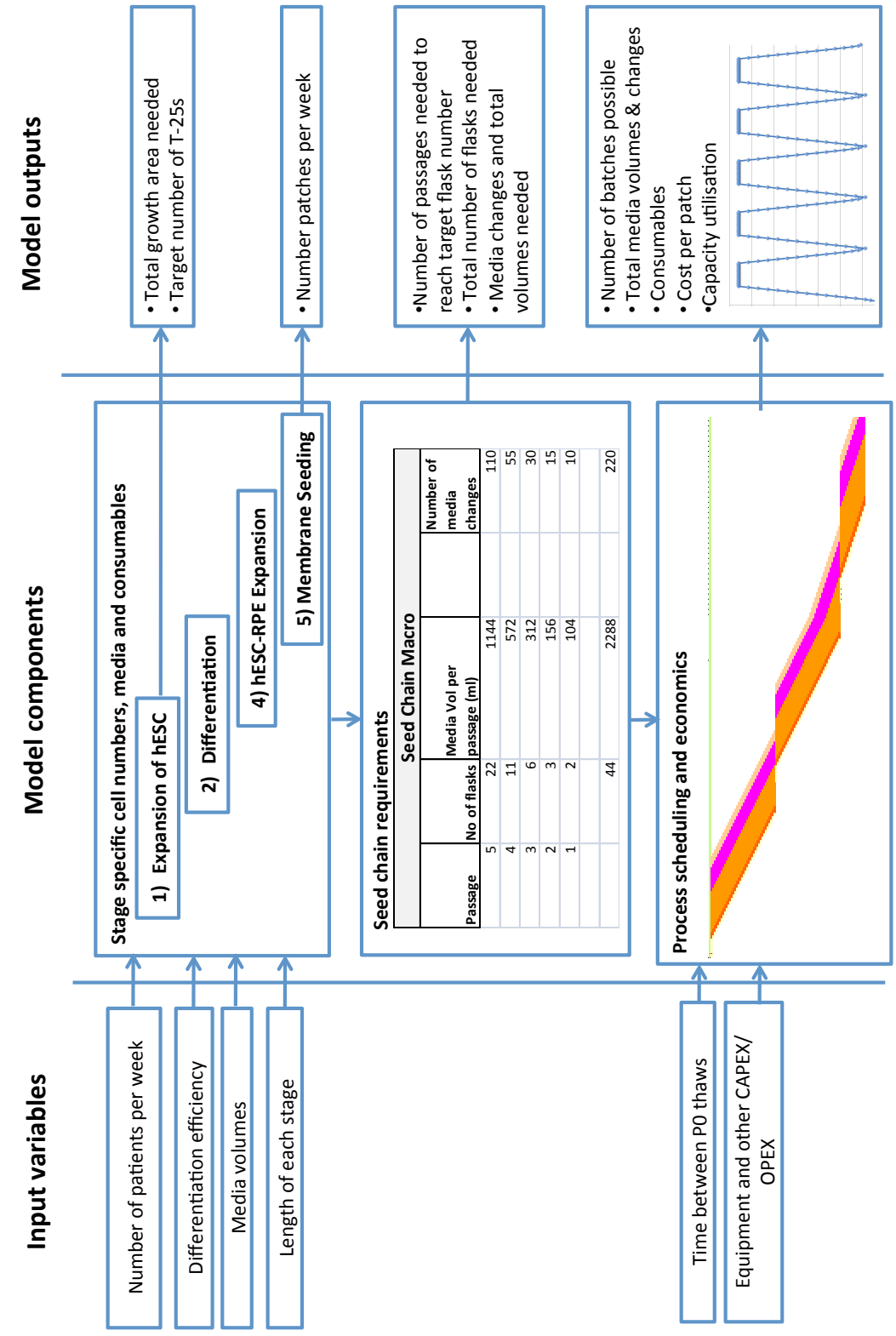

Figure 6.3: Overview of the PSC-RPE economic and resource model. The model takes in the input variables and calculates the resources required using data such as seeding densities for each of the stages to create a scheduling model and deliver the model outputs.

a) Media requirements per batch (mL)

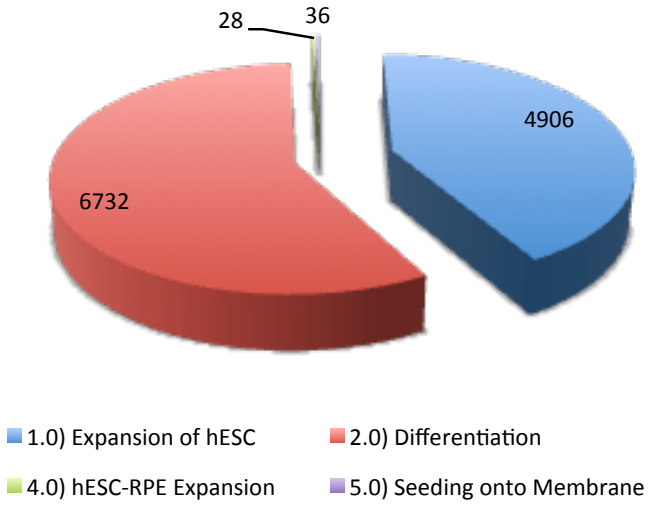

b) Culture period per stage (weeks)

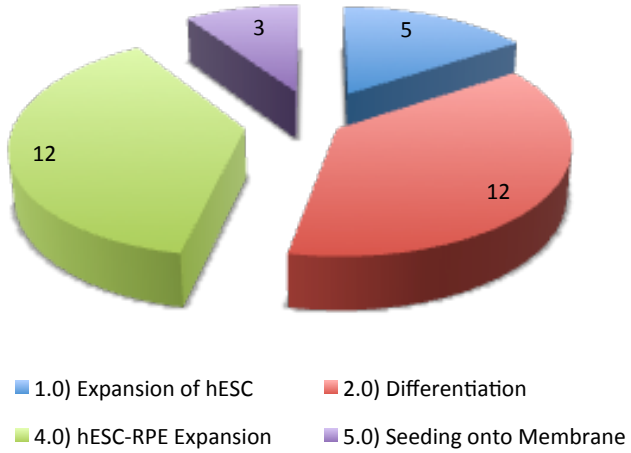

c) Number of media changes

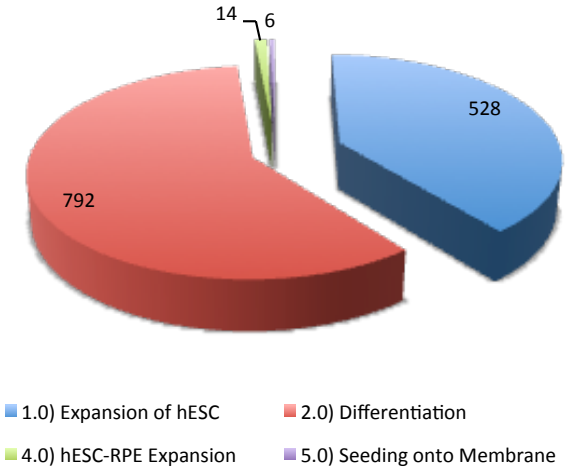

Figure 6.4: Results of the PSC-RPE economic and resource model. The media required a), the time required b) and the number of media changes needed c) for a process producing 1 batch a week yielding 3 patches (with an additional patch for QC).

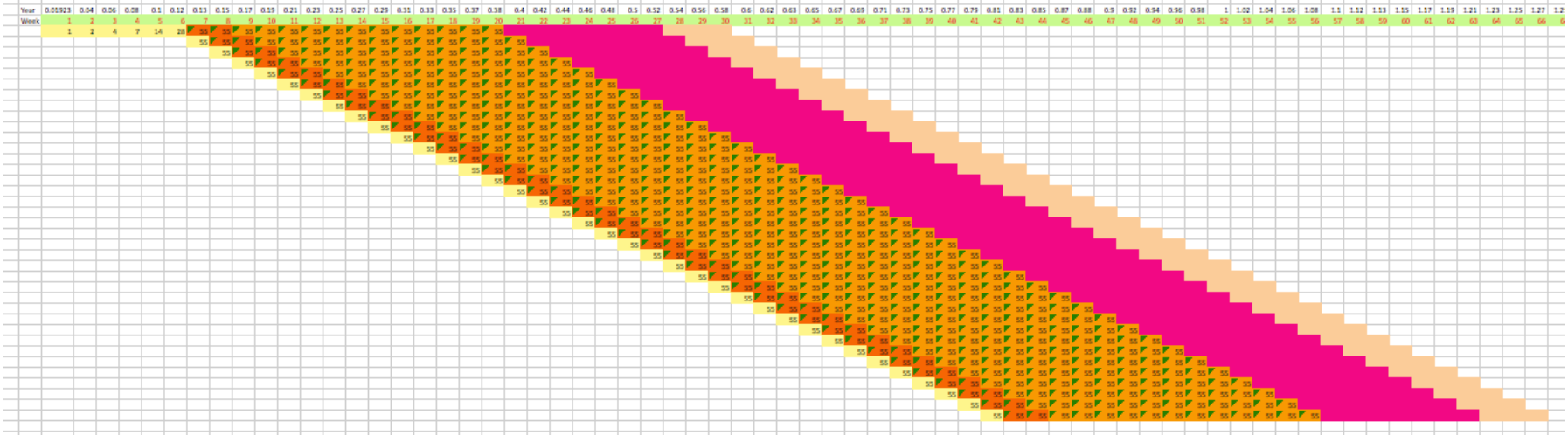

Figure 6.5: Visual representation of the Batch Timings. Each colour represents a different stage of the process which is linked to different resourcing calculations. Yellow is the expansion stage, dark orange is the time taken to achieve confluence, light orange for the differentiation stage, pink for the PSC-RPE expansion and cream for the PSC-RPE expansion on the trans well plates.

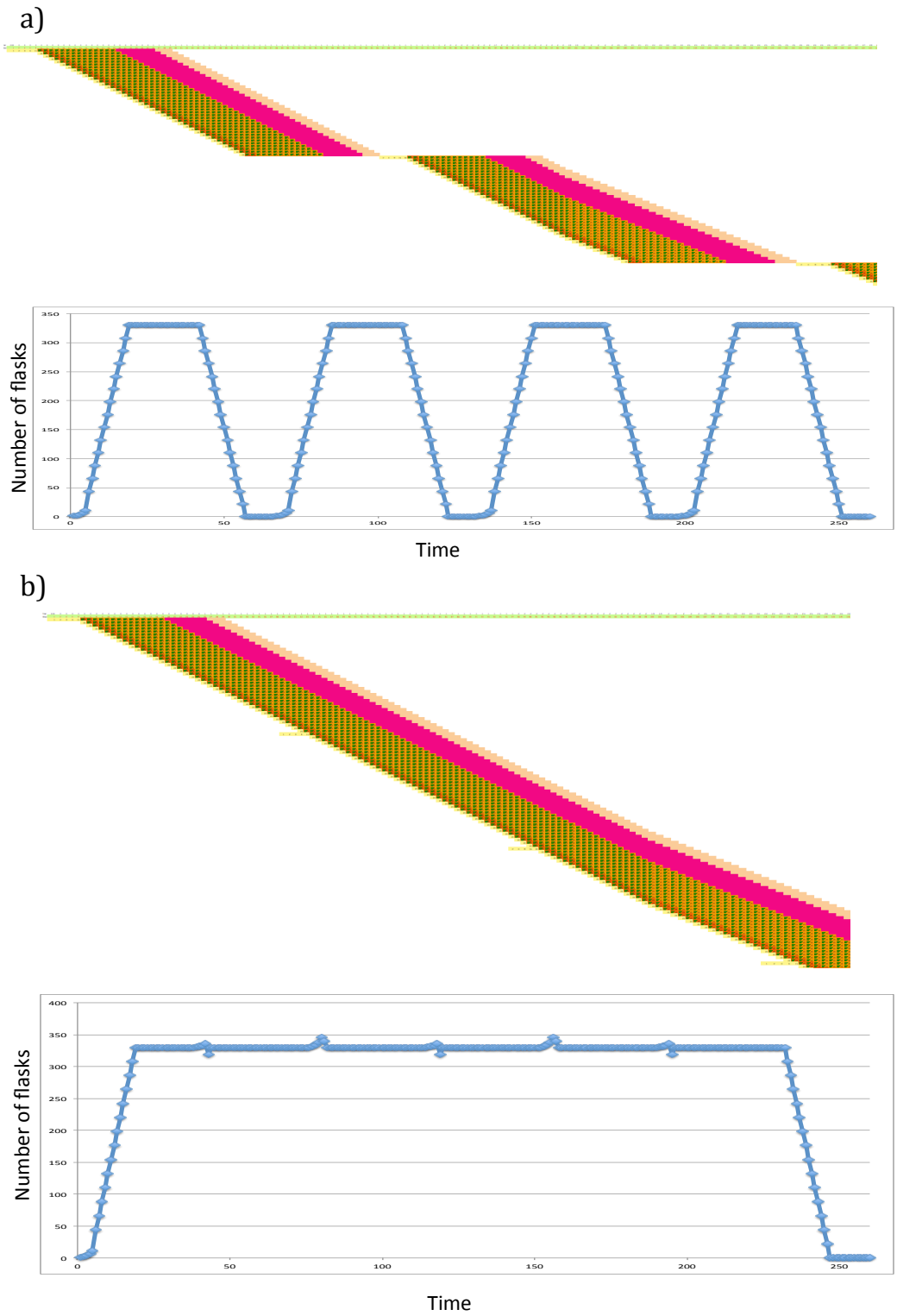

Figure 6.6: Comparison of capacity utilisation scenarios. The visual representation from the Excel macro and accompanying plot in a) show the readout for scenario i) where the next working cell bank vial is thawed only after the last batch is completed from the vial before. The representation and plot in b) show the readout for scenario ii).

ADRION, R. F., G. R. SIEBERT, C. J. WECK, D. YEN, AND R. MANSON 1984. Optimization of in vivo monoclonal antibody production using computer-assisted expermental design. *Proceedings of the First Carolina Biomedical Engineering Conference*

ALAZZAM, A., ROMAN, D., NERGUIZIAN, V., STIHARU, I., BHAT, R., YASMEEN, A. & AL MOUSTAFA, A. E. Real-time continuous dielectrophoretic separation of malignant cells. Microsystems and Nanoelectronics Research Conference, 2008. MNRC 2008. 1st, 15-15 Oct. 2008 2008. 45-48.

ALGE, C. S., SUPPMANN, S., PRIGLINGER, S. G., NEUBAUER, A. S., MAY, C. A., HAUCK, S., WELGE-LUSSEN, U., UEFFING, M. & KAMPIK, A. 2003. Comparative proteome analysis of native differentiated and cultured dedifferentiated human RPE cells. *Invest Ophthalmol Vis Sci,* 44**,** 3629-41.

ALGVERE, P. V., BERGLIN, L., GOURAS, P., SHENG, Y. & KOPP, E. D. 1997. Transplantation of RPE in age-related macular degeneration: observations in disciform lesions and dry RPE atrophy. *Graefes Arch Clin Exp Ophthalmol,* 235**,** 149-58.

ALLISON, M. 2009. Genzyme backs Osiris, despite Prochymal flop. *Nat Biotech,* 27**,** 966-967.

AMPS, K., ANDREWS, P. W., ANYFANTIS, G., ARMSTRONG, L., AVERY, S., BAHARVAND, H., BAKER, J., (...) & ZHOU, Q. 2011. Screening ethnically diverse human embryonic stem cells identifies a chromosome 20 minimal amplicon conferring growth advantage. *Nat Biotechnol,* 29**,** 1132-44.

ANISIMOV, S. V., MORIZANE, A. & CORREIA, A. S. 2010. Risks and Mechanisms of Oncological Disease Following Stem Cell Transplantation. *Stem Cell Rev*.

BAXTER, L. L. & PAVAN, W. J. 2003. Pmel17 expression is Mitf-dependent and reveals cranial melanoblast migration during murine development. *Gene Expr Patterns,* 3**,** 703-7.

BOATRIGHT, J. H., DALAL, N., CHRENEK, M. A., GARDNER, C., ZIESEL, A., JIANG, Y., GROSSNIKLAUS, H. E. & NICKERSON, J. M. 2015. Methodologies for analysis of patterning in the mouse RPE sheet. *Mol Vis,* 21**,** 40-60.

BRINDLEY, D. A., DAVIE, N. L., CULME-SEYMOUR, E. J., MASON, C., SMITH, D. W. & ROWLEY, J. A. 2012. Peak serum: implications of serum supply for cell therapy manufacturing. *Regen Med,* 7**,** 7-13.

BRUNK, U. T. & TERMAN, A. 2002. Lipofuscin: mechanisms of age-related accumulation and influence on cell function. *Free Radical Biology and Medicine,* 33**,** 611-619.

BUCHHOLZ, D. E., PENNINGTON, B. O., CROZE, R. H., HINMAN, C. R., COFFEY, P. J. & CLEGG, D. O. 2013. Rapid and Efficient Directed

Differentiation of Human Pluripotent Stem Cells Into Retinal Pigmented Epithelium. *Stem Cells Translational Medicine,* 2**,** 384-393.

CARPENTER, M. K., FREY-VASCONCELLS, J. & RAO, M. S. 2009. Developing safe therapies from human pluripotent stem cells. *Nat Biotechnol,* 27**,** 606-13.

CARR, A. J., VUGLER, A. A., HIKITA, S. T., LAWRENCE, J. M., GIAS, C., CHEN, L. L., BUCHHOLZ, D. E., AHMADO, A., SEMO, M., SMART, M. J., HASAN, S., DA CRUZ, L., JOHNSON, L. V., CLEGG, D. O. & COFFEY, P. J. 2009. Protective effects of human iPS-derived retinal pigment epithelium cell transplantation in the retinal dystrophic rat. *PLoS One,* 4**,** e8152.

CHAMBERS, S. M., FASANO, C. A., PAPAPETROU, E. P., TOMISHIMA, M., SADELAIN, M. & STUDER, L. 2009. Highly efficient neural conversion of human ES and iPS cells by dual inhibition of SMAD signaling. *Nat Biotech,* 27**,** 275-280.

CHEN, X., CHEN, A., WOO, T. L., CHOO, A. B., REUVENY, S. & OH, S. K. 2010. Investigations into the metabolism of two-dimensional colony and suspended microcarrier cultures of human embryonic stem cells in serum-free media. *Stem Cells Dev,* 19**,** 1781-92.

CHOPDAR, A., CHAKRAVARTHY, U. & VERMA, D. 2003. Age related macular degeneration. *BMJ,* 326**,** 485-8.

CLAASSEN, D. A., DESLER, M. M. & RIZZINO, A. 2009. ROCK Inhibition Enhances the Recovery and Growth of Cryopreserved Human Embryonic Stem Cells and Human Induced Pluripotent Stem Cells. *Molecular Reproduction and Development,* 76**,** 722-732.

COOKE, M. J., STOJKOVIC, M. & PRZYBORSKI, S. A. 2006. Growth of teratomas derived from human pluripotent stem cells is influenced by the graft site. *Stem Cells Dev,* 15**,** 254-9.

CSASZAR, E., CHEN, K., CALDWELL, J., CHAN, W. & ZANDSTRA, P. W. 2013. Real-time monitoring and control of soluble signaling factors enables enhanced progenitor cell outputs from human cord blood stem cell cultures. *Biotechnol Bioeng*.

DA CRUZ, L., CHEN, F. K., AHMADO, A., GREENWOOD, J. & COFFEY, P. 2007. RPE transplantation and its role in retinal disease. *Prog Retin Eye Res,* 26**,** 598-635.

DAVIS, A. A., BERNSTEIN, P. S., BOK, D., TURNER, J., NACHTIGAL, M. & HUNT, R. C. 1995. A human retinal pigment epithelial cell line that retains epithelial characteristics after prolonged culture. *Invest Ophthalmol Vis Sci,* 36**,** 955-64.

DECARIS, M. L. & LEACH, J. K. 2011. Design of experiments approach to engineer cell-secreted matrices for directing osteogenic differentiation. *Ann Biomed Eng,* 39**,** 1174-85.

DOH, I. & CHO, Y.-H. 2005. A continuous cell separation chip using hydrodynamic dielectrophoresis (DEP) process. *Sensors and Actuators A: Physical,* 121**,** 59-65.

DRAPER, J. S., SMITH, K., GOKHALE, P., MOORE, H. D., MALTBY, E., JOHNSON, J., MEISNER, L., ZWAKA, T. P., THOMSON, J. A. & ANDREWS, P. W. 2004. Recurrent gain of chromosomes 17q and 12 in cultured human embryonic stem cells. *Nat Biotech,* 22**,** 53-54.

DUPIN, E., GLAVIEUX, C., VAIGOT, P. & LE DOUARIN, N. M. 2000. Endothelin 3 induces the reversion of melanocytes to glia through a neural crest-derived glial-melanocytic progenitor. *Proc Natl Acad Sci U S A,* 97**,** 7882-7.

DUTT, K., WALDREP, J. C., KAPLAN, H. J., DEL MONTE, M., SEMPLE, E. & VERLY, G. 1989. In vitro phenotypic and functional characterization of human pigment epithelial cell lines. *Curr Eye Res,* 8**,** 435-40.

EBRAHIMI, K. B. & HANDA, J. T. 2011. Lipids, lipoproteins, and age-related macular degeneration. *J Lipids,* 2011**,** 802059.

EVANS, J. R. 2001. Risk factors for age-related macular degeneration. *Prog Retin Eye Res,* 20**,** 227-53.

FERNANDES, A. M., MARINHO, P. A., SARTORE, R. C., PAULSEN, B. S., MARIANTE, R. M., CASTILHO, L. R. & REHEN, S. K. 2009. Successful scale-up of human embryonic stem cell production in a stirred microcarrier culture system. *Braz J Med Biol Res,* 42**,** 515-22.

FLANAGAN, L. A., LU, J., WANG, L., MARCHENKO, S. A., JEON, N. L., LEE, A. P. & MONUKI, E. S. 2008. Unique Dielectric Properties Distinguish Stem Cells and Their Differentiated Progeny. *Stem Cells,* 26**,** 656-665.

FORRISTAL, C. E., WRIGHT, K. L., HANLEY, N. A., OREFFO, R. O. & HOUGHTON, F. D. 2010. Hypoxia inducible factors regulate pluripotency and proliferation in human embryonic stem cells cultured at reduced oxygen tensions. *Reproduction,* 139**,** 85-97.

HAALAND, P. D. 1989. *Experimental Design in Biotechnology*, Taylor & Francis.

HAGEMAN, G. S., LUTHERT, P. J., VICTOR CHONG, N. H., JOHNSON, L. V., ANDERSON, D. H. & MULLINS, R. F. 2001. An integrated hypothesis that considers drusen as biomarkers of immune-mediated processes at the RPE-Bruch's membrane interface in aging and age-related macular degeneration. *Prog Retin Eye Res,* 20**,** 705-32.

HERNANDEZ, D., RUBAN, L. & MASON, C. 2011. Feeder-free culture of human embryonic stem cells for scalable expansion in a reproducible manner. *Stem Cells Dev,* 20**,** 1089-98.

HEWITT, C. J., LEE, K., NIENOW, A. W., THOMAS, R. J., SMITH, M. & THOMAS, C. R. 2011. Expansion of human mesenchymal stem cells on microcarriers. *Biotechnol Lett,* 33**,** 2325-35.

HIRAMI, Y., OSAKADA, F., TAKAHASHI, K., OKITA, K., YAMANAKA, S., IKEDA, H., YOSHIMURA, N. & TAKAHASHI, M. 2009. Generation of retinal cells from mouse and human induced pluripotent stem cells. *Neurosci Lett,* 458**,** 126-31.

HUNT, M., MENG, G., RANCOURT, D., GATES, I. D. & KALLOS, M. S. 2013. Factorial Experimental Design for the Culture of Human Embryonic Stem Cells as Aggregates in Stirred Suspension Bioreactors Reveals the Potential for Interaction Effects Between Bioprocess Parameters. *Tissue Eng Part C Methods*.

IDELSON, M., ALPER, R., OBOLENSKY, A., BEN-SHUSHAN, E., HEMO, I., YACHIMOVICH-COHEN, N., KHANER, H., SMITH, Y., WISER, O., GROPP, M., COHEN, M. A., EVEN-RAM, S., BERMAN-ZAKEN, Y., MATZRAFI, L., RECHAVI, G., BANIN, E. & REUBINOFF, B. 2009. Directed differentiation of human embryonic stem cells into functional retinal pigment epithelium cells. *Cell Stem Cell,* 5**,** 396-408.

JOUSSEN, A. M., HEUSSEN, F. M. A., JOERES, S., LLACER, H., PRINZ, B., ROHRSCHNEIDER, K., MAAIJWEE, K. J. M., VAN MEURS, J. & KIRCHHOF, B. 2006. Autologous Translocation of the Choroid and Retinal Pigment Epithelium in Age-related Macular Degeneration. *American Journal of Ophthalmology,* 142**,** 17-30.e8.

KEHOE, D. E., JING, D., LOCK, L. T. & TZANAKAKIS, E. S. 2010. Scalable stirred-suspension bioreactor culture of human pluripotent stem cells. *Tissue Eng Part A,* 16**,** 405-21.

KLIMANSKAYA, I., HIPP, J., REZAI, K. A., WEST, M., ATALA, A. & LANZA, R. 2004. Derivation and comparative assessment of retinal pigment epithelium from human embryonic stem cells using transcriptomics. *Cloning Stem Cells,* 6**,** 217-45.

KNOSPEL, F., SCHINDLER, R. K., LUBBERSTEDT, M., PETZOLT, S., GERLACH, J. C. & ZEILINGER, K. 2010. Optimization of a serum-free culture medium for mouse embryonic stem cells using design of experiments (DoE) methodology. *Cytotechnology,* 62**,** 557-71.

KOROHODA, W. & WILK, A. 2008. Cell electrophoresis — a method for cell separation and research into cell surface properties. *Cellular & Molecular Biology Letters,* 13**,** 312-326.

LANE, A., PHILIP, L. R., RUBAN, L., FYNES, K., SMART, M., CARR, A., MASON, C. & COFFEY, P. 2014. Engineering Efficient Retinal Pigment Epithelium Differentiation From Human Pluripotent Stem Cells. *Stem Cells Transl Med*.

LARSEN, K. B., LUTTERODT, M., RATH, M. F. & MOLLER, M. 2009. Expression of the homeobox genes PAX6, OTX2, and OTX1 in the early human fetal retina. *Int J Dev Neurosci,* 27**,** 485-92.

LAWRENZ, B., SCHILLER, H., WILLBOLD, E., RUEDIGER, M., MUHS, A. & ESSER, S. 2004. Highly sensitive biosafety model for stem-cell-derived grafts. *Cytotherapy,* 6**,** 212-22.

LENSCH, M. W. & INCE, T. A. 2007. The terminology of teratocarcinomas and teratomas. *Nat Biotechnol,* 25**,** 1211; author reply 1211-2.

LI, F., CHONG, Z. Z. & MAIESE, K. 2006. Cell Life Versus Cell Longevity: The Mysteries Surrounding the NAD(+) Precursor Nicotinamide. *Current medicinal chemistry,* 13**,** 883-895.

LI, Q., CHEUNG, W. H., CHOW, K. L., ELLIS-BEHNKE, R. G. & CHAU, Y. 2012. Factorial analysis of adaptable properties of self-assembling peptide matrix on cellular proliferation and neuronal differentiation of pluripotent embryonic carcinoma. *Nanomedicine,* 8**,** 748-56.

LIAN, X., HSIAO, C., WILSON, G., ZHU, K., HAZELTINE, L. B., AZARIN, S. M., RAVAL, K. K., ZHANG, J., KAMP, T. J. & PALECEK, S. P. 2012. Robust cardiomyocyte differentiation from human pluripotent stem cells via temporal modulation of canonical Wnt signaling. *Proc Natl Acad Sci U S A,* 109**,** E1848-57.

LUND, R. D., WANG, S., KLIMANSKAYA, I., HOLMES, T., RAMOS-KELSEY, R., LU, B., GIRMAN, S., BISCHOFF, N., SAUVE, Y. & LANZA, R. 2006. Human embryonic stem cell-derived cells rescue visual function in dystrophic RCS rats. *Cloning Stem Cells,* 8**,** 189-99.

MARMORSTEIN, A. D., MARMORSTEIN, L. Y., RAYBORN, M., WANG, X., HOLLYFIELD, J. G. & PETRUKHIN, K. 2000. Bestrophin, the product of the Best vitelliform macular dystrophy gene (VMD2), localizes to the basolateral plasma membrane of the retinal pigment epithelium. *Proc Natl Acad Sci U S A,* 97**,** 12758-63.

MARUOTTI, J., WAHLIN, K., GORRELL, D., BHUTTO, I., LUTTY, G. & ZACK, D. J. 2013. A simple and scalable process for the differentiation of retinal pigment epithelium from human pluripotent stem cells. *Stem Cells Transl Med,* 2**,** 341-54.

MASON, C. & DUNNILL, P. 2009. Quantities of cells used for regenerative medicine and some implications for clinicians and bioprocessors. *Regen Med,* 4**,** 153-7.

MCGILL, T. J., LUND, R. D., DOUGLAS, R. M., WANG, S., LU, B. & PRUSKY, G. T. 2004. Preservation of vision following cell-based therapies in a model of retinal degenerative disease. *Vision Research,* 44**,** 2559-2566.

MEYER, J. S., SHEARER, R. L., CAPOWSKI, E. E., WRIGHT, L. S., WALLACE, K. A., MCMILLAN, E. L., ZHANG, S. C. & GAMM, D. M. 2009. Modeling early retinal development with human embryonic and induced pluripotent stem cells. *Proc Natl Acad Sci U S A,* 106**,** 16698-703.

MILLMAN, J. R., TAN, J. H. & COLTON, C. K. 2009. The effects of low oxygen on self-renewal and differentiation of embryonic stem cells. *Curr Opin Organ Transplant,* 14**,** 694-700.

MITALIPOVA, M. M., RAO, R. R., HOYER, D. M., JOHNSON, J. A., MEISNER, L. F., JONES, K. L., DALTON, S. & STICE, S. L. 2005. Preserving the genetic integrity of human embryonic stem cells. *Nat Biotech,* 23**,** 19-20.

MULLEN, R. J. & LAVAIL, M. M. 1976. Inherited retinal dystrophy: primary defect in pigment epithelium determined with experimental rat chimeras. *Science,* 192**,** 799-801.

NAKANO, T., ANDO, S., TAKATA, N., KAWADA, M., MUGURUMA, K., SEKIGUCHI, K., SAITO, K., YONEMURA, S., EIRAKU, M. & SASAI, Y. 2012. Self-formation of optic cups and storable stratified neural retina from human ESCs. *Cell Stem Cell,* 10**,** 771-85.

NGUYEN, M. & ARNHEITER, H. 2000. Signaling and transcriptional regulation in early mammalian eye development: a link between FGF and MITF. *Development,* 127**,** 3581-91.

NIE, Y., BERGENDAHL, V., HEI, D. J., JONES, J. M. & PALECEK, S. P. 2009. Scalable culture and cryopreservation of human embryonic stem cells on microcarriers. *Biotechnol Prog,* 25**,** 20-31.

NISTOR, G., SEILER, M. J., YAN, F., FERGUSON, D. & KEIRSTEAD, H. S. 2010. Three-dimensional early retinal progenitor 3D tissue constructs derived from human embryonic stem cells. *Journal of Neuroscience Methods,* In Press, Uncorrected Proof.

OSAKADA, F., IKEDA, H., SASAI, Y. & TAKAHASHI, M. 2009a. Stepwise differentiation of pluripotent stem cells into retinal cells. *Nat Protoc,* 4**,** 811-24.

OSAKADA, F., JIN, Z. B., HIRAMI, Y., IKEDA, H., DANJYO, T., WATANABE, K., SASAI, Y. & TAKAHASHI, M. 2009b. In vitro differentiation of retinal cells from human pluripotent stem cells by small-molecule induction. *J Cell Sci,* 122**,** 3169-79.

PERA, M. F. 2004. Unnatural selection of cultured human ES cells? *Nat Biotech,* 22**,** 42-43.

PHILLIPS, B. W., HORNE, R., LAY, T. S., RUST, W. L., TECK, T. T. & CROOK, J. M. 2008. Attachment and growth of human embryonic stem cells on microcarriers. *J Biotechnol,* 138**,** 24-32.

POWERS, D. E., MILLMAN, J. R., BONNER-WEIR, S., RAPPEL, M. J. & COLTON, C. K. 2010. Accurate control of oxygen level in cells during culture on silicone rubber membranes with application to stem cell differentiation. *Biotechnol Prog,* 26**,** 805-18.

PRUSZAK, J., SONNTAG, K.-C., AUNG, M. H., SANCHEZ-PERNAUTE, R. & ISACSON, O. 2007. Markers and Methods for Cell Sorting of Human

Embryonic Stem Cell-Derived Neural Cell Populations. *Stem Cells,* 25**,** 2257-2268.

RAMSDEN, C. M., POWNER, M. B., CARR, A. J., SMART, M. J., DA CRUZ, L. & COFFEY, P. J. 2013. Stem cells in retinal regeneration: past, present and future. *Development,* 140**,** 2576-85.

RATCLIFFE, E., HOURD, P., GUIJARRO-LEACH, J., RAYMENT, E., WILLIAMS, D. J. & THOMAS, R. J. 2013. Application of response surface methodology to maximize the productivity of scalable automated human embryonic stem cell manufacture. *Regen Med,* 8**,** 39-48.

ROBERTS, I., BAILA, S., RICE, R. B., JANSSENS, M. E., NGUYEN, K., MOENS, N., RUBAN, L., HERNANDEZ, D., COFFEY, P. & MASON, C. 2012. Scale-up of human embryonic stem cell culture using a hollow fibre bioreactor. *Biotechnol Lett,* 34**,** 2307-15.

ROSS, P. J., SUHR, S. T., RODRIGUEZ, R. M., CHANG, E. A., WANG, K., SIRIPATTARAPRAVAT, K., KO, T. & CIBELLI, J. B. 2010. Human-induced pluripotent stem cells produced under xeno-free conditions. *Stem Cells Dev,* 19**,** 1221-9.

ROWLAND, T. J., BUCHHOLZ, D. E. & CLEGG, D. O. 2012. Pluripotent human stem cells for the treatment of retinal disease. *J Cell Physiol,* 227**,** 457-66.

SAUVE, Y., KLASSEN, H., WHITELEY, S. J. & LUND, R. D. 1998. Visual field loss in RCS rats and the effect of RPE cell transplantation. *Exp Neurol,* 152**,** 243-50.

SAVOLAINEN, V., JUUTI-UUSITALO, K., ONNELA, N., VAAJASAARI, H., NARKILAHTI, S., SUURONEN, R., SKOTTMAN, H. & HYTTINEN, J. 2011. Impedance Spectroscopy in Monitoring the Maturation of Stem Cell-Derived Retinal Pigment Epithelium. *Ann Biomed Eng*.

SCHRIEBL, K., LIM, S., CHOO, A., TSCHELIESSNIG, A. & JUNGBAUER, A. 2010. Stem cell separation: A bottleneck in stem cell therapy. *Biotechnology Journal,* 5**,** 50-61.

SCHWARTZ, S. D., REGILLO, C. D., LAM, B. L., ELIOTT, D., ROSENFELD, P. J., GREGORI, N. Z., HUBSCHMAN, J.-P., DAVIS, J. L., HEILWELL, G., SPIRN, M., MAGUIRE, J., GAY, R., BATEMAN, J., OSTRICK, R. M., MORRIS, D., VINCENT, M., ANGLADE, E., DEL PRIORE, L. V. & LANZA, R. 2014. Human embryonic stem cell-derived retinal pigment epithelium in patients with age-related macular degeneration and Stargardt's macular dystrophy: follow-up of two open-label phase 1/2 studies. *The Lancet*.

SERRA, M., BRITO, C., SOUSA, M. F., JENSEN, J., TOSTOES, R., CLEMENTE, J., STREHL, R., HYLLNER, J., CARRONDO, M. J. & ALVES, P. M. 2010. Improving expansion of pluripotent human embryonic stem cells in perfused bioreactors through oxygen control. *J Biotechnol,* 148**,** 208-15.

SHEN, C.-C., HUANG, H.-M., OU, H.-C., CHEN, H.-L., CHEN, W.-C. & JENG, K.-C. 2004. Protective effect of nicotinamide on neuronal cells under oxygen and glucose deprivation and hypoxia/reoxygenation. *Journal of Biomedical Science,* 11**,** 472-481.

SHI, Y. & CLEGG, D. O. 2008. *Stem Cell Research and Therapeutics*, Springer.

SHIH, C. C., FORMAN, S. J., CHU, P. & SLOVAK, M. 2007. Human embryonic stem cells are prone to generate primitive, undifferentiated tumors in engrafted human fetal tissues in severe combined immunodeficient mice. *Stem Cells Dev,* 16**,** 893-902.

STACHELSCHEID, H., WULF-GOLDENBERG, A., ECKERT, K., JENSEN, J., EDSBAGGE, J., BJÖRQUIST, P., RIVERO, M., STREHL, R., JOZEFCZUK, J., PRIGIONE, A., ADJAYE, J., URBANIAK, T., BUSSMANN, P., ZEILINGER, K. & GERLACH, J. C. 2012. Teratoma formation of human embryonic stem cells in three-dimensional perfusion culture bioreactors. *Journal of Tissue Engineering and Regenerative Medicine***,** n/a-n/a.

STEINER, D., KHANER, H., COHEN, M., EVEN-RAM, S., GIL, Y., ITSYKSON, P., TURETSKY, T., IDELSON, M., AIZENMAN, E., RAM, R., BERMAN-ZAKEN, Y. & REUBINOFF, B. 2010. Derivation, propagation and controlled differentiation of human embryonic stem cells in suspension. *Nat Biotech,* advance online publication.

STRAUSS, O. 2005. The retinal pigment epithelium in visual function. *Physiol Rev,* 85**,** 845-81.

SUN, X., LONG, X., YIN, Y., JIANG, Y., CHEN, X., LIU, W., ZHANG, W., DU, H., LI, S., ZHENG, Y., KONG, S., PANG, Q., SHI, Y., HUANG, Y., HUANG, S., LIAO, B., XIAO, G. & WANG, W. 2008. Similar biological characteristics of human embryonic stem cell lines with normal and abnormal karyotypes. *Hum Reprod,* 23**,** 2185-93.

TAKAHASHI, K., TANABE, K., OHNUKI, M., NARITA, M., ICHISAKA, T., TOMODA, K. & YAMANAKA, S. 2007. Induction of pluripotent stem cells from adult human fibroblasts by defined factors. *Cell,* 131**,** 861-72.

TESTORF, M. F., LUNDSTRˆM, I. & ÷BERG, P. K. 2001. The electric charge of pigment granules in pigment cells. *Biosensors and Bioelectronics,* 16**,** 31-36.

THOMSON, J. A., ITSKOVITZ-ELDOR, J., SHAPIRO, S. S., WAKNITZ, M. A., SWIERGIEL, J. J., MARSHALL, V. S. & JONES, J. M. 1998. Embryonic stem cell lines derived from human blastocysts. *Science,* 282**,** 1145-7.

TITMARSH, D., HIDALGO, A., TURNER, J., WOLVETANG, E. & COOPER-WHITE, J. 2011. Optimization of flowrate for expansion of human

embryonic stem cells in perfusion microbioreactors. *Biotechnology and Bioengineering,* 108**,** 2894-2904.

VUGLER, A., CARR, A. J., LAWRENCE, J., CHEN, L. L., BURRELL, K., WRIGHT, A., LUNDH, P., SEMO, M., AHMADO, A., GIAS, C., DA CRUZ, L., MOORE, H., ANDREWS, P., WALSH, J. & COFFEY, P. 2008. Elucidating the phenomenon of HESC-derived RPE: anatomy of cell genesis, expansion and retinal transplantation. *Exp Neurol,* 214**,** 347-61.

WANG, L., LU, J., MARCHENKO, S. A., MONUKI, E. S., FLANAGAN, L. A. & LEE, A. P. 2009. Dual frequency dielectrophoresis with interdigitated sidewall electrodes for microfluidic flow-through separation of beads and cells. *Electrophoresis,* 30**,** 782-791.

WEIL, B. & VERAITCH, F. 2014. Bioprocessing Challenges Associated with the Purification of Cellular Therapies. *In:* AL-RUBEAI, M. & NACIRI, M. (eds.) *Stem Cells and Cell Therapy.* Springer Netherlands.

WONG, W. L., SU, X., LI, X., CHEUNG, C. M. G., KLEIN, R., CHENG, C.-Y. & WONG, T. Y. Global prevalence of age-related macular degeneration and disease burden projection for 2020 and 2040: a systematic review and meta-analysis. *The Lancet Global Health,* 2**,** e106-e116.

YANG, X. M., YAFAI, Y., WIEDEMANN, P., KUHRT, H., WANG, Y. S., REICHENBACH, A. & EICHLER, W. 2012. Hypoxia-induced upregulation of pigment epithelium-derived factor by retinal glial (Muller) cells. *J Neurosci Res,* 90**,** 257-66.

YOUNG, R. W. 1987. Pathophysiology of age-related macular degeneration. *Surv Ophthalmol,* 31**,** 291-306.